

Raffaele Vitulli

ESA/ESTEC, Keplerlaan 1, 2201AZ Noordwijk, The Netherlands

e-mail: Raffaele.Vitulli@esa.int

Peter Vörsmann

Institute of Aerospace Systems, Technical University Brunswick, Germany

Shui-Lin Weng

NSPO, Satellite System Development Program, 8F, 9 Prosperity 1st Road, Hsinchu Science Park, Hsinchu City 30078, Taiwan

e-mail: jsw.weng@nspo.org.tw

Alex Wishart

Astrium Satellites Ltd, Gunnels Wood Road, Stevenage, SG1 2AS, England

e-mail: alex.wishart@astrium.eads.net

Lance Wu

National Space Organization (NSPO), 8F, 9 Prosperity 1st Road, Science Park, Hsinchu, Taiwan 30078

e-mail: lancewu@nspo.org.tw

An-Ming Wu

National Space Organization (NSPO), 8F, 9 Prosperity 1st Road, Science Park, Hsinchu, Taiwan 30078

Seung-Uk Yang

Satrec Initiative, 461-26 Jeonmin-Dong, Yuseong-Gu, Daejeon 305-811, Republic of Korea

Zizung Yoon

Berlin Technical University, Institute of Aeronautics and Astronautics, Department of Astronautics, Marchstr. 12, 10587 Berlin

e-mail: zizung.yoon@tu-berlin.de

Tino Zehetbauer

German Aerospace Centre (DLR), Microwave and Radar Institute, Department Reconnaissance and Security, Oberpfaffenhofen, D-82234 Wessling, Germany

e-mail: Tino.Zehetbauer@dlr.de

L.M. Zelenyi

Space Research Institute (IKI), RAS, Profsoyuznaya 84/32, 117997 GSP-7 Moscow, Russia

Session 1

Programmatics

NASA Earth Observation Programs and Small Satellites

Steven P. Neeck and Theodore F. Hammer

Abstract NASA's strategic goal in Earth science is motivated by the fundamental question: "How is the Earth changing and what are the consequences for life on Earth?" NASA's mission in Earth science as mandated by the U.S. Space Act is to "... conduct aeronautical and space activities so as to contribute materially to . . . the expansion of human knowledge of the Earth and of phenomena in the atmosphere and space". Therefore, NASA's role is unique and highly complements those of other U.S. Federal agencies by continually advancing Earth system science from space, creating new remote sensing capabilities, and enhancing the operational capabilities of other agencies and collaborating with them to advance Earth science goals. NASA's Earth Science Division (ESD) currently has a system of spacecraft collecting observations of the Earth system and in the months and years ahead will deploy new satellites and constellations with advanced measurement capabilities. Small satellites ($\sim 500\text{kg}$ or less) have been crucial contributors to achieving NASA's Earth science measurements and will continue to be so in the future. The U.S. National Research Council (NRC) is just now completing its first decadal survey for Earth science and applications from space. This survey will be used to set priorities for future missions to 2017 and beyond. Current status of ESD flight programs, preparations for the NRC decadal survey, and the role of small satellites will be discussed.

1 NASA Earth Science

The complexity of the Earth system requires that an organized scientific approach be developed for addressing the complex, interdisciplinary problems that exist, taking good care that in doing so there is a recognition of the objective to integrate science across the programmatic elements towards a comprehensive understanding of

S.P. Neeck

NASA Headquarters, Science Mission Directorate, Washington, DC 20546, USA
e-mail: steven.neeck@nasa.gov

T.F. Hammer

NASA Headquarters, Science Mission Directorate, Washington, DC 20546, USA

the Earth system. In the Earth system, these elements may be built around aspects of the Earth that emphasize the particular attributes that make it stand out among known planetary bodies. These include the presence of carbon-based life; water in multiple, interacting phases; a fluid atmosphere and ocean that redistribute heat over the planetary surface; an oxidizing and protective atmosphere, albeit one subject to a wide range of fluctuations in its physical properties (especially temperature, moisture, and winds); a solid but dynamically active surface that makes up a significant fraction of the planet's surface; and an external environment driven by a large and varying star whose magnetic field also serves to shield the Earth from the broader astronomical environment.

The resulting structure is comprised of six interdisciplinary Science Focus Areas:

| | |
|--------------------------------|----------------------------|
| Atmospheric Composition | Weather |
| Carbon Cycle and Ecosystems | Water and Energy Cycle |
| Climate Variability and Change | Earth Surface and Interior |

These six focus areas include research that not only addresses challenging science questions but drives the development of an Earth observing capability and associated Earth system models as well. In concert with the research community, NASA developed a hierarchy of science questions. The fundamental question: "How is the Earth changing and what are the consequences for life on Earth?" leads to five associated core questions, representing a paradigm of variability, forcing, response, consequences and prediction mitigate natural hazards? Figure 1 illustrates the cross-cutting and interdisciplinary nature of the science questions and their links to each science focus area.

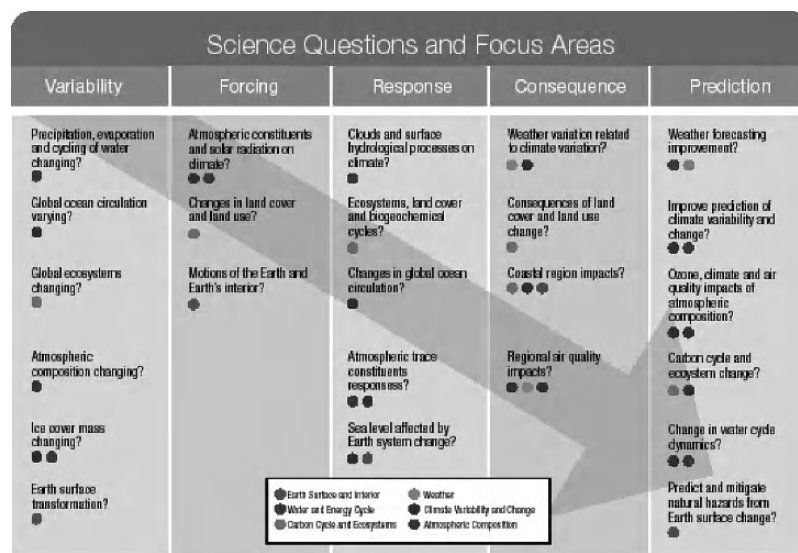


Fig. 1 Links and interrelationships between science focus areas and science questions

NASA's Earth science programs are essential to the implementation of three major Presidential initiatives: Climate Change Research (June 2001), Global Earth Observation (July 2003), and the U.S. Ocean Action Plan (December 2004).

NASA's Earth science program is an end-to-end one that starts with the development of observational techniques and the instrument technology needed to implement them; tests them in the laboratory and from an appropriate set of suborbital (surface, balloon, aircraft) and/or space-based platforms; uses the results to increase basic process knowledge; incorporates results into complex computational models that can be used to more fully characterize the present state and future evolution of the Earth system; and develops partnerships with other national and international agencies that can use the generated information in environmental forecasting and in policy and resource management. Accordingly, ESD is divided into the following major program elements: Research and Analysis, Flight, and Applied Sciences, and Technology [1].

2 ESD Flight Program Status

ESD's Flight Program encompass the space based and suborbital remote sensing observational capabilities supporting NASA's Earth science activities. Ground segment elements such as data and information systems are an important part of the Flight Program in addition to space and suborbital missions. Synergy between different classes of observations, basic research, modeling, and data analysis, as well as field and laboratory studies is the hallmark of the. Three types of space flight missions were distinguished in the recent past: systematic observation missions (SYSP), exploratory missions (PI-led), and operational precursor or technology demonstration missions. The identification of these categories represents a significant evolution of the original architecture of the Earth Observing System, which combined studying basic processes, assembling long-term measurement records, and introducing innovative measurement techniques. The Flight Program also develops geostationary-orbiting meteorological and polar-orbiting environmental satellites for the National Oceanic and Atmospheric Administration (NOAA) through the Geostationary Operational Environmental Satellite (GOES) and the Polar Operational Environmental Satellite (POES) programs.

Figure 2 provides the timeline of Earth science systematic and exploratory missions, including placeholders for future missions. 14 ESD missions are currently operating while 7 are in formulation or development. Of these 21 missions, 9 fall into the small satellite (~ 500 kg or less) category. The Ocean Surface Topography Mission (OSTM), Orbiting Carbon Observatory (OCO), Glory, and Global Precipitation Measurement (GPM) are related upcoming missions. This emphasis reflects advancements in compact sensor, small satellite bus, and launch vehicle technologies, in addition to management innovations (e.g. Principal Investigator mission management and streamlined "catalog" acquisition approaches). Advanced planning suggests this trend will continue including their use in constellations as is

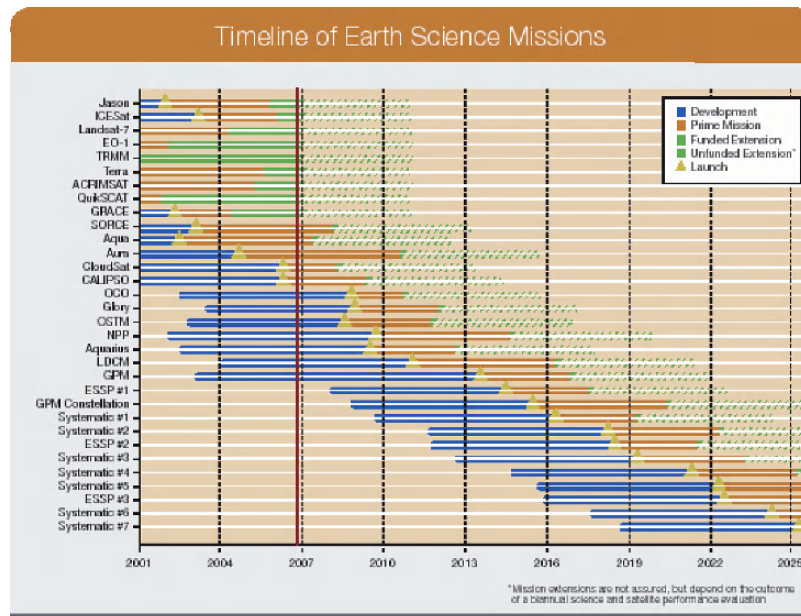


Fig. 2 Earth science mission timeline (includes placeholders for future missions)

now the case in the five satellite A-Train. Descriptions of the four upcoming small satellite missions follow.

OSTM will measure sea surface height to an accuracy of < 4 cm every ten days. Its primary objectives are to provide continuity of ocean topography measurements beyond the Jason mission and to provide a bridge to an operational mission to enable the continuation of multi-decadal ocean topography measurements. OSTM uses a Thales Alenia PROTEUS minisatellite bus. It is a collaboration with CNES, EU-METSAT, and NOAA. OSTM is in implementation (Phase C/D) and is scheduled for 2008 launch with a 3 year lifetime.

OCO provides space-based observations of atmospheric Carbon Dioxide (CO₂), the principal human-initiated driver of climate change. It will generate precise global maps of the abundance of CO₂ in the Earth's atmosphere using an optical spectrometer. OCO uses an Orbital Sciences Corporation LeoStar-2 minisatellite bus. OCO is in implementation (Phase C/D) and is scheduled for launch in 2008 with a 2 year lifetime.

The Glory mission will increase our understanding of black carbon soot and other aerosols as causes of climate change as well as continue the measurement of the total solar irradiance. Aerosol properties will be measured by an advanced polarimeter. The total solar irradiance measurement will be made based by a SORCE-heritage instrument. Glory uses an Orbital Sciences Corporation LeoStar minisatellite bus. It will carry two optical instruments. Glory is in implementation (Phase C/D) and is scheduled for launch in 2008 with a 3 year lifetime.

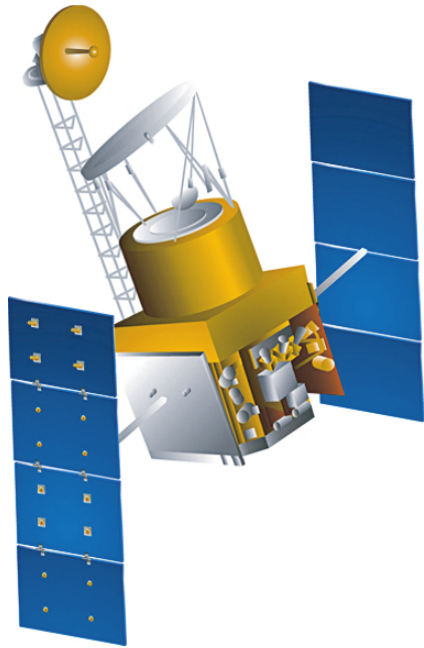
Fig. 3 Ocean Surface Topography Mission



Fig. 4 Orbiting Carbon Observatory



The Global Precipitation Measurement (GPM) mission initiates the measurement of global precipitation, providing uniformly calibrated measurements every 3 hours for scientific research and societal applications through a constellation of dedicated and operational satellites carrying active and passive microwave sensors. It is a collaboration with JAXA and other international partners. In addition to the precipitation radar carrying Core Spacecraft, NASA supplies a single instrument minisatellite observatory. The GPM Constellation Spacecraft flies in a low-inclination orbit to improve spatial coverage and sampling frequency, near real-time monitoring and prediction of hurricanes/typhoons, diurnal sampling of precipitation, cross-calibration of polar-orbiting constellation satellites. GPM Constellation will use a RSDO catalog minisatellite bus. GPM Constellation is in formulation (Phase B) and is scheduled for launch in 2014.

Fig. 5 Glory**Fig. 6** GPM Constellation

3 NRC Decadal Survey and ESD Preparations

The U.S. NRC recently completed its first decadal survey for Earth science and applications from space [2]. This survey will be used by ESD to set priorities for future missions and research and develop an integrated strategic roadmap of its space activities. Among its recommendations, the decadal survey prioritized 15 missions for ESD to launch during 2010–2020. During the latter half of 2006, in preparation for the decadal survey and to facilitate strategic roadmapping, ESD conducted “building

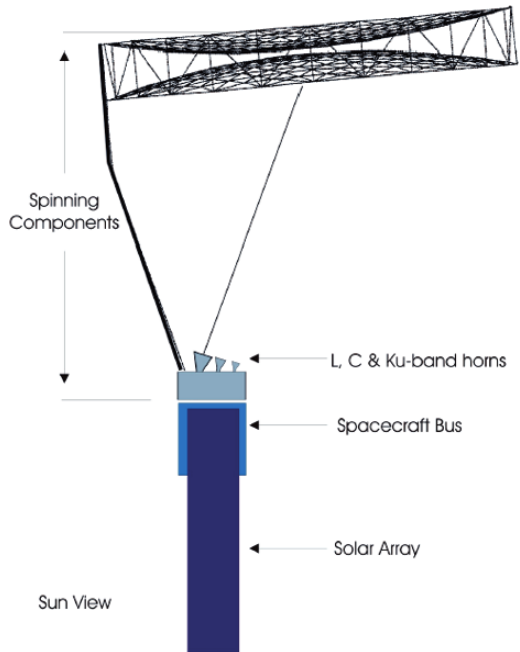
block” mission concept definition studies under NASA Headquarters direction at the Goddard Space Flight Center (GSFC), Jet Propulsion Laboratory (JPL), and the Langley Research Center (LaRC). These consisted of 13 individual and 6 integrated mission concepts based on earlier Science Focus Area roadmaps. ESD is presently using the engineering, programmatic, and budgetary data from the “building block” studies to construct the priority order of its space science missions through the next decade. In both the decadal survey missions and the ESD “building block” studies a number of concepts used small satellites in individual or multi-satellite configurations. Four small satellite concepts from the 15 missions recommended by the NRC decadal survey follow.

The Climate Absolute Radiance and Refractivity Observatory (CLARREO) will provide a global, accurate, and tested climate benchmark. Key observations include incident and reflected solar irradiance and spectrally resolved radiance emitted to space that carries the spectral signature of IR forcing of climate and the resulting response of that climate system. The observing elements are shared between NASA and NOAA. The NASA component consists of three microsatellites in polar orbits separated by 60 degrees in orbit plane, two carrying redundant IR interferometers and the third carrying in addition a UV/VNIR/SWIR redundant interferometer. GPS occultation receivers are carried on all three microsatellites. CLARREO is recommended to launch in the 2010–2013 timeframe. The NOAA component of CLARREO is the reflight of the TSIS incident solar irradiance and CERES broadband Earth radiation instruments on NPP and NPOESS.

Soil Moisture Active-Passive (SMAP) will provide global high-resolution 3–10 km soil moisture mapping. It addresses critical science questions in the water and energy cycle and enhances the forecasting and mitigation of flash-floods, severe storms, and regional droughts. Additionally, it extends the predictability of processes influenced by surface moisture states and fluxes. SMAP is based on a single minisatellite in low Earth orbit and includes both active and passive L band microwave measurements. Its technology readiness benefits from the recent Hydros risk reduction efforts. SMAP is recommended to launch in the 2010–2013 timeframe.

Surface Water and Ocean Topography (SWOT) will address science and applications questions related to the storage and movement of inland waters, the circulation of the oceans and coastal waters, and the fine-scale bathymetry and roughness of the ocean floor. SWOT carries a Ka band swath altimeter that will produce high resolution measurements of water surface elevations over inland waters, as well as near-coastal regions and the open ocean. It also carries a Ku band nadir altimeter, a microwave radiometer, and a precision GPS receiver. It uses a minisatellite bus and is recommended to launch in 2013–2016 to overlap with the NOAA-recommended ocean vector winds mission.

Gravity Recovery and Climate Experiment-II (GRACE-II) will measure temporal variations in Earth’s gravity field at a higher resolution than that demonstrated by the NASA-DLR GRACE mission. For the hydrological cycle, GRACE-II will observe large-scale evapotranspiration, soil moisture inventory, and depletion of large aquifers; detect changes in deep ocean currents to differentiate between sea

Fig. 7 CLARREO**Fig. 8** SMAP

level rise and addition of freshwater from the continents; and detect changes in the mass and global spatial distribution of ice and permafrost. In addition, GRACE-II will identify constraints on the strength of Earth's interior by observing changes in the flow in Earth's core. GRACE-II will have more accurate measurement of

inter-satellite range using either an improved version of the GRACE microwave ranging system or a laser satellite-to-satellite interferometer. The pair of microsatellites is recommended to be launched in 2016–2020.

Fig. 9 SWOT

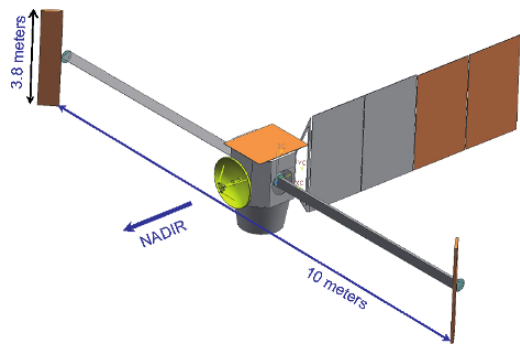
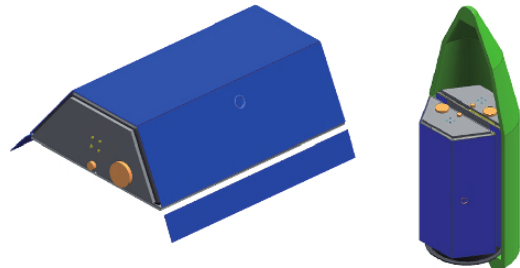


Fig. 10 GRACE-II



4 Role of Small Satellites

In the decade 2007–2017, ESD will develop and demonstrate new sensors and interacting constellations of satellites. Expanded operational capabilities will be complemented with the delivery of reliable data products from the space observing system and the continual improvement of predictive models based on emerging scientific research. In the future, as more data is collected and analyzed from a multi-disciplinary viewpoint and as predictive model development moves toward increased coupling of Earth system components, there will be increasing requirements for scientific research. Likewise, the number of space-based observations required for assimilation into the coupled models will also grow with the complexity of the system. In order to meet the increasing demands of data volume and model complexity, ESD will pursue the following strategies:

- *Work with the scientific community to create interdisciplinary teams that help focus research and resources on key uncertainties and model deficiencies;*

- *Develop in concert with commercial partners, new, decentralized approaches to data archiving and management that emphasizes broad, creative uses of multi-disciplinary data sets;*
- *Develop, launch and operate a cost effective suite of space-borne missions that observe multiple key Earth system parameters; and,*
- *Coordinate with other U.S. and international partners to ensure that a core set of key measurements are made on a sustained basis.*

In implementing the third of these strategies, ESD anticipates using the increasing capabilities of small satellites and their constellations.

References

1. NASA, Science Plan for NASA's Science Mission Directorate 2007–2016, 42–71 (2007)
2. National Research Council, Earth Science and Applications from Space: National Imperatives for the Next Decade and Beyond (2007)

Incubating Domestic Space-Qualified Manufacturers Through ROCSAT Programs

Jeng-Shing Chern, Arthur Huang, and Lance Wu

Abstract Taiwan's space program started from 1991. There was no space-qualified manufacturer in Taiwan before that time. The Government decided to incubate domestic space-qualified manufacturers in Taiwan through the development of space program. Consequently, the Government assigned the role of incubating domestic space-qualified manufacturers to the National Space Organization (NSPO). The role is partly completed after 16 years of effort. Major reasons are that Taiwan's space budget is small and all manufacturers are commercially oriented. Fortunately there are still some successful examples. This paper reviews the process of incubating Taiwan's domestic space-qualified manufacturers through ROCSAT space projects (currently called FORMOSAT projects) and introduces the successful examples. It then foresees the potential "blue sea" (or say blue ocean) of NSPO's future space program. There were three space projects in Taiwan's first phase space program which spans 15 years from 1991 to 2006: FORMOSAT-1 (FS1), FORMOSAT-2 (FS2) and FORMOSAT-3 (FS3). A total of 8 companies had been incubated with 23 products manufactured: 5 in FS1, 8 in FS2 and 10 in FS3. Among the 8 incubated companies, 6 continue to participate NSPO's second phase space program started at 2004 and shall end in 2018. Simply speaking, NSPO's experience can be summarized in two points: (1) it is not easy, and (2) it is a long but right way to go. For the potential "blue sea" in the future, NSPO's is developing the "super cluster project" currently. Tens or hundreds or thousands of cheap microsatellites called "astrochicken" with about 2 years of mission life shall be launched for various missions. One important point is that they must be very responsive. Under

J.-S. Chern

National Space Organization (NSPO),
8F, 9 Prosperity 1st Road, Science Park, Hsinchu, Taiwan 30078
e-mail: jschern@nspo.org.tw

A. Huang

National Space Organization (NSPO),
8F, 9 Prosperity 1st Road, Science Park, Hsinchu, Taiwan 30078

L. Wu

National Space Organization (NSPO),
8F, 9 Prosperity 1st Road, Science Park, Hsinchu, Taiwan 30078

this strategy, Taiwan could be able to copy its successful experience in developing computer industry.

1 Introduction

Taiwan's first phase space program spanned 15 years, from 1991 to 2006; and its second phase spans another 15 years, from 2004 to 2018. There are 3 years of overlap. The National Space Program Office (NSPO) of Taiwan was established in 1991 to perform the space program. It was then changed to the current name National Space Organization with the same acronym NSPO in 2005. Three satellite projects had been successfully completed with 8 satellites launched in the first phase space program: 1 small satellite in FORMOSAT-1 (FS1) project, 1 small satellite in FORMOSAT-2 (FS2) project, and 6 micro satellite as a constellation in FORMOSAT-3 (FS3) project.

One of the major roles of Taiwan's space program is to incubate the domestic space-qualified manufacturers. Therefore, from the beginning NSPO adopted a strategic policy to construct some satellite components by domestic manufacturers in order to build up space industry in Taiwan. A few carefully selected manufacturers obtained technology transfer agreements of space-qualified satellite components from foreign manufacturers. Using the transferred technical know-how, these manufacturers were able to fabricate some spacecraft components for FS1, FS2 and FS3 projects, respectively.

This paper introduces the domestic space-qualified manufacturers incubated and their products. [1] Then the super cluster concept for NSPO's future blue sea policy is presented.

2 Space-Qualified Manufacturers Incubated in FS1 Project [1]

The FS1 project was started in 1994 and completed in 1998. This is a cooperation project between NSPO and TRW of US for developing a small scientific satellite. Four domestic space-qualified manufacturers had been incubated with 5 products provided.

2.1 Acer Incorporation

Acer Incorporation built the on-board computer (OBC) to handle the satellite operation. The computer also performs data and signal processing, command decoding and executing, and subsystems interface control. More details of the on-board computer are listed below:

- Dimension: 21.6cm × 21.3cm × 11.9cm
- Central processing unit (CPU): 80186
- Weight: 3.3 kg

- Maximum power dissipation: 10.3 watt
- Read-only memory (ROM): 512 K Bytes
- Random access memory (RAM): 512 K Bytes
- Subsystem interface: TT&C, C&DH, EPS, ADCS, TCS, RCS, GSE, Payload, etc.
- Data interface: 1553B, RS-422

2.2 Trans System Incorporation

Trans System Incorporation manufactured the remote interface unit (RIU) which decodes and distributes commands to the experimental communication payload. The unit also receives telemetry signals as input and then digitizes them for output to the on-board computer. Its details are as follows:

- Dimension: 27.9 cm × 18.7 cm × 14.1 cm
- Weight: 3.91 kg
- Maximum power dissipation: 3.76 watt
- Signal input module: Bilevel, Serial, Analog

2.3 Victory Industry Company

Victory Industry Company built the diplexer to isolate and filter radio frequency (RF) signals. It has the following details:

- Dimension: 25.4 cm × 21.6 cm × 8.1 cm
- Weight: 1.7 kg
- Uplink frequency: 2039.6 MHz
- Downlink frequency: 2215 MHz
- Bandwidth: Uplink \pm 15 MHz, Downlink \pm 15 MHz
- Downlink power: 6 watt

Victory Industry Company also built the antenna to transmit and receive S-band RF signals at 2 GHz. The antenna has a diameter of 15.24 cm and an emitting power of 5 watt. Its details are:

- Dimension: 15.24 cm (φ) × 15.24 cm (h)
- Weight: less than 562 grams
- Reception frequency: 2039 \pm 5 MHz
- Transmit frequency: 2215 \pm 5 MHz
- Polarization: RHCP
- Power: 5 watt
- Characteristic resistance: 50Ω

2.4 Shihlin Electric & Engineering Corporation (SEEC)

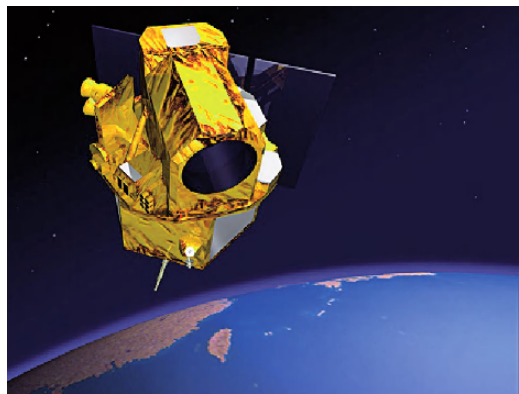
SEEC assembled the silicon solar cells into the solar panel. The cells with electrostatic clean coating have an efficiency of more than 14.6 % and a maximum power of 645 watt:

- Units: silicon solar cells, cover glass, blocking diode, structure and harness
- Weight (two wings): 21.36 kg
- End-of-life maximum power: 547.79 watt
- Maximum power: 645.36 watt
- V open circuit max: 99.0 V (DC)
- I short circuit min: 6.24 A (DC)
- Silicon solar cell efficiency: $\geq 14.6\%$
- V operate at maximum power: 48.07 V (DC)

3 Space-Qualified Manufacturers Incubated in FS2 Project [1]

The FS2 project was started in 2000 and completed in 2004. It is a cooperation project with EADS Astrium of France for the development of a small remote sensing satellite, as shown in Fig. 1.

Fig. 1 FS2 satellite

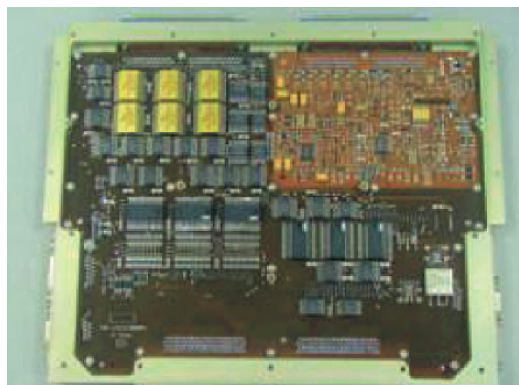


3.1 Acer Incorporation

In cooperation with EADS Astrium, Acer Incorporation participated in the design, manufacture, and test of the on-board management unit (OBMU) of FS2. It is the satellite's central control unit and the core of the secondary system for central command and data processing. The main function of the management unit is to control the satellite's operations, including the processing and execution of uploaded

commands, and the collection, processing, storage, and downloading of the satellite's status data. Figure 2 shows the board manufactured by Acer Incorporation.

Fig. 2 FS2 OBMU board



3.2 Tatung System Technology Incorporation (TSTI)

The flight software (FSW) of FS2 was co-developed by TSTI and EADS Astrium. Its functions are for managing and controlling the satellite orbit, position, and operation. The FSW is responsible for the calculation of satellite position/orbit, operation of scientific instrument payload, and communication with ground antenna.

3.3 SEEC

The sun sensor of FS2 as shown in Fig. 3 was developed by SEEC. It determines the satellite's relative position to the sun according to the direction of the source of sunbeam.

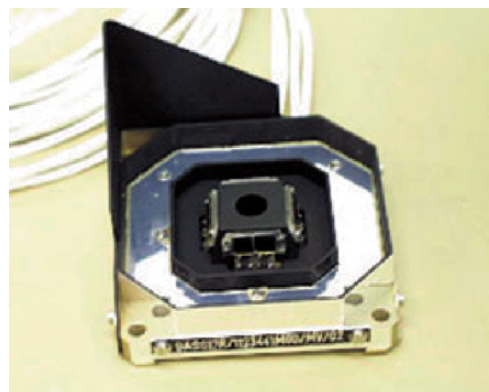


Fig. 3 Sun sensor of FS2

3.4 Victory Industry Company

The two S-band antennas of FS2 as shown in Fig. 4 were designed and manufactured by Victory Industrial Corporation. These antennas are used for receiving commands and transmitting microwave signals. They allow the uploading of ground commands and downloading of satellite information.

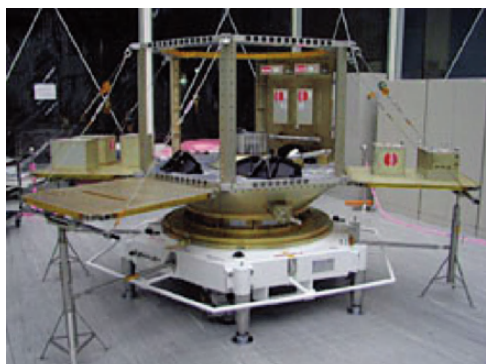
Fig. 4 S-band antennas of FS2



3.5 Aerospace Industrial Development Corporation (AIDC)

AIDC manufactured the flight harness by itself, and the primary structure (Fig. 5) along with Taiwan Aerospace Corporation (TAC). The harness wirings are used for connecting satellite modules, components and payloads, and for transmitting power, commands, and signals. The primary structure is designed and analyzed by NSPO, and manufactured by AIDC, and then tested by NSPO. All modules, components harness and payloads of the satellite are mounted to the primary structure, just like a human skeleton system.

Fig. 5 Primary structure (upper part) and VID of FS2 (lower part in white color)



3.6 Taiwan Aerospace Corporation (TAC)

TAC manufactured the vertical integration dolly (VID, Fig. 5) by itself and the primary structure along with AIDC. VID is the main loading equipment during the satellite integration and test procedures. It has anti-shock and anti-tilting functions and can prevent people from approaching too close to the satellite. TAC also manufactured the payload cone for adapting the satellite to the launch vehicle.

4 Space-Qualified Manufacturers Incubated in FS3 Project [1]

The FS3 project was started in 2002 and completed in 2006. It is a cooperation project with OSC of US for the development of 6 microsatellites to form a constellation observing system for meteorology, ionosphere and climate (COSMIC). Therefore, the whole system is known as FORMOSAT-3/COSMIC internationally. To further promote the domestic manufacturers' participation in the space industry and to solidify Taiwan's space industry development, NSPO incorporated 5 domestic manufacturers to produce 14 modules and components for FS3.

4.1 Acer Incorporation

Acer Incorporation manufactured the OBC of FS3 for the major function of satellite operation control, including data and signal processing, command interpretation and execution, and other secondary system interface control. As shown in Fig. 6, the computer has the following characteristics:

- CPU: Motorola 68302
- ROM: 3M Bytes
- Read-write memory: 512K Bytes
- Data interface: RS-422, RS-485 standard interface
- Weight: 2.6 kg

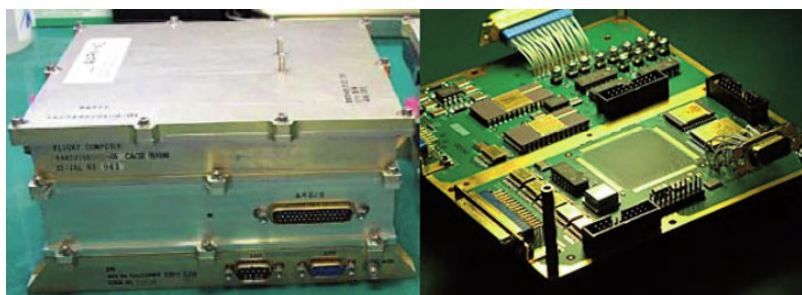


Fig. 6 OBC of FS3

- Dimension: 17cm × 16cm × 9cm
- Max power dissipation: 7.5 watt

Acer Incorporation also manufactured the mission interface unit (MIU, see Fig. 7) to provide the function of communication between satellite and ground system, including the uplink of operation commands and the download of remote sensing and scientific data:

- Secondary system interface: radio frequency secondary system, satellite computer, payload computer, solid-state memory, current converter, and attitude control processing unit
- Weight: 0.68 kg
- Dimension: 17.3cm × 18.6cm × 2.8cm
- Maximum power dissipation: 2.8 watt

Fig. 7 MIU of FS3



4.2 SEEC

SEEC manufactured three modules: solar sensor, rechargeable storage battery and current converter. Major functions of the solar sensor are to detect the sun's position and provide the information for the determination of satellite attitude. It weighs 10.8 grams with the dimension of 6cm × 3.5cm × 0.5cm. The rechargeable storage battery is a part of the secondary power system which provides power to the satellite. It weighs 4.75 kg and has a dimension of 45cm × 20cm × 10cm. Finally, the current converter provides power required for the three payloads: GPS occultation experiment (GOX), tiny ionosphere photometer (TIP) and tri-band beacon (TBB). The weight is 700 grams and the dimension is 16cm × 17cm × 25cm.

4.3 Victory Industry Company

Three modules of FS3 were manufactured by the Victory Industry Company: S-band antennas (Fig. 8), receiving coupler (Fig. 9) and transmitting filter (Fig. 10). FS3's antenna system includes an S-band transmitting antenna for sending satellite microwave signals to ground and an S-band receiving antenna for accepting command

signals from ground. The antenna system is able to provide a circular range greater than 85 %. Its weight is 227 grams and its dimension is 10.2cm × 10.2cm × 1.3cm. The receiving coupler has a weight of 100 grams and a dimension of 2.5cm × 3.8cm × 1.3cm. It is used to couple the single transmitter/receiver signal with two S-band antennas in order to provide near-spherical coverage. Finally, the filer can provide effective isolation of the noise and interference. It weighs 348 grams with 1 watt power dissipation and 5.1cm × 5.1cm × 15.2cm dimension.

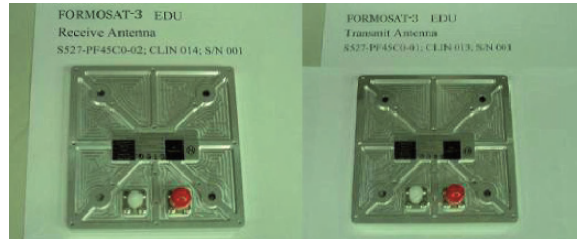


Fig. 8 S-band antennas of FS3



Fig. 9 Receiving coupler of FS3

Fig. 10 Transmitting filter of FS3



4.4 Yung Tien Industrial Corporation (YTIC)

The satellite heating elements were manufactured by YTIC. These heating elements ensure the proper operation of three modules, rechargeable storage battery, fuel tank and thruster wiring. Allowed temperature range is from -65°C to 200°C .

4.5 AIDC

Again, AIDC manufactured the flight structure. This is the first time of AIDC to develop a set of multi flight structures which needs to be stacked together for launch in one vehicle. Each of the 6 flight structures has the same diameter of 103 cm and height of 16 cm, as shown in Fig. 11.

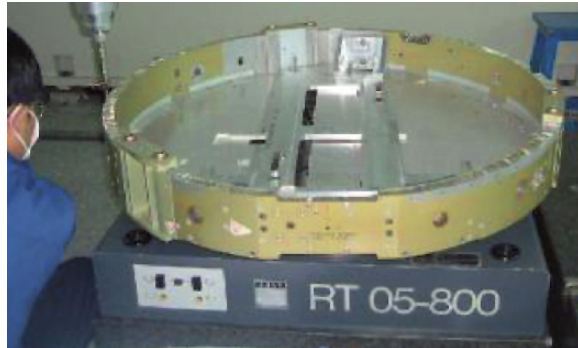


Fig. 11 Flight structure of FS3

5 Statistics of the Incubation Results

There are 8 space-qualified domestic manufacturers incubated during the first phase space program of Taiwan. Among them, TAC had been closed at about 5 years ago due to policy change of the company. All the others keep participating NSPO's current space projects except Trans System Incorporation. However, we can only say that a few space-qualified manufacturers have been successfully incubated. There is still no real space industry in Taiwan. The reason is simply because that the percentage of the space product value is negligibly small in the whole industrial community. Consequently, NSPO is seeking a possible breakthrough in Taiwan's second phase space program which already started in 2004.

6 NSPO'S Future Development Concept—Super Cluster of Microsatellites

6.1 Insights of Freeman Dyson [2]

In his book, Freeman Dyson mentioned that in order to control the price of a new generation spacecraft to be within several tens thousands US dollars, we need to develop the technologies far more advanced beyond 1988. The spacecraft must be cheaper, lighter and simpler. Further, the weight of the spacecraft should be in the order of pounds

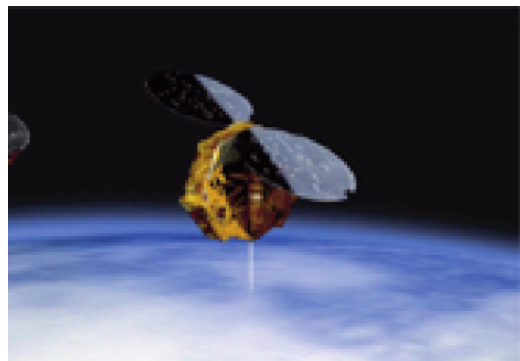
instead of tons. Also, each spacecraft could have several missions everyday instead of every year. There are two ways to reach the achievement: “nano- technology” and “genetic engineering”. Three paragraphs from his book are quoted bellow:

“I have sketched in a rough fashion how space-technology jumped in the past thirty years, from 1958 to 1988. The von Braun Mars Project represented the technology of 1958. The International Ultraviolet Explorer (IUE) represented the technology of 1988. The Mars Project was the best you could have done with space exploration in 1958, while the IUE was the best you could do in 1988. The point of this comparison is that the jump in cost-effectiveness from the Mars Project to the IUE is not just a factor of 10 or 100 but more like a factor of 10,000 or 100,000.”

“When we look forward to 2018 (e.g., thirty years from 1988), we should expect big steps forward in science to come once again from changes in style rather than from marginal improvements in technology. I am saying that another jump by a factor of ten thousand in cost-effectiveness is possible.... To improve cost-effectiveness by a factor of ten thousand, we need spacecraft that are radically cheaper, smaller, and quicker than anything we can build with 1988 technology. Spacecraft should weigh pounds rather than tons, they should cost tens of thousands rather than tens of millions of dollars, and they should fly missions at a rate of several per day rather than several per year.... Both mechanical nanotechnology and genetic engineering are vigorously growing industries, and are likely to be transforming our Earth-bound economy during the next thirty years.”

“Here is a rough sketch of one possible shape that the 2018 spacecraft might take. I call this model astrochicken because it is about as big as a chicken and about as smart. It is a product of genetic engineering. It does not look like a chicken. It looks more like a butterfly....” Coincidentally, the shape of FS3 microsatellite is just like a butterfly, as shown in Fig. 12.

Fig. 12 FS3 microsatellite (6 as a constellation)



6.2 “Blue Sea” Policy

Through the analysis of the strengths of Taiwan industrial community, one very important point is the strength in the area of semiconductor, computer and information

technology (IT). On the other hand, two of the weaknesses of NSPO are that both the scale of Taiwan space program and the number of satellite projects are too small. It is very obvious that the current space community is a “red sea” (or say, red ocean) dominated by NASA of USA, ESA of European Countries, JAXA of Japan, China National Space Administration (CNSA) of China, ISRO of India, etc. Within this environment and with the two weakness points, NSPO needs to find its way to go ahead and possibly to win in the future. Consequently, it is necessary for NSPO to seek the “blue sea” (or say blue ocean) policy on how to use the Taiwan’s strength in IT. [3, 4] The astrochicken could be one of the ways NSPO can choose. Under the idea of astrochicken, tens or hundreds or even thousands of microsatellites shall be flying in the orbit or even in the interplanetary space. Taiwan can apply the similar road map of its IT industry in the development and mass production of microsatellites.

6.3 Super Cluster Concept

The tens or hundreds or thousands of microsatellites flying in the orbit and the interplanetary space shall form a kind of constellation. We call it the “Super Cluster” temporarily. As long as the microsatellites are so cheap, no high reliability is required. Whenever needed, new satellites can be assembled and launched within a short time. [5, 6] These astrochickens can communicate with the ground stations and also among themselves. The ground stations shall be very powerful so that they can do the job of coordination, tracking, telemetry, command, and data processing. Both image and scientific data shall be collected. Since 2006, NSPO has started the preliminary study phase of this project.

7 Summary and Conclusions

Incubating Taiwan’s domestic space-qualified manufacturers was the Government’s policy since the first phase space program started at 1991. Four manufacturers made 5 products for the FORMOSAT-1 (FS1), 6 manufacturers made 8 products for the FORMOSAT-2 (FS2), and 5 manufacturers made 10 products for the FORMOSAT-3 (FS3). A total of 8 domestic space-qualified manufacturers had been incubated and 6 of them continue to participate NSPO’s current second phase space program which spans from 2004 to 2018. Therefore, it can be concluded that the way is not easy although it is right. In order to conquer the difficulty, NSPO started to develop the super cluster project at 2006. This policy has been made after analyzing NSPO’s weakness points and Taiwan’s strength in computer industry. It is expected that tens or hundreds or thousands of cheap astrochicken microsatellites capable of doing various missions with reasonable mission life and reliability can be launched responsively in the future. Complicated command and coordination work shall be accomplished by the ground system. Also, the new image processing system and scientific data processing system shall be developed to satisfy the tremendous data processing requirement.

References

1. Website of NSPO, www.nspo.org.tw, (2007)
2. F. Dyson, *From Eros to Gaia*, Chapter 5 “Sixty Years of Space Science, 1958–2018,” Pantheon Books, Knopf Publishing Group, Random House, Inc., New York (1992)
3. W. Chan Kim, *Blue Ocean Strategy: How to Create Uncontested Market Space and Make Competition Irrelevant*, Harvard Business School Press (2005)
4. L. Wu, Space Technology in 21st Century – Talk About Taiwan’s Space Program, a presentation at the Chang Jung Christian University, Tainan, Taiwan (2006)
5. T. Davis, “Responsive Space Launch Initiatives,” the Small Satellites Systems and Services Symposium (The 4S Symposium), Chia Laguna, Sardinia, Italy (25–29 September 2006)
6. S. Mike Hurley, T. Doyne, P. Wegner, R. Riddle, K. Weldy and T. Duffey, “Tacsat and Operationally Responsive Space Activity,” the 4S Symposium, Chia Laguna, Sardinia, Italy (25–29 September 2006)

Trends and Visions for Small Satellite Missions

Rainer Sandau, Larry Paxton, and Jaime Esper

Abstract Small satellite missions can be achieved by using different approaches and methods. One possible approach takes full advantage of ongoing technology development efforts leading to miniaturization of engineering components, development of micro-technologies for sensors and instruments, and others which allow the design of dedicated, well-focused Earth observation missions. Application Specific Integrated Micro-instruments (ASIM) are enabled by Micro-Electro-Mechanical Systems (MEMS) using microelectronics for data processing, signal conditioning, power conditioning, and communications. These micro- and nano-technologies have led to the concepts of nano- and pico-satellites, constructed by stacking wafer-scale ASIMs together with solar cells and antennas on the exterior surface. Space sensor webs are one outcrop of this technology. Further milestones in the cost-effective Earth observation mission developments are the availability and improvement of small launchers, the development of small ground station networks connected with rapid and cost-effective data distribution methods, and cost-effective management and quality assurance procedures. The paper is based on the outcomes of the study “Cost-Effective Earth Observation Missons” by an international team of experts in the framework of the International Academy of Astronautics [1]. It deals with general trends in the field of small satellite missions for Earth observation as well as trends specific for the segments of a misson: space segment, launch segment, ground segment. Visions are given for their further developments in the direction of improvement of cost-effectiveness of Earth observation missions.

R. Sandau

DLR, German Aerospace Center, Rutherfordstr. 2, 12489 Berlin, Germany
e-mail: rainer.sandau@dlr.de

L. Paxton

The Johns Hopkins University, Applied Physics Laboratory, 11100 Johns Hopkins Rd., Laurel MD 20723-6099, USA

J. Esper

NASA, Goddard Space Flight Center, Mail Code 532, Greenbelt, MD 20771, USA

1 Introduction

Since the advent of modern technologies, small satellites using off-the-shelf technologies or missions focused on specific physical phenomena have also been perceived to offer an opportunity for countries with a modest research budget and little or no experience in space technology, to enter the field of space-borne Earth observation and its applications. This is very much in line with the charter of the IAA Study Group on Small Satellite Missions for Earth Observation. One of its intentions is to bring within the reach of every country the opportunity to operate small satellite Earth observation missions and utilize the data effectively at low costs, as well as to develop and build application-driven missions. In this context the study group supports all activities to develop and promote concepts and processes by various user communities to conduct or participate in Earth observation missions using small, economical satellites, and associated launches, ground stations, data distributions structures, and space system management approaches.

Generally, the study [1, 2] provides a definition of cost-effective Earth observation missions, information about background material and organizational support, shows the cost drivers and how to achieve cost-effective missions, and provides a chapter dedicated to training and education. The focus is on the status quo and prospects of applications in the field of Earth observation. The conclusions and recommendations of the study are the focus of this paper. They are summarized here in terms of

- more general facts that drive the small satellite mission activities,
- recommendations of the study
- trends in Earth observation missions, and
- some visions concerning the future of cost-effective Earth observation missions.

2 Conclusions and Recommendations of the IAA Study

The study presented the state of the art of small satellite missions and examined the factors that enable one to produce a cost-effective small satellite mission for Earth observation. We find that, while there are several examples of such missions flying today, the lessons that must be learned in order to produce cost-effective small sat missions have neither been universally accepted nor understood by all in the space community. In the study we intended to point out how a potential user can produce a cost effective mission. One of the key enablers of designing a cost-effective mission is having the key expertise available. As the number of successfully space-faring nations grows, the pool of expertise available to meet the challenges of small mission grows.

2.1 General Facts

Cost-effective missions can be achieved by using different approaches and methods.

Since the advent of modern technologies, small satellites have also been perceived to offer an opportunity for countries with a modest research budget and little or no experience in space technology, to enter the field of space-borne Earth observation and its applications.

One of the possible approaches is to take full advantage of the ongoing technology developments leading to further miniaturization of engineering components, development of micro-technologies for sensors and instruments which allow to design dedicated, well-focused Earth observation missions. At the extreme end of the miniaturization, the integration of micro-electromechanical systems (MEMS) with microelectronics for data processing, signal conditioning, power conditioning, and communications leads to the concept of application specific integrated micro-instruments (ASIM). These micro- and nano-technologies have led to the concepts of nano- and pico-satellites, constructed by stacking wafer-scale ASIMs together with solar cells and antennas on the exterior surface, enabling the concept of space sensor webs.

More generally small satellite missions are supported by four contemporary trends:

- advances in electronic miniaturization and associated performance capability;
- the recent appearance on the market of new small launchers (e.g. through the use of modified military missiles to launch small satellites);
- the possibility of “independence” in space (small satellites can provide an affordable way for many countries to achieve Earth Observation and/or defense capability, without relying on inputs from the major space-faring nations);
- ongoing reduction in mission complexity as well as in those costs associated with management; with meeting safety regulations etc.

These trends are complemented by

- the development of small ground station networks connected with rapid and cost-effective data distribution methods
- and cost-effective management and quality assurance procedures

The advantages of small satellite missions are:

- more frequent mission opportunities and therefore faster return of science and application data
- larger variety of missions and therefore also greater diversification of potential users
- faster expansion of the technical and/or scientific knowledge base
- greater involvement of local and small industry.

After some years of global experience in developing low cost or cost-effective Earth observation missions, one may break down the missions into general categories such as:

- Commercial – requiring a profit to be made from satellite data or services
- Scientific/Military – requiring that new scientific/military data to be obtained

- New technology – developing or demonstrating a new level of technology
- Competency demonstration – developing and demonstrating a space systems competency
- Space technology transfer/training – development of an organic capability
- Engineering competency growth – developing engineering competence using space as a motivation
- Education – personal growth of students via course projects or project team participation

In the study we find that large and small satellite missions are complementary rather than competitive. The large satellite missions are sometimes even a precondition for cost-effective small satellite solutions.

2.2 Some Recommendations and Observations from the Study

The situation in the field of small satellite missions for Earth observation has matured in the last ten years. This may be, for instance, observed from the topics and the quality of contributions to the series of, to date, five biannual IAA Symposia on Small Satellites for Earth Observation in Berlin, Germany. The 5th Symposium took place in April, 2005.

We propose a simplified nomenclature for subsets of small satellites:

- mini satellites <1000 kg
- micro satellites <100 kg
- nano satellites <10 kg
- pico satellites <1 kg

Additionally, the cost and duration from the decision for a mission to getting the satellite into the orbit usually decrease with decreasing satellite complexity and mass.

There is no single, accepted, broad method for reducing mission cost. Instead, the builders of low-cost missions are aggressive competitors, just like their more expensive colleagues who create large programs for ESA, NASA, or the US Department of Defence. Each low-cost program has found and have to find a set of solutions to fill its particular need and programmatic style. The full paper gives a summary of cost reduction methods which are selectively used by the builders of low-cost missions.

To reduce cost, alternatives to dedicated launches of satellites should also be taken into consideration. Although each of the alternatives given and explained in the full paper has limitations, dramatic reductions in cost are possible for missions such as equipment testing that do not necessarily need a long period on orbit.

Cost-effectiveness also depends on the quality and engagement of the specialists participating in planning and implementing an Earth observation mission. Countries taking their first steps in space need to learn relevant techniques from more experienced space users, thereby acquiring a cadre of appropriately trained

personnel before going on to establish a national agency and to maintain a presence in space. Technology transfer through small satellite related training programs has been successfully implemented between Surrey University in the U.K. and customers in Chile, Malaysia, Pakistan, Portugal, the Republic of Korea, South Africa and Thailand.

Small satellites programs provide a natural means for the education and training of scientists and engineers in space related skills since they allow direct, hands-on, experience at all stages (technical and managerial) of a particular mission (including design, production, test, launch and orbital operations).

3 Some Trends in Earth Observation Missions

Different Earth observation applications need different approaches for cost-effective missions. The individual prospects are shown in chapter “Application Fields, Status Quo and Prospects”. The general prospects for disaster warning and support may serve as an example for the trends in Earth observation missions. They can be grouped into the following main topics: space, ground, and program segment.

3.1 Trends in the Space Segment

The trends of technology development in the space segment relevant for disaster management are characterized by:

- Higher performance of micro-satellites busses due to new developments on the component and subsystem level such as onboard computers, data handling systems, transmitters, solar arrays, batteries, GPS-receiver and others,
- Higher performance optical payloads for small satellites suitable for disaster monitoring tasks (high geometric and radiometric resolution, more spectral channels),
- Investigation of the feasibility of passive Radar (SAR) micro-satellites flying in formation with an active Radar satellite,
- Low-cost satellite technology makes operational satellites affordable for dedicated constellations,
- Novel international partnerships show new ways for new space nations to achieve effective systems through collaboration,
- Building of disaster monitoring constellations with small and micro-satellites,
- Decreasing the revisit time for monitoring tasks by using different satellites and constellations,
- Experimental on-board remote sensing data processing to produce a high level data product.

In summary, one can say that small satellites can provide data more quickly with a better match to user needs.

Table 1 Cost reduction methods

| Method | Mechanism | Comments |
|---------------------------------------|--|---|
| Programmatic | | |
| Schedule Compression | Reduces overhead of standing army; forcing program to move rapidly does drive down cost | Often results in a poor design due to lack of up-front mission engineering; required work reduced to fit schedule |
| Reduce Cost of Failure | Allows both ambitious goals and calculated risk in order to make major progress | Fear of failure feeds cost-growth spiral; major breakthroughs require accepting the possibility of failure – particularly in test |
| Continuous, Stable Funding | Maintains program continuity; maintains team together | Program delay will be funding break + 2–4 months |
| Minimize Documentation | Reduces programmatic overhead for creating, reviewing, and maintaining | Critical to document reasons for key decisions and as-built design |
| Personnel | | |
| Improved Interpersonal Communications | Dramatically reduces errors and omissions; conveys understanding as well as data | Large programs use formal, structured communications through specified channels |
| Small Team | Clear, nearly instantaneous communications; high morale; strong sense of personal responsibility | Problem if a key person drops out – but in practice it rarely happens. |
| Co-located Team | Improves communications | Best communications are face-to-face, but AMSAT and others don't seem to need it |
| Empowered Project Team | Rapid decision making; strong sense of personal responsibility; can make “sensible” decisions | Eliminates a major function of the management structure |
| Systems Eng. | | |
| Trading on Requirements | Eliminates non-critical requirements; permits use of low-cost technology | Makes traditional competition difficult |
| Concurrent Engineering | Allows schedule compression; reduces mistakes; increases feedback | High non-recurring cost relative to lowest cost programs |
| Design-to-Cost | Adjusts requirements and approach until cost goal has been achieved; | Spacecraft have rarely used it |
| Large Margins | Reduces testing; better flexibility; reduces cost of eng, manufac., and ops | Margins traditionally kept small for best performance – drives up development cost |
| Technology | | |
| Use COTS Software | Immediate availability; dramatically lower cost; tested through use | May need modification and thorough testing; typically not optimal |
| Use COTS H/W | Same as software | Same as software |
| Use Existing Spares | Reduced cost; rapid availability; meant for space | Only works so long as spares exist – not applicable for operational programs |

Table 1 (continued)

| Method | Mechanism | Comments |
|--|---|---|
| Use of Non-Space Equipment | Takes advantage of existing designs and potential for mass production | Typically not optimal; must be space qualified |
| Autonomy | Reduces operations costs | Can increase non-recurring cost |
| Standardized Components and Interfaces | Reduces cost and risk by reusing hardware; standardization is a major req. for other types of manufacturing | Has been remarkably unsuccessful in space; sub-optimal in terms of weight and power |
| Extensive Use of Microprocessors | Minimizes weight; provides high capability in a small package; allows on-orbit reprogramming | Problem of single-event upsets; high cost of flight software; very difficult to manage software development |
| Common S/W for Test and Ops | Reduces both cost and schedule; avoids reinventing the wheel | May be less efficient, user-friendly than ops group would prefer |

3.2 Trends in the Ground Segment

The trends in technology development for the ground segment relevant to disaster management are characterized by:

- increasing the flexibility of mission operations of satellites by building a flexible ground segment,
- building of networks of ground stations for increasing the satellite operational performance and data access without time delay,
- improving response time in imaging according to user requirements,
- data processing and distribution to the final user without delay,
- data policy is in many cases too restrictive for fast disaster response and must be addressed beforehand,
- distribution of data and algorithms for support of disaster management using COTS products running on personal computers will enable better use of the data,
- distributed permanent GNSS stations with radio links for fast data transmission are available to a certain extent and have to be extended,
- very small ground stations for in-situ measurements with data transmission facilities via satellites are available and they are independent on existing infrastructure,
- data processing and modeling of disaster conditions by experts are in progress, but there are gaps in the information extraction process for decision makers,
- tailoring of information for particular users
- improving and disseminating knowledge of the utility of space-based sensor information

In summary, technology developments in the ground segment address networking, improving response time and providing user-oriented space-segment control.

Table 2 Historical alternatives to dedicated satellites

| Option | Characteristics | Mass Limits | Principal Constraints | Con- | Approximate Cost | Sources |
|--------------------|---|--|--|-----------------------------|--|---------|
| Balloon Flights | Hours to days at ≈ 30 km altitude | Up to 70 kg for low-cost flights Up to 1,000 kg | Not in space, not zero-g, weather concerns | \$5K to \$15K | U. of Wyoming, USAFIA, NSBF | |
| Drop Towers | 1 to 10 sec of 0-g with immediate payload recovery | | Brief “flight,” 5 to 50 g landing acceleration, entire experiment package dropped | ≈ \$10K per experiment | ZARM, JAMIC, NASA LeRC and MSFC, Vanderbilt U. | |
| Drop Tubes | 1 to 5 sec of 0-g with immediate sample retrieval | <0.01 kg | Brief “flight,” 20 to 50 g landing acceleration, instrumentation not dropped with sample | ≈ \$0.02K per experiment | ZARM, JAMIC, NASA LeRC and MSFC, Vanderbilt U. | |
| Aircraft | Fair 0-g environment, repeated 0-g cycles | Effectively unlimited | Low gravity is only 10^{-2} g | \$6.5K to \$9K per hour | NASA LeRC and JSC, Novespace | |
| Parabolic Flights | Good 0-g environment, altitude to 1,200 km, duration of 4 to 12 minutes | Up to 600 kg | Much less than orbital velocities | \$1M to \$2M | NASA GSFC, NRL, ESA/Sweden, OSC, EER, Bristol Aerosp. | |
| Sounding Rockets | Days to weeks of 0-g on board the Shuttle | Up to 90 kg | Very limited external interfaces | \$27K for largest container | Ariane, OSC, MDA, Russia | |
| GAS Containers | Capacity that is available in excess of primary's requirements | Up to ≈ 1,000 kg | Subject to primary's mission profile | <\$10M | NASA GSFC | |
| Secondary Payloads | | | | | | |
| Shared Launches | Flights with other payloads having similar orbital requirements | Up to ≈ 5,000 kg | Integration challenges | Up to ≈ \$60M | Ariane, OSC, Russia | |

The education in using spaceborne data has to be improved but also the information extraction process for decision makers has to be tailored and optimized to their needs.

3.3 Trends in the Program Segment

The trends in the program segment of cost effective Earth observation missions for disaster warning and support are focused on new applications and new data products. Some key points are:

- tele-medicine applications are important for disaster management and should be extended,
- medical weather maps should be integrated into public health applications,
- tele-education should be built up for disaster applications,
- national disaster preparedness should be improved and should include the appropriate use of the space segment,
- new monitoring applications using space technologies (GPS) should be applied to rescue teams and people in high risk areas,
- integration of space-based sensors into the spectrum of sensors that includes ground- and aircraft-based systems,
- use of new airborne platforms such as UAVs (Unmanned Air Vehicle) or transportable tethered balloons or dirigible airships may augment the space segment,
- integration and fusion of data from all available sources and the development of models related to disaster conditions are progressing to the point where expert systems may become available
- multi-temporal analysis of regional changes and conditions based on already existing satellite data is currently done by experts and must be simplified or improved to address a broader potential user community

In summary, tele-health and tele-education applications should be included in a disaster monitoring program. In addition, the entire spectrum of assets, from ground to space, must be integrated into an environment that provides the information needed to make decisions. This “expert system” needs to be developed: too much of the data is of meaning to, and accessible, only to experts and too little is in a form that can be used for disaster relief and mitigation personnel.

4 The Future of Cost-Effective Earth Observation Missions

In the study we have considered the past experience of the global small satellite community and reviewed and incorporated the work of other studies and bodies that deal with disseminating information about small satellite missions and in promoting the appropriate use of such technology and we have surveyed the state of our current

knowledge. The study brings to light new capabilities as well as challenges that must be addressed in order to produce successful, cost-effective small satellite missions.

4.1 New Capabilities

There are three new developments that may prove to greatly enhance the capabilities of small satellite missions. These are:

1. the convergence of data acquisition and data visualization technologies
2. the ready availability of new small launchers and the rise of “space tourism”
3. the development of smaller, lighter, lower power satellites that can act as a constellation or independently

While there are many other developing technologies that hold promise, these factors may well transform the small satellite enterprise in the next ten years. A mission can be cost-effective and achieve all its measurement requirements without having to actually make all the measurements itself. To put this in concrete terms, NASA has a series of research satellites (Aqua, CloudSat, CALIPSO, PARASOL, Aura, and OCO) called the “A Train” that fly in formation. These satellites make individual measurements that support cross platform science. Many of the instruments that image the surface also use ancillary information, such as digital elevation maps, to add context to their products. One could readily envision a small satellite mission that was intended to provide some niche product, such as crop yield forecasting, in a particular region. Such a small satellite could produce a very specific measurement, say normalized difference vegetative index (NDVI), which would be corrected for aerosols and clouds using data from the A Train. Another approach, as evidenced in SSTL’s DMC, is to decrease the ground repeat delay by forming a cooperative that shares data which are produced among the elements of the constellation. Membership is acquired by contracting for the production of an element of the constellation. Each member of the cooperative then gets the benefit of a much shorter revisit time. In short, the economies of scale begin to operate as more members join the cooperative.

Getting into space is still a challenge. During the last ten years there have been more small launchers available and at prices that are quite reasonable compared to the cost of a small satellite. One of the newest and, potentially, most vigorous areas of development of small launchers has come about under the impetus of “space tourism”. On October 4th, 2004, Burt Rutan and Paul Allen, built and flew the world’s first private spacecraft to the edge of space to win the \$10 million Ansari X Prize. Perhaps the early history of the development of commercial aviation presages the next twenty years of space access. At the turn of the century, air travel was relatively risky and quite expensive. As the commercial market for air transport grew, costs dropped as did risk. Now, air transport is so cost-effective that it is used to ship bulky agricultural goods, such as apples, half-way around the world at prices that are competitive with local transport and production. To make space tourism viable the cost of putting a person in space will have to be

reduced to of the order of \$1M. At those kinds of costs for mass to orbit, small satellite missions will no longer be strongly constrained by launch costs. If we step back from the purely speculative, commercial launch services are now available on most launch systems, many of which are new vehicles designed or modified specifically for international commercial market. The most dramatic shift has been the entry of the Russian and Ukrainian launch systems operated as joint ventures with US or European companies. New launch systems around the world are even beginning to use major components built in other countries, further blurring national divisions. This international trend is important because some nations still insist on the use of a “national” launch capability. The increasing availability of these low-cost launchers and the development of dispensers has opened up possibilities for single launches of a constellation as well as individual payloads. The launch of the NASA / DLR GRACE satellites used Eurockot Launch Services, the joint venture owned by Astrium and the Russian company Khrunichev, to place two satellites in a closely controlled formation via a dispenser is a good example. This launch was the first commercial use of the Russian SS-19 ICBM which provides the two booster stages for the ROCKOT launch vehicle. This vehicle has a heritage of 150 flights. At the other end of the cost and mass spectrum, Ariane 5 has been used to launch 6 auxiliary payloads along with the primary Helios satellite. This included Nanosat, Spain’s first small satellite, built by the country’s INTA national space agency (Instituto Nacional de Técnica Aeroespacial), with a mass of less than 20 kg. In another example, the Cluster mission formed a constellation of four satellites, flying in formation, using two separate launches.

Once the spacecraft are in orbit, the remaining costs are largely associated with operating the spacecraft (including monitoring its health and safety) and collecting the data. As the number of spacecraft increases in a constellation there would be, without a change in the operations paradigm, a concomitant increase in the costs to operate the constellation. In order to have a cost effective constellation of micro- or nano-satellites, the operations costs have to be low on a per satellite basis, especially since some of these constellations are envisioned as consisting of tens or even hundreds of micro- or nano-satellites. Powerful, cheap, microprocessors provide the means for increased autonomy at the individual satellite level and across the constellation. At issue, though, is developing the software to perform these operations and subsequently testing the software so that its operation can be verified before flight. Qualifying these systems for spaceflight will be a challenge that must be addressed.

4.2 Challenges

The biggest long-term challenge for the small satellite community is that of developing a robust commercial market that supports the infrastructure that has been developed to produce small satellites. Small satellites have appealed to some nations as an instrument of national pride and as a means to focus and enhance the industrial base as well as providing a means of attracting students to a high tech industry. This is, of course, a finite market. After the first few satellites there has to be reason other than

becoming a space-faring nation to invest in, develop, and fly the next space mission and continue the development and training of students. To develop a robust market, small satellite manufacturers must remain relevant and cost-effective. It appears that in many markets space technology has entered the era of diminishing returns – for example, if you can achieve imagery from space with a spatial resolution of about one meter, do you really gain anything marketable by imaging at one centimeter? This plateau effect means that more vendors can aspire to provide the same product. How many suppliers can the market support? It may be that the market can support more suppliers of imagery if revisit time is a key driver. The user then must draw products from several sources and understand enough about each independent data source so that the desired product can be produced. Raw data products, though, are not likely to capture many more users: tailored products that address specific needs can be supplied by small satellites. The vertical integration of the industry, to provide instruments, data and integrated data products, is likely to spur significant growth.

Until that robust commercial market has been developed, government support will continue to be the financial mainstay of the small satellite community. This situation will remain in force until some economies of scale can be achieved. At this time, SSTL and RapidEye are two notable examples of commercial ventures that have achieved some stability. They did this by identifying and cultivating a niche market that they are able to address. Much of the small satellite community is still tied to education and research activities – activities that rely on government support. Inter-government cooperative agreements provide the means of broadening the opportunities available to the community. Bureaucracies are averse to risk, however, and small organizations and cooperative agreements are often viewed as risky.

Managing risk is a key problem, then. Since no complex system can be designed and tested against all failure modes, experience is often the best and only guide to making trades. Large organizations tend to have more restrictions on what can fly and may have stringent risk assessment processes. In NASA terms the confidence in a subsystem or system is called the Technology Readiness Level or TRL of the item. Higher TRLs mean the element has significant flight experience. The highest TRL is assigned to elements with direct flight heritage. Small satellites can be quite effective as platforms to raise the TRL of an element to be used in a latter design. The challenge faced by the small satellite community is to gain a broader acceptance of the notion that TRLs can be raised as an integral part of a mission rather than by implementing a dedicated mission such as the JPL-led Deep Space missions.

Making small satellites more cost-effective calls for new technologies but who then pays to certify these new technologies for spaceflight? There is certainly a higher risk associated with unproven technology. For example, the ready availability of large format detectors at relatively low cost shifts the design choices from being driven by the detector resolution to being driven by other factors such as the interplay between spacecraft stability and off-nadir pointing capability or downlink bandwidth and onboard storage, etc. Can a system be designed that can use these new detectors? How do they behave in space? A small mission is arguably the best way to perform a flight verification because even a failure to operate on orbit, or even to achieve orbit, can still be a successful demonstration from an educational or

developmental viewpoint. Cost-sharing between a larger, richer, risk-averse partner and a smaller, poorer, more risk-tolerant partner may prove beneficial to both parties.

4.3 Success and Failure of Cost-effective Missions

The study examined both what we know about small satellites and their uses for Earth observation. What makes a mission cost effective? The simplest answer is that the desired end is achieved for a price that is acceptable to all parties. While some mission objectives may only be achieved by the large, complex instruments and spacecraft, there are many uses for small missions. For many potential customers the best price point is established by sharing risk. If the risk is borne broadly, even a failure to achieve launch can still yield a cost-effective mission because the partners view the educational and infrastructure return as sufficiently high and the other shared aspects of the partnership yield some of the required information. To remain cost-effective in the commercial arena, small missions must be able to incorporate new technologies that reduce costs and improve performance. Small satellite missions face growing competition in regional markets from GPS-based solutions, UAVs, balloons, and sensor webs, for example. The chief advantage of satellites is their global access. Exploiting that, and successfully marketing that advantage, will hold the long-term key to keeping small satellites cost-effective.

Assessing whether a mission is successful or not involves many different measures. Assuring that a small-satellite mission is considered successful means that these differing measures must be addressed and considered in the design of the mission. Some of these measures of success are, in fact, much more likely to be fulfilled by a small-satellite mission than a large one. For example, students are much more likely to be involved in a small satellite mission. The experience gained in the design, construction, test, flight, operation, and data analysis phase of the mission will guarantee “success” in terms of the educational experience of the students. Small satellites can demonstrate new technologies or measurement techniques. If they achieve these goals they are “successful” even if the scope of the goal is small (for example, a small satellite mission need not inventory the global carbon budget but it could provide a measure of the amount of carbon produced in boreal forest fires). In terms of impact at the national level, a small satellite that is produced by a country may well evoke more pride of ownership than an instrument or participation in a large-scale investigation. In this study we have laid out the reasons how to design and implement a small cost-effective Earth-observation mission. In the end, success is subjective: the true measure is whether the program continues and flourishes.

References

1. Sandau, Rainer (ed.), International Study on Cost-Effective Earth Observation Missions, Balkema Publishers, a member of Taylor & Francis Group plc, Leiden, The Netherlands, 2006. ISBN 10: 0-415-39136-9, ISBN 13: 9-78-0-415-39136-8, 160 p.
2. <http://iaaweb.org/iaa/Studies/earthobservation.pdf>

Session 2

Missions (1)

Development of the MicroSat Programme at INTA

**Manuel Angulo, Juan Maria Mi, Pedro de Vicente, Manuel Prieto,
Oscar Rodriguez, Enrique de la Fuente, Jordi Palau**

Abstract This paper presents the INTA μ SAT programme initiative and its development status. With a mass ranging from 80 to 150 Kg and compatible with the Ariane-5 ASAP, the Phase-A one year study was initiated in Oct. 05. At this moment we are running the Phase-B started in Nov. 06 that will finish with a PDR in Dec. 07. The first INTA μ SAT-1 will be a very agile Earth observation mission using CMGs, with a launch tentative date by the beginning of 2010. This enlarged μ SAT class is a further step after the NANOSAT programme success [1] with a launch onboard Ariane-5 V-165 in Dec. 04 (Nanosat-01 still working OK in orbit), and the next Nanosat-1B planned to be launched most probably in a DNEPR by the middle of 2008. It will be followed by Nanosat-2, an evolved 15–40 Kg satellite with improved service module resources and a separated payload module design, set for launch by 2011.

Main objectives of the INTA μ SAT initiative are similar to the NANOSAT programme: 1-Keep running at our Institute an internal space programme with limited resources; 2-Most of the subsystems are developed at INTA, but with collaborations in the research and bilateral work with several universities and other research

M. Angulo

Departamento de Programas Espaciales y Ciencias del Espacio, INTA (Instituto Nacional de Técnica Aeroespacial), Carretera de Ajalvir, Km 4, forrejón de Ardoz 28850 – MADRID, Spain
e-mail: angulom@inta.es

J. Maria Mi

INTA (Instituto Nacional de Técnica Aeroespacial)

P. de Vicente

INTA (Instituto Nacional de Técnica Aeroespacial)

M. Prieto

Departamento de Automática, Universidad de Alcalá

O. Rodriguez

Departamento de Automática, Universidad de Alcalá

E. de la Fuente

Universidad Politécnica de Madrid

J. Palau

AD Telecom Barcelona

institutions in Spain; 3-We also offer specific tasks or satellite units to the small business Spanish industries, to encourage their entering into the space technology; 4-Offer small missions flight opportunities to the Spanish research community, at an affordable budget target each 3–4 years.

1 Introduction

First Spanish satellite INTASAT, still in a 1440 Km sun synchronous orbit since Nov. 1974 (dead after 2 years end life timer) and put in orbit by a Delta rocket from Vandenberg-USA, and MINISAT-01 (launched in a Pegasus-XL above the Canary Islands) initiatives were relying on the traditional “big” Spanish space industries. Now in the NANOSAT & INTA μ SAT programmes they are almost out of the game. Most of the subsystems are developed at INTA, but we also rely on bilateral work with several Spanish universities and other research institutions. At the same time, we try to offer parts of HW or SW to the small business Spanish industries, to promote and encourage their entering into the space technology.

The launch of the first Nanosat-01 mission was made on 18 Dec. 04 by an Ariane-5 ASAP from Kourou. Next sister Nanosat-01B with the same store & forward communication mission and an enhanced UHF antenna, is planned to be launched in 2008.

2 Roots and Logic of the INTA μ SAT Programme

MINISAT, a well focused 150–250 Kg small satellite programme started in 1989, was in fact a precursor of the actual success on this s/c category, but unfortunately it was stopped after the first mission launch in 1997. Even after almost 5 years working perfectly in orbit that gave remarkable science returns, this was the second deceleration after Intasat 1st generation 15 years stop from 1974 to 1989. At the time of Minisat-01, a joint development effort with the “big” national space industries was the right approach for a minisatellite mission in Spain.

Fortunately and in order not to stop the space mission’s activity in our Institute, the much smaller Nanosat programme started at the right moment (1998) little after Minisat-01 launch. This time it was focused to an almost internal R&D initiative at INTA, based mainly in our own human and facilities resources. The National Space Plan founded partially the Phases A & B studies to all the participant institutions (universities and other research centres). Phases C/D, launch campaign and the actual in orbit operations, have been fully founded by our INTA internal budget.

2.1 Why not a Bigger INTA μ SAT?

Just as a logical further step to the original Nanosat initiative, in Oct. 05 we started the INTA μ SAT programme Phase-A feasibility study, to take full advantage of



Fig. 1 The INTASAT satellite (1974)

the Ariane-5 launch using ASAP. In our view and considering the evolved space industry reality in Spain today, we can state that the same approach is also applicable to a microsatellite programme. This class now is going up to 150 Kg total mass due to the actual Ariane-5 ASAP bigger size, compared with the previous 50 Kg capability of the Ariane-4 ASAP. However, the MicroSat missions can be adapted to a bigger mass (<200 Kg) or different small launchers.

3 Programme Support Team: Universities, National Research Institutes, and Small Business Spanish Industries

To fully develop a small satellite project internally is not an easy task at INTA, even having the resources of 1400 people and very capable test facilities, because it is very difficult to cover all the necessary disciplines. Besides that, other



Fig. 2 MINISAT-01 satellite (190 Kg) & Pegasus-XL at INTA facilities in Torrejón de Ardoz Madrid (March 1997)

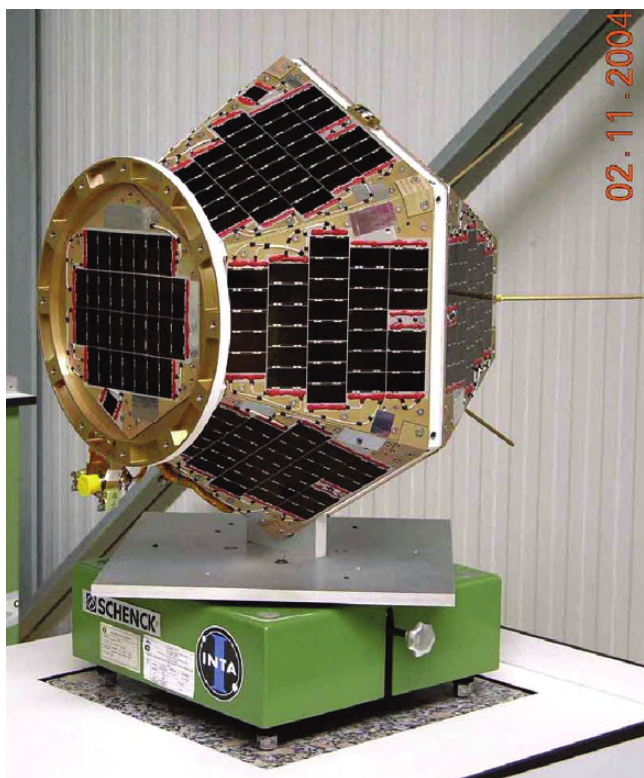


Fig. 3 Nanosat-01 FM s/c during Xs MoI measurements (Oct. 04)

important and much specialised external contributions for space experiments, technologies and new missions can be missed. Next team members are contributing till now:

- **SRG-UAH:** the Space Research Group belongs to the Universidad de Alcalá near Madrid. They started with space activities on the Payload processor for an instrument on board SOHO. During the development phase of Nanosat-01 they were responsible for the on board and EGSE SW. Now they are also working with INTA in the design & development of the OBDH processor for the INTA μ SAT Service Module (SVM).
- **RM-EUITA-UPM:** the Structural Group at the Escuela Universitaria de Ingenieros Técnicos Aeronáuticos belongs to the Universidad Politécnica de Madrid (UPM), was responsible for the Nanosat-01 structure NASTRAN analysis. Now they are doing the same job for INTA μ SAT satellite.
- **UCM:** The Automatic Control Research Group from the Universidad Complutense de Madrid, have previous experience in control laws design and implementation. They are integrated in the AOCS design & testing group, with INTA as leader.
- **AD Telecom:** is a small private company in Barcelona that was responsible of the UHF transceiver (20 Kbps) development. Now they are working on a new S-Band transceiver with 2 Mbps capability, for INTA μ SAT TTC and payload telemetry.
- **TTI Norte:** is another little company in Santander, which was responsible of the specific communications protocol development for Nanosat-01. They are now developing the INTA μ SAT TTC protocol, that is compatible to ESA CCSDS recommendations.
- **DEIMOS:** is a well known private Spanish small company in the GN&C activities for ESA and other European programmes. Within INTA μ SAT they are participating in the mission analysis and supporting the AOCS design and testing group.

4 Microsat System Approach

INTA μ SAT is focused at a multimission system optimised for 600–700 Km LEO orbits, with inclinations ranging from 0° to 100°. The satellite design is modular with a neat physical separation between the Service Module (SVM) and Payload Module (PLM), that will ease the design and integration phases for different payloads (P/L) in parallel with the SVM. The subsystems (S/S) design philosophy is also modular to allow specific resources to be matched to each particular mission, most probably with different flight configurations. The AOCS should cope with Earth, Sun and Space Pointing, from 1° to few arc seconds. The baseline design is with fixed solar panels, but a design rotating along Xs axis is available if specifically required. Propulsion will be an add-on module when needed.

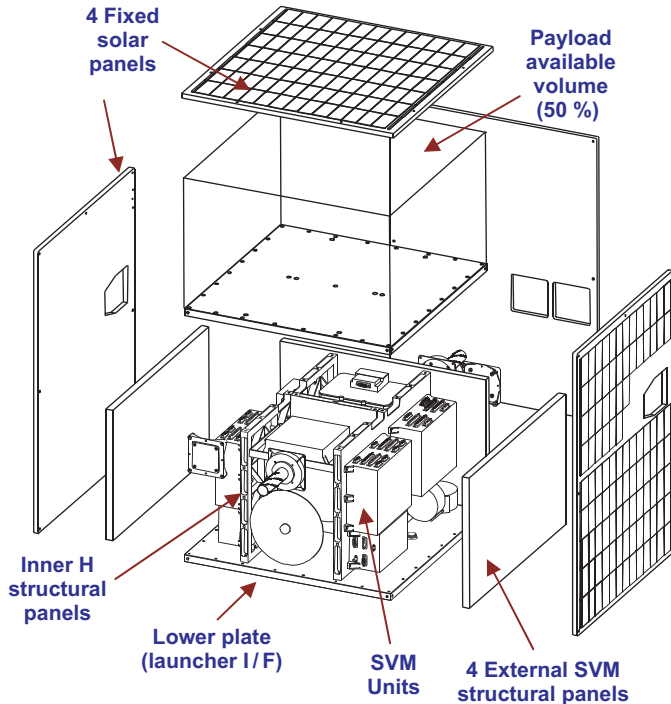


Fig. 4 MicroSat exploded view

There are 6 S/S: Structure, thermal control, Communications, AOCS, OBDH (HW & SW) and Power. Next Fig. 5 provides the block diagrams for a generic SVM and the PLM. Each mission is particular in its design or configuration, and the blocks will change in accordance with the needs.

4.1 Units Design

The volume available inside a Nano or μ SAT is typically much reduced and for this reason, it was decided after a trade-off study for Nanosat-01 also applicable to the MicroSat SVM, to have several quite small electronic boxes instead of big ones. This approach gives much more flexibility for accommodation, and optimises the volume occupation. Figure 6 shows as an example the Nanosat-01 PDU four level boards and mother board (total mass is 1,4 Kg). To improve the modularity, we selected a common and small board size for most satellite units: single Europe 100 \times 160 mm. Due to the increased capabilities and power consumption reasons, in some INTA μ SAT units we need also double size: 200 \times 160 mm. This applies to the OBDH box and Power Distribution Unit (PDU), with total masses around

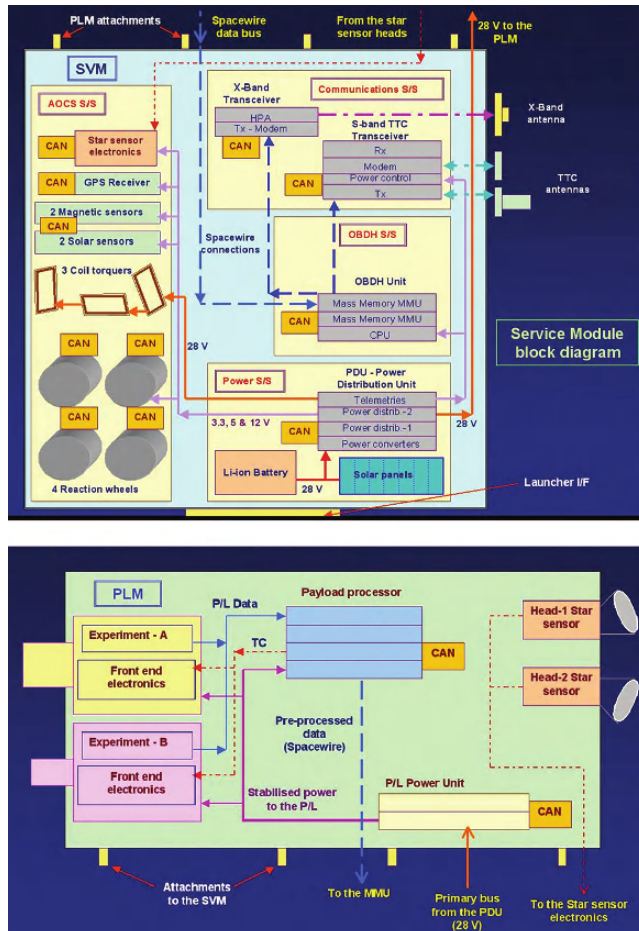


Fig. 5 SVM & PLM block diagrams

2,5 Kg per unit. When required by a specific box, a common back plane design is also available to interconnect the different boards inside that particular unit.

4.2 Models Philosophy

After a full development of all units and subsystems that must be reused in other Nano or μ SAT missions, it was difficult to establish a simplified baseline model philosophy. For new electronics unit level we use: EBB, EM, QM and FM. For limited redesigns we go directly to PFM after delta qualifications. There are some applications –typically for experiments–where we decide EQM & PFM. Nevertheless, we usually apply important simplifications:

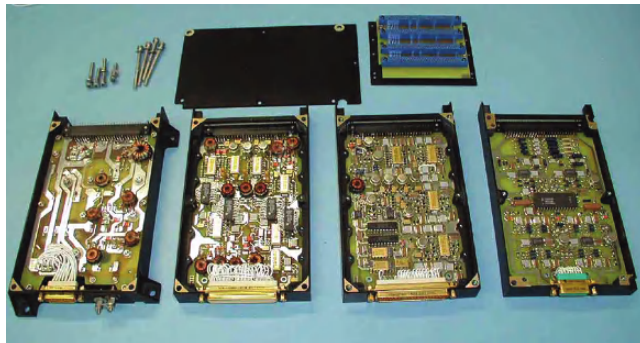


Fig. 6 Power Distribution Unit – PDU for Nanosat-01 (similar for INTA μ SAT)

1. The EM units are submitted to a temperature cycle at ambient pressure, to check the behaviour of the design at the limits.
2. The QM units are not fully qualified isolated (thermal vacuum, shock & vibration tests), but all interconnected at system level with the satellite QM harness, not yet assembled in the s/c (see Fig. 7).

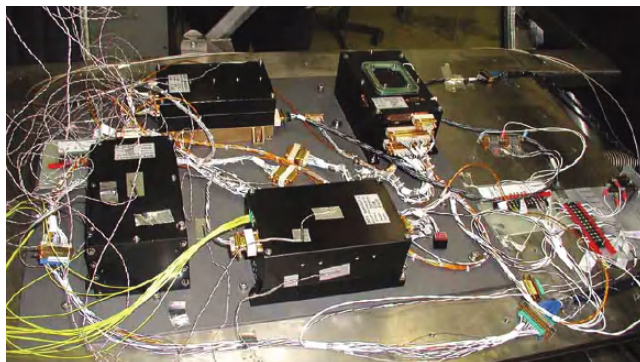


Fig. 7 All Nanosat-01 QM units with the s/c harness at the TV test at system level

3. After the required functional test, the Flight units passed just the environmental acceptance tests at satellite level.

For the satellite level we usually build STM, QM and FM. Here again the STM structure is reused for the QM model after limited refurbishment. Is it a luxury to have a full functional QM satellite? To some extent yes. In our case it is justified due to the need of building up some further sister satellites (i.e Nanosat-1B that will be launched in 2008), because we typically use the original QM satellite to make the delta qualification tests when developing a new unit or element. On top of that, it is of great benefit to have two operational satellites during the development and during the in orbit acceptance campaign.

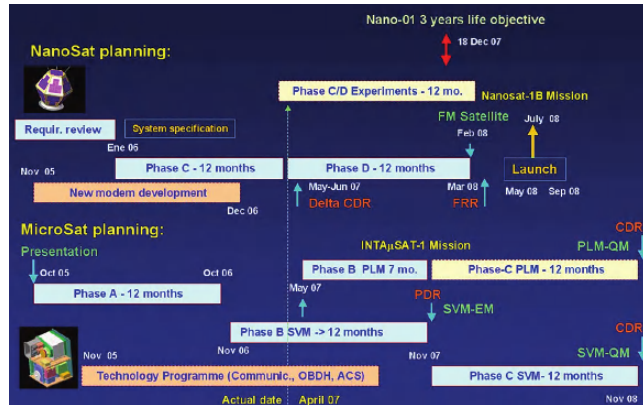


Fig. 8 Nano & Microsat plannings

5 Structure and Thermal S/S

The structure design is based on a traditional concept with separated SVM and PLM. The SVM has a primary structure with an H shape where all its units are attached. Just the antennas and the HPA final stage of the X-Band transmitter (for thermal reasons), are supported by the 4 external panels made in a light Aluminium honeycomb. Given the size of the inner panels and the load factor that also supports the Payload mass they are made from a solid aluminium alleviated plate. This configuration also provide thermal benefits, as it distributes the heat from “hot” to “cold” units inside the SVM, and then to the cold space with surface adjustable radiators placed in the lower SVM plate (-Z_s side, also I/F with the launcher).

Thermal control is based on the classical passive design, using when required multilayer thermal isolations in the external sides, and radiators where required. Inside the satellite all units are finished in black and in good thermal contact with the structure when adequate for heat rejection. Only the Lithium-ion battery carries heaters to keep it between adequate limits, but most of the time they are off.

All the Payload instruments are attached to the P/L I/F base plate that hold all the loads and transmit them to the SVM structure. Thermal control in principle shall be independent from the SVM, but certain coupling is unavoidable.

6 OBDH S/S

The OBDH is crucial for the mission success once in orbit and should provide the best performances available today for this kind of small satellites. The Central Processing Unit (CPU) uses Atmel microprocessor TSC-695 (ERC-32), that is a good compromise between performances and full space qualification (Radhard). This is critical, as the design is just single string. Only the TTC transceiver is redundant

on board, because we use a lot of commercial level components (COTS). The CPU single PCB occupies the lower floor of the OBDH Unit, while the second and third are taken by the Mass Memory Unit (MMU) boards.

A good connectivity between P/L instruments, all SVM S/S units and the central processor is mandatory in view of performance, flexibility and modularity. The CAN bus concept is used for H/K, TC distribution, and for ACS sensors & actuators communications in real time with the CPU.

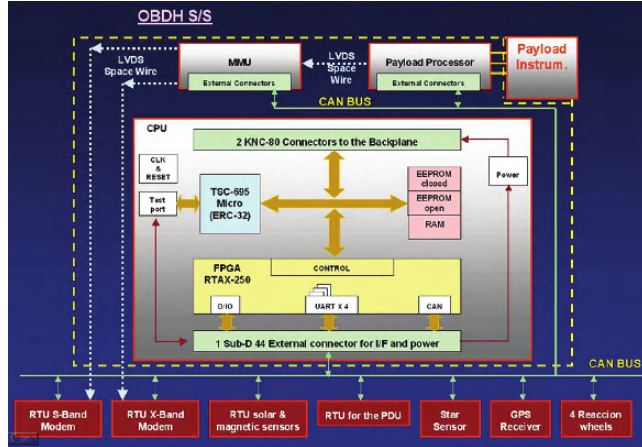


Fig. 9 OBDH block diagram

Dedicated Remote Terminal Units (RTU) with a local 80C32 microcontroller embedded in a RTAX 250 FPGA, are used to interface with the CAN bus at <500 Kbps. Higher speeds (from 1 Mbps to 200 Mbps TBC) needed by the P/L data I/F with the Mass Memory Unit (MMU), and also during downloads from the MMU to the S & X Band modems, is based in a LVDS physical layer and ESA's SpaceWire protocol.

The MMU will be placed in the same OBDH Box, and it will use the LEON-2 SPARC V8 microprocessor embedded in a RTAX-2000 FPGA, together with SDRAM memory banks (several Mbits). This "System on chip" design will have fast processing power and will provide the required I/F with CAN and SpaceWire buses in a quite open and reconfigurable way.

7 Communications S/S

After developing the original UHF transceiver for the Nanosat-1 (18 Kbps) in 2003 and the new improvement for Nano-1B (up to 80 Kbps), we did realise that a further step to S-Band was mandatory for TTC and TM speeds around 2 Mbps for the next Nanosat-2 and MicroSat missions. The new design was initiated in Nov. 05 within the technology programme, and performed by the same bilateral team AD Telecom – INTA. Right now the first EM is already running and been tuned in Barcelona after

the EBB development, and the performances seem well for the RF side. The new digital Modem design uses an Actel RTAX-2000 FPGA, although the EBB & EM models are based on a Xilinx chip that gives more flexibility in the VHDL SW development, as it allows several programmations.

This new Modem takes the 70 MHz IF (Inter-mEDIATE Frequency), and after a conversion to the digital domain and filtering, it performs several functions: the automatic IF signal tone tracking using a PLL (Phase Locked Loop), automatic IF chain gain control, QPSK demodulation, symbol & block synchronization, and extraction of the base band information. At the same time it takes care of both I/F with the CAN (CPU) and SpaceWire (MMU) buses. In the uplink mode, it sends out the TTC received information to the OBDH-CPU through the CAN Bus. When performing the downlink to ground, the data is taken either from the CPU RAM or the MMU, because both hold recorded data (Housekeeping or payload TM). As this channel speed is above the CAN capabilities, we have decided to use the SpaceWire bus. This decision is also challenging due to this recent and still in development high speed technology for space, sponsored by ESA.

Recently, we have organised a development team to start the design of a completely new X-Band transceiver (R&D project), together with AD Telecom, ACORDE (Santander) and INTA. Although only the transmitter is sufficient for MicroSat, we will make also a receiver in order to qualify it in orbit for other applications. Additionally, it could provide a backup TTC channel for the uplink that will increase the mission reliability. Part of the development effort spent on the new digital Modem, will be reused in this band with speed requirements going up to 20–40 Mbps.

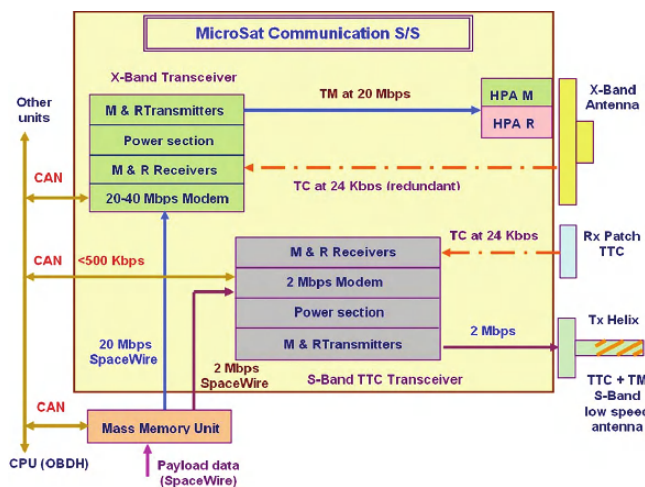


Fig. 10 Communications S/S block diagram and interfaces

All the satellite antennas are developed at INTA, were we have long time experience and nice testing facilities.

8 Attitude & Orbit Control S/S

The Nanosat-1 ACS is a quite simple spinning design with 2 groups of coarse Sun Sensors (SS) with 3 cells each, 4 simple axis Magnetic Sensors (MS), and 3 coil actuators (CA), all developed and qualified at INTA. Nanosat-1B is an Earth pointing satellite due to the medium gain UHF helix antenna, required to improve the store and forward communications with mobile terminals on ground. In this case we will use a single momentum wheel, to guaranty the required pointing range between 5° and 10°. In MicroSat and for the coarse pointing, we will use the same 3 axes MS design based on a Honeywell magneto resistance COTS chip, and 3 new improved SS with 5 cells each. They have dedicated electronics and a common CAN I/F with the CPU. Additionally, a Star Tracker (STR) is mandatory when the pointing requirements are stringent. For the first mission we will use the well known DTU μ Star sensor with probably 2 optical heads 90° apart.

Either air coils or magnetorods together with 4 reaction wheels are the baseline actuators. There will be a new development Control Moment Gyro (CMG) also called Advanced Gyroscopic Actuator (AGA-150 patented), with two degrees of freedom that will allow fast slewing manoeuvres up to 3°/s in a bang-bang mode, because the gyroscopic torque provided by this device is very high. It only takes one second to give such angular speed to the satellite. Nevertheless, it is envisaged that the reaction wheels will be needed for the fine pointing after any rotation manoeuvre, and to desaturate the AGA when required. The initial plan is to check first in orbit the behaviour and real performances of this R&D actuator, and if it will be OK, then try to apply it for nominal image taking during the exploitation phase of the earth observation mission.

In terms of pointing and slewing requirements, at present we are working with 3 mission scenarios:

- Fixed Nadir pointing with 0,1° to 1°
- Earth image taking along and across track ($\pm 35^\circ$) with 1' to 30'' accuracy
- Space inertial pointing with 30'' to 1'' accuracy and low speed slewing for retargeting astronomic payloads

The baseline design is to relay in fixed solar panels for most of the missions, although if needed by a particular application, there will be a deployable and rotating design along the $\pm Y_s$ axis (symmetrical wings). Number of modes and transition rules are now been studied.

9 Power S/S

The primary bus power provided by the 4 fixed solar panels will be a 28 V non regulated bus concept (battery voltage tracker). The number of strings connected to this bus in real time will be in accordance with the required power in the satellite. The PDU will be responsible for this regulation and for the distribution of secondary regulated

voltages ($3.3, \pm 5$ and ± 12 V) to the SVM units that could need them. The battery will be an 18 Ah (SAFT) design already qualified for PROBA-2.

10 INTA μ SAT-1 Mission Description

For the first flight it has been selected an Earth observation mission, relying on previous experience with the following cameras at INTA: IRIS engineering model 5m PAN camera development (1999), OMC for Integral (2001), and OSIRIS NAC & WAC contributions for ESA mission Rosetta (Jan. 2004).

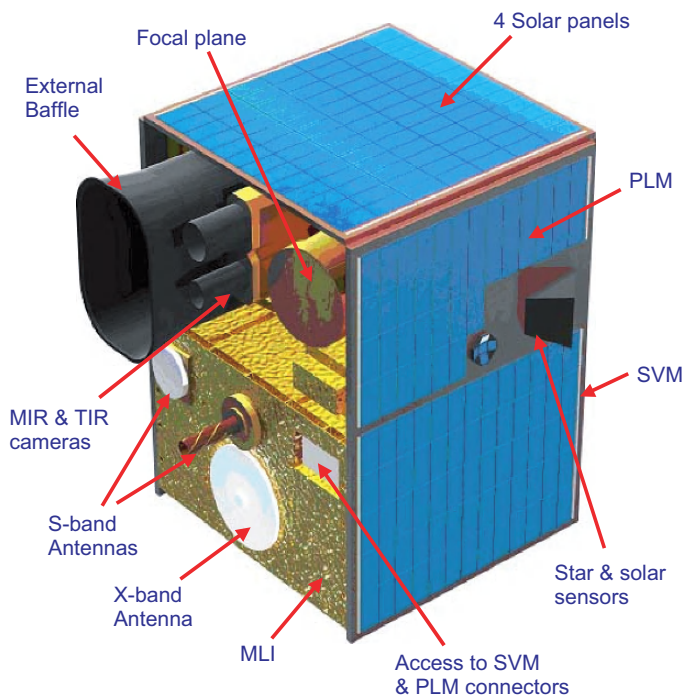


Fig. 11 INTA μ SAT-1 general view

This is very challenging for a completely new development, considering both the SVM and the camera at the same time; however, it has an R & D purpose and not a full operational need. For this reason, the satellite will make use of almost all its resources and S/S capabilities now in the development phase (most probably it will not have a propulsion S/S). The Control Centre will be installed at INTA in Torrejón (same for Minisat-01 and Nanosat-01). The 5 m dish S-Band antenna is already there but needs some refurbishment, and the 10 m X-band antenna will be shared once installed with the bigger SEOSAT (Spanish Earth Observation Satellite), now in phase-A. The previous experience developing and operating other small satellites will be of great benefit.

11 Conclusions

1. Very interesting micro & nano-technology and diffuse IR OWLS experiments are running OK in Nanosat-1, in orbit since 18 Dec. 04.
2. We have developed with success all the units, subsystems and space & ground segment at INTA, with the help of other national research centres, some Spanish Universities, and a small RF company in Barcelona.
3. Nanosat-1B is a sister satellite, that will be launched in 2008 to complement the store and forward communication mission of the first mission. It will carry new nano & micro technology experiments.
4. Nanosat-2 is an improved new generation with increased capabilities (ERC-32 OBDH, 2Mbps TTC+TN transceiver, 3 axis control ACS, etc.) but with the same philosophy.
5. Since Nov. 05 we have started the MicroSat programme, a 100–150 Kg microsatellite as a further step. This again will follow the same principles and development rules of Nanosat, together with the acquired know-how and lessons learned up to now.
6. The target for the MicroSat development planning since the programme presentation in Oct. 05, was to have ready the first mission in 4 years (end 2009–beginning of 2010). At this stage near to the middle of Phase-B and thanks to the R+D technology effort dedicated to new developments, this objective seems realistic and reachable.
7. Apart INTA internal budget, the programmes are been supported by external founding since 2005 (PNE-CDTI) to develop an Advanced CMG that will be qualified in orbit (SAGAS-150). This will provide to INTAμSAT-1 a torque 500 times higher when compared with traditional reaction wheels. The baseline is to use it to rotate very fast the satellite ($3^\circ/\text{s}$) in an experimental mode. The wheels and coil torquers will be the nominal actuators.
8. We have just made a new proposal to the PNE-07 (CDTI) to fully develop an Advanced Communications S/S in X-Band (AD Telecom). This includes new antennas (INTA) and power amplifiers (ACORDE from Santander).
9. The first mission will carry a Mid Resolution Multispectral Camera (10–12 m GSD) with 3 to 4 channels. We are starting by now the work and setting the requirements for this new camera that will be fully develop at INTA, as the first Payload for INTAμSAT-1.

Acknowledgements The Nanosat and MicroSat programmes are running thanks to several funding from the National Space Plan, either Scientific (PNE) or Technical (CDTI), and from our internal budget. We will like also to thank INTA top level management, for their big support and encouraging recommendations along the past years.

Reference

1. M. Angulo, MR. Canchal, JM. Mi, P. de Vicente; *Development and qualification of the Nanosat programme at INTA*. 57th IAC Valencia 2006.

Moving Towards Commercial Earth Observation Services with Small Satellite Constellations

Adam M. Baker, Philip Davies, and Lee Boland

Abstract This paper outlines the heritage and future plans of SSTL in enabling high performance cost effective Earth observation services through constellations of small spacecraft. The paper will discuss two new spacecraft for customers in Spain and Nigeria, and how these meet traditional needs for Earth Observation data at a low cost. The range of payload options which SSTL can offer for a wide variety of Earth imaging applications covering high and medium resolution, wide area coverage, frequent revisits and near real-time tasking and data return in various wavebands, including visible light and microwave will be discussed. Applications enabled through SSTL's heritage platform capability, the optical payload group (formerly Sira Space group) and SSTL's business unit DMC Imaging International, DMCii will be discussed to illustrate the utility of small satellites for real, commercial applications.

1 SSTL Small Satellite Heritage

The first five satellites of the Disaster Monitoring Constellation (DMC) launched in 2002–2005 demonstrated the humanitarian value of Earth imaging using cost-effective small satellites and, having met the primary objectives of their buyers, are now facilitating the delivery of commercial earth observation data services. The British National Space Centre provided £15M in funding through the MOSAIC (MicroSatellite Applications in Collaboration) programme from 2000 which helped develop the SSTL ‘enhanced’ microsatellite platform and camera through three funded missions. MOSAIC also funded the TOPSAT consortium, lead by QinetiQ

A.M. Baker
Surrey Satellite Technology Ltd, United Kingdom
e-mail: a.baker@sstl.co.uk

P. Davies
Surrey Satellite Technology Ltd, United Kingdom

L. Boland
Surrey Satellite Technology Ltd, United Kingdom

with an SSTL platform and a RAL camera, and initial development of the GeMini low cost geostationary microsatellite platform.

MOSAIC has now leveraged significant export sales, commencing with AlSat-1 for the Algerian Space Agency (CNTS), and the first DMC satellite the Nigerian Agency for Space Research & Development (NASRDA), the Turkish Ministry of Science and Technology research institute BILTEN TUBITEK and the Chinese Ministry of Science & Technology have since purchased Disaster Monitoring Constellation spacecraft.

The partners formed the DMC consortium, agreeing to reserve 5% of system capacity for disaster management, to operate as part of a constellation, to share data, and to investigate commercial exploitation of the data. In November 2005, the DMC, coordinated by SSTL's business unit DMC Imaging International (DMCii) officially joined the "International Charter: Space and Major Disasters", supplying broad daily image coverage during disasters such as hurricane Katrina and the Indian Ocean Tsunami.

The Beijing-1 microsatellite was added to the constellation after launch in October 2005. Beijing-1 is the first DMC+4 spacecraft built by SSTL [1]. DMC+4 combines the basic DMC wide area multispectral payload with a 4 m Ground Sample Distance (GSD) panchromatic instrument, to provide continuity of DMC data (for example generating a cloud free map of China within 6 months) and to carry out systematic mapping at a higher resolution (in support of the 2008 Beijing Olympic Games).

2 The Benefits of Constellations

The key benefit of a constellation of small spacecraft is that high temporal resolution can be matched with high spatial resolution, at a mission cost well within that of a single conventional large remote sensing spacecraft. Metrics comparing the performance of various constellations typically compare timeliness, where satellites require days but terrestrial systems can deliver hours, against either area coverage/field of regard, or resolution. Satellites can cover hundreds to hundreds of thousands of square kilometres, depending on the resolution, against hundreds of square kilometres for aerial platforms. The latter however can offer resolution in the tens of cm range, although satellites are rapidly catching up, with the latest generation of 'Orbview-5' spacecraft designed by Digital Globe claiming 0.41 m GSD at nadir. However the revisit period of such spacecraft is typically 2–3 days, the maximum resolution is only gained in the image centre, and capability itself has cost in the order of \$500M to develop (based on the NextView contract value). In contrast, a typical small spacecraft such as NigeriaSat-2 can be built for an order of magnitude less, will offer a GSD as low as 2 m, and can offer daily repeat with as few as 2 spacecraft, both of which can be positioned using a single low cost launcher.

The plots above demonstrate the increasing capability of cameras and sensor arrays available for small satellite platforms, enabling attractive combinations of wide field of regard, rapid repeat and high resolution to be affordable.

Fig. 1 Timeliness v. area coverage for different sensor options, focus on tactical applications

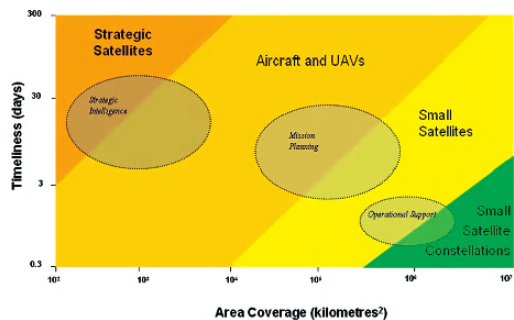
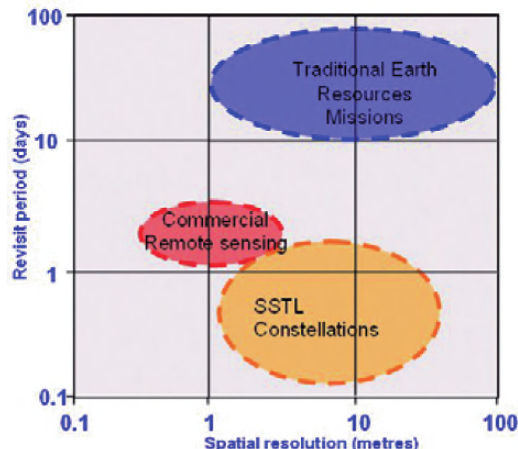


Fig. 2 Revisit period v. spatial resolution for traditional v. small satellite space-based options, focus on Earth resources



Despite the obvious value of small satellite constellations for tactical applications, and the successful operation of Topsat launched in October 2005, the first purpose built small satellite constellation for a single customer, RapidEye, was funded with commercial returns in mind.

RapidEye aims to deliver Earth agricultural and insurance industry specific information products derived from multispectral wide area Earth Observation data.

RapidEye will serve 3 markets:

1. Agricultural Insurance: supporting the loss adjustment process by provision of regularly updated field maps.
2. Agricultural Producers: assisting precision farming by regularly providing information about crop conditions and yield predictions.
3. International Institutions: assessing expected crop harvests and monitor usage of subsidies for disaster relief.

SSTL, acting as platform provider and satellite integrator to MDA in Canada, will launch the RapidEye constellation of 5 satellites in the second half of 2007.

The five RapidEye platforms take some features from TOPSAT and Beijing-1, while additionally focusing on meeting the mission requirements in the shortest possible time (24 months) at the lowest overall price for a constellation ($\sim \text{£}20\text{M}$).

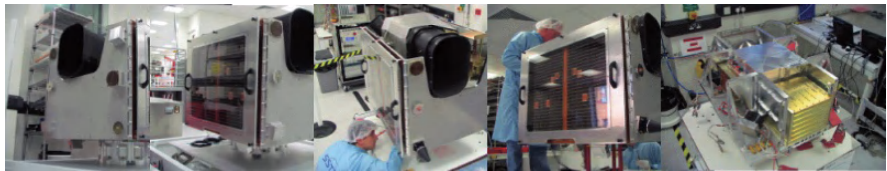


Fig. 3 RapidEye during camera/platform integration at SSTL

3 New Optical Spacecraft for SSTL

SSTL is designing two new Earth Observation spacecraft for customers in Spain and Nigeria. Spain DMC is funded through anticipated data sales to a small set of countries, and will reach new levels of image throughput performance for the next generation DMC constellation.

3.1 Spain DMC

The principal mission level improvement of Spain DMC compared to previous DMC spacecraft is to increase image throughput, such that the cost of spacecraft can be offset by data sales. To this end, subsystem design changes include

- i. Addition of X-band data downlink, increasing the data rate from the 8 Mbps of the early DMC S-band system to over 20 Mbps.
- ii. Replacement of NiCd battery with higher capacity, greater Depth of Discharge, higher energy density and longer life Li-Ion battery.
- iii. Improving the imager resolution has been increased from 32 m to 22 m at nadir without reducing swath, by utilising a custom lens and the latest CCD linear array, while maintaining overall mass, envelope and power consumption. Digitisation fidelity has also been improved from 8 to 10 bit.

The spacecraft envelope & mass at 100 kg, as well as orbit at 686 km with LTAN 10:30 am, a lifetime of 5 years, compatibility with the DMC ground segment and an 18 month build are identical to the current DMC spacecraft.

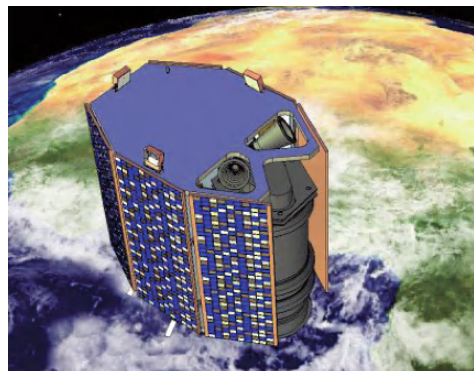
The operations strategy targets maximum imaging time in the sunlit part of the orbit. Operating modes with imaging and downlinking data during each orbit, and imaging orbits followed by downlinking orbits have been developed. A key customer requirement is to deliver complete coverage of Spain and Portugal within 5 days using a combination of operating modes. This requires a significant increase in the number of scenes per day delivered to the customer, compared to the original

DMC spacecraft. A balance is struck between covering the maximum area per orbit, which requires a subsequent orbit or orbits to downlink all the data, and reducing the area covered but allowing all operations to be conducted within an orbit. A future goal for SSTL missions is to allow stripmap imaging, where the imager can be run continuously in parallel to downlinking for the sunlit part of the orbit. This would deliver up to 12M km^2 of imagery per orbit, assuming the ground segment could handle this data throughput!

Fig. 4 SSTL-100 platform,
Spain-DMC



Fig. 5 SSTL-300 platform,
NigeriaSat-2



3.2 *NigeriaSat-2*

NigeriaSat-2 will offer the most capable high performance imaging system based on small satellites for the price. Through a combination of wide area multispectral imagery compatible with SPOT and Landsat ETM, and 2.5 m resolution VHR panchromatic and 5 m multispectral imagery, a range of imaging modes will be possible to enable agricultural, mapping, security and disaster monitoring services.

NigeriaSat-2, weighing about 300 kg at launch, will feature a high-capacity solid-state onboard recorder with a 16-gigabyte memory and an X-band downlink capacity exceeding 100 megabits per second. In excess of 150 accurately geolocated images with a 2.5 m GSD (PAN) and 5 m GSD (multispectral) per day will be produced from the 686 km altitude orbit over a period of seven years.

NigeriaSat-2, shown above will be built in 30 months and is scheduled for launch in mid-2009 along with a co-passenger NigeriaSat-X which will be an advanced training model for the Nigerian engineers who began their training with the NigeriaSat-1 DMC spacecraft launched in 2003.

The table below compares SSTL's three Earth Observation platform products:

Table 1 Comparison of SSTL spacecraft platform product lines

| | SSTL-100 (<i>Spain DMC</i>) | SSTL-150 (<i>RapidEye, Beijing-I</i>) | SSTL-300 (<i>NigeriaSat-2</i>) |
|--------------------------|--|---|----------------------------------|
| PAN imager GSD and swath | N/A | 2.8–4 m, 17–22 km | \leq 2.5 m, 20–30 km |
| M/S imager GSD and swath | 22–32 m, 600 km | 5.6–8.7 m, 78–104 km, 1500 km long swath | \leq 32 m, 300 or 600 km |
| Colour wavebands | 3: R, G, NIR | 5: VNIR | 4: R, G, B, NIR |
| Image throughput | >4/day (600 km \times 600 km) | Typically 80–100 km \times 1500 km swath per orbit using MR camera | >100/day |
| Lifetime | 5 years | 7 years | >7 years |
| On-orbit data archive | 2 Gb | Up to 8 Gb | >120 Gb |
| Downlink data rate | >8 Mbps | 40 Mbps | >100 Mbps |
| Off pointing | No | Yes | Yes |
| Image quality | 8–10 bit. SNR > 100 | 12 bit. SNR > 130. | 10 bit. SNR > 140. |
| Typical orbit altitude | 600–800 km (686 km for DMC, 620 km for RapidEye) | | |

Following the launch of the 5 RapidEye spacecraft in early 2008, SSTL's Earth Observation launch manifest can be summarised as:

| | |
|----------|--------------|
| Q1, 2008 | Spain DMC |
| Q1, 2008 | UK-DMC2 |
| Q4, 2008 | KANOPUS 1–3 |
| Q3, 2009 | NigeriaSat-2 |
| Q3, 2009 | NigeriaSat-X |

KANOPUS platforms are being manufactured for the Russian Federal Space Agency, procured by the Russian Research and Production Enterprise Pan-Russian Research Institute for Electromechanics (FSUE NPP VNIEM) and Radioexport of Russia, and will support the monitoring of disasters, agricultural planning and the management of water and coastal resources.

4 Payloads for Small Satellites

SSTL has carefully studied the Earth Observation market, and has made efforts to ensure that its platforms are applicable to a range of payloads operating in various wavebands outside the visible spectrum, and carrying out activities in addition to electro-optical imaging. Missions studies have ranged from altimetry, geolocating electronic intelligence signals, spectrometry of a wide range of atmospheric species and greenhouse gases, and both active and passive microwave imaging.

Mindful of the breadth of the market for Earth Observation and small satellites, SSTL spacecraft continue to be designed in an adaptable modular fashion which can support multiple payload options. Two popular options are detailed below:

SSTL developed the wide area medium resolution SLIM-6 camera, shown below, and in 2006 acquired the optical instrument capability of the UK firms Sira electro-optics, which developed the Beijing-1 microsatellite high resolution imager, also shown below:

Fig. 6 SLIM-6, medium resolution ultra-wide field camera developed for DMC

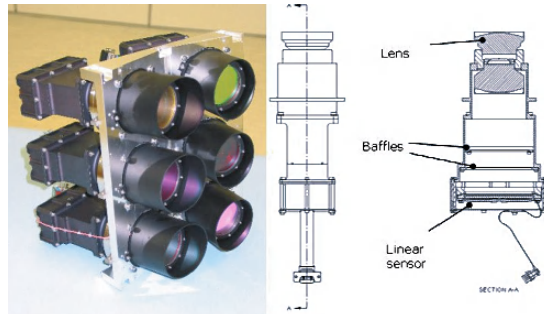


Fig. 7 High resolution narrow angle panchromatic and multispectral camera



SSTL can now offer a range of payloads covering visible and infrared wavebands and microwave frequencies, delivering a unique blend of high resolution, wide area coverage, frequent revisits and near real-time tasking & data.

Table 2 SSTL camera options for Earth Observation

| Imager | GSD at nadir, 686 km ref altitude (m) | Swath at reference altitude (km) | Wavebands | Tele-scope mass (kg) | Envelope (cm) | Power (W) |
|------------------------------------|---|--|---|-------------------------|--|--------------|
| VHR PAN and M/S | ≤ 2.5 (PAN) ≤ 5 m M/S | 20–30 | Up to 4, NIR, R, G, B | <50 | Primary micro- satellite payload | <50 |
| Medium Res. M/S | 7.1 | 91 | 5 across VNIR | <30 | | <50 |
| Wide Area M/S | 22 | 300–600 | Up to 4, NIR, R, G, B | <10 | Primary on SSTL-100, secondary on SSTL-300 | <20 |
| CHRIS hy- perspectral camera | 17 m in best mode | 13 km ² sampling area | Up to 62, 0.4–1.05 μ m, 1.25–11 nm spectral res. | 14 | | 8 |

The key point which the last 3 columns in the above table show is that all the instruments fit comfortably within the typical 1m × 1m × 1m envelope of a microsatellite, and both wide area M/S camera and CHRIS can be accommodated as secondary imager payloads on the SSTL-300 platform

Concept designs for short wave and thermal infra-red cameras have also been developed, targeting 30 m GSD in the 1.55–1.75 μ m wavebands with 150 km swath (Landsat ETM 5+ equiv.) for the former and 300 m resolution in the 3–5 and 8–12 μ m bands and up to 400 km swath for the latter, respectively. SSTL's microsatellites have also attracted the interest of ESA as gapfillers for its GMES programme an Sentinel spacecraft.

Sub-1 m GSD performance using a microsatellite platform is being examined by SSTL in collaboration with a leading UK payload provider, allowing additional production capacity to meet the requirements of future constellations.

SSTL is also working with a leading payload provider to be able to offer a Synthetic Aperture Radar (SAR) payload ready for launch as early as the end of 2010. This mission would deliver 10–30 m GSD, swath widths of 50–100 km in a single polarisation, X- or C-wavebands and <−25 dB Ne σ_0 radiometric resolution.

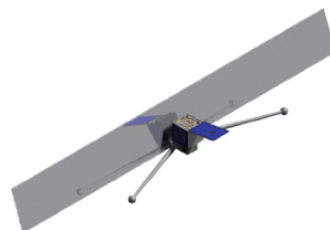
Further payloads being studied by SSTL and in collaboration with other companies include GNSS-reflectometry for monitoring wave height and wind speed to complement buoy data, and compact uncooled imaging spectrometers for greenhouse gas monitoring such as CO₂.

Two example mission configurations under study include an Earth mapper designed to provide continuity to LandSat VII using a constellation of 4 small satellites, and an ultra-low cost SAR mission delivering performance comparable to DMC and priced comparable to optical SSTL-300 based missions, shown below:

Fig. 8 Concept for LandSat Data Continuity Mission, with SWIR imager and 4-band VNIR wide swath multispectral camera



Fig. 9 Concept for Ultra Low Cost SAR spacecraft based on RapidEye platform, delivering all-weather and day-night data equivalent to the DMC



5 Applications

Example applications of DMC which have led to the creation of the DMCii value added data sales business unit of SSTL include:

- Field level monitoring of crop health in the UK and Europe, in combination with high resolution aerial images.
- Illicit crop mapping & classification, for example Opium production in Afghanistan at the request of the United Nations Office on Drugs & Crime.
- Monitoring Amazonian logging and deforestation management for INPE (the Brazilian Space Agency), imaging the entire Amazon basin annually.
- Monitoring the rate of calving of the Greenland ice sheet, which would raise global sea level temperatures by 7 m, were it to melt entirely.

Furthermore, SSTL's CHRIS (Compact High Resolution Imaging Spectrometer) hyperspectral instrument, hosted by the ESA PROBA spacecraft celebrated its 5th birthday in September 2006. A user forum in Frascati, Italy attended by 60 delegates demonstrated how CHRIS and PROBA instrument data supports the research of 100 EO projects from nearly 30 countries worldwide. CHRIS is currently the highest resolution capability spectrometer in orbit, and with a mass of only 14 kg and a power draw of 8 W is a highly attractive payload for a small spacecraft. Example applications include mapping aerosol concentrations, water and land surface use, and chlorophyll concentrations. Two key applications from DMCii and CHRIS/PROBA are shown below:

Fig. 10 DMCii – Amazonian rain forest mapping to show deforestation

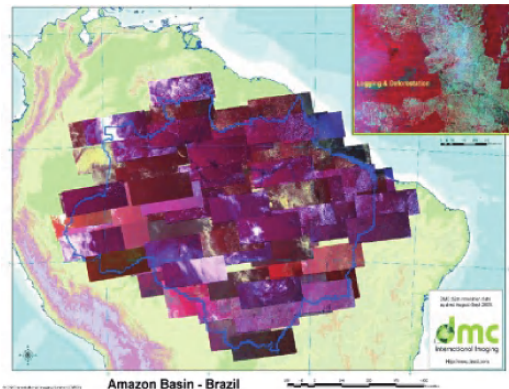
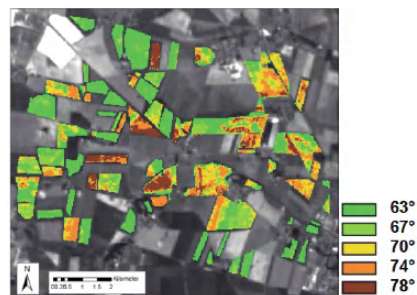


Fig. 11 Leaf area angle of wheat crops in Germany taken with 5 different views from CHRIS/PROBA. Leaf angle is indicator of crop ripeness



6 Supporting Mission Elements

SSTL also offers a number of supporting capabilities to give a spacecraft mission appropriate utility:

- Ground stations, fixed or mobile.
- Launch contracts, operations and operational support contracts, as well as image data processing, sales and marketing.
- Sale of a complete range of ITAR free spacecraft subsystems.
- Know-How transfer and Training, in the form of (i) Improving customer ability to specify and procure low cost space systems, (ii) Training technical organisations in the SSTL approach to space systems development and (iii) Training spacecraft operators.

Reference

1. Cawthorne A, da Silva Curiel A, Sweeting M, *The next generation DMC small satellite platform for high-resolution imaging*; IAC-05-B5.4.01, presented at the 56th International Astronautical Congress, Fukuoka, Japan, October 2005; p. 9.

PROBA Spacecraft Family

Small Mission Solutions for Emerging Applications

Jo Bermyn and Chris Dorn

Abstract Small Satellites are now being developed by many organisations. These are now a mature technology and have demonstrated their potential as a product with complementary performances to more conventional mission solutions.

Recent successes with the PROBA 1 (with more than 5 years of operations in orbit) and the UK's Topsat spacecraft show the potential to use these platforms in flexible and low-cost ways for Earth Observation missions. ESA's Earth Observation Directorate uses PROBA 1 on a daily basis in support of research related to vegetation, disaster monitoring, land use, volcano observations, etc. Topsat supports a number of users with up to date imagery and has demonstrated several new approaches to data downlink & distribution.

With continued advances in technology, new areas in Earth observation are being explored and applications like high resolution-, hyper spectral- and small SAR radar missions become feasible with a PROBA scale platform and its derivatives.

As small satellite missions become more ambitious, so the space industry is adapting to the challenge of creating organisations which can deliver the advantages of small satellite technology while retaining compatibility with international data standards and operating practices. The merging of Verhaert Space and QinetiQ's Space Division is a first step in the creation of a solid mid-tier player dedicated to small mission solutions, combining complementary skills in mission design, system integration and key areas of technology development to offer end-to-end solutions to customers worldwide.

This paper will outline high-performance solutions for future Earth observation missions, highlighting the role that cutting-edge technologies have to delivering unique capability to meet customer needs.

J. Bermyn

Verhaert Space, Hogenakkerhoekstraat 9, B-9150 Kruibeke, Belgium
e-mail: jo.bermyn@verhaert.com

C. Dorn

QinetiQ – Space Division, Cody Technology Park, Ively Road, Farnborough, UK

1 Small Missions Heritage

1.1 *Proba 1/Proba 2*

Mid nineties, ESA initiated the idea for building a small satellite for technology demonstration purposes, called PROBA (Project for On-Board Autonomy). With the financial support from the Belgian Science Policy Office to ESA's General Support Technology Programme (GSTP), Verhaert Space finally could win the phase C/D contract that started in February 1998.

PROBA 1 is the first Belgian small satellite and is developed by Verhaert Space as prime contractor. The satellite, only weighing 94 kg with dimensions $80 \times 60 \times 60$ cm, was realised in about 3 years. The strong features of the PROBA platform lie in the field of autonomous operation (low operational cost), its simplicity in operation, its performant attitude control system and its strong Léon based computing capability. PROBA's 3-axis attitude control system provides fine-pointing capabilities, resulting in precise snapshot images (e.g. HRC instrument – 4 m pan images) and has agility to execute demanding mapping and push-broom scanning scenarios (e.g. CHRIS instrument – 18 m multispectral images).

Although designed for a lifetime of only 2 years, PROBA 1 is now functioning in-orbit for more than 5 years and providing earth observation images through ESA to the science community on a daily basis.

In the meantime, its successor PROBA 2 carrying sun observation instruments is under final integration at Verhaert Space and is planned for launch early 2008.

The PROBA platforms are operated through a small ground station (2,4 m dish) located at the ESA Redu site in the Belgian Ardennes.



Fig. 1 PROBA 1 on PSLV launcher (ISRO/Antrix)

Fig. 2 PROBA/HRC Image of pyramids of Gizeh (ESA)



Fig. 3 PROBA/Chris image of 3 gorges dam China (ESA/SIRA)



Fig. 4 PROBA 2 under integration at Verhaert Space



1.2 TopSat 1

On 27th October 2005, TopSat was successfully launched. It has since been producing high quality imagery to satisfy a range of user requests.

The purpose of the programme is primarily to demonstrate the ability to build and operate a low cost optical satellite capable of generating high quality imagery.

Fig. 5 TopSat spacecraft platform (outer panels removed for clarity)



Fig. 6 Image of Marseilles, France



The satellite produces panchromatic imagery ($17 \times 17\text{km}$) with a spatial resolution of 2.8 m, and multi-spectral imagery ($12 \times 18\text{km}$) with 5.6 m resolution. Imagery is

routinely downloaded to QinetiQ's ground station at West Freugh, Scotland, where it is forwarded to the Payload Operations Centre in Farnborough for processing and dissemination to users.

Fig. 7 The West Freugh ground station



Fig. 8 The RAPIDS mobile ground station



In addition, QinetiQ has developed a mobile ground station, consisting of a 2.7 m receiving dish towed by a Land Rover, which has demonstrated the ability to downlink near-real time TopSat imagery directly to end users.

1.3 New Approaches

Missions such as Topsat and Proba are made possible by the pragmatic application of key technologies and new approaches to the programmatic and system design. A flexible response to the customers needs is the hallmark of the QinetiQ-Verhaert approach. Simplified programmatic structures, integrated teams, on-board automation and new technologies all have their part to play in reducing costs. The mission must be

viewed as a complete system and the component segments design to minimise through life costs by matching risk with customer expectation and technical solutions.

2 Small Mission Solutions

Small satellites can play an important role for earth observation applications, which is proven in the meantime by the successful PROBA/Topsat missions.

To date, the application field stays limited to imagery with up to a few meters of ground resolution and a few spectral bands in the visible and near-infrared spectrum. Clearly, this is driven by the resources and performances available on small platforms but thanks to the evolving technologies on payloads and platform side a lot of other applications come within our reach.

A nice example of this capability improvement is demonstrated on PROBA 2; compared to PROBA 1 the payload carrying capability is increased from 30% to 40%. A major contribution in this improvement is coming from our on-board computer based on the Léon chip, 3,3 V and SMD component technology.

Small missions will never be suited, and are not intended, to replace the full capability of large systems, but they will be a very interesting complement to it. Small missions may be able to provide solutions for 80% of the requirements at only 20% of the cost and as such are very interesting as gapfiller, precursor or stand-alone solution.

Over the years, several concepts and ideas were worked out to show the potential of our PROBA platform for emerging applications. Indeed, we can talk about the Proba Spacecraft Family of which some key potential is highlighted hereafter.

2.1 Small Satellites for Earth Observation

Future important application fields for small missions lie in the area of high-resolution images (security – dual use), more spectral bands (vegetation – precision farming) and SAR imagery (overnight visibility).

Clearly, this type of instruments requires more power, more volume, more data storage & downlink capability, but smart solutions and optimisations allow overcoming of the challenges.

Several studies were carried out to demonstrate the feasibility of following missions based on a PROBA platform:

2.1.1 High Resolution

The major challenge for this type of missions is the thermal stability on the instrument and platform stability required to provide sharp images.

Availability of high performance gyro's in combination with a performant attitude control system on the satellite, allow to build PROBA satellites which can provide ground resolutions up to 1 meter (e.g. ARGUS phase A study for ESA).

2.1.2 Multispectral/Hyperspectral/Lidar

Access to QinetiQ's specialised hollow wave guide technologies offer the possibility of smaller sensors which will deliver comparable optical performance on small satellites. New mission solutions including Lidar and microwave sounder systems will become possible with QinetiQ's Gallium Nitride technologies. These offer the possibility of even smaller and more electrically efficient sub-systems. Currently a study for a multispectral mission, called PROBA Landobs, is ongoing.

Multi – and hyper spectral instruments work typical at lower resolutions but generate huge amounts of data. Here solutions can be worked out in several areas, starting with data capturing optimisation (to reduce the capture of un-useable data), data compression and storage and high power downlink capacity.

2.1.3 Radar

Radar missions on a small satellite are a challenge since we have to deal with relatively large antenna systems and large peak power requirements.

Studies are ongoing to fly optimised systems with shorter lifetime (less redundancy) on a small platform, and investigation continues in to low altitude missions.

2.1.4 Formation Flying

Formation flying with small platforms is demonstrating the usefulness for pré-cursor missions. Before entering in a very ambitious science mission, critical technologies can be developed and demonstrated in orbit in a fast and cost-effective way.

Currently, two parallel phase A studies are on-going for ESA for a PROBA 3 formation flying mission.

2.1.5 Microgravity Platform

Verhaert Space performed for ESA a study (Wakeshield type of platform for high-quality microgravity research). In this concept, we use a PROBA based free-flyer which operates in the vicinity of the ISS. The challenges added to the platform are related to docking & payload exchange and the triple redundancy required for safety related aspects.

2.1.6 Small Satellites for Interplanetary Mission

NEO missions such as SIMONE, as well as ESMO and Don Quijote are predicated on the use of electronic propulsion (EP) to access regions of the inner solar system (beyond Earths gravitational influence).

In addition to the existing LEO applications of small spacecraft, new missions are being developed to utilise small satellites in other Earth orbits. Access to MEO, GTO and even GEO is becoming possible with new upper stages and launchers. These can be coupled with a range of propulsion systems for new mission solutions.

2.2 Small Satellites for Great Science

Small satellites offer the following advantages for science missions in LEO, GEO, GTO and the inner solar system:-

- More measurements = better science
- Lower cost = affordable where previously assumed not
- Single primary instrument = optimised missions
- Smaller consortia = less compromise (on mission issues)
- Shorter build times = faster response
- Lower cost and faster response = more missions

QinetiQ-Verhaert is involved in the following key areas that make such missions possible:-

- Concept Development (technical and consortia)
- System prime
- Core bus with Electric propulsion options
- Technology insertion (into science group designed instruments)
- Technology adoption at bus level (for greater payload capacity)
- Technology delivery (key subsystems with flight heritage)
- Mission Management and operations

3 Qinetiq & Verhaert Space, Your Partner for Small Space Missions

The acquisition by QinetiQ of Verhaert Space in September 2005 paves the way in the creation of THE small space missions company in Europe. The joining of skills from QinetiQ's space division – with a lot of heritage in mission design and innovative technologies, and Verhaert Space – a seasoned small (smart) space systems integrator, creates an entity that can offer attractive small mission solutions to governmental and commercial customers worldwide.

As small missions prime, we enter the so-called Mid-Tier segment, where challenging missions based on small satellite platforms will be developed.

Small missions require smart and innovative solutions but at the same time they have to stay affordable and require realisation within reasonable timescales. In fact, these projects are too big for small companies (risk & capabilities) and too small for large companies (priority & cost effectiveness).

The QinetiQ-Verhaert teaming allows such mission to be undertaken in an appropriate and efficient way, with the right priority (small mission are a key account for us). Furthermore, we combine the flexibility and cost efficient approach of smaller organisations with the quality standards, facilities and credibility of larger organisations. As such we provide optimum value-for-money while delivering flexible solution that meet the customer's *real* needs.

4 Conclusion

The Verhaert Space – QinetiQ team can offer a wide range of small satellite solutions based on the PROBA spacecraft family.

The strong points are:

Reliable/robust platform

- Five years in orbit and still in excellent shape (original mission: 1 year)

Demonstrated its potential as Earth observation platform:

- Originally pure technology demonstration, but now part of earth observation user programme
- Used on daily basis by ~60 user groups

Autonomous Operation

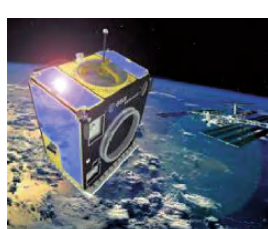
- Onboard Autonomy (orbit & attitude determination, FDIR)
- Ground Segment Automation (low operational cost)
- Simple commanding : 1 image = 1 command (coordinates)
- Performant on-board computer

Fine Pointing & Stability

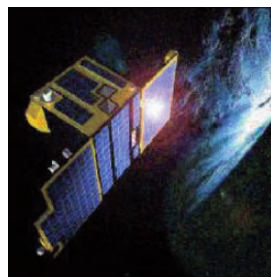
- Agile platform (3-axis stabilized)
- High pointing accuracy
- High pointing Stability (point & stare – snapshot imaging)
- Complex manoeuvring (motion compensation – push broom imaging – multiple backward / forward scanning)

Modularity and flexibility in design

ESA Quality Label



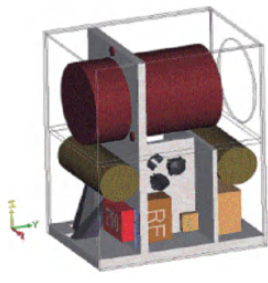
μ G platform



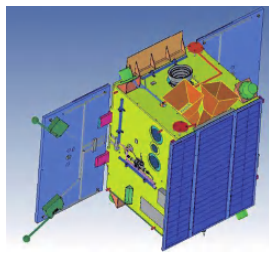
Science mission



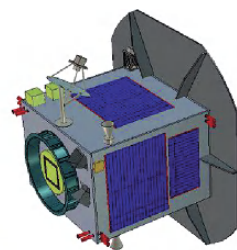
Formation Flying



High-resolution concept



Multispectral mission



Near Earth Object spacecraft

Session 3

Instruments

Small Satellites and Earth Observation Systems for Small Countries and Regions

Annelie Schoenmaker

Abstract Earth Observation (EO) data are useful tools for managing and improving various aspects of regional and national resources. During the summer 2006, 33 students from the International Space University (ISU) worked on a project aiming at making EO accessible to small countries and regions. Although EO programs are costly to initiate, they are often feasible and beneficial for small countries and regions. However an information gap exists between EO providers and decision makers. This is the reason why a prototype software “selection” tool was developed to assist regional and national leaders in determining which EO capabilities are useful to them and how to initiate a program. As small satellites are amongst the cheapest systems to develop and launch, this will often be the preferred option of small countries and regions, and the selection tool is thus likely to bring benefits to the small satellite industry. The region of Catalonia, one of the three test cases studied in the project, is used as example to illustrate this statement.

1 Introduction

Throughout the last several decades, civil Earth Observation programs have become valuable tools for decision makers at various levels. Examples of such decision makers include resource managers, urban and regional planners; agricultural producers and disaster first responders. Examples of EO applications include facilitating public services and natural resource management. Earth Observation data can be especially useful for small countries and regions in assisting their future development. However a gap often exists between the capabilities of EO systems to serve applications and the knowledge base of decision makers about EO capabilities, especially at the level of small countries and regions. EO programs are often technologically complex and costly to initiate and are therefore difficult to develop with the limited budget of a small country or region. However, in some cases, small countries and regions that

A. Schoenmaker

International Space University, Strasbourg Central Campus, 1 rue Jean-Dominique Cassini,
Parc d’Innovation, 67400 Illkirch-Graffenstaden, France
e-mail: schoenmaker@isu.isunet.edu

carefully investigate and develop EO programs can establish their own EO programs despite the cost and complexity issues. Alternatively, cooperation between regions or small countries can allow regions to overcome resource constraints and lack of expertise to harness the potential of these powerful technologies. Small countries and regions establishing EO capacity, whether they are cooperating or not, must determine the most cost-effective way of implementing this capacity. Several options exist for these actors to take full advantage of EO technology to answer their needs. Amongst them, buying existing data, obtaining data free of charge or commercially, or developing their own system, are the most realistic ones. Developing a space-based system for a small country or region with a limited budget almost automatically implies small satellites.

2 The Sol Project

Thirty-three students of the International Space University (ISU), from sixteen different countries, during the Summer Session Program (SSP) 2006, worked on this issue and completed a project named SOL (Système d'Observation Locale or Local Observation System)[1]. To bridge the identified gap between EO providers, who possess the data, and decision makers, who could apply the information, the project developed a prototype software “selection” tool, using background information and expertise about EO operating at regional scales, that would assist small countries and regions in identifying options for the most useful and cost-effective EO programs. The prototype was developed using three test cases that have shown an interest in developing an EO program: Catalonia, Spain; Alsace, France; and the Island of Mauritius.

Earth observations are a technologically complex and costly set of tools that can be instituted effectively for small countries and regions, if developed appropriately. Five major, non-exclusive options for developing EO capacity were identified:

1. Obtain EO data from existing aerial and satellite EO data providers;
2. Establish aerial EO programs;
3. Develop locally owned and operated satellite EO systems (small satellites);
4. Create a data processing centre that converts data to information for decision makers; or
5. Any or all of the above in cooperation with another small country or region.

EO developers must assess the applications, needs, technical capabilities, and policy and legal implications of using the technology. Developing an Earth Observation project is a truly interdisciplinary work, and this is how this project was put together.

The following figures show how the same EO process can be seen from different perspectives: technical and financial.

Indeed, the technical process is a very important aspect of an EO system, but a country or region envisaging building its own EO system should not overlook

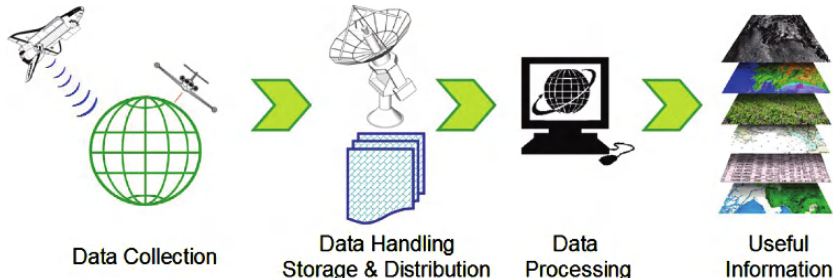


Fig. 1 EO process flow

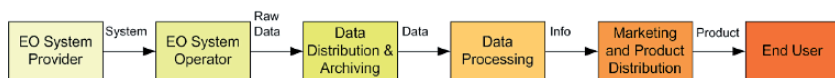


Fig. 2 EO value chain

the importance of other aspects of the program. An understanding of the financial considerations for EO programs is one of the most essential points. A proposed value chain for EO systems, from the EO provider and to the end users who exploit the information is shown in Fig. 2. The principal concepts applied to the value chain are the EO ventures analyzed, cost estimating methods and financing options.

When a small country or region develops EO programs, the national and international policies and legal framework for space should also be considered, in concert with the technological development path and program financing. EO system licensing and data access policies are particularly important because, if ignored, they can obstruct the users' ability to obtain data.

Given this technological, financial and legal context for EO program development, small countries and regions are often best served by employing a cooperative model, e.g. public-private-partnership (PPP). Using a cooperative model, small countries and regions can overcome obstacles and develop EO programs that meet the specific needs of the region.

The SOL project encompasses all these different aspects of EO to find out the best options for small countries or regions, whose decision makers are the targets of this study. Apart from providing an interdisciplinary background in Earth Observations the project also includes three test cases and the idea of a tool, which will be discussed next.

3 Catalonia as a Test Case

The example of Catalonia, an autonomous community of Spain, is the best suited example amongst the test cases studied, to illustrate the importance of small satellite technology in small countries and regions. The local economy of Catalonia is highly

dependent on tourism and industry. Agriculture, including viticulture and cereals, is also an important factor for the economy. Currently, private industry and academic research centers comprise the extent of EO capabilities in Catalonia; however, interest in expanding EO capability locally has grown recently. This project has identified an opportunity for Catalonia to consider developing a regional EO system to stimulate local industry and to improve the use of EO for current and future applications.

EO can be useful in Catalonia for viticulture, mapping, environmental monitoring, disaster management, and humanitarian aid. Catalonia is currently using EO data for some applications, but the region could further capitalize on EO technology and build capacity in EO system development.

Given the current capacity and the potential budget for EO systems, a small dedicated satellite is one viable option for Catalonia. Such a system could satisfy some of the technical EO needs (*e.g.*, high spatial resolution) for the applications identified above. Discussions between the SOL students and the regional industry resulted in an estimated budget of 12 M€ for the region for the test case, taking into account possible future cooperation with other regions.

Different sectors where EO could be useful for Catalonia have been analyzed, starting with vineyards. The analysis of the density and vigor of the vine canopy is an essential tool to assess the yield and quality of the wine. To achieve such target, a minimum spatial resolution of at least 1.5 m is required, regardless of the temporal and radiometric resolution constraints. This requirement is driven by the conventional vineyard row spacing.

Considering current available technology and the proposed budget cap of 12 M€, one of the options is the use of a multispectral RALCam1 sensor running on a microsatellite platform, with a maximum resolution of 2.5 m. Unfortunately this resolution does not provide sufficient resolution for the development of precise viticulture. Therefore, another proposed option which should supplement the space-based solutions is based on airborne systems in combination with on-site ground observations. A CASI (Compact Airborne Spectrographic Imager) sensor could be installed in an airplane to do the observations. This sensor is an optical multispectral sensor, offering a typical spatial resolution below 1 m, depending on the flight altitude.

Concerning environmental applications, there is a wide range of EO applications that could be tackled by means of different solutions (space-, airborne- or ground-based), and within the set budget constraints. Considering the general approach of this particular example, the possible solutions are very broad. One of the alternatives would be to buy data from the huge number of currently orbiting satellites and sensing systems scattered around the world. Another possibility would be to make use of airborne systems in combination with on-site ground observations.

A feasible space-based solution could be based on the use of a micro-satellite, with medium-to-high resolution sensors. An example of implementation would be the use of a suitable platform to be integrated in the DMC-2 constellation, with a CHRIS sensor achieving spatial resolutions of about 17 m. With this proposed system operating in LEO orbits, a vast range of applications could be developed, as is the case of mapping and monitoring to assess the change of the territory over time, precision agriculture, urban planning in coastal areas to avoid denaturalization

of the seashore, forestry, water shed control, wetlands monitoring in the Ebro river delta, coastal erosion control, snow measurement in the Pyrenees, etc.



Fig. 3 Ebro river delta [2]

Although this proposal is just one of the possible solutions, it is interesting to note the recent signing of a contract between the Spanish company, Deimos Imaging, and Surrey Satellite Technology Limited (SSTL) on the DEIMOS satellite to be added to the DMC constellation.

This new development is very encouraging for the small satellite industry in Spain, and is related to the third important application in Catalonia: Disaster management. In this case, the SOL report advised that the revisit time of the EO systems should be relatively short. Revisiting times below one or two days would be desired for a proper management of river flooding, as well as for the identification of the current state of infrastructures under the effects of any natural disaster of short life time. That is why any new satellite should be integrated into an already flying constellation, such as DMC. The same kind of micro-satellite could be used by Catalonia for mapping purposes.

After this analysis it is thus striking to see all the possible applications of the capabilities of a micro-satellite in this region, whilst staying in a limited budget.

These proposed systems would however be best developed in cooperation with other regions or countries in order to facilitate technology transfer, to encourage political ties between regions, to improve EO system capabilities (*e.g.*, revisit time), and to offset some of the system construction and operational costs. This is an aspect that is now being addressed by Deimos Imaging by entering into the DMC constellation.

EO capacity building in Catalonia could result in valuable economic and social spin-offs for the region. High-tech EO systems can be beneficial for the local economy by stimulating economic growth, industry, commercial development, and fostering new ventures in EO. This would occur if Catalonia began developing its own satellites or if the region established other EO competencies. A data processing center, for example, could serve regional data processing needs, stimulate revenues for the region, and provide a mechanism for Catalonia to assist other regions in harnessing the potential benefits from EO. A center of this type could be based on a public-private partnership (PPP) model. EO capacity building in Catalonia could also encourage scientific and technology competitiveness and promote scientific education.

This detailed analysis of one particular region was carried out in order to show the different options to use EO for a small country or region but also to show the parameters that the future “EO decision tool” would take into account to help decision-makers.

4 EO Decision Software

The identified gap between the knowledge of EO providers and decision makers about EO systems, and the conclusion that each region or country has specific needs, led the group to develop a prototype software named SOL Selection Tool (SOLST).

The idea of this tool came after assessing the existence of tools such as GEOSS. GEOSS is a project that attempts to centralize the existing EO databases in order to facilitate gap analysis in available data and enhance dissemination and sharing of existing EO data. However the scope of GEOSS is limited to sharing observational data and connecting information from separate sources. The usefulness of the GEOSS centralized database will be limited to experienced users that have already identified the datasets that they need. Accessing GEOSS requires technical expertise in EO technology; potential users need a simple tool to help them target needed data and assess the cost. As a result, the need to map and centralize existing technologies, research centers, and added-value actors remains despite the more recent efforts. A tool such as SOLST could assist users to target the appropriate options of datasets for a particular application or interest. This issue is pressing for small regions and countries with limited resources. The restricted financial capacity places emphasis on a tool that can facilitate a search for existing and future EO tools, giving preferential consideration to cooperation models with other participants in EO.

The system architecture of the proposed tool is composed of databases, an electronic interface, and linkages between the databases and interface. The databases consist of specific information about EO applications, data types and availability, and estimated system and data costs. These databases link together in such a way that multiple outputs can be selected, depending on the level of detail sought by the tool user. The tool selects EO options with a set of criteria like budget, technical requirements, applications, and cooperation opportunities. The criteria are not ranked by order of importance. The outputs serve as options for the EO system and/or data that are recommended for the region and the application being investigated.

The intentions of the user are divided into three main options: building a system; searching for datasets; searching for added-value services (*e.g.*, data processing know-how). A combination of these three options could be selected. A cooperation entry can lead to both an output tutorial on cooperative models and an access to posted inquiries. The four entries can be independently left blank if unknown by the user. If all are left blank, the user will be directed to a high level introduction to EO applications and its potential.

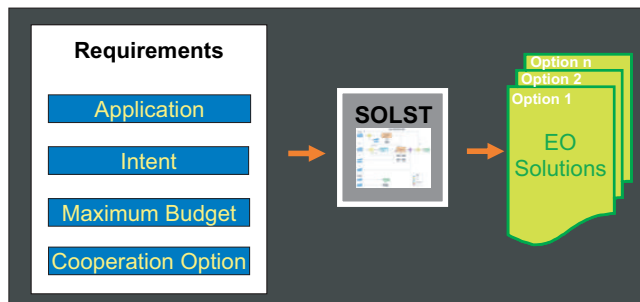


Fig. 4 SOLST methodology

Organizing and centralizing the applications, platforms, sensors, and data sources is an essential first step in helping local decision makers and potential users. A search and selection tool can help accomplish this. SOLST would be a tool that accesses a centralized database listing EO users, applications, available and emerging technologies, and EO databases such as the GEOSS database.

The beneficiaries of SOLST could include decision makers at different levels, technical EO users, and small countries and regions that are open to collaboration. The primary objectives of SOLST are:

- To increase the awareness of the potential of EO through a high level introduction and application-based description;
- To bridge the gap between the potential users of EO systems;
- To provide an initial set of available EO options based on user selection criteria, and to give a preliminary overview of options prior to making a local or global decision;
- To guide small countries or regions through the decision-making process by facilitating the identification and definition of an EO system that meets their needs;
- To enhance collaboration options particularly for small countries or regions through the use of a Forum and a posted inquiries compartment; and
- To provide technical EO users an accessible database of EO systems.

SOLST incorporates three primary functions. Apart from the search selection tool, an information request option and a forum section should also be included, to answer the needs of the users that are not met in the tool itself. For example it will allow them to ask for a summary describing the legal aspects of remote sensing, or to interact with other users of the tool to enhance communication and help cooperation.

Several implementation and maintenance options for the tool have been proposed and a prototype database has been constructed. However, this needs further and long-term development and testing to evolve in an operational tool.

5 Benefits of the Project for Small Satellites

The importance of the tool for small satellites is non negligible. First, it would increase the awareness of decision makers about the capabilities of small satellite technology and therefore increase the demand. For a region like Catalonia, which already has an interest in Earth Observation technology, the tool mainly confirms the option that a small satellite would best suit their needs. It adds however that cooperation would be the best way to go about it, and gives an approximation of the total cost that would have to be invested in such a system. This rapidly accessible information might quicken the process for local decision-makers. The EO documents available in the tool also give them information about already existing small satellite programs. In this case the tool gives an easy access to information about the sought after technology. In other cases, the tool and the available EO introductory documents might be the first exposure a user has to EO and small satellite technology. The tool would then fulfill its mission of increasing awareness amongst worldwide decision makers about EO, and in this case small satellites. Increasing awareness and giving easy access to information will surely help increase the demand for small satellites but also improve the technology, as a variety of payloads might be carried on small satellites. As mentioned earlier, cooperation is often the most reliable and realistic way for small countries and regions to gain access to EO data, and this seems to be favorable to small satellites as well. Surrey Satellite Technology Limited (SSTL) is a good example of a cooperative venture that led to the development, building and launching of several identical small satellites.

Second the tool will help in addressing the limitations of small satellites by emphasizing possible trade-offs. For small countries or regions, budget, technical capability and human resources are critical factors. As mentioned before, a small satellite will not usually be feasible for them; cooperation with other entities will allow them to spread the costs and the risks and to take advantage of a range of sensors or resolutions even if they develop only one themselves.

Third, some specific programs involving small satellite technology such as Know-How Transfer programs and Rent-a-Sat options seem to prove to be very well adapted to the needs of small countries and regions, as they are solutions both to lack of capacity and lack of funds, two of the main issues for small countries and regions.

6 Conclusion

EO is a powerful tool that has great potential for assisting with environmental management and other important applications for small countries and regions. The SOL project is a proposal for EO capacity building in terms of the unique circumstances

of small countries and regions. The utility of EO for such countries and regions, however, rests on the ability of an organizing body for the EO program to identify and select the most suitable option(s) for EO in the region. This selection must fall within the technical and budgetary constraints, which are case specific. Combining cooperation and small satellites is here often a winning solution.

To assist in identifying and selecting the best option for the small countries and regions, this project has identified one method and illustrated that method using the SOLST prototype. In the long term, it is proposed that this method and prototype be developed in conjunction with other initiatives that are attempting to facilitate this type of EO program decision.

References

1. International Space University, *SOL*, Strasbourg, 2006
2. Image courtesy: NASA Earth Observatory

Development of a High-Performance Optical System for Small Satellites

Young-Wan Choi, Seung-Uk Yang, Myung-Seok Kang, and Ee-Eul Kim

Abstract Funded by the Ministry of Commerce, Industry, and Energy of Korea, Satrec Initiative has initiated the development of the prototype model of a TMA-based electro-optical system as part of the national space research and development program. Its optical aperture diameter is 120 mm, the effective focal length is 462 mm, and its full field-of-view is 5.08 degrees. The dimension is about 600mm × 400mm × 400mm and its weight is less than 15 kg.

To demonstrate its performance and versatility, hyper-spectral imaging using a linear spectral filter was chosen as the application of the prototype. The spectral resolution will be less than 10 nm and the number of channels will be more than 40 in visible and near-infrared region.

In this paper, the progress made so far on the prototype development and the future plan will be presented.

1 Introduction

Satrec Initiative (SI) has continued the development of new technology for electro-optical sensor systems for several Earth observation missions using small satellites. Recently, the technology development efforts within SI have been focused on advanced optical and opto-mechanical systems to meet the increasing demand from

Y.-W. Choi

Satrec Initiative, 461-26 Jeonmin-Dong, Yuseong-Gu, Daejeon 305-811, Republic of Korea

S.-U. Yang

Satrec Initiative, 461-26 Jeonmin-Dong, Yuseong-Gu, Daejeon 305-811, Republic of Korea

M.-S. Kang

Satrec Initiative, 461-26 Jeonmin-Dong, Yuseong-Gu, Daejeon 305-811, Republic of Korea

E.-E. Kim

Satrec Initiative, 461-26 Jeonmin-Dong, Yuseong-Gu, Daejeon 305-811, Republic of Korea

e-mail: eek@satreci.com

scientific and remote sensing communities. Funded by the Ministry of Commerce, Industry, and Energy of Korea in 2005, SI has initiated the development of the prototype model of an advanced high-performance optical system, the TIS system as part of the national space research and development program.

The TIS system is designed to be versatile with a wide field-of-view, no obscuration, and no refractive element. Therefore, it can be used for various missions such as super-swath imaging, hyper-spectral imaging, infrared imaging, and aerial imaging. In addition, its compactness and light weight are ideal for small satellites.

The development of two prototype models is planned together with a field test for each model. The progress made so far on the 1st prototype development will be presented: optical design, analysis, and manufacturing; opto-mechanical design, analysis, and manufacturing; and demonstration of hyper-spectral imaging.

2 System Overview

The TIS system is based on an un-obscured three-mirror-anastigmat (TMA) telescope that consists of three mirrors. The optical design was simplified to use an on-axis spherical secondary mirror. The primary and tertiary mirrors are off-axis segmented aspheric mirrors. Its optical aperture is 120 mm, its effective focal length is 462 mm, and its full field-of-view is 5.08 degrees. It has a box-type structure with a dimension of 600mm × 400mm × 400mm and the weight is less than 15 kg.

The key features of the TIS system are listed in Table 1. As can be seen in Table 1, the TIS system is designed for dual applications of high-resolution panchromatic (PAN) imaging and hyper-spectral (HS) imaging. The ground sample distance (GSD) at 470 km altitude is 5 m for a PAN and 15 m for HS imaging channels. The spectral band range is from 450 to 890 nm and the spectral resolution is less than 10 nm for HS channels. The number of HS channels is more than 40.

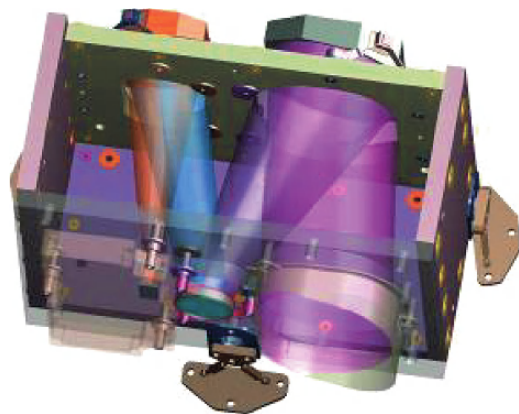
Table 1 Key features of TIS 1st prototype model

| Clear Aperture Size | | 120 mm | | | |
|------------------------------|-----------------------|---------|--------------|--|--|
| Number of Imaging channels | | PAN | 1 | | |
| | | HS | ≥ 40 | | |
| GSD (m) @ 470 km | | PAN | 5 m | | |
| | | HS | 15 m | | |
| Swath width @ 470 km | | ≥ 40 km | | | |
| MTF (%) | | PAN | ≥ 10 | | |
| | | HS | ≥ 20 | | |
| Spectral Range | | PAN | 500 ~ 700 nm | | |
| | | HS | 450 ~ 890 nm | | |
| Spectral Resolution for H-ch | | ≤ 10 nm | | | |
| Dimension | 600mm × 400mm × 400mm | | | | |
| Weight | ≤ 15 kg | | | | |

Fig. 1 Front view of 1st TIS Telescope



Fig. 2 Exploded view of 1st TIS Telescope



The box-type structure of the TIS system is based on honeycomb panels with composite face-sheets designed to minimize mass and to have enough stiffness. The reference planes for the optical surfaces are implemented with invar inserts through the honeycomb panels.

The spectrometer of the TIS system is implemented with a linear variable filter (LVF) on a two-dimensional detector array instead of conventional dispersive elements such as prism and grating. The spectral resolution is less than 10 nm, typically less than 1% of central wavelength over $450 \sim 890$ nm spectral range.

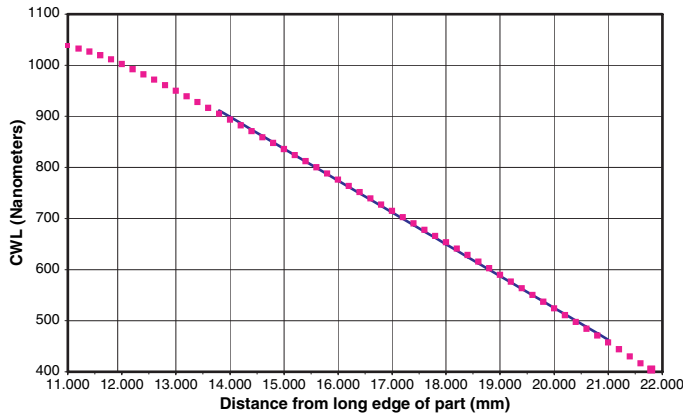


Fig. 3 Spectral range, dispersion and linearity of LVF

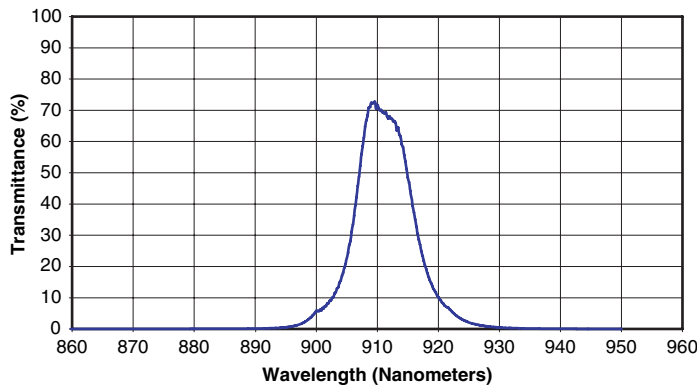


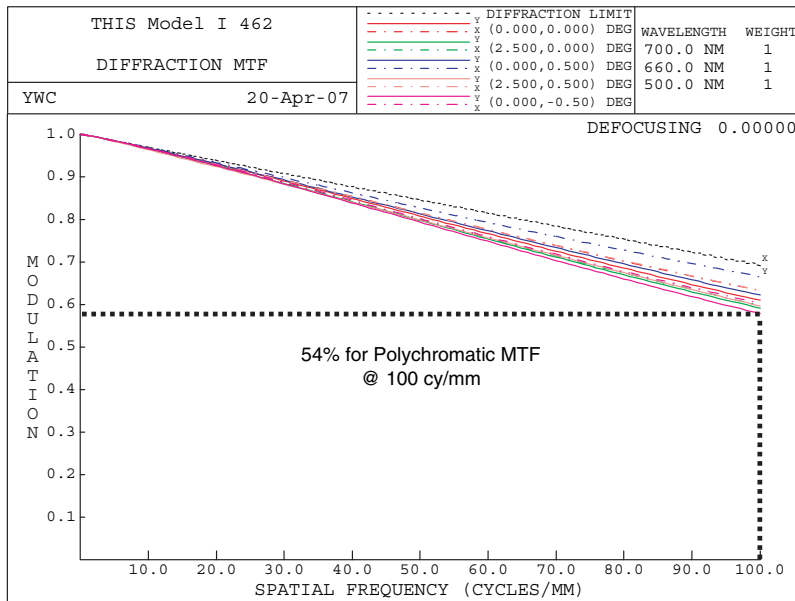
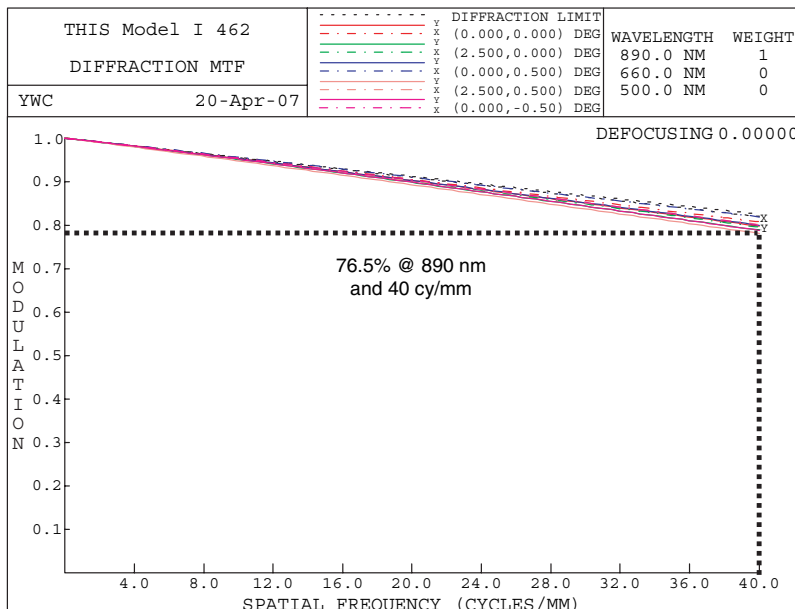
Fig. 4 Spectral resolution and transmittance of LVF at 910 nm

3 Development of Prototype Model

3.1 Optical Design and Analysis

The optical design of the TIS system has two advantages compared with conventional TMA designs: manufacturing and alignment. Using aspheric surfaces for an optical system usually gives high performance but, it will increase the manufacturing cost and needs a complex alignment process. To minimize the manufacturing cost and to make the alignment process simpler, the secondary mirror of the TIS system is an on-axis spherical mirror and the tertiary mirror has a small deviation from a spherical surface.

The primary mirror has a hyperbolic surface of conic constant of about -1.3 and the tertiary mirror has an oblate elliptical surface of conic constant of about 0.2 .

**Fig. 5** MTF estimation for PAN band**Fig. 6** MTF estimation for 890 nm

These two mirrors are manufactured to have a surface quality of $\lambda/17$ rms and the secondary mirror of $\lambda/10$ PV at λ of 632.8 nm.

The design MTF (modulation transfer function) is estimated to be more than 54% at 100 cycles per mm for the panchromatic band and is more than 76% at 40 cycles per mm for 890 nm. The design MTF at shorter wavelength is higher than that of 890 nm.

To predict the telescope performance, a tolerance analysis is performed in wavefront error (WFE) and MTF. The tolerance analysis includes manufacturing, assembly, and alignment errors. The parameters used for the analysis includes the surface quality of mirrors. The analysis shows a wavefront error of 0.149λ at the corner of the image plane and the panchromatic MTF of 34% in across-track and 32% in along-track direction at 100 cycles per mm. If the detector MTF is assumed to be 45%, the TIS system will give MTF values of 15.3 and 14.4% in across and along-track directions, respectively.

3.2 Alignment of Optics

The alignment of the telescope started with the precision installation of the tertiary mirror (M3) with respect to the primary mirror (M1). From the tolerance analysis, the alignment result showed that the installation of M3 was successful within 100 μm for de-center and 10 arc-min for tilt.

The secondary mirror (M2) was aligned in two steps: coarse alignment and precision alignment. The coarse alignment of M2 was performed with respect to M1 using CMMs (coordinate measurement machines) and alignment telescopes. CMMs were used to correct the M2 de-center and de-space and alignment telescopes to correct the M2 tilt. It is estimated that the coarse alignment of M2 was successful within 50 μm for de-center and 5 arc-min for tilt.

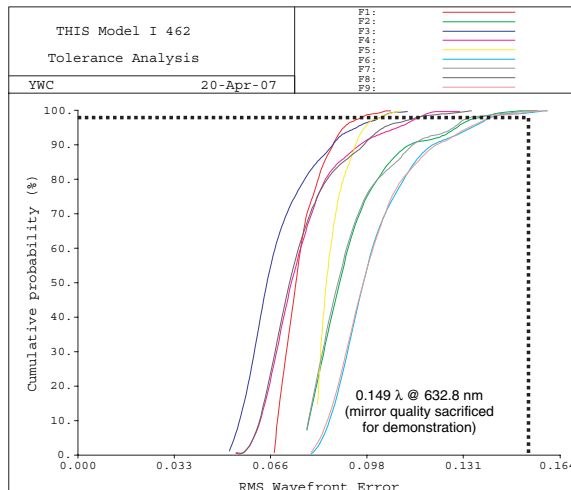


Fig. 7 WFE prediction for secondary mirror alignment

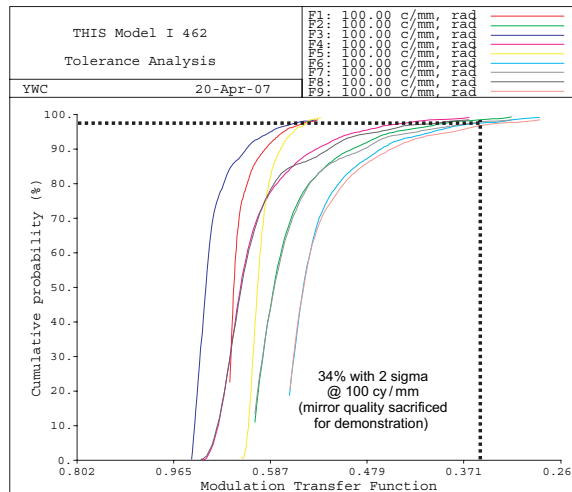


Fig. 8 MTF prediction for PAN in across-track direction

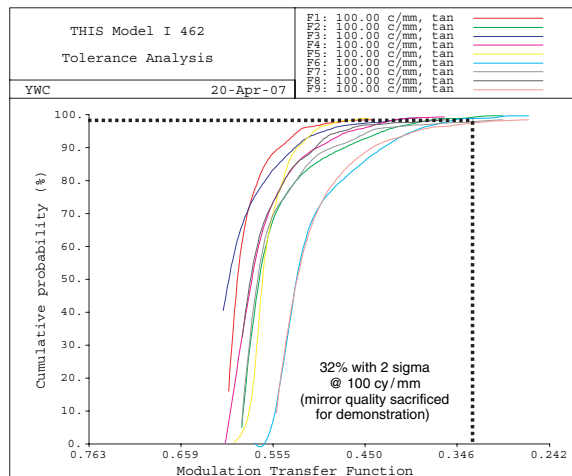


Fig. 9 MTF prediction for PAN in along-track direction

For the precision alignment of M2, a computer-aided alignment (CAA) based on the Zernike sensitivity was planned but it was not successful. It is believed that this was caused by the fact that the Zernike calculation perpendicular to the exit pupil was not correct because the image plane is slanted against the optical axis.

For the precision alignment of M2, the sensitivity of M2 movement was measured. The optimum position and tilt was estimated based on the measured sensitivity. To verify the alignment, a tolerance analysis on WFE and MTF was performed for a monochromatic band (632.8 nm).

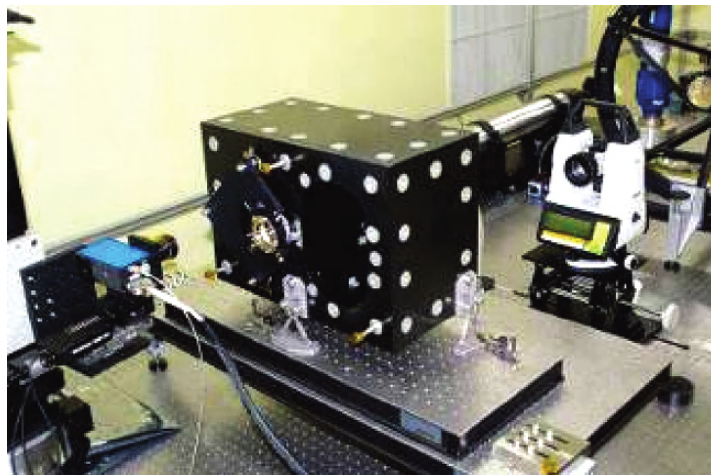


Fig. 10 M2 Alignment

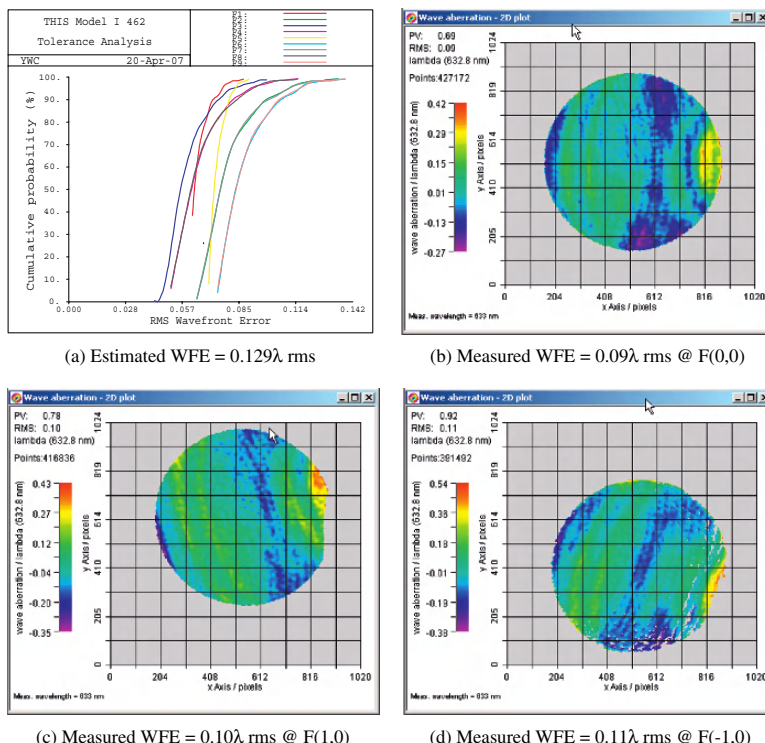


Fig. 11 Estimated and Measured WFE for M2 Alignment (a) Estimated WFE = 0.129λ rms, (b) Measured WFE = 0.09λ rms @ F(0,0), (c) Measured WFE = 0.10λ rms @ F(1,0), (d) Measured WFE = 0.11λ rms @ F(-1,0)

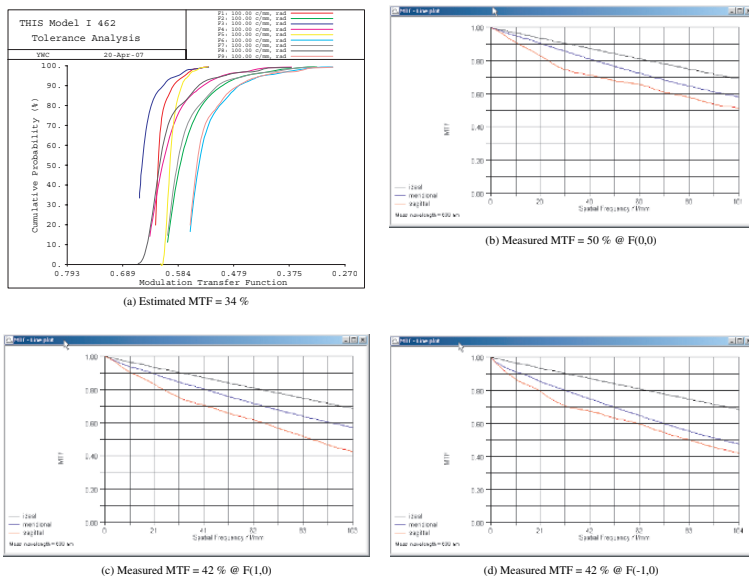


Fig. 12 Estimated and Measured MTF for the Alignment of M2(a) Estimated MTF = 34 %, (b) Measured MTF = 50 % @ F(0,0), (c) Measured MTF = 42 % @ F(1,0), (d) Measured MTF = 42 % @ F(-1,0)

3.3 Structure Verification

A random vibration test for the TIS structure model (SM) was performed before the optical alignment to investigate the structural stiffness and to obtain the notching profile. The first excitation was measured at 130 Hz from the interface flexure of the main structure. Others were measured at frequencies higher than 300 Hz from translational and local motions of the structure and at frequencies higher than 900 Hz for the motion of mirror assemblies.

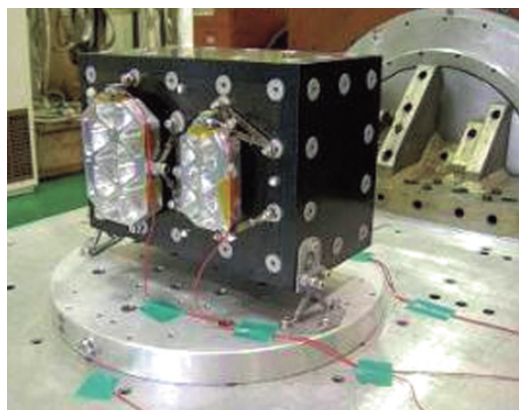


Fig. 13 Random vibration test of SM

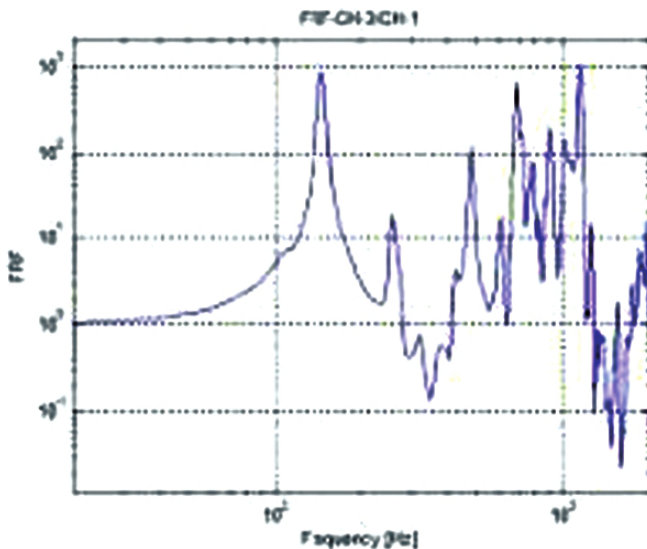


Fig. 14 M1 FRF in Y axis

3.4 Demonstration of Spectrometer

For the verification of the spectrometer of the TIS system, a commercial lens and a target simulator were used. Figure 15 shows the images acquired in the channel 22 (551 nm), 30 (588 nm), 47 (665 nm), and 62 (734 nm).

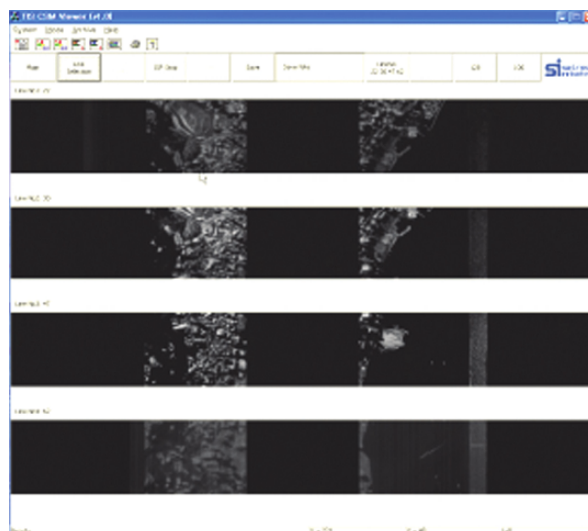


Fig. 15 Demonstration of Spectrometer performance in different channels

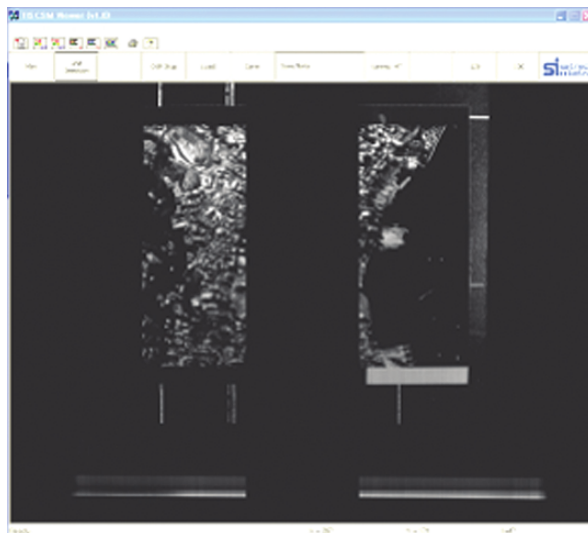


Fig. 16 Image captured in channel 47

4 Future Plan

With the completion of the optical alignment and test for the 1st prototype model, a random vibration test will be performed with actual mirrors in early May, 2007. The development of the 1st prototype model will be completed by the end of August, 2007 with the hyper-spectral imaging demonstration through a field test.

In parallel, the development of 2nd prototype model has been initiated. The 2nd model will have a bigger optical aperture of 150 mm and thus, the complete system will become larger and will give higher performance compared with the 1st model. The 2nd model will give 5 m GSD for one panchromatic and 10 m GSD for four multi-spectral bands at the design orbit of 685 km. The imaging swath width will be larger than 60 km at the design orbit. With the estimated system MTF values of 10% for the panchromatic band and 20% for multi-spectral bands, the 2nd model will produce high-resolution images of high quality.

Comparison of Atmospheric Ozone Measurements Between NASA's Total Ozone Mapping Spectrometer (TOMS) and the FASAT-BRAVO Ozone Mapping Detector (OMAD)

Juan A. Fernandez-Saldivar, Craig I. Underwood, and Stephen Mackin

Abstract The Ozone Layer Monitoring Experiment (OLME) on board the FASAT-Bravo microsatellite, launched in July 1998, observed backscattered UV to retrieve total atmospheric ozone concentrations using two instruments: the Ozone Ultra-violet Backscatter Imager (OUBI) and Ozone Mapping Detector (OMAD). Initial results from this experiment have shown good qualitative agreement with NASA's Total Ozone Mapping Spectrometer (TOMS) [1]. Recent studies on OMAD and TOMS data found quantitative agreement in the radiances and indicated the detection of the volcanic eruption plume of Nyamuragira volcano (due to its sulphur dioxide content) [2].

A new analysis of OMAD data using an improved version of the simplified algorithm to find ozone content has been developed and tested. Multiple days were analysed using composites of up to 15 days and ozone contents ranging from 150 DU to 400 DU. Recent findings indicate a relative error of between 3–10% in the vertical column content of ozone given in Dobson Units (DU) when compared with TOMS-Earth Probe data, depending on the geographical area analysed from the tropics to mid-latitudes.

The results obtained are in good agreement overall, despite the instrumental differences between OMAD and TOMS. The potential of small satellites for atmospheric missions is discussed, including factors to consider when planning such missions.

J.A. Fernandez-Saldivar

Surrey Space Centre, University of Surrey, GU2 7XH
e-mail: j.fernandez@surrey.ac.uk

C.I. Underwood

Surrey Space Centre, University of Surrey, GU2 7XH

S. Mackin

Surrey Satellite Technology Ltd., University of Surrey, GU2 7XH

1 Introduction

In 1994, a collaborative programme was set up between the University of Surrey and the Chilean Air Force (FACH), to design and build a low-cost 50 kg micro-satellite with instrumentation capable of monitoring the distribution and concentration of stratospheric ozone – particularly over Chilean territory. This resulted in the joint design and development of the Ozone Layer Monitoring Experiment (OLME) which was flown on-board the resultant *FASAT-Bravo* micro-satellite, launched in July 1998 into an 820 km altitude Sun-synchronous orbit. The experiment comprised two miniature low-cost instruments: the Ozone Ultraviolet Backscatter Imagers (OUBI), which used a UV-sensitive dye-coated CCD, and the Ozone Mapping Detector (OMAD), which is based on enhanced-UV-sensitive silicon photodiodes. The latter is a 4-channel radiometer with 10-nm resolution bands at 289, 313, 334 and 380 nm working continuously with a Field of View (FOV) of $11^\circ \times 11^\circ$ providing a ground resolution of approximately 150×150 km. Each channel uses a single fused silica anti-reflection coated lens with a focal length of 12.5 mm and an F-number of 1.1. The signals are sampled continuously to 12-bit resolution, and the entire instrument draws only 500 mW when in operation [1].

2 Methodology

The new algorithm obtains empirical factors to derive the total ozone content in the vertical column from the un-calibrated slant column content of the original algorithm. In order to minimise retrieval errors, the factors are derived by restricting the reflectance conditions to 20%, thus ignoring cloudy scenes. Once the factors are derived these are applied to all cloud conditions where we are aware of the errors in determining the ozone content below clouds due to their properties: height and thickness. Tropospheric ozone under the cloud can reach up to ~ 20 DU according to TOMS v.8 L2 products and [2]. The expected errors after the retrieval should be within this error range.

2.1 Reflectivity

The first step in filtering out cloudy scenes requires knowledge of the surface reflectance. The 380 nm surface reflectivity is low (2–8 %) over most surfaces, water and land, the observed reflectivity changes are mostly caused by changes in the amount of snow/ice, cloudiness, and aerosols [3, 4]. Reflectivity is then derived through vicarious calibration between reflectivity data from the TOMS 360 nm channel and the OMAD 380 nm channel, based on radiometric calibration from [5] once the data has been referenced to a common grid (0.125° longitude \times 0.1° latitude).

Once OMAD's reflectivity or albedo is determined, we observe a good linear relation when this is plotted versus TOMS' reflectivity; their cross-correlation is high. The 1-sigma absolute reflectivity error of TOMS minus OMAD reflectivities is in the range between $\sim 3\%$ at the Equator to $\sim 8\%$ near the Poles. This is shown in Fig. 1 below for tropical regions based on 15 days of data taken in October 1998.

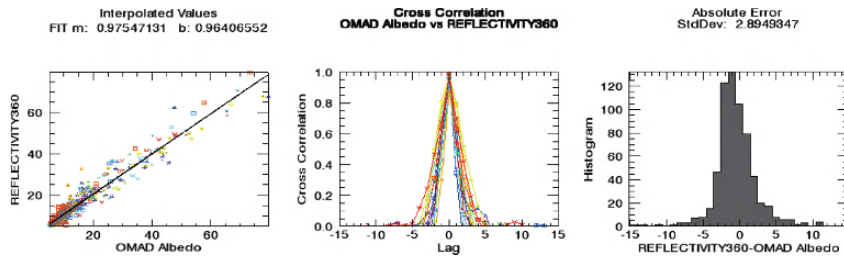


Fig. 1 Relation between OMAD albedo at 380 nm and TOMS reflectivity at 360 nm (left). Cross-correlation (centre) and absolute error (%) (right)

Discrepancies between the two may be explained by taking into account the differences in their wavelengths and spectral bandwidth. Furthermore, the pixel sizes and time of overpass are different accounting for dissimilar cloud fractions covering the scene. Finally aerosols would introduce another variation however those are ignored here. Reflectivity is not directly taken into account in the retrieval procedure but it allows a selection of low cloud cover from where the empirical factors are derived thus the discrepancies just described do not affect the algorithm directly.

2.2 Retrieval Algorithm

The new algorithm is applied to low reflectivity ($<20\%$) scenes representing low or cloud free conditions. Figure 2 shows 15 days of OMAD tracks that meet this condition.

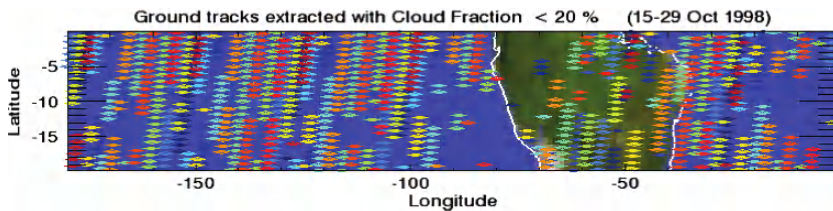


Fig. 2 Ground pixels with cloud fractions $<20\%$ between 15th–29th October 1998

The procedure to retrieve ozone total column content products is detailed below and consists of four basic steps. Firstly, we obtain a slant column amount based on a

logarithmic ratio between two OMAD channels (334-nm and 313 nm). Secondly the geometrical observing conditions are taken into account with the solar zenith angle, this is known as geometrical air mass factor and is then subtracted in its logarithmic form from the slant column. Finally the empirical factors convert this un-calibrated vertical column into a real vertical column content. The algorithm works as follows:

The un-calibrated slant column amount is derived from the initial simplified algorithm based on the estimated radiance from two channels (L_{334} and L_{313}).

$$uO3_{\text{Slant}} = \text{Log}(L_{334}/L_{313}) \quad (1)$$

It is then corrected using a Geometrical Air Mass Factor (GAMF) based on the solar zenith angle (θ) given the observing conditions defined as:

$$\text{GAMF} = 1/\cos(\theta) \quad (2)$$

From (1) and (2), we obtain a representative value of the vertical ozone content OMAD_{O_3} .

$$\text{OMAD}_{\text{O}_3} = uO3_{\text{Slant}} - \text{Log}(\text{GAMF}) \quad (3)$$

In order to obtain the real vertical column content from (3) we used an empirical linear function based on geographical zones

$$\text{O3}_{\text{vertical}} = M_{\text{zone}} * \text{OMAD}_{\text{O}_3} + B_{\text{zone}} \quad (4)$$

Where, M_{zone} is the empirical slope factor for given zone

B_{zone} is the empirical intercept factor for given zone

These two empirical factors allow us to account for various aspects: the most important is due to variations in ozone profiles that normally change with latitude; atmospheric profiles of temperature and pressure also vary with geography and continental/ocean masses. Other aspects include: the different spectral resolution of OMAD, (10 times wider than TOMS-EP) and its ground sample area (also 10 times larger than TOMS) and the fact that OMAD is nadir-only viewing, whilst TOMS scans across-track, which also affects the air mass factor.

3 Empirical Function

Twelve regions were defined for analysis based mainly on solar angle conditions and geographical zones. Even though it seems a rather arbitrary designation, the purpose is to have multiple reduced datasets with similar ozone profile and content for each zone. This consideration also excludes the latitudes closer to the poles since these areas have the most extreme conditions on solar angle, radiance values and ozone

content; polar regions would need a different analysis. The evaluated regions are illustrated in Fig. 3 showing a monthly ozone climatology of the average column content during the period under analysis (October 1998).

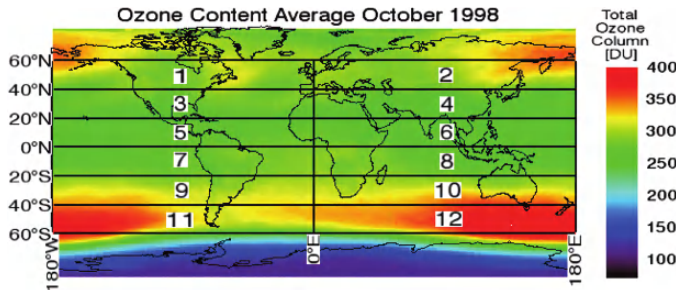


Fig. 3 Ozone content average October 1998

The factors for the empirical function described in (4) are obtained by analysing, on various days, the linear relation between the OMAD representative value of ozone content given by (3) and TOMS total ozone column content from version 8 of the processing algorithm.

The scatter plot OMAD vs TOMS and a linear fit with 5% error bars are shown in Fig. 4 for various days obtaining the corresponding daily M_{day} and B_{day} parameters. All analysed days show a similar linear trend and most data points fall within the 5% error for the daily fit. However, it is desired to have single linear parameters M and B that would apply to all days, these will be the final empirical parameters described in (4).

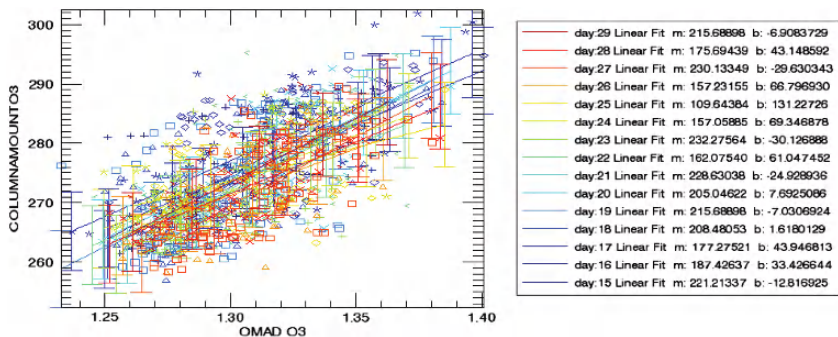


Fig. 4 Linear fits for days under analysis with their M and B parameters

For the complete dataset of all zones and all days, the M and B parameters were obtained. The temporal and regional dimensions were analysed considering the variations of these parameters represented in the contour maps shown in Fig. 5.

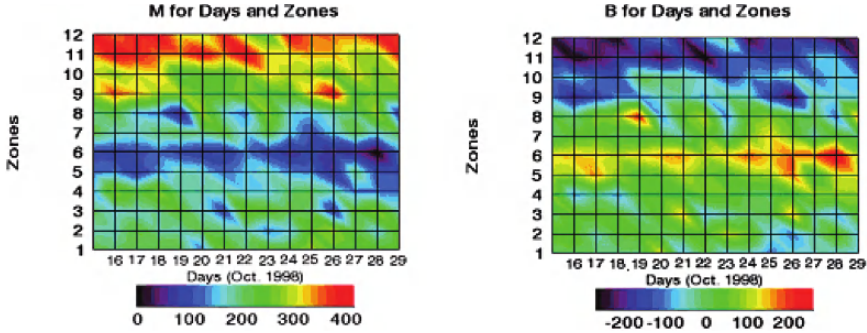


Fig. 5 (left) M factor and B factor (right) for days vs zones

The lowest M parameters (~ 100) are centred on equatorial regions and they reach the maximum of (~ 400) in southernmost regions 11 and 12. This would be a rather large variation in slope (M) if we do not take into account that the intercept (B) parameter behaves somehow inversely having the lowest values (~ -200) in the southernmost regions. This is partly due to the fitting method resulting in certain coupling between M and B; nonetheless this is useful for deriving the other by having defined one of them once proper relationship between them is identified.

In order to help the definition of regional parameters, the corresponding 1-sigma uncertainty estimates of each parameter the fit are included so that the best daily fits are weighted accordingly before obtaining their regional representatives for all those days.

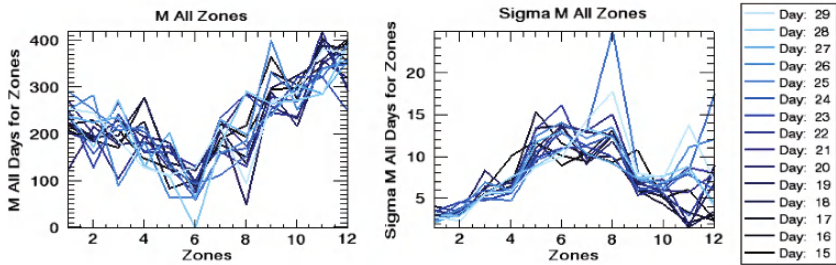


Fig. 6 (left) M factor and 1-sigma uncertainty of M factor (right) for the considered zones

The M parameter and its 1-sigma uncertainty for each day analysed are shown in Fig. 6 above. A trend is observed throughout the days indicating the validity of the empirical parameters to represent each zone condition. The M-parameter trend is non-symmetrical with respect to the equator neither to the solar angle indicating the different ozone profiles for each region. The sigma-M also shows a trend that is somehow symmetrical with respect to the equatorial zones except in the southernmost regions where an ozone hole condition normally develops around this time of year.

The uncertainties of the fit are explained by the different conditions over the regions where the overpass occurred on a specific day. In order to get day-independent representative regional parameters, an average of the M-parameter is obtained with 10 out of 15 days when the uncertainty estimates are lowest; a representative value is then obtained and the B-parameter is derived from there through the coupling between them. Figure 7 below shows a linear relationship between these two parameters for all zones.

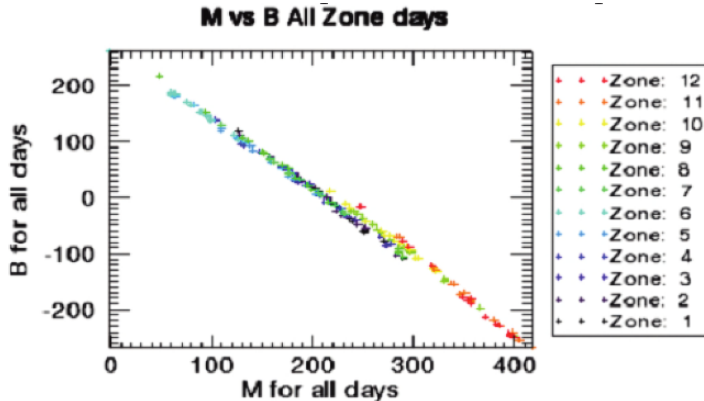


Fig. 7 Linear relationship between M and B parameters for all zones

4 Results

Once the empirical M and B parameters were obtained, these were then applied to all days under analysis for each zone taking into account all reflectances and not just the ones <20% from where parameters were derived.

As an example, zone 7 shown in Fig. 2 is analysed below (Fig. 8) with its corresponding factors. On the left plot, data points are scattered but clustered around the fitted line mostly within the 5% error bars. On the right plot, the histogram shows the daily relative error between OMAD and TOMS for the period under analysis.

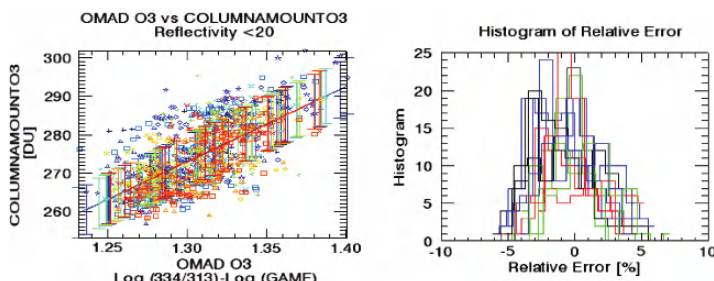


Fig. 8 Representative ozone value from (2) and (right) its correlation for zone 7

The same analysis is carried out for all zones with consistent results. Knowing that higher reflectances will introduce an error due to the unaccounted ozone below the cloud, another analysis was carried out expecting the errors to be reduced as the data points were constrained to reflectivities below 20%, 30%, 40% and 50%. The parameters used are the same as before but the number of data points included varies.

Table 1 shows the results of the four different reflectance limits considered and the empirical factors used. Errors are lowest near equatorial regions where the smallest solar angle occurs; as we get closer to the poles the GAMF increases and the errors increase accordingly.

Table 1 Relative error and corresponding histogram for zone 7

| Zones | M | B | Absolute 1-Sigma Error in OMAD O3 [DU] | | | | Relative 1-Sigma Error in OMAD O3 [%] | | | |
|-----------------------------------|---------|----------|---|--------------|--------------|-------------|--|--------------|--------------|--------------|
| | | | 50% | 40% | 30% | 20% | 50% | 40% | 30% | 20% |
| Reflectivity | 20% | 20% | | | | | | | | |
| 1 | 227.927 | -24.259 | 14.16 | 12.72 | 10.59 | 7.87 | 4.70 | 4.23 | 3.53 | 2.68 |
| 2 | 201.325 | 12.036 | 14.52 | 13.00 | 14.11 | 9.20 | 4.91 | 4.41 | 3.85 | 3.23 |
| 3 | 213.459 | -3.531 | 12.09 | 11.12 | 10.14 | 8.49 | 4.50 | 4.13 | 3.75 | 3.16 |
| 4 | 187.006 | 26.741 | 10.97 | 10.42 | 9.75 | 8.34 | 3.96 | 3.77 | 3.54 | 3.05 |
| 5 | 145.384 | 78.466 | 5.60 | 5.50 | 5.28 | 4.72 | 2.10 | 2.06 | 1.98 | 1.78 |
| 6 | 80.232 | 161.690 | 6.42 | 6.44 | 6.41 | 5.88 | 2.41 | 2.42 | 2.41 | 2.21 |
| 7 | 195.810 | 18.558 | 9.33 | 9.15 | 8.32 | 7.33 | 3.31 | 3.20 | 2.99 | 2.66 |
| 8 | 191.104 | 26.172 | 7.14 | 6.99 | 6.71 | 6.32 | 2.58 | 2.53 | 2.43 | 2.30 |
| 9 | 289.933 | -92.257 | 13.96 | 13.09 | 11.86 | 9.56 | 4.34 | 4.09 | 3.75 | 3.11 |
| 10 | 278.727 | -74.309 | 13.70 | 13.16 | 12.27 | 11.06 | 4.42 | 4.26 | 4.00 | 3.65 |
| 11 | 351.321 | -177.655 | 16.00 | 14.56 | 12.41 | 14.91 | 4.66 | 4.15 | 3.46 | 4.06 |
| 12 | 365.279 | -199.791 | 16.95 | 15.65 | 13.92 | 9.07 | 5.14 | 4.79 | 4.30 | 2.93 |
| All Regions Average Errors | | | 11.74 | 10.98 | 10.15 | 8.56 | 3.92% | 3.67% | 3.33% | 2.90% |

Both absolute and relative errors are reduced as the reflectivity limit decreases. The absolute 1-sigma error decreases from ~ 20 DU when all zones are averaged with no reflectivity constraints (i.e. all data points considered) to a minimum of 8.56 [DU] when the <20% reflectivity limit is considered. These figures are in agreement with the typical amounts of ozone in the troposphere below the cloud mentioned in section 2. On the other hand, the relative 1-sigma errors drop from $\sim 10\%$ for the unconstrained case to 2.9% for the lowest reflectivity constraint.

5 Conclusions

The new algorithm under development, despite the rather large and inhomogeneous zones, offers a significant improvement over its predecessor thus extending the previously known capabilities of micro-satellites for atmospheric remote sensing. The errors between OMAD and TOMS are explained by changes in real cloud fraction due to difference timing of overpasses and also the determination of ground reflectance for different viewing conditions.

The days and zones analysed here, even though they represent a relatively narrow window to observe the complex ozone dynamics, nevertheless provide an insight into the processing required to obtain valuable scientific data at low-cost and without the heavy computational burden required by recursive radiative transfer methods. Because of the temporal variations of ozone, further analyses are required for other months and also polar regions need to be included in order to observe phenomena such as the known ozone hole development. This region is likely to need special treatment due to the extremely low solar elevation angles encountered.

Acknowledgement The authors would like to thank the Royal Academy of Engineering, CONACYT and SSTL for their financial support. We would also like to acknowledge and thank the original FASAT-Bravo Team and the Chilean Airforce (FACH).

References

1. Underwood, C., Valenzuela, A., Schoenherr, M., Arancibia, M., Fouquet, M., *Initial in-orbit results from a low-cost atmospheric ozone monitor operating on board the FASat-Bravo microsatellite*. Philosophical Transactions Of The Royal Society A, 2003. **361**: pp. 71–76.
2. Newchurch, M.J., Liu, X., Kim, J.H., Bhartia, P.K., *On the accuracy of Total Ozone Mapping Spectrometer retrievals over tropical cloudy regions*. Journal of Geophysical Research, 2001. **106**(23): pp. 32315–32326.
3. Herman, J.R., Celarier, E., *Earth's surface reflectivity climatology at 340–380 nm from TOMS data*. Journal of Geophysical Research, 1997. **102**(28): pp. 003–012.
4. Herman, J.R., Larko, E., Celarier, E., Ziemke, K., *Changes in the Earth's UV reflectivity from the surface clouds, and aerosols*. Journal of Geophysical Research, 2001. **106**(6): pp. 5353–5368.
5. Fernandez-Saldivar, J.A., Underwood, C.I., Mackin, S. Low-cost microsatellite UV instrument suite for monitoring ozone and volcanic sulphur dioxide. in *Remote Sensing of Clouds and the Atmosphere XI*. 2006. Stockholm, Sweden: SPIE.

Session 4

Constellations

Serious Microsats Need Serious Instruments, MIBS and the First Results

J. Leijtens, B. de Goeij, E. van der Meché, M. Eschen, and A. Court

Abstract To go beyond the point where micro satellites are seen as a way to qualify technology for use on a “real” satellite, small instruments are needed that can perform a socially or scientifically significant task. MIBS is a spectrometer operating in the thermal infrared wavelength region, designed in the frame of the phase A study for the ESA EarthCARE mission, which uses an uncooled 2D microbolometer array detector instead of the more common MCT detectors, which allows for a significant reduction in size, and power consumption. Although the detectivity of microbolometers is less than for MCT detectors, they offer specific advantages due to the wider wavelength response, which can be tailored to suit the application. This allows the design of an instrument that can image both the 3 . . . 5 and 8 . . . 12 micron bands simultaneously, and which can be seen as an instrument that can be used to assist in weather prediction during everyday use (its original goal) and in addition be used for forest fire detection and monitoring. In order to demonstrate feasibility of the concept a breadboard has been designed and built of which the first measurement results are presented here.

1 Introduction

The microbolometer spectrometer is a prism spectrometer that uses a combination of reflective optics and a high speed camera in order to obtain an as high as possible NETD. (Fig. 1)

J. Leijtens
TNO science and Industry, Stieltjesweg 1, 2628 CK Delft
e-mail: johan.leijtens@tno.nl

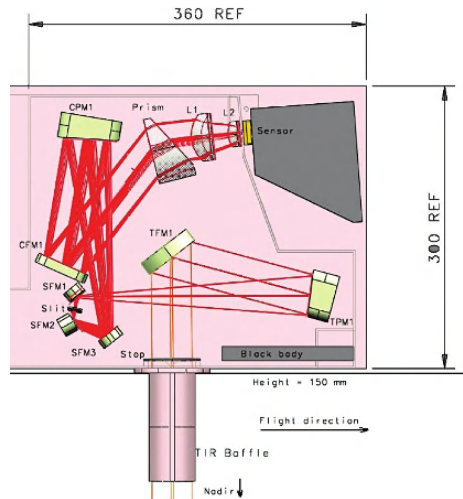
B. de Goeij
TNO science and Industry, Stieltjesweg 1, 2628 CK Delft

E. van der Meché
TNO science and Industry, Stieltjesweg 1, 2628 CK Delft

M. Eschen
TNO science and Industry, Stieltjesweg 1, 2628 CK Delft

A. Court
TNO science and Industry, Stieltjesweg 1, 2628 CK Delft

Fig. 1 Principle optical diagram of MIBS



The nadir view is looking down in this picture, and the incoming radiation is deflected by TFM1 to the collimator TPM1 which focuses on the slit via compensation mirror SFM1. The slit image is again formed into a collimated beam via compensation mirror SFM2, foldmirror SFM3, collimation mirror CPM1 and foldmirror CFM1. The radiation is then dispersed by the prism and imaged on the detector via Germanium lenses L1 and L2. TFM1 is the calibration mirror which is used to point at either one of two blackbody's incorporated in the design or the scene. For this purpose the mirror of the MIBS breadboard can be rotated by means of a small stepper motor.

Given the close proximity of the parts CFM1, SFM1, slit and SFM2 (and the desire to assemble the entire system on basis of manufacturing tolerances as much as possible) a single mechanical assembly is created out of these parts. This so called slit assembly (Fig. 2) is used as the starting point of the alignment procedure.

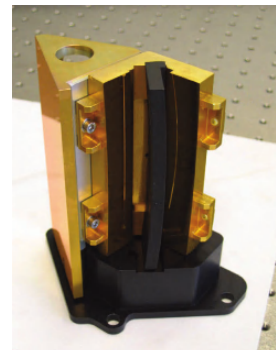
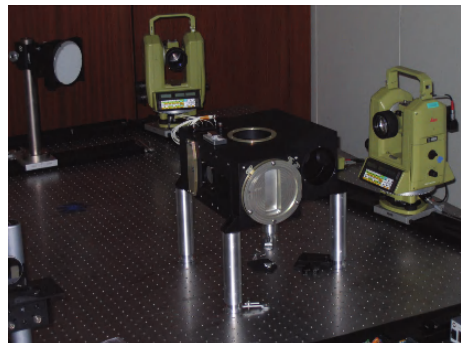


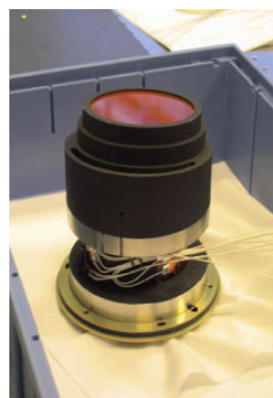
Fig. 2 Slit assembly

Fig. 3 Alignment setup

Subsequent mounting of SFM3 and CPM1 completes the installation of the collimating branch. Mounting of TPM1 and TFM1 completes the telescope branch. The alignment of the optical parts is facilitated through the availability of wedged shims that allow to adjust the tilts of the components in an easy way and a number of dedicated alignment openings are provided in the housing in order to be able to measure the position of the optical components.

Since the entire system up to the prism is reflective (with a transmissive slit) all of the measurements can be done using standard theodolites. During the assembly and alignment of the system it was proven that the alignment philosophy worked well in the sense that although additional shimming possibilities where provided, they where not needed during the alignment and all parts are mounted using manufacturing tolerances and dedicated alignment shims only.

The camera assembly consists of the mount for the prism and the camera lenses. It is a selfstanding assembly which is made of titanium in stead of the aluminium which is the base material for the rest of the instrument. (Fig. 4). Until now no further measurements have been made on this assembly with exception of the mounting position of the prism.

**Fig. 4** Camera assembly ready for mounting

The camera assembly has dedicated heaters and temperature sensors in order to enable accurate temperature stabilization. This stabilization is required in case absolute temperature measurements are to be made with the instrument. The need to stabilize the temperature is related to the absorption in the Germanium. Since the absorption in the Germanium is less for lower temperatures, and the change in absolute radiation is less for lower temperatures, there is a preference to operate the optical bench at as low as possible temperatures in order to have an as high as possible absolute radiometric accuracy.

2 Current Status

The MIBS breadboard has been assembled and is ready for the measurement and verification phase (Fig. 5). Since the setup has only been used to do NETD measurements, the thermal control hardware has been mounted but has not yet been operated.

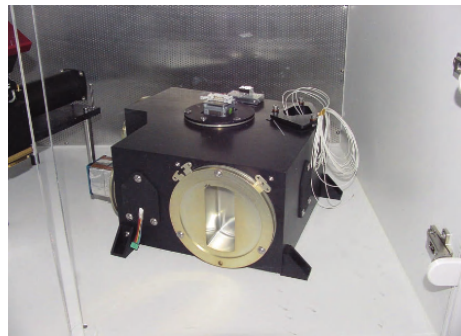


Fig. 5 MIBS in space incubator

3 Measurements Performed

Since the obtainable NETD is inherently lower when comparing a filter based instrument and a spectrometer, and absolute radiometric accuracy may be easier to obtain with a spectrometer, the prime focus for the measurements performed were optical alignment and NETD.

3.1 Optical Measurements

The optical alignment went very well with the exception of mounting of the prism. The rotation of the prism in its holder is slightly above spec (1, 3 mrad instead of 1 mrad) which will potentially influence the co-registration for the end of swath. This however is not considered to be a serious deviation and is left as is for the

moment. In case full performance is required in a later stage, this mis-alignment can be solved through a more elaborate alignment procedure, but for the moment it is deemed more important to know what the deviation from nominal is, then to be within the nominal tolerances as there are no real fixed requirements for the breadboard and recalculation (with the actual values) will allow the correlation of real life measurements with theoretical predictions.

As for the other optical tolerances everything else with exception of the nadir pointing repeatability has been proven to be well within spec. The nominal optical axis is positioned at 90 ± 0.001 degrees with respect to the front face of the instrument well within the 0.1 mrad requirement. The repeatability of the stepper-motor used to rotate the calibration mirror however has been proven to be within 0.08 degrees, the 0.08 degrees repeatability is less than required (0.14 mrad against 0.1 mrad required) but this is not seen as a serious issue at this moment in time. The lower than required repeatability should be weighed against the need to design a new calibration unit anyway in case the instrument is to be operated in vacuum. As all blackbodies used are oversized, the reduced repeatability is not seen as a serious constraint for this stage of the project. The final alignment of the detector behind the camera has not yet been performed because it was felt that a slight defocus would not have dramatic effects on the NETD to be measured. Therefore, in order to find the largest noise contributors and possible large deviations, we decided to do a set of preliminary NETD measurements.

3.2 NETD Measurements

Until now, the NETD measurements have proven to be more difficult than the optical alignment. The first images produced gave us the confirmation that the optical curvature correction seems to be working, (Fig. 6) but the measured NETD was about a factor of two above the expected NETD and the camera was mounted in a fashion that caused all the data to be in the same column.

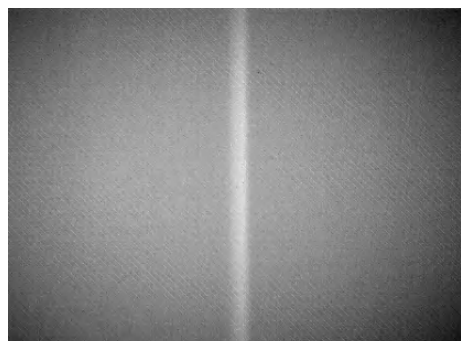


Fig. 6 Picture showing slit signature at first light

In order to mitigate some of the column effects noticed during the first measurements the camera was rotated so as to allow reference measurements to be taken in

each column, and a calibration sequence was used, with a cold flat plate blackbody to calibrate gain and offset. The gain and offset uses a cold flat plate blackbody (at room temperature) and another hot plate blackbody (at approximately 60 degrees. (it should be noted that this will decrease the measured NETD due to the low effective emissivity of the blackbody(approx 0.9) with about 10%)

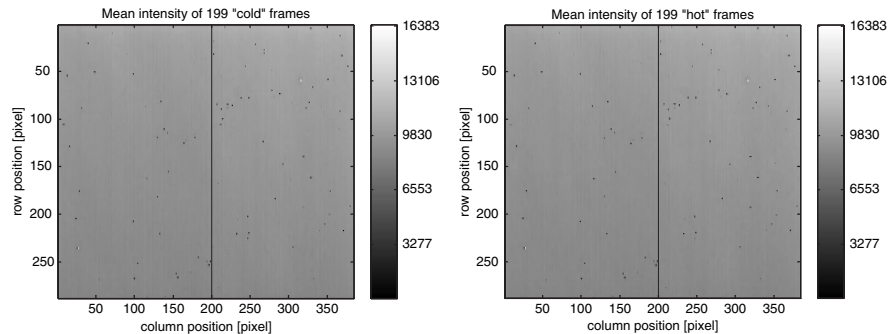


Fig. 7 Temporal average of 199 frames of “cold” and “hot” target

As can be seen in Fig. 7 there seem to be a number of pixels that give significant differences as compared to the rest. Some bright pixels can be discerned as well as some dark pixels showing less than average signal levels but no signal is visible in the raw image. (the line in the picture indicates the selected line used for further data evaluation)

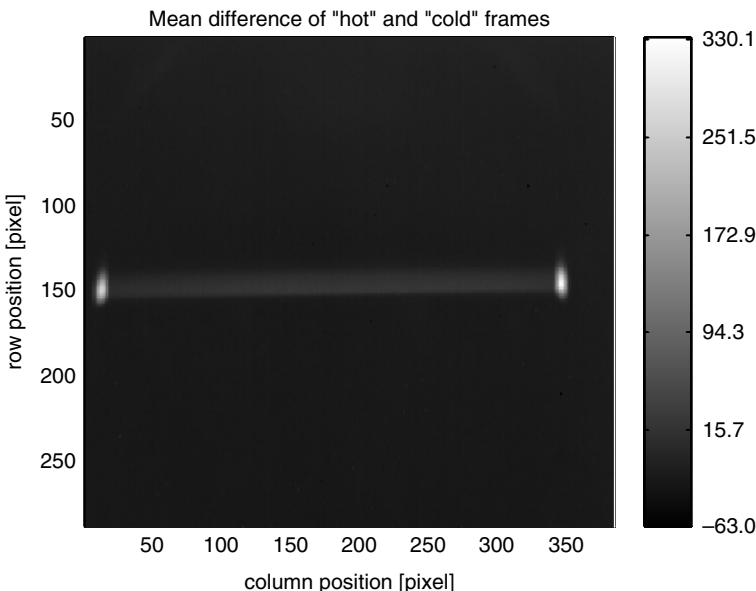


Fig. 8 Difference of time averaged “hot” and “cold” frames

The signal becomes visible only after correction of gain and offset. Nevertheless the slit image at the detector can be clearly seen as well as the image of the two starting and endingpoints of the slit. (The bright spots left and right in the image are caused by drilled holes at the beginning and end of the slit used for the spark erosion manufacturing process.

In order to do some NETD measurements, one column was selected for further analysis. (Fig. 9) which shows that a measureable signal is present.

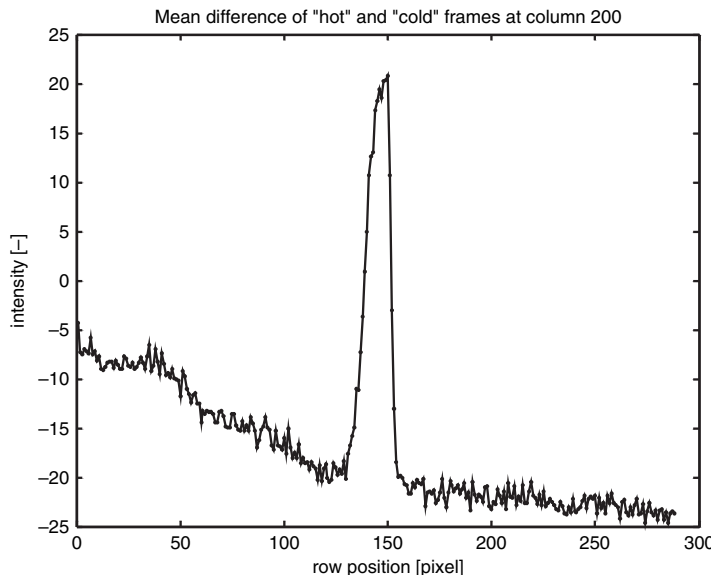


Fig. 9 Difference of 199 time averaged “hot” and “cold” frames at pixel column 200

The signal has a pulse shaped response with a significantly steeper trailing than leading edge. This is in line with expectations and can be explained when looking at the response of the microbolometer detector. The leading edge is determined by the long wavelength response which gradually improves with decreasing Germanium absorbtion. (Longer wavelengths are to the left) Shorter wavelengths will be transmitted by the high pass filter deposited on the detector window, and a combination of filter damping and decreased bolometer response cause the response to decrease fast with wavelength.

3.3 Lower than expected NETD and way forward

As mentioned before, the measured NETD is currently about a factor 2 higher then expected. This prompted some investigations aimed at providing additional insight into the cause of the lower then expected NETD.

During these investigations a number of contributors have been identified. Although the investigations have not been exhaustive a good feeling has been developed regarding the optical throughput of the system.

First of all the reflection of a spare mirror that was coated at the same time as the mirrors used in the breadboard was measured. The results of these measurements showed the reflection to be less than presumed during the NETD calculations. The average reflection at the wavelengths of interest proved to be only 96% whilst 98.5% was anticipated. In first instance this may not seem to be dramatic, but considering that the beam passes 7 surfaces, the total system transmission is 0.75 in stead of 0.90 which is more than 16% less.

Furthermore during the initial measurements it was found that the intensity variations of the entire image are quite significant. When tracking the average intensity of the image over time, it can be seen (Fig. 10) that the variation is in the order of 16 AD counts and drift is 8 AD counts. As compared to the signal found in Fig. 9 (40 AD counts) this is considered very significant. Preliminary calculations have shown that this effect has reduced the measured NETD by approximately 35%.

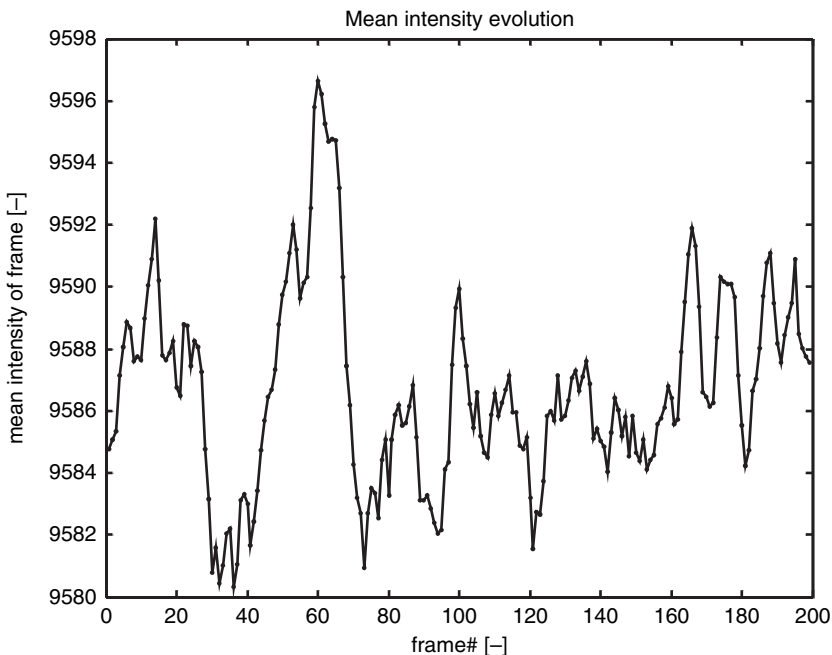


Fig. 10 Changes in average level over time

The drift shown is more or less expected and is related to the temperature control of the detector and optical bench. The large fluctuations however were not directly expected but may be related to some limit cycling in the thermal control hardware. For normal imaging applications this will not be a real problem, but this becomes a significant effect for the spectrometer application where the input signal is reduced

due to the fact that the available signal is dispersed over a number of pixels. It is not expected that this effect can be easily remedied for the breadboard, as it would involve interference with the thermal control hardware of the camera used.

Another significant contribution to the lower measured NETD is the EMC problems that are currently experienced. Most probably due to a parasitic groundloop, the image is disturbed by a moiré pattern. (Fig. 11) This pattern disturbs the measurements and should be accounted for during the NETD measurements.

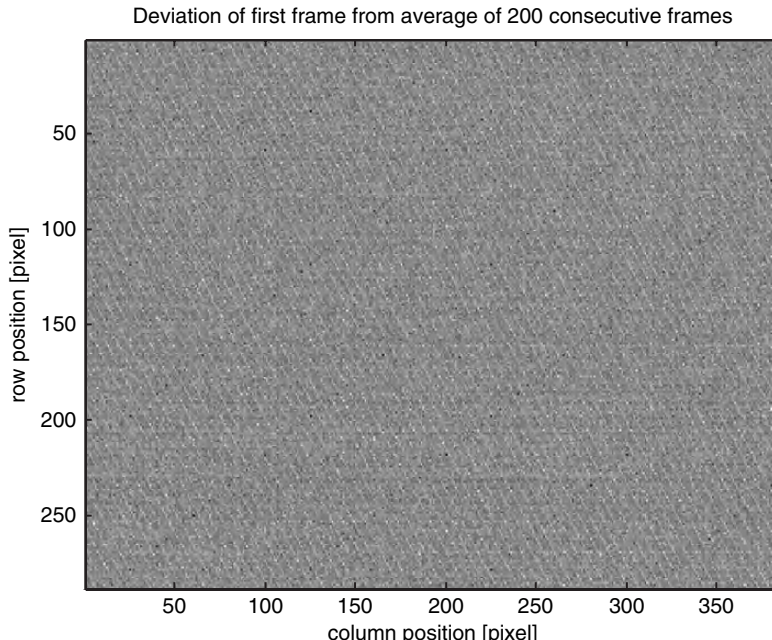


Fig. 11 Deviation of first “cold” frame from time-averaged mean

In order to estimate the obtainable performance without this interference, a 2D FFT of the images was taken and the higher order components removed. This leads to a considerably improved image quality (Fig. 12) and NETD calculated with this improved average where improved by 30% (although some artefacts still exist).

The performed exercises show that the measured NETD is above the expected NETD, but a number of contributors have been identified:

- Poor quality of the blackbody used
- Lower than expected reflection of mirrors
- High average image intensity variations
- EMC disturbance

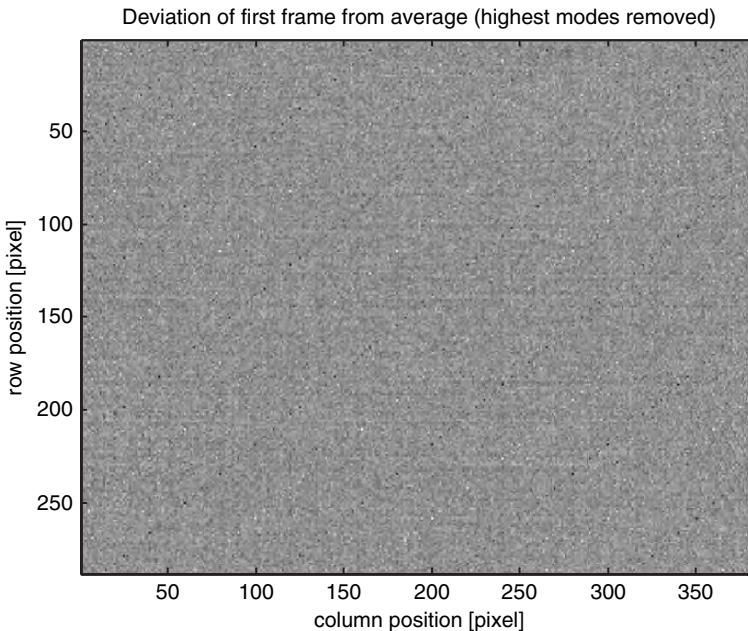


Fig. 12 Deviation of first “cold” frame from time-averaged mean with spatial harmonic interference removed (43 modes with highest amplitude in 2D FFT)

4 Conclusions

Given the actual situation of the spectrometer as described above and their estimated or calculated influence on NETD it has been concluded that the original NETD calculations will be in line with the measurements results once the above issues are solved. Furthermore a number of potentially relevant issues have not been specifically investigated yet.

- Absorption in the Germanium lenses of the camera
- Effects of defocus on NETD

Furthermore until now the TNO approach of designing an instrument that can be assembled for the majority based on manufacturing tolerances (largely decreasing costs for assembly and alignment) has proven to be working for as far as measurements have been performed. This will lead to an instrument that can be manufactured and aligned at a competitive price. During this year TNO will continue with the characterization of the MIBS breadboard and further results can be expected in the course of this year.

Feasibility of a Constellation of Miniature Satellites for Performing Measurements of the Magnetic Field of the Earth

**Michael Thomsen, José M. G. Merayo, Peter Brauer, Susanne Vennerstrøm,
Nils Olsen, and Lars Tøffner-Clausen**

Abstract This paper studies the requirements for a small constellation of satellites to perform measurements of the magnetic field of the Earth and a payload and boom design for such a mission is discussed. After studying communication, power and mass requirements it is found that it is feasible to develop a $10 \times 10 \times 30 \text{ cm}^3$ satellite with a mass of about 2.5 kg, which can fulfill such a mission. We also study the feasibility of controlling a constellation of such small satellites by means of air drag by extracting one or more flaps. It is found that it is indeed possible, but for best performance it is limited to altitudes around 450 to 550 km, depending on the time of launch with regard to the solar sunspot cycle.

1 Introduction

The dynamics and unpredictability of the Earth's magnetic field requires a continuous mapping of Earth's magnetic field from space. Description of the geomagnetic

M. Thomsen

Danish National Space Center, Technical University of Denmark (DTU), Elektrovej, Building 327, 2800 Kgs. Lyngby, Denmark
e-mail: mt@spacecenter.dk

J.M.G. Merayo

Danish National Space Center, Technical University of Denmark (DTU), Elektrovej, Building 327, 2800 Kgs. Lyngby, Denmark

P. Brauer

Danish National Space Center, Technical University of Denmark (DTU), Elektrovej, Building 327, 2800 Kgs. Lyngby, Denmark

S. Vennerstrøm

Danish National Space Center, Technical University of Denmark (DTU), Elektrovej, Building 327, 2800 Kgs. Lyngby, Denmark

N. Olsen

Danish National Space Center, Technical University of Denmark (DTU), Elektrovej, Building 327, 2800 Kgs. Lyngby, Denmark

L. Tøffner-Clausen

Danish National Space Center, Technical University of Denmark (DTU), Elektrovej, Building 327, 2800 Kgs. Lyngby, Denmark

field for the twenty years between Magsat (1979–80) and Ørsted (1999–present) is therefore of much reduced quality compared to what could have been obtained with satellite data. Unfortunately it is still expensive to integrate and launch large satellites. Instead this paper investigates the possibility of performing continuous measurements of the Earth’s magnetic field – knowledge which is essential for many practical applications like navigation and exploration – with a small, low mass satellite concept, which can also be used as a pioneer platform for future deployments of a nanosatellite fleet for other multipoint measurements missions.

2 Scientific Objectives

The scientific objectives for the mission discussed in this paper are two-fold: Geopotential research and investigation of the solar wind interactions with the magnetosphere.

Magnetic field readings will allow for a determination of “IGRF-type” models of the Earth’s magnetic field (up to spherical harmonic degree of about $n = 13$). Due to the lack of high-precision attitude data, only the magnetic field intensity will be used for this purpose. The practical inversion of the ill-posed problem of determining a potential field from intensity measurements only can be solved by utilizing a-priori information on the location of the dip-equator (defined by the places on Earth’s surface where the magnetic field is purely horizontal). Mapping of Earth’s magnetic field requires knowledge of the exact position. The availability of GPS position measurements for just a fraction of the time (e.g. one orbit/day) combined with models of the Earth’s gravity field and air density allows determining position with an accuracy of down to one hundred meters, sufficient to measure magnetic field intensity with an accuracy of a few nT. Fortunately, along-track position errors result in much smaller magnetic field errors compared to vertical and across track position errors.

Solar wind interactions with the Earth magnetic field generates a number of different current systems in Earth’s magnetosphere and ionosphere: Distant currents in the outer magnetosphere, the magnetospheric boundary and the tail, the ring-current in the inner magnetosphere, currents flowing along field-lines from the outer magnetosphere to the polar ionosphere close to the Earth and ionospheric currents flowing horizontally in the polar ionosphere acting to close the field-aligned current loop. All of these current systems will influence the magnetic field as measured by a low Earth orbiting (LEO) satellite, and can therefore in principle be investigated by such. The current systems are highly dynamic, varying at a large range of time scales, partly due to the time variations of the solar wind and partly due to internal magnetospheric and ionospheric dynamics.

Measurements of the time variations of the total magnetic field intensity at low earth orbit can be used to investigate the magnetospheric currents and also the ionospheric currents. During geomagnetic storms the magnetospheric ring-current increase and act to decrease the magnetic field near the Earth. This means that energetic particles trapped in the Earth’s radiation belts will be able to penetrate to lower altitudes, thereby endangering astronauts and spacecraft instruments.

A detailed description of this magnetic field decrease, its spatial variation and relationship to the solar wind, is therefore of high priority. The spatial variations can be investigated statistically by combining single satellite measurements with solar wind data, or instantaneously by using multipoint measurements from widely separated spacecraft.

A LEO satellite will pass through the field-aligned currents (FACS) in the upper polar ionosphere, and can be used to investigate time-variations in their structure and intensity, provided that the satellite attitude is stable during the passage. The structure of the FAC's is known to be highly filamentary, but by using a single satellite it is not possible to distinguish spatial variations from time variations. Two or more closely orbiting satellites can contribute significantly to our knowledge of the space/time structure of FAC's.

3 Requirements

In order to realize the science objectives the following is required:

- Accurate clock (1 ms or better)
- Inter satellite time synchronization (1 ms or better)
- Accurate orbit determination (better than 0.5 km)
- Attitude determination better than 1°
- Near polar orbit
- No magnetic contamination

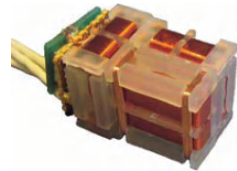
The first 3 requirements can easily be fulfilled with a GPS receiver, and the attitude can for the sunlit part of the orbit be determined using sun sensors. DTU has developed some very small MEMS sun sensors providing accuracy better than 1° [1], but commercial sun sensors with similar performance are also available, for instance from AeroAstro [2]. During eclipse periods the attitude can be found using a magnetometer. The last requirement is fulfilled by mounting the magnetometer on a deployable boom and by designing the entire spacecraft with respect to a magnetic cleanliness program.

4 Payload and Operations Description

The payload consists of two instruments: A miniature three axis fluxgate magnetometer mounted on a boom and a GPS receiver. The current control electronics for the magnetometer consists of one circuit board of $95 \times 48 \times 10 \text{ mm}^3$. It features A/D converters, voltage references, circuits to generate the necessary excitation currents for the fluxgate magnetometer and a FPGA to control the system.

The magnetometer will be mounted in a carbon-fiber cylinder on the top of a short boom. A number of boom design options will be discussed in the following section. It may be possible to mount MEMS sun sensors on the side of the magnetometer

Fig. 1 Miniature magnetometer



sensor. Likewise it is possible to mount a passive GPS patch antenna at the end of the boom, but another location may be required in order to archive the best signal strength.

The GPS receiver could either be embedded into the magnetometer FPGA, by adding an RF front-end to the design. Correlation and position calculations can be done in the FPGA, possibly using a softcore microcontroller. Alternatively a separate GPS unit can be used such as Surrey Satellite Technology Ltd's SGR-05U, which measures $70 \times 45 \times 10$ mm³, has a mass of 20 g (excluding antenna) and consumes 0.5 to 0.8 W at 5V [3].

The attitude does not need to be very well controlled, as long as the spacecraft is not spinning unreasonably fast. Since we are performing measurements of the magnetic field, attitude control based on permanent magnets is not possible. On the other hand attitude control based on magnetorquers can be used but may only be operated at known intervals in order to correlate to the magnetometer data.

In order to control the distance between the two satellites in the constellation, flaps on the sides of the satellites can be extracted to increase the area facing the flight direction and therefore increase the air drag on one of the satellites, thus reducing or increasing the inter-satellite distance. It should be noted that if this system is to be used the orbit must be reasonably low; otherwise the air density is too small to generate a sufficient drag, we will look further into this issue in a later section.

To minimize the power consumption, it may be desirable to only operate the GPS receiver part of the time. One scenario would be to operate the GPS receiver for one orbit per day. On board (and later ground) propagation of the GPS data can later be used to determine the position accurately.

5 Boom Design

For a mission performing precise measurements of the Earth's magnetic field it is necessary to place the magnetometer some distance away from the spacecraft in order to minimize the noise from the satellite body. For the small spacecraft proposed here a required boom length has been estimated to about 25 cm. Three different designs are considered: A telescopic boom made from carbon fiber, a miniature version of the Ørsted satellite boom, and a fixed carbon fiber boom which does not require deployment mechanisms, but requires a larger area and may have issues with regard to vibrations during launch. The two deployable designs are shown mounted on a cubesat on the illustration below. Both designs will be stowed in the spacecraft during launch and will be deployed by releasing a locking mechanism.

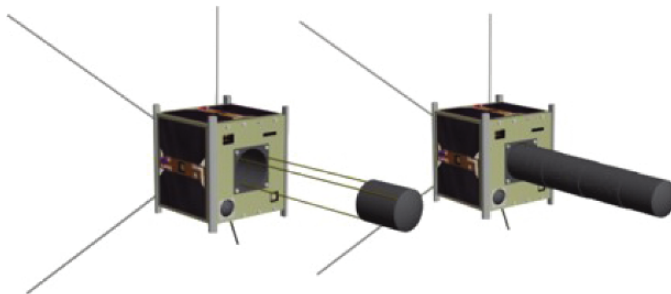


Fig. 2 Cubesats ($10 \times 10 \times 10 \text{ cm}^3$) with two different deployable boom designs (*left*: Miniature Ørsted boom; *right*: Telescopic boom)

The telescopic boom will consist of 4 elements that will be deployed by a strong spring. A slightly conical design of the cylinder elements will ensure the rigidity and stability of the boom in the deployed position.

The Ørsted boom consists of three $1 \times 1 \text{ mm}^2$ longerons made of an epoxy/fiber glass compound. They are fixed at the bottom of the well in the satellite, and mounted through hinges on the top mercedes-structure of the boom. The longerons are very flexible allowing the complete structure to be stowed in a very small space. The spring-like properties of the longerons ensure that the boom will be unfolded to a fairly rigid structure, although the carbon fiber boom will be more rigid it also has a higher mass.

6 Communication

The magnetometer can be used in several different modes, some that are interesting for a mission like this are:

| Mode | Resolution @ Frequency | Scalar measurements | Vector measurements |
|----------|------------------------|---------------------|---------------------|
| Burst | 20 bit res @ 50 Hz | 3042 bytes/min | 9046 bytes/min |
| Nominal | 22 bit res @ 10 Hz | 642 bytes/min | 1846 bytes/min |
| High-res | 24 bit res @ 1 Hz | 102 bytes/min | 226 bytes/min |

This amount of data includes magnetic measurements, house keeping data (2 temperatures and 2 voltages), status information, a time stamp and protocol overhead. The calculations are based on the ESA ECSS-E-70-41A protocol, packet size equals one minute of measurements, and data compression is utilized. However for vector measurements attitude information is required, which is not included in the data calculations. Note that data compression based on offset/deltas requires that the spacecraft is not spinning too fast. The GPS has been estimated to generate less than 1 kB per 10 minutes, including protocol overhead.

Depending on the orbit of the satellite the window for communication varies drastically. Simulations using STK based on a sun synchronous orbit and a minimum elevation angle of 10 degrees result in the following windows for a ground station at the same latitude as Copenhagen (55.4°N):

| Altitude | 450 km | 650 km | 850 km |
|----------------------|------------|------------|------------|
| Communication Window | 23 min/day | 39 min/day | 55 min/day |

Considering 650 km altitude and allocating 75% of the downlink capacity to science data, a TM link of 60 kbps is required to run the vector burst mode continuously. This can be mitigated by using additional ground stations, or by choosing a location at higher latitude. It may be better to reduce the amount of data, and thus reduce the amount of power required to transmit the data. This can be done by operating in vector burst mode only part of the time, for instance when a magnetic pole is passed, which allows for study of the field aligned currents. Scalar measurements are fine for the magnetic mapping campaign.

By selecting a TM link of 19200 bps, an average downlink window of 39 minutes per day and allocating 75% of the downlink capacity for the payload results in the possibility of transferring just over 4 Mb per day. This means that the magnetometer can be operated for the following durations:

| Mode | Resolution @ Frequency | Scalar measurements | Vector measurements |
|----------|------------------------|---------------------|---------------------|
| Burst | 20 bit res @ 50 Hz | 23 hours/day | 7.7 hours/day |
| Nominal | 22 bit res @ 10 Hz | 109 hours/day | 38 hours/day |
| High-res | 24 bit res @ 1 Hz | 688 hours/day | 310 hours/day |

7 Budgets

The magnetometer chosen for this design analysis is the miniature DTU fluxgate sensor, which consists of a sensor mounted on a small boom and some control electronics. The mass and volume of these components can be seen in Table 1. Power consumption is up to 250 mW when operating at 50 Hz sampling rate.

The AeroAstro sunsensors have a mass of 36 g each, and does not consume any power. The GPS receiver data is based on the SSTL SGR-05, which consumes 0.5 to 0.8 W. As explained earlier it is possible to reduce this power consumption by operating the GPS only part of the time.

Assuming a $10 \times 10 \times 30 \text{ cm}^3$ satellite body and $76 \times 37 \text{ mm}^2$ solar cells 6 of such cells can be mounted on four sides. With an efficiency of 25% and a power supply conversion and battery storage efficiency of 65%, the total output with the sun orthogonal on the cells is 3.7 W, which is sufficient to power the satellite and charge the batteries after an eclipse period.

At worst case a satellite in LEO will be in the eclipse for 35 minutes of a 98 minute orbit. With three 1500 mAh CGR18650H Li-ion cells the depth of

Table 1 Satellite budgets

| | Volume (mm) | Mass (g) | Power (mW) |
|----------------------------------|----------------------------|-------------|--------------|
| Magnetometer sensor head | 25 × 25 × 45 | 50 | |
| Telescopic carbon fiber boom | 50 × 50 × 70 | 40 | |
| Magnetometer PCB w/electronics | 48 × 95 × 10 | 100 | < 250 |
| GPS receiver | 70 × 45 × 10 + antenna | < 50 | < 800 |
| Sunsensors (AeroAstro) | Ø35 mm × 10 each | 216 | 0 |
| Communication TM/TC | one pcb, 90 × 90 + antenna | 250 | 2000/75 |
| Onboard data handling | one pcb, 90 × 90 | 100 | 150 |
| Flaps | | 150 | |
| Magnetotorquers | | 150 | < 150 |
| Power Subsystem | one pcb, 90 × 90 | 150 | |
| Batteries (3 pcs CGR18650H) | | 120 | |
| Structure, incl solar panels | | 600 | |
| Harness | | 100 | |
| Subtotal | | 2076 | 1425 |
| 15% margin for partly new design | | 311 | 210 |
| Total | | 2387 | 1635* |

* plus 2000 mW when transmitting.

discharge of the batteries will not exceed 8%, even when an entire 15 minute transmission window takes place during an eclipse. With current Li-ion technology this should provide well over 10000 cycles, or more than 2 years of operation [4].

This analysis suggests that it is indeed possible to build a small satellite to monitor the magnetic field of the earth.

8 Constellation Control

Based on the above analysis a $10 \times 10 \times 30 \text{ cm}^3$ satellite of 2.5 kg seems feasible to fulfill part of the mission. However to fulfill the entire mission two or more satellites are required in order to perform multipoint measurements of the magnetic field. During such a mission it will be useful to be able to control the distance between each satellite. Typically this is done by means of propulsion systems, but here we will look at the feasibility of controlling the intersatellite distance by utilizing airdrag.

For a LEO satellite the, although very thin, atmosphere brakes the satellite and eventually causes reentry. Two satellites of equal mass orbiting at equal altitude but with a different surface area of the satellite facing the forward direction will be subjected to a different amount of drag, which will change the distance between them. By mounting extractable flaps on the satellite it should therefore be possible to control the along-track distance between the satellites.

The density of the air at LEO depends on the amount of radiation from the sun, which follows an 11-year pattern related to the sunspot cycle. When the number of sunspots is high the solar radiation increases. This will heat the atmosphere of the Earth, which will therefore expand and thus result in an increased density at a given altitude. This will cause increased drag so a satellite will deorbit faster during

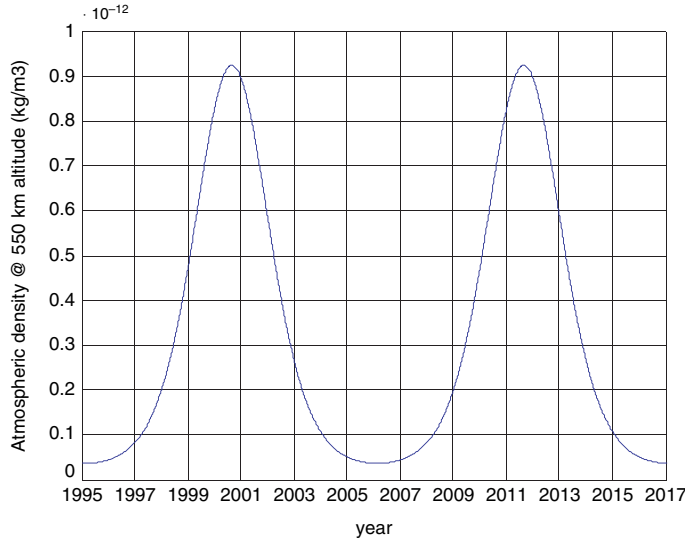


Fig. 3 Modeled air density

solar maximum. The simplified model used for this analysis takes this 11-year solar sunspot cycle into consideration. Figure 3 shows how the air density at 550 km altitude varies over time according to the model.

The lifetime of a LEO satellite is therefore dependent on the time of launch, since it may deorbit sooner if launched near solar maximum than near a solar minimum. Figure 4 shows how fast a $10 \times 30 \text{ cm}^2$ forward facing, 2.5 kg satellite will deorbit if launched around solar maximum (January 1st, 2011) and solar minimum, around January 1st, 2015.

It can be seen that when launched to 550 km near solar maximum we can expect an orbital lifetime of close to two years (blue line), while if launched to 450 km near solar minimum, we can expect almost twice as long before the satellite deorbit (blue line).

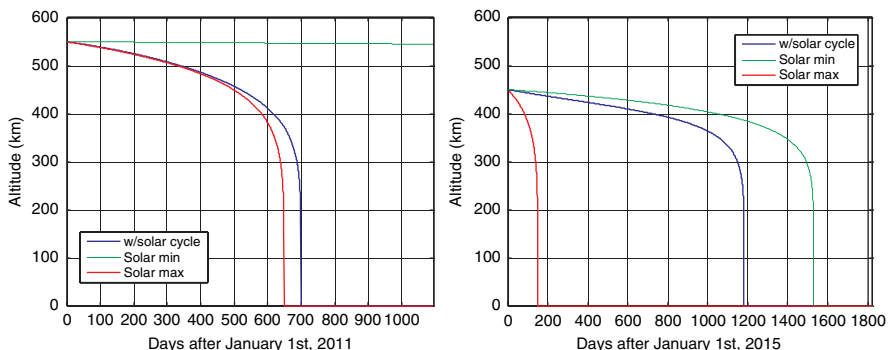


Fig. 4 Altitude characteristics of similar (mass, volume) satellite launched near maximum sunspot activity (left) and near minimum sunspot activity (right)

Table 2 Along track difference between one $10 \times 30 \text{ cm}^2$, 2.5 kg satellite and one $20 \times 30 \text{ cm}^2$, 2.5 kg satellite at various altitudes

| Altitude (km) | Along track difference (m) after one orbit | |
|---------------|--|-------------|
| | 2011 launch | 2015 launch |
| 400 | 166 | 38.4 |
| 450 | 79.7 | 14.8 |
| 500 | 39.9 | 6.1 |
| 550 | 20.6 | 2.7 |
| 600 | 11.0 | 1.3 |
| 650 | 6.0 | 0.7 |
| 700 | 3.4 | 0.4 |

Table 3 Along track difference between one $10 \times 30 \text{ cm}^2$ satellite and one satellite with flaps of varying size, both satellites 2.5 kg

| Size of second satellite | Along track difference (m) after one orbit | |
|--------------------------|--|----------------------|
| | 2011 launch (550 km) | 2015 launch (450 km) |
| 30×10 | 0 | 0 |
| 30×15 | 10.3 | 7.4 |
| 30×20 | 20.6 | 14.8 |
| 30×25 | 30.9 | 22.2 |
| 30×30 | 41.2 | 29.6 |

Next we look at how much we can change the along-track difference by extracting flaps which will double the area of one of the satellites. As can be seen from Table 2, during a solar maximum this will change the difference by 20.6 m per orbit at 550 km altitude. A value of similar magnitude is found for a 450 km altitude orbit during solar minimum. If, on the other hand the satellites are launched to a 550 km altitude orbit during solar minimum, the change in distance between the two satellites is only 2.7 m per orbit, which does not seem sufficient.

Table 3 shows the along-track difference for satellites with different flap size. The simulations suggest that it is indeed feasible to control inter-satellite distances of small spacecraft by means of air drag. It also shows that the launch altitude and time with regard to the solar sunspot cycle are important factors for determination of mission lifetime and the time it takes to change the inter-satellite distance.

9 Conclusion

We have here described the scientific objectives for a mission performing measurements on the magnetic field of the earth. A mission that requires multiple simultaneous measurements, which can be obtained by launching several small satellites. The science payload along with a boom design, communication, power and mass budgets are analyzed. It is shown that compact, low power hardware already exists to fulfill these requirements, and that a constellation of 2.5 kg $10 \times 10 \times 30 \text{ cm}^3$

satellites can fulfill the mission. Finally it is shown that it is feasible to control the constellation based on air drag, but for best performance it is limited to altitudes around 450 to 550 km, depending on the time of launch with regard to the solar sunspot cycle.

References

1. M. Pedersen, J.H. Hales, R.W. Fleron: "Linear Two-axis MOEMS Sun Sensor and the Need for MEMS in Space", IAC-03-U.2.b.02 (2003)
2. AeroAstro "Medium Sun Sensor", Datasheet, <http://www.aeroastro.com/datasheets/MSS.pdf>
3. Surrey Satellite Technology Ltd: "SSTL SGR-05 Series Space GPS Receivers", Datasheet, <http://www.sstl.org/documents/SGR-05%20GPS%20Receiver.pdf>
4. H. Croft, P. Kasztenjna, B. Staniewicz: "Li Ion Cell Performance for Space Applications", IEEE 17th Battery Conference on Applications and Advances, 179–182 (2002)

Preliminary Concepts and Analysis of Future Earth Observation Missions Based on Distributed Radars

Marco D'Errico and Giancarmine Fasano

Abstract Spaceborne synthetic aperture radars can gain great advantage from the concepts of formations and distributed space systems. In fact, combination of signals from multiple coherent receivers allows to overcome intrinsic performance limitations of monolithic SAR systems. This paper deals with an overview of recent advances and ideas in the field of distributed sparse/filled aperture radar concepts and required signal processing. Then, preliminary system considerations are given and a preliminary conceptual analysis of a distributed P-band SAR is presented. At low frequency distributed SARs offer greater advantages in overcoming the minimum area constraint (order of several tens of meters) and reduce the impact on formation control feasibility (requirement depends on λ). A formation of 6 cooperating satellites carrying a $2\text{ m} \times 2\text{ m}$ antenna operating at an undersampling pulse repetition frequency of 1000 Hz would allow to achieve 1 m azimuth resolution (ionospheric effect not included) over the whole range swaths.

1 Introduction

In the last decades, spacecraft mass and power have been reduced to limit costs and risks leading to shorter development time, possibility to fly up-to-date technology, and frequent re-flight. The possibility to use coordinated systems of platforms instead of a large single spacecraft has been introduced. Not only can a system of platforms replace a monolithic system, but it has also the capability of realizing performance otherwise unachievable. New technology plays a fundamental role in enabling high performance, which are required to implement new missions based on distributed systems: near term developments involve microtechnology, while nanotechnology impacts far term goals.

M. D'Errico

Second University of Naples – Department of Aerospace and Mechanical Engineering, Via Roma 29, 81131, Aversa (CE), Italy
e-mail: derrico@unina.it

G. Fasano

University of Naples “Federico II” – Department of Aerospace Engineering, P.le Tecchio 80, 80125, Napoli, Italy

There seems to be a high degree risk in developing formation-based missions. Nevertheless, formation concept is widely considered as a unique tool to perform missions otherwise impossible and has been recognized as an enabling technology by NASA and U.S. Air Force. A number of space missions are under development which, in full or in part, make use of the formation concept: Earth Orbiter, Space Technology 3, Space Technology 5, Starlight by NASA; the American University Nanosatellites Program, which is based on several nanosatellites developed by several American Universities under private and public sponsorships; Cluster, Darwin, and Smart-2 by ESA; LISA jointly by NASA and ESA; TechSat21 by the Air Force Research Laboratory.

The first applications of formations were proposed by astronomers to obtain optical interferometry able to cancel out star light in order to identify distant planets, which imposes very demanding (nm order) requirement on satellite relative position knowledge and control [1]. To identify mission scenarios for future Earth observation missions, let us schematically consider near, mid, and far term time frames and define the following wording: (A) a “formation” is a system of at least two platforms where relative motion must be at least measured by at least one of the formation spacecrafts (that is to say, at least one spacecraft integrates a metrology subsystem); (B) a “formation mission” is flown by a formation and payloads on-board different spacecrafsts are used in synergy to derive new data (thus, new data are generated by combination of data from different payloads); (C) a “distributed mission” is flown by a formation and the payload itself is split over the different platforms (a single payload on a single spacecraft is practically useless: mission data are only obtained by on-board combination of data from different platforms). Thus, missions where different spacecrafsts only contribute to enhance space and time distribution of gathered data (constellations) are not considered. It is worth underlining that formations, formation missions, and distributed missions pose incrementally challenging issues.

Formation missions exploiting microwave Earth remote sensing are already under development: SABRINA in Italy and Tandem-X in Germany. SABRINA [2] is scheduled for 2011 and it will perform Synthetic Aperture Radar interferometry (InSAR) and large baseline Synthetic Aperture Radar bistatic acquisitions (BSAR) by two SARs flying on a non-cooperative COSMO satellite and on an additional satellite (BISSAT). Tandem-X [3, 4] is due for launch in 2009 and will perform InSAR by two cooperative TerraSAR-X satellites.

Other missions bearing similarities with SABRINA and Tandem-X had been proposed in [5, 6] in the framework of the TOPSAT project. Then, it was proposed a small mission flying in formation with Envisat [7] and COSMO/Skymed [8, 9]. In addition, the cartwheel concept [10, 11] was introduced to perform InSAR by microsatellites flying in coordination with a large active SAR satellite.

Besides InSAR and BSAR mission, SAR has been considered for other interesting formation missions. TechSat21 [12], studied at US Air Force Research Laboratory, integrated 5 lightweight SAR payloads on-board 5 lightweight spacecrafsts (<100 kg), which were designed to fly at distances ranging from 100 m to about 5 km [13]. One of the objectives of TechSat-21 was the assessment of space-based, sparse-array aperture used to synthesize a large radar antenna. In fact, the radars

were designed to work in three modes [14, 15]: synthetic aperture radar imaging, moving target indication, geo-location. TechSat21, though being a formation mission, had working modes typical of distributed missions, with strong interactions among different payloads.

Real breaking concepts for future remote sensing missions, including microwave Earth observation, rely on realization of large apertures, unachievable with standard design technique and technology [16] but with massive use of micro/nano technologies.

The general goal of filled large aperture is simple in principle: bringing antenna apertures form the order of magnitude of few to tens square meters to hundreds square meters or square kilometers. The concept of such systems does not differ from standard system since there is a primary microwave mirror and a feed. Nonetheless, implementation is substantially different because standard rigid or inflatable structures have mass density well above what is needed to achieve feasible system masses. Thus, the primary mirror is realized by a thin film membrane (gossamer concept), non rigid in nature but assuming a prescribed figure thanks to an electron beam scanning its surface and commanding embedded actuators. The electron beam generator (free flying spacecraft with loose orbit control) is activated by a free flying spacecraft (loose orbit control) which sense current figure of membrane. Finally a free flying spacecraft carrying feed array is precisely station-kept with respect to the mirror.

The concept of sparse aperture has its roots in the work on optical interferometry over one-hundred years ago and on the development of radio astronomy about half century ago [17]. The basic idea is not to use the overall aperture, rather it is segmented and only a sparse subset of segments are really implemented. If amplitude and phase are received from each segment Fourier inversion can be implemented reconstructing images of the observed target. A sparse radar aperture can be implemented with a swarm of simple, free flying antennas, which autonomously set their time delay to compensate for different distance from target. In particular, free flyer can be loosely controlled thanks to virtual control obtained by selectable delay lines. The advantage of sparse arrays is that they can be virtually combined generating different apertures and beam widths, multi-beam systems, different beam forms. Of course, such combination can be dynamically changed in orbit to realize a very versatile Earth observation system. Sparse aperture have been recently studied for microwave remote sensing [18].

In the following, the concept of distributed radar aperture is analyzed in further details and a potential mission is preliminarily highlighted.

2 Rationale and Potential of Distributed Radar

Recent research on distributed synthetic aperture radar systems is due to the necessity of overcoming intrinsic limitations of monolithic SAR systems. In particular, the trade-off between swath width and azimuth resolution leads to the minimum

antenna area constraint if best possible resolution and widest possible swath are the design goals [19]. The minimum area constraint can be expressed as follows:

$$A > \frac{4V\lambda R_s \operatorname{tg}\Phi_i}{c} \quad (1)$$

where V is the satellite speed, λ is wavelength, Φ_i is the incidence angle, R_s is the slant range and c is the speed of light. It can be seen that minimum area increases for increasing incidence angle and wavelength. In Fig. 1 minimum area is plotted as a function of altitude and off-nadir angle. It is worth noting that for low frequency the constraint is of the order of 100 m^2 . Smaller antennas can be built at the cost of worse azimuth resolution and/or smaller swath, but with degraded observation potential.

To overcome this constraint, multiple receiving channels are required to improve both observed areas and spatial/temporal sampling. The first ideas in this framework is referred to the possibility of using multi-channel SAR antennas [20, 21]. The same concept can be implemented by using a sparse set of coherent transmitters/receivers [18]. A preliminary overview of techniques, potentials, and criticalities of sparse SAR is given in [18, 22–24]. Multiple coherent receive apertures can be used to improve illumination coverage while maintaining azimuth resolution. Illuminated area is determined by size of individual antenna, while spatial information provided by multiple antennas is used to resolve range-Doppler ambiguities. Since it is the sum of antenna areas that must satisfy minimum SAR antenna area constraint, each aperture can be smaller and illumination area can be improved over the single-receiver case by a factor equal to the number of receivers. It is interesting to note that data from each satellite can be processed alone, accepting a reduced swath width and/or a worse azimuth resolution (processed Doppler bandwidth). Moreover, quality of single SAR images does depend on antenna dimensions which strongly affect SNR. However, it is the processing of all received echoes that enables high performance. Nevertheless, a definitive solution for 3d, random array patterns is not given [18, 22–24]. Furthermore, it is worth noting that many receive apertures are necessary in order to reduce array pattern sidelobe levels.

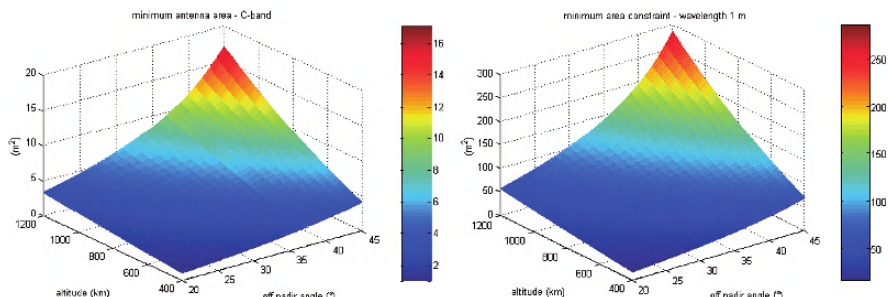


Fig. 1 Minimum area constraint for C ($\lambda = 6 \text{ cm}$) and P ($\lambda = 1 \text{ m}$) bands

More recently, studies have been focusing on linear sparse arrays as a more immediate solution for distributed SAR and GMTI systems. For example, Raman et al. [25] demonstrate the possibility to suppress azimuth ambiguities for these configurations.

SAR train concept [26, 27] is also proposed to solve the minimum antenna constraint by splitting a wider antenna over a given number of smaller antennas. A similar approach (multi-aperture azimuth sampling) is followed in [28, 29, 30] for the proposed, virtually filled aperture. That is to say, that the SAR distributed system simulates a virtual monostatic SAR antenna. N smaller antennas work at an under-sampling PRF, but signals acquired at different positions eventually by different antennas are coherently combined to gather the signal of the virtual antenna. Once the virtual SAR signal is reconstructed, standard SAR processing can be applied.

3 System Considerations

Sparse SAR systems performance rely directly on relative dynamics, platform synchronization and coordination. Thus, there is a close connection between payload and system design, which is an innovative aspect with respect to classical SAR missions. Furthermore, these systems can be operated in monostatic or bistatic modes (Fig. 2).

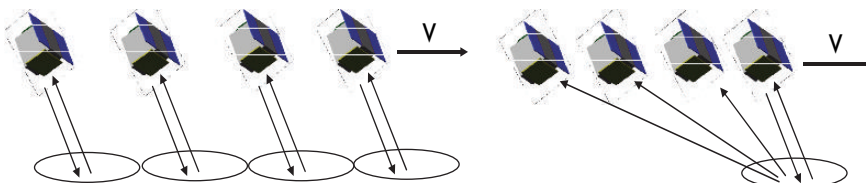


Fig. 2 Monostatic and bistatic distributed linear SAR systems (not to scale)

In monostatic distributed SARs, all the platforms are Tx/Rx. Since the antennas are small, they are characterized by large patterns and swaths. As a consequence, interference among the different radars can be a problem. It can be avoided by different approaches: (1) using large satellite separations (depending on frequency: hundreds of kilometers for P-band); (2) using slightly different Tx signals for the different radars; (3) ad-hoc coding of Tx signals. Large separation among platforms poses major problems in knowledge and control of relative position and attitude. In fact, the most precise metrology systems (lasers) can typically operate at short distances, whereas differential GPS accuracy decreases for increasing satellites separation.

Another option is to acquire data in a bistatic configuration, with a separate transmitter and all the other antennas working as receiving-only systems. Different approaches can be utilized to implement the system. A single, larger satellite could be in charge for transmitting the radar signals, with lighter satellites as receivers. As an alternative, all satellites can be identical, but one at a time is used for transmission and transmission times per orbit are equally shared by different radars. With this approach, satellite orbit average power can be reduced and the formation is more

reliable since it does not depend on a single platform for operation. Peak power is not relaxed.

From a dynamics point of view, different constraints arise for monostatic and bistatic cases. In the first case, major effort is to control radar burst times among different satellites order to achieve adequate and regular azimuth sampling (common time reference probably mandatory). Whereas for bistatic solutions, it is necessary to control relative positioning up to λ -fraction, which is harder at higher frequencies. On-going researches will probably allow to relax these requirements: algorithms for azimuth signal reconstruction from non uniform samples [30] and auto-focus techniques [28, 29].

It is worth noting that a sparse aperture gives more possibilities/flexibility with respect to multi-channel systems implemented on a physical antenna (given distance among phase centers leads to given PRF). With a distributed radar, PRF can be dynamically selected in conjunction with a given satellite distance. Since required PRF depends on single antenna size and on number of flying antennas, this capability allows an incremental development of the system with incremental achievement of performance. Signal to Noise Ratio (SNR) is a critical issue for small antennas. However, it is useful to remind that SNR for final SAR image not only depends on raw data SNR, but it is also related to range and azimuth oversampling factors. Thus, it is possible to enhance SNR increasing virtual PRF for a given Doppler bandwidth, which is obtained either increasing elementary radar PRF or the number of flying radars (or a combination of both). Approaching higher and higher PRF can again lead to ambiguity problem.

4 Low Frequencies as a Test Case for Distributed Radars

Low frequency (below L-band) radars have never been used in Earth observation spaceborne applications. This is mostly due to technological problems in realization of very large antennas, required to get adequate SNR and to avoid range/azimuth ambiguities. Necessity of full polarization to remove ionospheric effects is another factor that limits performance of classical SAR systems. Nevertheless, climatology and biosphere scientific community is in clear need of information which can only be provided on a global scale by a spaceborne P-band SAR [32]. In fact, P-band backscatter has been found to have a strong correlation with biomass in forested areas [33–35], allowing for global biomass measurements and realization of accurate forest and deforestation maps. Furthermore, P-band capability to penetrate ice can be used for Antarctica subsurface analyses which can have a great impact on prediction of ice sheet dynamics and climate/sea level changes. Past studies in this framework [36] showed that a nadir looking geometry is necessary to isolate the return from subsurface ice layers removing surface echos. However, a multi-platform approach allows to apply interferometric SAR, so that surface clutter can be removed even in side-looking geometries [37].

Thus, a P-band distributed systems can be considered as a great scientific opportunity, allowing for both biomass and glaciology studies. Furthermore, from the

engineering point of view, relative position knowledge and control requirements are relaxed thanks to longer wavelength (~ 70 cm considering latest ITU allocation). To get preliminary quantitative insights, let us consider $2\text{ m} \times 2\text{ m}$ P-band SAR antennas flying in along-track formation at an altitude of 550 km with off-nadir angles within $20\text{--}30^\circ$. Doppler bandwidth corresponding to the 3 dB azimuth aperture is 6674.9 Hz, which lead to a minimum required PRF of about 8000 Hz (1.2 azimuth sampling factor). Since, cross-track swath is about 210 km, such a PRF would lead to range ambiguities. Maximum PRF required to avoid range ambiguities would vary from about 2100 Hz (at 20° off nadir angle) to about 1150 Hz (30° off nadir angle). Thus, there are two choices: reduction of elevation swath or reduction of azimuth swath (process a smaller Doppler bandwidth). The former approach leads to small imaged swaths, the latter one to reduced azimuth resolution. Utilizing more SARs allows to improve either range swath or processed bandwidth (or a combination of both).

Choice of PRF and distance among platforms depends on required performance. Figure 3 shows the potential of distributed SAR reporting unambiguous swath and achievable 1-look azimuth resolution as a function of PRF and number of satellites. Off nadir angle is selected at 25° , and it is supposed that maximum desired swath is the one corresponding to 3 dB antenna aperture in elevation (this is why there is an upper limit for unambiguous swath). The performance improvement brought by an increasing number of platforms is very considerable.

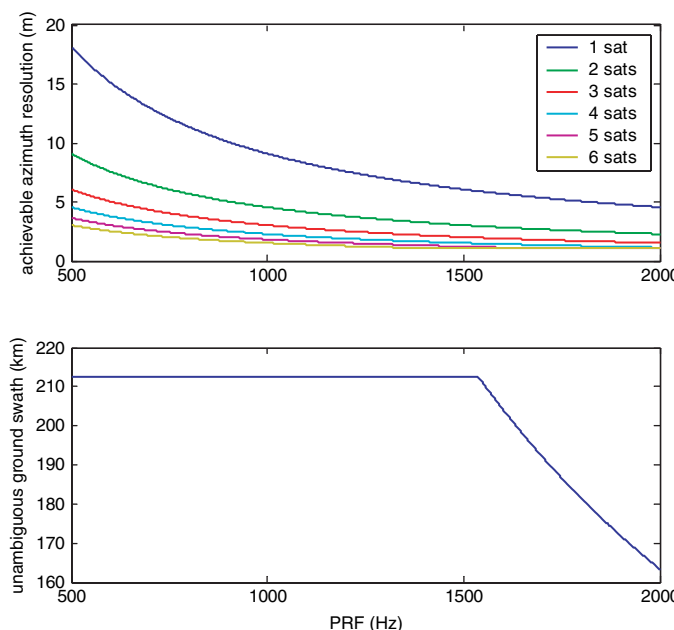


Fig. 3 Unambiguous swath and 1-look azimuth resolution as a function number of satellites

For the sake of clarity, let us underline that Fig. 3 represents limit cases in a simplified scenario (for example, impulse duration is neglected), whereas in real sensor design PRF must be defined in order to obtain required low values for azimuth and range ambiguity-to-signal ratios. It is also worth noting that Fig. 3 was obtained without considering full polarization. If this is the case, then for any given PRF achievable azimuth resolution doubles and the advantage of distributed sensor approach with respect to monolithic system design is more evident.

5 Conclusions

Distributed radars can in principle allow to overcome limitations of classical, monolithic radars. After an overview of current researches covering both sparse and filled (or virtually filled) radar apertures, an analysis has been presented in the case of a low frequency (P-band) distributed SAR. In particular, if on the one hand SAR antennas should be as small as possible to improve azimuth resolutions, on the other hand they must be large enough to avoid ambiguities. Distributed SARs allow to overcome this limitations.

References

1. R.L. Duren and O.P. Lay, The Starlight Formation-Flying Interferometer System and Architecture. *Proc. of the IEEE Aerospace Conf.*, Vol. 4, pp. 1703–1719, Big Sky (2002).
2. G. Fasano and M. D'Errico, Gathering SAR Data Under Different Bistatic Angles: A New Potential of COSMO/SkyMed Constellation. *Proc. of 5th IAA Symp. on Small Sat. for Earth Obs.*, Berlin (2005).
3. A. Moreira, G. Krieger, I. Hajnsek, S. Rieger, and E. Settlemeyer, TanDEM-X: A TerraSAR-X Add-On Satellite for Single-Pass SAR Interferometry. *Proc. of IGARSS*, pp. 1000–1003 (2004).
4. G. Krieger, A. Moreira, H. Fiedler, I. Hajnsek, M. Zink, and M. Werner, TanDEM-X: Mission Concept, Product Definition and Performance Prediction. *Proc. of EUSAR*, pp. 4, Dresden (2006).
5. H.A. Zebker, T.G. Farr, R.P. Salazar, and T.H. Dixon, Mapping the World's Topography Using Radar Interferometry: The TOPSAT Mission, *Proc. of the IEEE*, **82** (12), 1774–1786 (1994).
6. M. D'Errico, A. Moccia, and S. Vetrella, Attitude Requirements of a Twin Satellite System for the Global Topography Mission, *45th IAF Congress*, IAF-94-B.2.077, Jerusalem (1994).
7. M. D'Errico, M. Grassi, and S. Vetrella, A Bistatic SAR Mission for Earth Observation Based on a Small Satellite. *Acta Astronaut.*, Vol. 39, No. 9–12, pp. 837–846 (1997).
8. M. D'Errico and A. Moccia, Attitude and Antenna Pointing Design of Bistatic Radar Formations. *IEEE TAES*, Vol. 39, No. 3, pp. 949–960 (2003).
9. A. Moccia, G. Salzillo, M. D'Errico, G. Rufino, and G. Alberti, Performance of Spaceborne Bistatic Synthetic Aperture Radar. *IEEE TAES*, Vol. 41, No. 4, pp. 1383–1395 (2005).
10. D. Massonnet, The Interferometric Cartwheel: A Constellation of Passive Satellites to Produce Radar Image to be Coherently Combined. *Int. J. of Remote Sensing*, Vol. 22, No. 12, pp. 2413–2430 (2001).
11. D. Massonnet, Capabilities and Limitations of the Interferometric Cartwheel. *IEEE TGRS*, Vol. 39, No. 3, pp. 507–520 (2001).
12. R. Burns, C.A. McLaughlin, J. Leitner, and M. Martin., TechSat21: Formation Design, Control, and Simulation. *Proc. of IEEE Aerospace Conf.*, pp. 19–25, Big Sky (2000).

13. Chien et al., The Techsat-21 Autonomous Sciencecraft Constellation. *Proc. of the 6th Int. Symp. on Artificial Intelligence and Robotics & Automation in Space*, p. 8, St-Hubert, Canada, (2001).
14. H. Steyskal, J.K. Schindler, P. Franchi, R.J. Mailloux, Pattern Synthesis for TechSat21 – A Distributed Space-Based Radar System. *Proc. of IEEE Aerospace Conf.*, pp. 725–732, Big Sky (2001).
15. H. Steyskal and J.K. Schindler, Separable Space-Time Patter Synthesis for the TechSat21 Space-Based Radar System. *IEEE Aerospace Conf.*, p. 6, Big Sky, (2003).
16. I. Bekey, Advanced Space System Concepts and Technologies – 2010–2030+. AIAA (2003).
17. T.A. Pauls, Origins of Sparse Aperture Imaging. *Proc. of IEEE Aerospace Conf.*, Vol. 3, pp. 1421–1427, Big Sky (2002).
18. N.A. Goodman and J.M. Stiles, Resolution and Synthetic Aperture Characterization of Sparse Radar Arrays. *IEEE TAES*, Vol. 39, No. 3, pp. 921–935 (2003).
19. A. Freeman, W.T.K. Johnson, B. Huneycutt, R. Jordan, S. Hensley, P. Siqueira, and J. Curlander, The “Myth” of the Minimum SAR Antenna Area Constraint. *IEEE Trans. Geosc. Rem Sens.*, **38**, 320–324 (2000).
20. A. Currie and M.A. Brown, Wide-swath SAR. *IEE Proc-F*, 139, 122–135 (1992).
21. G.D. Callaghan and I.D. Longstaff, Wide-swath space-borne SAR using a quad-element array. *IEE Proc. Radar, Sonar Navig.*, **146**, 159–165 (1999).
22. N.A. Goodman, S.C. Lin, D. Rajakrishna, and J.M. Stiles, Processing of Multiple-Receiver Spaceborne Arrays for Wide-Area SAR. *IEEE TGRS*, Vol. 40, No. 4, pp. 841–852 (2002).
23. N.A. Goodman and J.M. Stiles, Radar Satellite Constellations: SAR Characterization and Analysis. *Proc. of the Advanced SAR Workshop*, Montreal, Canada, June, p. 10 (2003).
24. J.M. Stiles and N.A. Goodman, Wide Area, Fine Resolution SAR From Multi-Aperture Radar Arrays. *Proc. of the Advanced SAR Workshop*, Montreal, Canada, June, p. 10 (2003).
25. J.R. Raman, J.C. Nelander, J.W. Garnham, J.D. Keisling, and L.M. Black, Suppression of Doppler Ambiguities for Linear Sparse Arrays. *Proc. of IEEE Radar Conf.*, 650–656 (2006).
26. R. Marechal, T. Amiot, S. Attia, J.P. Aguttes, and J.C. Souyris, Distributed SAR for Performance Improvement. *Proc. of IGARSS*, pp. 1030–1033 (2004).
27. J.P. Aguttes, The SAR Train Concept: An Along-Track Formation of SAR Satellites for Diluting the Antenna Area Over N Smaller Satellites, While Increasing Performance by N. *Acta Astronautica*, Vol. 57, pp. 197–204 (2005).
28. Z. Li, H. Wang, T. Su, and Z. Bao, Generation of Wide-Swath and High-Resolution SAR Images From Multichannel Small Spaceborne SAR Systems. *IEEE GRSL*, Vol. 2, No. 1, pp. 82–86 (2005).
29. Z. Li, Z. Bao, H. Wang, and G. Liao, Performance Improvement for Constellation SAR Using Signal Processing Techniques. *IEEE TAES*, Vol. 42, No. 2, pp. 436–452 (2006).
30. N. Gebert, G. Krieger, and A. Moreira, High Resolution Wide Swath SAR Imaging with Digital Beamforming – Performance Analysis, Optimization, System Design. *Proc. of EUSAR* (2006).
31. C. Le, S. Chan, F. Cheng, W. Fang, M. Fischman, S. Hensley, R. Johnson, M. Jourdan, M. Marina, B. Parham, F. Rogez, P. Rosen, B. Shah, and S. Tafi, Onboard FPGA-Based SAR Processing for Future Spaceborne Systems. *Proc. of the Radar Conf.*, pp. 15–20 (2004).
32. ESA EOP-SFP/2006-09-1240, Statement of Work for the Phase 0 Study of the Six Candidate Earth Explorer Core Missions, Annex 1: Missions Description and Technical Requirement, Paragraph A1.1 The BIOMASS Mission, pp. 1–3 (2006).
33. T. LeToan et al., Relating Forest Biomass to SAR Data, *IEEE TGRS*, Vol. 30, pp. 403–411 (1992).
34. E. Rignot, R. Zimmerman, R. and J.J. van Zyl, Spacebome Applications of P Band Imaging Radars for Measuring Forest Biomass, *IEEE TGRS*, Vol. 33, No. 5 (1995).
35. B. Hallberg, G. Smith, A. Olofsson, and L.M.H. Ulander, Performance Simulation of Spaceborne P-band SAR for Global Biomass Retrieval, *Proc. of IGARSS* (2004).
36. A. Herique, W. Kofman, P. Bauer, F. Remy, and L. Phalippou, A Spaceborne Ground Penetrating Radar: MIMOSA, *Proc. of IGARSS*, Vol. 1, pp. 473–475 (1999).
37. E. Rodriguez, A. Freeman, K. Jezek, and X. Wu, A New Technique for Interferometric Soundings of Ice Sheets, *Proc. of EUSAR* (2006).

The Swarm Magnetometry Package

José M. G. Merayo, John L. Jørgensen, Eigil Friis-Christensen, Peter Brauer,
Fritz Primdahl, Peter S. Jørgensen, Thomas H. Allin, and Troelz Denver

Abstract The Swarm mission under the ESA's *Living Planet Programme* is planned for launch in 2010 and consists of a constellation of three satellites at LEO. The prime objective of Swarm is to measure the geomagnetic field with unprecedented accuracy in space and time. The magnetometry package consists of an extremely accurate and stable vector magnetometer, which is co-mounted in an optical bench together with a star tracker system to ensure mechanical stability of the measurements.

J.M.G. Merayo

Danish National Space Center, Technical University of Denmark (DTU), Elektrovej, Building 327, 2800 Kgs. Lyngby, Denmark
e-mail: jmm@spacecenter.dk

J.L. Jørgensen

Danish National Space Center, Technical University of Denmark (DTU), Elektrovej, Building 327, 2800 Kgs. Lyngby, Denmark

E. Friis-Christensen

Danish National Space Center, Technical University of Denmark (DTU), Elektrovej, Building 327, 2800 Kgs. Lyngby, Denmark

P. Brauer

Danish National Space Center, Technical University of Denmark (DTU), Elektrovej, Building 327, 2800 Kgs. Lyngby, Denmark

F. Primdahl

Danish National Space Center, Technical University of Denmark (DTU), Elektrovej, Building 327, 2800 Kgs. Lyngby, Denmark

P.S. Jørgensen

Danish National Space Center, Technical University of Denmark (DTU), Elektrovej, Building 327, 2800 Kgs. Lyngby, Denmark

T.H. Allin

Danish National Space Center, Technical University of Denmark (DTU), Elektrovej, Building 327, 2800 Kgs. Lyngby, Denmark

T. Denver

Danish National Space Center, Technical University of Denmark (DTU), Elektrovej, Building 327, 2800 Kgs. Lyngby, Denmark

1 Introduction

High precision measurements of the geomagnetic field have been and are essential to provide insight into the internal structure of the Earth and the solar interaction with the Earth's magnetic field. These measurements reveal the resulting magnetic field that stems from the superposition of three sources: the core field, the crustal field and the current driven field. The spatial and temporal structure of these sources are very different from each other, and therefore not only signal extraction methods and modelling but also measurement strategies have to be taken into account in order to successfully separate these signal contributors. Furthermore, this decomposition process requires that the global field is known at any given time with a relatively high accuracy, wherefore accurate magnetic field mapping is only viable using spaceborne observations.

The data obtained from one single spacecraft is extremely valuable. The first mission to ever map the Earth's magnetic field vector at LEO was the NASA MAGSAT (1978–9). Twenty years later, the Danish Ørsted micro satellite (1999–), the German CHAMP (2000–), the Argentine SAC-C (2000–5) have been designed specifically for mapping the LEO magnetic field. Common to these resent missions is the magnetometry package, which utilizes a vector field magnetometer co-mounted with a star tracker (2 in the case of CHAMP) on an optical bench.

As the accuracy of the instrument package has constantly increased, as well as the modelling methods have been improved towards optimized signal decomposition, it has been realized that simultaneous data from several points in space is needed, if the ultimate modelling barrier, the spatial-temporal ambiguity, has to be broken.

The ESA Swarm mission under the Living Planet Programme consists of three identical spacecraft orbiting in near polar orbits with altitudes varying between 400 km and 550 km. This constellation is to map the magnetic field of the Earth with unprecedented spatial and temporal accuracy. For this purpose, each spacecraft will be equipped with a vector field magnetometer and three star trackers co-mounted in an optical bench, which will ensure 100% data coverage over the orbit with arcsecond accuracy. This accuracy of the magnetometry package is essential for fulfilling the mission objectives.

This paper describes the basic design characteristics and the performance potentials of the Swarm Magnetometry Package. The key performance parameter is an absolute attitude recovery accuracy in the arcsecond range over time, temperature and aging. The methods used to achieve and validate this accuracy are discussed, as well as the potential for using this methodology on other future missions with extreme stability and accuracy demands.

2 The Swarm Mission

The Swarm mission [1] was selected as the 5th mission in ESA's Earth Explorer Programme in 2004. The mission will provide the best ever survey of the geomagnetic

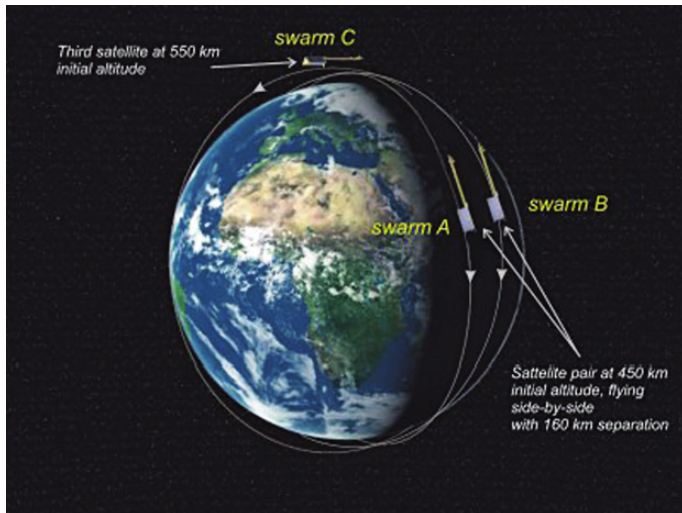


Fig. 1 Swarm constellation of three satellites

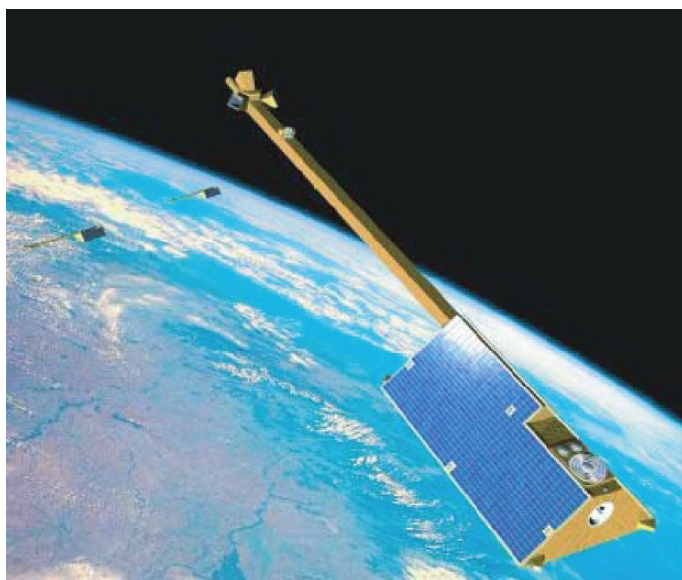


Fig. 2 Swarm satellite will be about 8 m long and have a weight of 300–400 kg

field and its temporal evolution that will lead to new insights into the Earth system by improving our understanding of the Earth's interior and its effect on Geospace, the vast region around the Earth where electrodynamic processes are influenced by the Earth's magnetic field. Scheduled for launch in 2010, the mission will comprise a constellation of three satellites, with two spacecraft flying side-by-side at lower

altitude (450 km initial altitude), thereby measuring the East-West gradient of the magnetic field, and the third one flying at higher altitude (530 km). High-precision and high-resolution measurements of the strength, direction and variation of the magnetic field, complemented by precise navigation, accelerometer and electric field measurements, will provide the necessary observations that are required to separate and model the various sources of the geomagnetic field. This results in a unique “view” inside the Earth from space to study the composition and processes of its interior. It also allows analysing the Sun’s influence within the Earth system. In addition practical applications in many different areas, such as space weather, radiation hazards, navigation and resource management, will benefit from the Swarm concept.

The research objectives of Swarm mission [2] are:

- Related to the Earth’s Interior:
 - Map the core flow
 - Determine core dynamics
 - Investigate jerks: their time-space structure and recurrence
 - Understand core-mantle coupling and its implication for Earth rotation
 - Perform 3D imaging of mantle conductivity
 - Determine remanent and induced magnetisation of the lithosphere
- Related to the Earth’s environment:
 - Determine the position and development of the radiation belts and their near-Earth effects
 - Investigate the time-space structure of the magnetospheric and ionospheric current systems on all time scales
 - Monitor the solar wind energy input into the upper atmosphere and sense its effect on the thermospheric density
 - Sound the electron density of the ionosphere/plasmasphere and relate it to magnetic activity

The scientific payload consists of the following instruments:

- Vector Field Magnetometer (VFM), which is co-mounted together with a stellar compass for determining the components of the magnetic field very accurately
- Absolute Scalar Magnetometer (ASM), which is used primarily for calibrating absolutely the vector field magnetometer.
- Electrical Field Instrument (EFI)
- Accelerometer (ACC)

3 The Magnetometry Package on Swarm

The high accurate magnetic field measurements are achieved by co-mounting the magnetometer in a very stable optical bench together with three μ ASC star trackers,

which ensures full (and continuous) data coverage regardless of the orientation of the satellite. I.e. in case of blinding of one of the star trackers due to the Sun or Earth being on the field of view, two star trackers can deliver full accurate attitude. The blinding of two camera heads (by both Sun and Earth) at the same time is also possible but extremely rare. The optical bench temperature gradients as well as the time thermal variation are designed to be as low as possible to minimize the potential effects that can be difficult to model to the level of accuracy required, i.e. few arc seconds.

3.1 Vector Field Magnetometer (VFM)

The Vector Field Magnetometer (VFM) from DTU is the prime instrument of the Swarm mission. It will provide ultra linear and low-noise measurements of the Earth's magnetic field vector components. The VFM full-scale range is $+/- 65 \mu\text{T}$ and it has been allocated a measurement random error of less than 1 nT integrated over frequencies up to 4Hz.

The proposed VFM (fluxgate type) consists of a Compact Spherical Coil (CSC) sensor, non redundant, mounted on the deployable boom, an internally redundant data processing unit (DPU) and the connecting harness.

The fluxgate magnetometer, which is based on the CSC (Compact Spherical Coil) sensor that exhibits extremely high directional linearity as well as thermal stability (30 ppm/C for the scale factors and very low for the non-orthogonal angles and offsets). The range of the magnetometer is $+/- 65536 \text{nT}$ with digitalization error of 21 bits, with a noise of less than $100 \text{ pT}_{\text{RMS}}$ in the band 0.1–10Hz (for the sensor this

| <i>VFM Specifications</i> | |
|------------------------------------|---|
| Mass | 1000 g |
| Power consumption | 1 W |
| Dimension Sensor Head | 82 mm Ø |
| Dimension DPU | 100 × 100 × 50mm |
| Data Rate | |
| Dynamic Range | $\pm 65536.0 \text{nT}$ to 0.0625nT (21 bits) |
| Omnidirectional Linearity | $\pm 0.0001\%$ of FS ($\pm 0.1 \text{nT}$ in $\pm 65536 \text{nT}$) |
| Intrinsic sensor noise | $15 \text{ pT}_{\text{RMS}}$ in the band 0.01–10Hz ($6.6 \text{ pT}_{\text{RMS}}/\sqrt{\text{Hz}}$ at 1Hz) |
| Intrinsic electronics noise | $50 \text{ pT}_{\text{RMS}}$ in the band 0.01–10Hz ($15 \text{ pT}_{\text{RMS}}/\sqrt{\text{Hz}}$ at 1Hz) |
| Sampling Rate | 50Hz, linear phase filter, -3dB frequency 13.1Hz |
| Temperature range | -20°C to $+40^\circ\text{C}$ (Operating performance) -40°C to $+50^\circ\text{C}$ (Survival performance) |
| <i>Thermal behavior</i> | |
| • Offset | $\sim 0 \text{nT}/^\circ\text{C}$ (csc), $\sim 0.1 \text{nT}/^\circ\text{C}$ (electronics) |
| • Scale Factors | $\sim 10 \text{ ppm}/^\circ\text{C}$ (csc), $\sim 2 \text{ ppm}/^\circ\text{C}$ (electronics) |
| • Non-orthogonality angles | $\sim 0''/^\circ\text{C}$ (0.06, 0.07, 0.04) |

| | |
|---|--|
| Zero stability (thermal & long term) | $< \pm 0.5 \text{ nT}$ |
| <i>Absolute accuracy of Ørsted magnetometer parameters (relative to ASM & STR):</i> | |
| •Offset | $< 0.2 \text{nT} (\sim 120 \text{dB})$ |
| •Scale Factors | $< 0.0005\%$ |
| •Axes orthogonality | $< 0.0006 \text{ deg} (\sim 2'')$ |
| •Axes alignment | $< 0.0002 \text{ deg} (\sim 7'')$ |
| <i>Ørsted magnetometer with 3 offsets, 3 scale factors & 3 angles for 6.5 year:</i> | |
| Accuracy | $< 0.5 \text{nT}$ |

figure is (15 pT_{RMS}). The sampling rate is 50Hz. The mass of the VFM is about 1 kg excluding harness and the power consumption is less than 1 W. The absolute accuracy as measured by the Ørsted mission in flight over 6.5 years is better than 0.5 nT.



Fig. 3 The VFM magnetometer configuration for the Swarm mission. *Left:* redundant electronics box with *Right:* CSC sensor (shown with a CHAMP holder)

3.2 The Absolute Scalar Magnetometer (ASM)

The objective of the Absolute Scalar Magnetometer (ASM) from LETI is to calibrate the vector field magnetometer (VFM) to maintain the absolute accuracy in the multi-year geomagnetic field mission. The required main performance characteristics of the ASM are: absolute accuracy of $< 0.3 \text{ nT}$ (2σ), resolution $< 0.1 \text{ nT}$ within its full-scale range of 15000–65000 nT. The ASM magnetometer is based on the Electron Spin Resonance (ESR) principle and makes use of the Zeeman effect which splits the emission and absorption lines of atoms in an ambient magnetic field. The pattern and amount of splitting is a signature of the magnetic field strength. The optically pumped helium magnetometer uses a High Frequency (HF) discharge within a gas cell to excite ${}^4\text{He}$ atoms from the ground state to the metastable state. This metastable level is split by the Earth magnetic field into 3 Zeeman sublevels. The separation of those sublevels is directly proportional to the ambient field strength and equals half the gyro frequency ($eB/2m$ with m – electron mass).

| <i>ASM Specifications</i> | |
|----------------------------------|-----------------------------|
| Mass | 3000 g |
| Power consumption | 5.3 W |
| Dimension Sensor Head | 40 × 60mm |
| Dimension DPU | 200 × 150 × 100mm |
| Data Rate | 0.35 Mbyte/ day |
| Dynamic Range | 15000 – 65000 nT full scale |
| Absolute Accuracy | <0.3 nT (2σ) |
| Omni-directional response | < 0.1 nT angular dependence |

3.3 The Star Tracker (STR)

The STR provides the attitude of the VFM and both are co-mounted in a common optical bench. The μ ASC (Advanced Stellar Compass from DTU) star tracker is a well proven instrument with an extensive space heritage. It features two fully cold/hot redundant DPU's. Full cross-strapping, each DPU can control one to four CHU's. Mission specific baffles can be designed for optimum performance. It can provide 22 true solutions per sec. The absolute accuracy is <1''. The mass is < 1400g (3 × CHU, BFL's & DPU). The power is < 5.7 W (3 × CHU+DPU). It can support asteroid science - Near Earth Object (NEO) detection and planets triangulation.



Fig. 4 The STR μ ASC for the Swarm mission. Central: redundant electronics box. Each side can operate up to four camera heads

3.4 The Optical Bench (OB)

The purpose of the Optical Bench is the transference of the attitude from the extremely precise star trackers to the magnetometer field components. The OB ensures a highly mechanical stable platform for the magnetometer and the star trackers.

A exhaustive thermo mechanical design and analysis is carried out to determine and minimize any thermal gradient that could cause a shift in the relative attitude between the two systems.

The STR are very magnetically clean, however the separation between the two (STR and VFM) is about 40 cm to reduce magnetic perturbation from the STR's. Exploitation of symmetric system has been resulted in a cylindrical tube holding the VFM sensor, minimizing transversal thermal gradients. Emphasis has been on the matching of material parameter, use of iso-static support interfaces and detailed analysis of loads.

The instruments are calibrated as stand alone and once integrated in the OB, a inter-calibration and system verification is carried out in order to determine the relative orientation between the VFM and STR and to verify that the stability is as required.

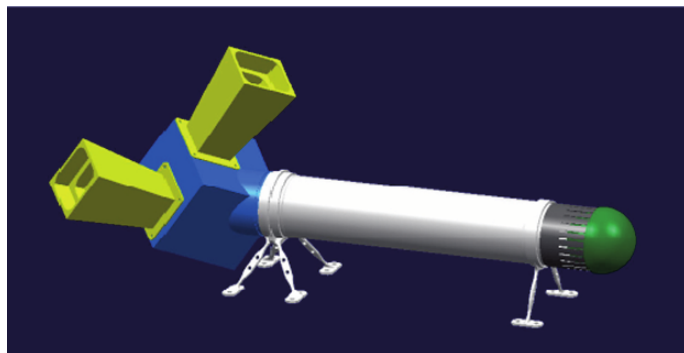


Fig. 5 The Optical Bench with three star tracker cameras (yellow, only two of them are shown) and the magnetometer sensor (green)

4 Discussion

The Ørsted, SAC-C and CHAMP satellites have had some overlapping during 1999–2007, whereas MAGSAT has produced a reference measurement point at 1980. These missions have produced a large amount of high quality magnetic field data and therefore contributed enormously for the understanding of the Earth's magnetic field. This has yielded models that can represent the many field contributions (Earth's core, Earth's crust, large scale ionospheric and magnetospheric currents, interactions with the Sun, galaxy, ocean currents, tidal currents, earthquakes, etc . . .).

In some occasions there has been conjunctions of the orbits of these satellites (Ørsted/CHAMP/SAC-C). However, the orbits are not optimized for certain field structures analysis. In addition, the instrumentation and platform in these satellites are not uniform. The field measure in space is the result of many sources, which can be spatial dependent but also time dependent. The volume out there in space is enormous, and therefore the space-time ambiguity can not be resolved with single

point measurements. Since it is not possible to have a fixed measuring point in space, constellations have been devised in order to separate these sources in the models. Other constellations have been launched (Cluster, Stereo, Themis, ...) for the investigation of structures in specific regions of the Earth environment.

The rationale behind Swarm is that the signal extraction of space-temporal signatures can be optimized by designing the orbits of a constellation of three satellites. This is of quite importance for further understanding the Earth and its evolution, and therefore its history.

5 Conclusion

The instruments planned for Swarm are the evolved counterparts of those flown on Ørsted, with slightly better performance as well as mounted in a more mechanically stable optical bench. Therefore one could expect a factor of 5 better in overall performance. The instruments are 10 times as stable and since there are three star cameras, a much better attitude can be determined in all directions.

The Ørsted orbit was 600–800 km whereas Swarm is planned for about 350 km. Ørsted is a low mass (60 kg) and gradient stabilized satellite, which need to be at high altitudes otherwise the air drag will unstabilize it and cause a fast orbital decay. On the other Swarm has higher mass ($\sim 300\text{kg}$), which allows it to fly in a more aerodynamical regime, and at a lower orbits. In addition it also carries fuel and the altitude can be controlled as opposed to the case of Ørsted. By using the cubic attenuation law (i.e. $850/350)^3 \sim 10$), this could give up to a factor 10 on the measurement of the field. Therefore, in principle one of the Swarm satellites could provide a precision up to 50 times better than Ørsted.

Finally, the instruments can be tested, calibrated and verified to probe the high performance as stand alone. However, the VFM, which has to be calibrated with the ASM, has to be related to a geographical coordinate system via the STR. Therefore, one has to ensure that the measurement performance and thermal stability is not degraded from the instrument level towards the satellite level. In addition, the long term stability and timing between the three satellites has to also be ensured for the constellation level.

References

1. E. Friis-Christensen, H. Lühr, and G. Hulot, *Swarm: A constellation to study the Earth's magnetic field*, Earth Planets Space, Vol. 58 (No. 4), pp. 351–358, 2006
2. http://esamultimedia.esa.int/docs/EEUCM/Swarm_handout.pdf
3. http://esamultimedia.esa.int/docs/EEUCM/SWARM_TPA.pdf

EO Formation Flying Applications for Small Satellite Missions

Tony Sephton, Alex Wishart, Karsten Strauch, and Frederic Teston

Abstract The aim of the ESA study on concepts for demonstration of advanced techniques and technologies on an EO (“Earth Observation”) small mission is to identify, assess and trade-off ideas for EO missions which are compatible with implementation on a small satellite such as PROBA-3, and which may benefit from Formation Flying using the PROBA-3 mission as reference. The output of the study will comprise a definition of a mission and required developments, along with estimated mission cost. In addition, and because the PROBA-3 mission has some capacity for implementing an additional payload, the study will identify such a payload of opportunity along with its required development and cost which can take advantage of the PROBA-3 orbit and possibly its Formation Flying opportunities. The study is led by Astrium Satellites Ltd, with support from Astrium SAS, Astrium GmbH, ENVEO, GMV and Verhaert Space.

1 Introduction

The scope of work comprises identification, study and analysis of candidate EO missions for implementation with small satellites of the PROBA-class flying either in formation, constellation or as single spacecraft. Requirements are derived on Formation Flying techniques and technologies and on the PROBA-3 demonstration mission to serve EO mission requirements.

T. Sephton

Astrium Satellites Ltd, Gunnels Wood Road, Stevenage, SG1 2AS, England
e-mail: tony.sephton@astrium.eads.net

A. Wishart

Astrium Satellites Ltd, Gunnels Wood Road, Stevenage, SG1 2AS, England

K. Strauch

ESTEC, Postbus 299, NL 2200 AG Noordwijk, Netherlands

F. Teston

ESTEC, Postbus 299, NL 2200 AG Noordwijk, Netherlands

A trade-off and selection process is followed by the outline of a reference candidate Formation Flying EO small mission. The estimation of the advantages of the implementation of the EO missions in Formation Flying assuming the performance demonstrated by PROBA-3 and the establishment of the approach to future utilization of the technology, tools and facilities developed for PROBA-3 is performed. The term “Small Mission” here implies small satellite platforms of the micro- and mini-sat class of up to 150 kg total spacecraft mass (e.g. PROBA, DMC, Myriade, etc.). An EO guest payload for the PROBA-3 platform will also be identified and analysed.

2 PROBA-3

PROBA-3 (Project for On-Board Autonomy) is an ESA precursor technology demonstration mission to prove techniques and technologies which will be required for future operational Formation Flying missions in the fields of space science, Earth Observation and surveillance. PROBA-3 will comprise two spacecraft with a combined mass in the range 500–600 kg. The spacecraft will combine standard platform technology with new technology for Formation Flying command, guidance, navigation and control (GNC), relative metrology sensors and thrusters. The PROBA-3 programme will also drive the development of advanced engineering processes for the specification, design and verification of Formation Flying systems. The operational lifetime of the mission will be two years, with a VEGA launch expected in the 2010–2011 timeframe.

The principal science payload carried on PROBA-3 will be ASPIICS (“Association de Satellite Pour Imagerie et l’Interferometrie de la Couronne Solaire”), which is a very large, externally occulted, solar coronagraph. The Occulter spacecraft carries an occulting disk which is approximately 1.5 m in diameter. The Coronagraph spacecraft carries the coronagraph optical instrument. For ASPIICS, the Coronagraph spacecraft flies in formation with respect to the Occulter, at a nominal separation of between 150 m and 250 m, maintaining the entrance pupil of the Coronagraph optics centred within the shadow formed by the occulting disk. In addition to ASPIICS, PROBA-3 will conduct demonstrations of other Formation Flying manoeuvres which are relevant for both future science and Earth Observation missions.

A fundamental system design aspect of PROBA-3 is the choice of the operational orbit. A highly elliptical orbit (HEO) has been selected (see Fig. 1), with an orbital period of three days. The high apogee of approx. 160,000 km provides a benign environment for precision science operations closely representative of the environment of future operational missions flying in Lagrange orbits, and the low perigee of (initially) 800 km provides an environment to demonstrate low Earth orbit (LEO) type Formation Flying which is of relevance for Earth Observation missions. The orbit period being an odd integer multiple of 24 hours means that apogee and perigee always occur over roughly the same longitude on the Earth’s surface. The orbit inclination is 32 degrees, which is a good compromise between the VEGA injection capability and visibility from the designated ground station at Redu in Belgium. The orbit is oriented with the apogee over the Northern hemisphere and

perigee mainly over Australasia. The perigee height will vary over the course of the two year mission due to lunar-solar perturbations of the orbit.

Non-Keplerian Formation Flying for both ASPIICS and other science demonstrations takes place during the apogee pass where the gravity gradient is very small. The perigee pass will be free-flying, with the natural evolution of the relative motion under the local gravity gradient.

It is planned that PROBA-3 will carry a guest EO payload of opportunity for which a nominal 30 kg mass allocation is reserved, whilst on the Coronagraph spacecraft there will be at least 40 W of power available away from apogee when the Coronagraph optics and the laser metrology systems are switched off.

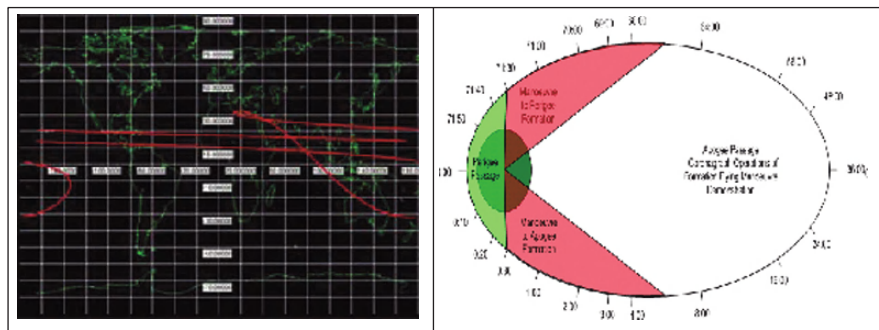


Fig. 1 PROBA-3 operational orbit – Ground trace (LHS) and Timeline (RHS)

3 Selection of EO Formation Flying Missions and Guest Payloads of Opportunity

Three broad categories of EO missions have been identified, i.e. missions requiring co-ordinated Formation Flying, missions benefiting from Formation Flying (“loose” Formation Flying, including also the single spacecraft case), and missions not requiring Formation Flying. The different applications of Formation Flying considered include:

- Synergy of observations by splitting the payload onto several satellites.
- Coincident observations of nadir and limb looking sensors, e.g. AceCHEM.
- Aperture synthesis techniques (radar or optical), e.g. SMOS.
- Synthesis of gradiometer baselines, e.g. GRACE / GOCE follow-on.
- Stereoscopic and bistatic observations, e.g. for generation of DEM’s.

Higher altitudes benefit from lower disturbance forces and hence accuracy of formation positional measurement and control, but may require larger instruments to achieve required resolution of the desired EO parameter.

A number of primary and secondary selection criteria have been used to down-select from an initial list of about 40 candidates to about 12 candidates now being analysed in more detail, particularly with respect to their Formation Flying characteristics, and accommodation on PROBA-3. A number of these candidates are described by way of example below.

3.1 EO Small Missions (with or without Formation Flying)

3.1.1 L-Band SAR and Single-Pass Interferometry

Single-pass interferometry removes the problem of temporal de-correlation that is always associated with interferometric image pairs acquired at different times, and as such is highly desirable. Simultaneous acquisition is achieved by implementation of a 2 (or more) satellite constellation in which the orbits of the component satellites are carefully controlled so that appropriate interferometric baselines can be established. This type of system is achievable with current technologies and is within the reach of small satellites. Only one of the spacecraft needs to carry a transmitter, and the other spacecraft receivers only.

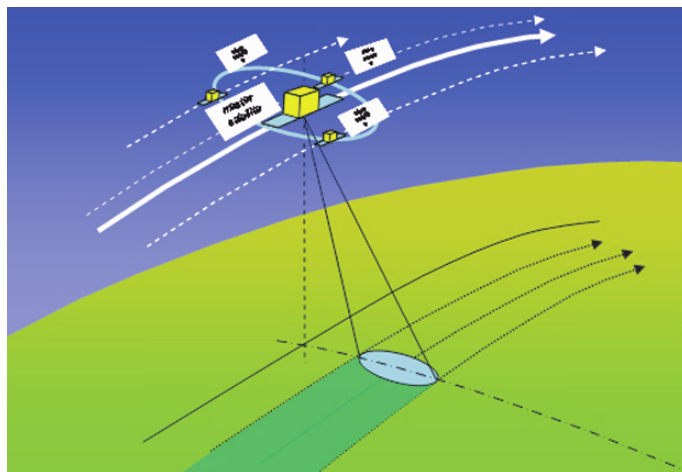


Fig. 2 L-Band SAR Single-pass interferometry concept

3.1.2 AERL – Aerosol Land Mission

Improved information on optical depth, type and size of aerosol is needed for climate and environmental research and for air pollution monitoring. Aerosols have an effect on the radiation balance of the Earth-atmosphere system that is not yet well known, and the possible contribution (cooling or warming) of aerosols to global warming is still a matter of controversy. In addition to direct radiative effects in the

clear atmosphere, their role as condensation nuclei is important. Another issue of increasing concern is adverse effects on human health of very fine particles (“fine dust”) that have only recently been recognized as a major menace in Europe, calling for urgent actions to reduce the concentrations of these particles. The UN/EC Convention on Long-Range Trans-boundary Air Pollution requires not only monitoring of trace gases, but also of tropospheric aerosol.

In view of these needs, the Aerosol Land Mission (AERL) has been proposed by ENVEO as a complement to the existing lower resolution (several km) global aerosol missions such as POLDER (on PARASOL). The AERL mission would enable the study of aerosol distribution and properties at regional scales with high spatial detail, measuring directional reflectance, polarization and aerosol layer height near-simultaneously. Spatial resolution of about 250 m is proposed, being more than an order of magnitude below the resolution of the global aerosol missions. This is of particular relevance for understanding and quantifying the main aerosol sources and types, and is also supportive for developing measures to reduce the concentration of fine dust in populated areas.

For retrieval of aerosol properties over land, it is necessary to separate the atmosphere signal from the surface signal of unknown or poorly known reflection properties. For this purpose it is necessary to obtain multiple viewing angle measurements of both intensity and polarizations.

For retrieval of aerosol optical depth (AOD) and type, the observations required are:

- Intensity of backscattered solar radiation in 9 bands within 350–940 nm, spectral resolution ca. 15 nm. Spatial resolution about 250 m to map aerosol sources.
- Polarized radiance in 3 bands.
- All observations in 3 pointing directions: $-55^\circ, 0^\circ, 55^\circ$; azimuth close to the principal plane ($\Delta\phi = 0^\circ$).

For information on aerosol layer height (ALH) and vertical aerosol distribution:

- Intensity of backscattered solar radiation in about 4 channels of the Oxygen A-band (760 nm), $\Delta\lambda \cong 1$ nm resolution. Spatial resolution about 500 m.
- All observations in 2 pointing directions: $0^\circ, 55^\circ$. Azimuth as above.

For complementary information on atmospheric water vapour content:

- Intensity of backscattered solar radiation about 6 channels in the H_2O bands (876 nm, 940 nm), $\Delta\lambda \cong 1$ nm resolution.
- All observations in 2 pointing directions: $0^\circ, 55^\circ$. Azimuth as above.

This leads to the combination of multispectral imaging radiometers and narrow band imaging spectrometer shown in Fig. 3.

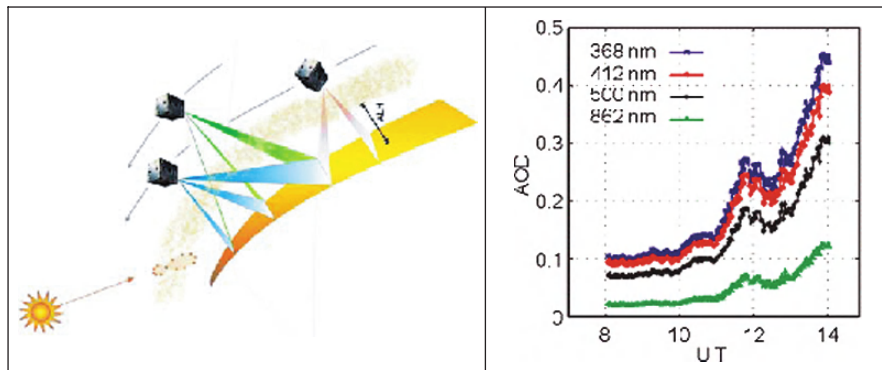


Fig. 3 LHS: Observation geometry of the AERL mission ($\times 2$ multispectral imaging radiometers with 3 view angles, narrow band imaging spectrometer with 2 view angles). RHS: Temporal variability of aerosols observed at Lago di Garda, 10 June 2003

3.1.3 Thermal Inertia mapping

Thermal inertia of bodies is a measure of their resistance to changing temperature under a time varying energy flux, and therefore it is proportional to the time involved in absorbing and losing heat; it increases with an increase in material conductivity, capacity and density.

Thermal inertia can be defined as the amplitude of the diurnal temperature curve as illustrated in Fig. 4, or the maximum minus minimum surface temperature, and so can be determined by observing a particular area at two different times. The temperature of a material with low thermal inertia changes significantly during the day, while the temperature of a material with high thermal inertia does not change as rapidly. Deriving and understanding the thermal inertia of the surface can help to recognize small-scale features of that surface. In conjunction with other data such as water vapour content, thermal inertia can help to characterize surface materials and the geological processes responsible for forming these materials.

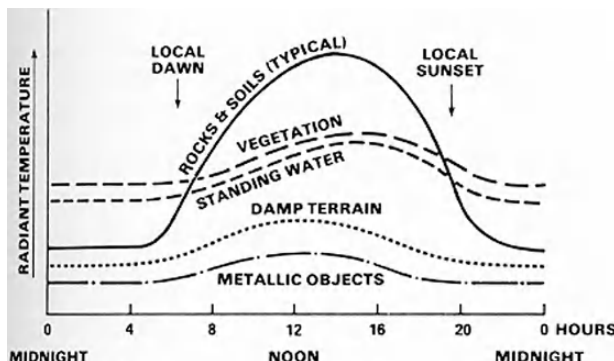


Fig. 4 Changes in radiant temperatures of 5 surface-cover types during a 24-hour thermal cycle [1]

Although a traditional approach in evaluating thermal inertia involves both day and night coverage (see Fig. 5), it is also possible to discriminate between surfaces with different thermal inertia using the thermal portion of the electromagnetic spectrum with coverage around noon: this is when the thermal contrast between dry and wet areas reaches maximum.

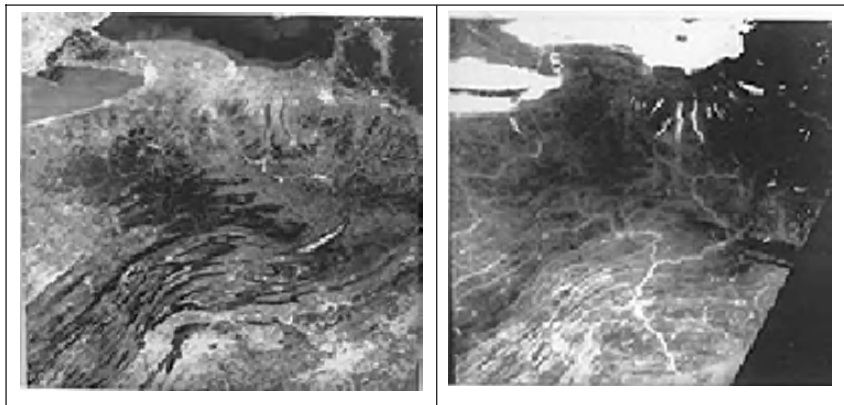


Fig. 5 Day (LHS) and night (RHS) thermal IR observations of North-East USA using Heat Capacity Mapping Radiometer data (ref. <http://www.fas.org/>)

Thermal inertia mapping requires a single broad bandwidth thermal channel (e.g. 10.5–12.5 microns) plus a single broad bandwidth visible channel to give surface albedo. Some atmospheric spectral bands are also useful (for water vapour, etc) to remove the atmospheric effects from the thermal signature.

This concept is being evaluated within the study using microbolometers to determine its feasibility as a potential EO Small Mission.

3.2 *Payloads of Opportunity*

3.2.1 Lightning Imagery Experiment (LIM)

The objective of this mission concept is to validate the measurement principle and usefulness of lightning imagery from near geo-orbit position. The mission is proposed as precursor for a lightning imager on the Meteosat Third Generation (MTG) satellite, and is intended to provide real-time capabilities in lightning detection and location in support to nowcasting and Very Short Range Forecasting of severe storm hazards and lightning strike warning. As lightning is strongly correlated with storm-related phenomena like precipitation, hail and gust, a further objective is to act as proxy for intensive convection related to ice flux, updraft strength and convective rainfall.

The frequency of lightning depends on the climate zone, the season and on regional characteristics like surface topology, ocean currents and wind direction.

Between 4 and 30 million lightning events per day occur worldwide (equivalent to 100 lightning events per second), about 10% of which strike the ground. Lightning is monitored by observing a neutral oxygen line in the near IR (e.g. at 777.4 nm).

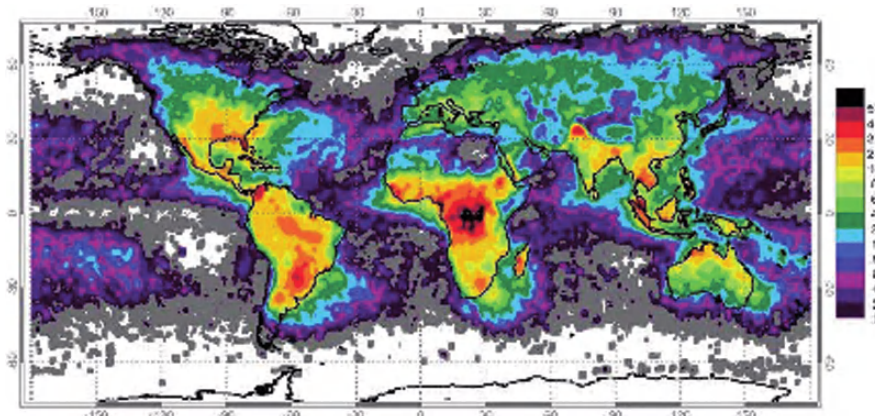


Fig. 6 Global lightning frequency

The LIM concept is being considered in this study as a potential payload of opportunity for PROBA-3, perhaps operated from apogee. The integral trapped proton spectrum caused by passage through the Van-Allen Belt is relatively high, and will require special protective measures for the detector. The lightning imager conceived for MTG has a mass of 48 kg and input power of 57 W.

3.2.2 PARIS Spaceborne Demonstrator

The concept of using signals of opportunity for sea surface altimetry is well documented. The importance of pursuing such an instrument as PARIS (Passive Reflectometry and Interferometry System) is the ability it has of providing a wide swath compared with the traditional nadir-looking radar altimeter, with the purpose of providing important oceanographic data to supplement that data already being acquired. This is achieved by selecting beams across the flight direction to look directly at the reflection specular point for opportunity signals from GNSS (Global Navigation Satellite System) satellites such as GPS and in the future GALILEO.

The instrument is a bi-static radar where the source is the GNSS transmitted signal, the target is the sea, land or ice surface, and the Receiver is mounted on a satellite which is at low altitude. By measurement of the Direct paths and the Reflected paths, the relative mesoscale altitudes can be deduced.

With a major interest in mesoscale ocean altimetry to identify ocean eddies and other important characteristics, the PARIS instrument is ideally suited as it can provide a wide swath (typically 1200 km for 500 km orbit) in line with the flight direction. It is important to note the flexibility of the GNSS-R approach, as with a relatively simple instrument it is possible to obtain scatterometry type of data for

sea-state measurements and sea surface wind speeds. The PARIS instrument is the next step with the measurement of mesoscale altimetry. The major difference in approaches is that the PARIS instrument requires a more sophisticated antenna and beam-steering system in order to achieve a good signal-to-noise ratio, as well as multiple frequencies (L1, L2 and L5) which can be used to reduce the effects of ionospheric errors and also to reduce/eliminate phase ambiguities.

Figure 7 shows the system block diagram. The direct signal is assumed to be received by a GPS Receiver onboard the platform. This receiver will also provide the navigation data to the instrument controller so that it can predict the location of the reflection area. Hence the instrument controller can provide the data for the steering of the antenna beam to the reflection point.

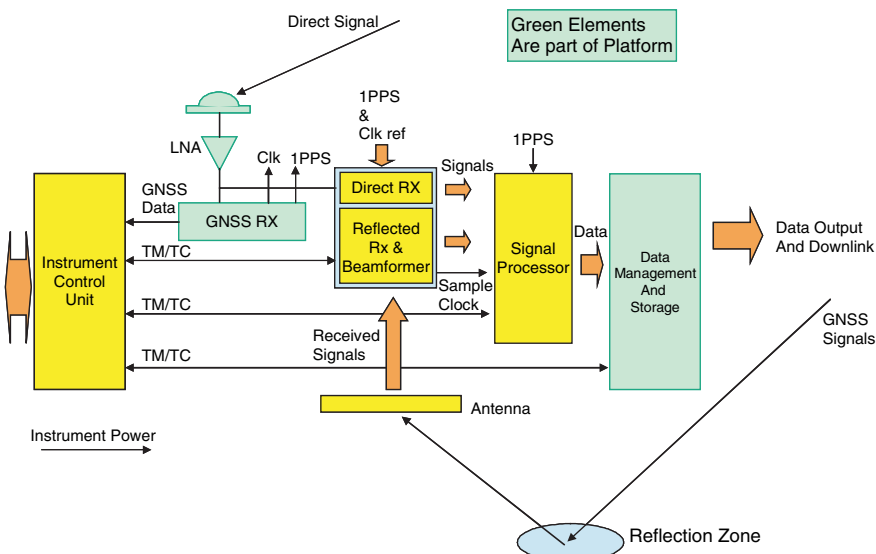


Fig. 7 PARIS system block diagram

PARIS would nominally require a LEO orbit so only the perigee phase of the PROBA-3 orbit can be used. The data-take is assumed to be 15 minutes (primarily over the ocean). Total mass of the PARIS Spaceborne Demonstrator is currently estimated at 20 kg, and power at 81 W for 3 frequencies (68 W for 2 frequencies).

4 Conclusions

This study has identified a large number of candidate EO missions that would benefit from Formation Flying, as well as potential EO payloads of opportunity on PROBA-3. The study is still ongoing, with selection of the reference mission and payload due to be made in Summer 2007, followed by a detailed mission and payload design in the second half of the study.

Acknowledgement This study is being performed for ESA under contract number 20395/06/NL/JA. The inputs from ENVEO and Astrium GmbH to this paper on the AERL and Lightning Imager concepts respectively are gratefully acknowledged.

Reference

1. F.F. Sabins Jr., Remote Sensing: Principles and Interpretation. 2nd Ed., 1987.

Session 5

Subsystems (1)

GPS for Microsatellites – Status and Perspectives

Oliver Montenbruck, Markus Markgraf, Miquel Garcia-Fernandez,
and Achim Helm

Abstract GPS receivers nowadays provide a well established system for tracking of spacecraft in low-Earth orbit (LEO). In addition, GPS receivers serve as instruments for geodetic and atmospheric research on an ever growing number of science missions. The paper provides an overview of existing GPS receivers for LEO satellites, covering both fully space qualified as well as commercial-off-the-shelf (COTS) systems. The needs of pure navigation receivers and advanced science instruments are independently discussed and directions for future systems are identified. Potential benefits of the new Galileo constellation are addressed and recommendations for future receiver developments are given.

1 Introduction

More than 30 years have past since the first spaceborne GPS receiver was flown on-board the Landsat-4 satellite. Since then, GPS has become a well accepted tool for spacecraft navigation and scientific investigations. With at least four GPS satellites in view, a spaceborne GPS receiver can provide instantaneous position and velocity as well as timing information onboard a user spacecraft. This enables new and powerful applications and promises relevant cost savings in ground operations and space equipment.

O. Montenbruck

DLR, German Space Operations Center, D-82234 Oberpfaffenhofen, Germany
e-mail: oliver.montenbruck@dlr.de

M. Markgraf

DLR, German Space Operations Center, D-82234 Oberpfaffenhofen, Germany

M. Garcia-Fernandez

DLR, German Space Operations Center, D-82234 Oberpfaffenhofen, Germany

A. Helm

GeoForschungsZentrum Potsdam, Telegrafenberg A 17, D-14473 Potsdam

Besides the navigation oriented applications, GPS sensors are more and more employed as science instruments for geodetic and atmospheric research. GPS tracking has enabled the generation of high-fidelity gravity field models and GPS radio occultation (RO) measurements support a global near-real-time monitoring of the troposphere and ionosphere. Finally, new science opportunities emerge through the analysis of ground reflected GPS signals.

So far, the distinction between the navigation and science applications is almost unambiguously reflected in the choice of single- versus dual-frequency receiver technology. The vast number of GPS receivers in orbit are designed to provide navigation and timing information with an accuracy that is well compatible with the GPS Standard Positioning Service (SPS) and thus the use of single-frequency technology. Science applications, on the other hand, demand the availability of dual-frequency measurements to measure (or eliminate) ionospheric path delays and to enable purely carrier-phase based navigation. In fact, high precision navigation marks the boundary between both receiver classes and a growing tendency to support these needs may be recognized in the receiver market.

Following a more detailed discussion of navigation and science applications, an overview of current single-and dual-frequency receiver technology is given in the subsequent sections. Thereafter, future technology needs and trends are discussed, giving proper attention to the upcoming Galileo system. In view of limited space, the presentation is confined to the use of Global Navigation Satellite System (GNSS) receivers on LEO satellites. These constitute the majority of missions and offer the largest market segment for spaceborne GNSS technology. Special applications, such as GEO and HEO missions are beyond the scope of this survey and left for future studies.

2 Spaceborne GNSS Applications

2.1 Navigation and Timing

With at least four GPS satellites in view, a spaceborne GPS (SGPS) receiver can provide instantaneous position and velocity as well as time information onboard a user spacecraft. The four-dimensional nature of the GPS navigation information distinguishes it from other spacecraft tracking systems. This enables new and powerful applications and promises relevant cost savings in ground operations and space equipment [1]. So far, the usefulness of GPS has already been demonstrated for

- precise orbit determination [2],
- onboard time synchronization and geocoding of payload information [3],
- autonomous orbit control and maneuver planning [4],
- spacecraft formation flying [5, 6], and
- onboard attitude determination [7, 8],

to mention just the most popular applications.

Following the deactivation of Selective Availability (S/A), representative accuracies for GPS based real-time navigation of spacecraft in low Earth orbit (LEO) are on the order of 10 m for kinematic single-frequency solutions. Associated timing accuracies for onboard clock synchronization are generally better than 1 μ s. Using dual frequency receivers and dynamical filtering the real-time navigation accuracy can further be improved to 1 m and below. In post-processing, accuracies of down to 5 cm have been achieved using dual-frequency GPS measurements in combination with sophisticated reduced dynamic orbit determination algorithms [2]. For relative navigation of two spacecraft based on carrier-phase differential GPS (CDGPS), accuracies of down to 1 mm have been demonstrated in real-time hardware-in-the-loop simulations [5] as well as offline analyses of actual flight data [6].

As illustrated by these examples, spaceborne GPS sensors offer remarkable positioning accuracies, that are hardly achieved with alternative tracking devices at competitive cost. Unfortunately, the same does not apply for GPS-based attitude determination, which generally suffers from short baselines and signal reflections at the spacecraft structure. Even though various successful flight demonstrations have been reported in the literature ([7, 8]), the achieved accuracies of 0.1°–1° are easily outperformed by other attitude sensors such as star cameras and optical gyros. Attitude capable GPS receivers have therefore gained little attention by spacecraft designers and have not reached a fully operational status.

2.2 Radio Science

Besides the navigation oriented applications, GPS sensors are more and more employed as science instruments for geodetic and atmospheric research [9]. This is nicely exemplified by the German CHAMP satellite, which carries a BlackJack dual-frequency GPS receiver. GPS measurements collected onboard this satellite have enabled the independent generation of high-fidelity gravity field models that notably outperformed the results derived from all previous space missions [10]. GPS radio occultation measurements, furthermore, enable a tomographic and low-latency monitoring of the troposphere and ionosphere for weather forecasts and atmospheric studies [11]. GPS instruments for occultation measurements are flown on the latest generation of European meteorological satellites (METOP, [12]) and a global constellation (COSMIC) of five satellites carrying GPS occultation receivers has been launched by the Taiwanese government in 2006.

While the use of GPS measurements for gravimetry and atmospheric research is now a well established technology, new science opportunities emerge through the analysis of ground reflected GPS signals. The GPS constellation offers a particularly large number of “natural” signal sources for bistatic altimetry and surface roughness or wind speed measurements. The feasibility of these techniques has been demonstrated the onboard CHAMP satellite [13, 14] and with a dedicated GPS receiver onboard the UK satellite of the Disaster Monitoring Constellation [15] and a variety of future space experiments has already been proposed by the science community.

3 Receiver Survey

A non-exhaustive list of present and planned GPS receivers for space applications is provided in Tables 1 and 2 for single- and dual-frequency receivers, respectively. Compared to terrestrial GPS receivers, the environmental robustness of space equipment is a continued source of concern. Key issues to be considered in this context include the resistance to thermal-vacuum conditions, vibration and shock loads as well as ionizing radiation and single event effects. Besides a cost driving test and qualification effort that is implied by applicable space engineering standards, suitably qualified electronic components are often less powerful and require higher resources (mass, power) than state-of-the-art consumer electronics.

The small market segment and high specialization of SGPS receivers as well as the associated test and qualification effort inevitably results in high unit cost ranging from roughly 100 k€ to 1 M€. Various companies and research institutes have therefore made efforts to come up with low cost solutions based on the use of commercial-off-the-shelf (COTS) components. Following the early work of SSTL, miniature single-frequency GPS receivers based on COTS components are now considered for numerous micro-satellites projects. An advanced example of these is DLR's check-card sized Phoenix GPS receiver, which has been selected for the Proba-2, Flying Laptop, TET, ARGO, and X-Sat missions. The receiver offers a power consumption of less than one Watt and can provide real-time and offline navigation down to the 1 m level [16]. It will also provide high-accuracy relative navigation for the first European formation flying mission, PRISMA.

Based on promising experience with single-frequency receivers, DLR has taken the initiative to investigate the use of commercial-off-the-shelf (COTS) dual-frequency receivers for space applications and perform a basic qualification program

Table 1 Single-frequency GPS receivers for space applications

| Manufact. | Receiver | Chan | Ant | Power Weight | TID [krad] | Missions, References |
|-----------------------------|--------------|-----------|-----|-----------------|---------------|---|
| Alcatel (F) | TopStar 3000 | 12–16 C/A | 1–4 | 1.5 W 1.5 kg | > 30 | Demeter, Kompsat-2; |
| EADS | MosaicGNSS | 6–8 C/A | 1 | 10 W 1 kg | > 30 | SARLupe, TerraSAR-X |
| Astrium (D) | | | | | | Aeolus; [17] |
| General Dynamics (US) | Viceroy | 12 C/A | 1–2 | 4.7 W 1.2 kg | 15 | MSTI-3, Seastar, MIR, Orbview, Kompsat-1 |
| SSTL (UK) | SGR-05 | 12, C/A | 1 | 0.8W, 20g | >10 | |
| | SGR-20 | 4 × 6 C/A | 4 | 6.3 W 1 kg | >10 | PROBA-1, UOSat-12 [8], BILSAT-1 |
| DLR (D) | Phoenix-S | 12 C/A | 1 | 0.9 W 20 g | 15 | Proba-2, X-Sat, FLP, ARGO, PRISMA; [16] |
| Accord (IND) | NAV2000HDCP | 8 C/A | 1 | 2.5 W 50 g | | X-Sat |

Table 2 Dual frequency GPS receivers for space applications

| Manufact. | Receiver | Chan | Ant | Power Weight | TID [krad] | Missions, References |
|------------------------|----------------------------------|------------------------------|----------------|--------------|------------|--|
| SAAB (S) | GRAS/ GPSOS | 12 C/A,P1/2 | 3 30kg | 30 W | | METOP [11] |
| Laben (I) | Lagrange | 16 × 3 C/A,P1/2 | 1 5.2 kg | 30 W | 20 | ENEIDE, Radarsat-2, GOCE; [18] |
| General Dynamics (US) | Monarch | 6–24 C/A,P1/2 | 1–4 4 kg | 25 W | 100 | |
| JPL (US) / BRE (US) | BlackJack / IGOR | 16 × 3 C/A,P1/2 | 4 3.2/4.6kg | 10 W | 20 | CHAMP, GRACE, Jason-1/COSMIC, TerraSAR-X; [19] |
| Alcatel (F) | TopStar 3000G2 | 6 × 2 C/A,L2C | 1 | | | Under development; PROBA-2; [20] |
| Austrian Aerospace (A) | Inn. GNSS Navigation Recv. | Up to 36 C/A,P1/2 | 2 | | >20 | Under development; SWARM; [21] |
| BRE (US) | Pyxis Nautica | 16–64 C/A,P1/2 L2C, L5 | 1–4 2.5 kg | 20 W | | Under development |
| NovAtel (CA) | OEM4-G2L | 12 × 2 C/A,P2 | 1 50 g | 1.5 W | 6 | CanX-2; CASSIOPE; [22] |
| Septentrio (B) | PolaRx2 | 16 × 3 C/A,P1/2 | 1 (3) 120 g | 5 W | 9 | TET; [19] |

as well as initial flight demonstrations. As part of this effort, NovAtel's OEM4-G2L receiver and Septentrio's PolaRx have been demonstrated to cope with the signal dynamics and the environmental conditions of a low Earth satellite [19, 22]. Extended flight demonstrations of these receivers are planned for 2008–2009 onboard the Canadian CASSIOPE mission and the German TET technology demonstration micro-satellite.

4 Technology Needs and Trends

The applications and available receiver equipment discussed in the previous sections nicely demonstrate that GNSS is a mature and well accepted technology for space missions. Despite these achievements, continued research and development are deemed necessary to properly respond to needs of future mission designers and scientists. Even though the evolution of the spaceborne receiver market is not expected to parallel the explosive evolution of the terrestrial GNSS market, a continued growth and technical evolution are likewise expected. Aside from an overall need for cost-reduction, the four key challenges have to be met: miniaturization, increased accuracy and robustness, support of new signals, and advanced science applications. These are addressed in more detail in the subsequent paragraphs.

4.1 Miniaturization

Shrinking space programs and the interest in faster mission implementations have raised the attractiveness of small and micro-satellites that can be implemented by individual research institutes or Small and Medium sized Enterprises (SMEs). These missions are generally characterized by limited engineering (and financial) budgets and benefit most from a further reduction in the size, mass and power consumption of avionics equipment. As a guideline, power consumptions below 1 W appear desirable for onboard radio navigation receivers that are continuously operated. This requirement can presently only be met by COTS-base receivers such as the SGR-05, Phoenix and CCA-370HJ [23] receivers. Further efforts will thus be required to achieve a similar performance with fully space hardened electronic components.

An extreme case of miniature satellites is represented by the CubeSat initiative, which has resulted in numerous student projects around the world. At a nominal size of $10 \times 10 \times 10 \text{ cm}^3$, and an average power budget of 1 W, the use of a GPS receiver onboard such satellites becomes highly demanding. Modified Garmin and Trimble receivers as well as Phoenix receivers are considered in some upcoming CubeSat missions, but no successful flight demonstration has yet been reported. Despite serious technical concerns and risks, the operation of GPS receivers onboard CubeSat satellites would ultimately be of benefit for the space community. Even sparse position fixes could assist a proper orbit determination and prediction in the absence of continuous and reliable NORAD tracking and thus facilitate a better maintenance of space object catalogues.

4.2 Accuracy and Robustness

Applications such as remote sensing, altimetry, and SAR interferometry drive the need for sub-decimeter orbit information that is traditionally served by dual-frequency GNSS receivers and ground-based precise orbit determination (POD) systems [2]. So far, a 10 m level accuracy has well been accepted for onboard purposes, but a 1 m or better position knowledge already becomes desirable for onboard geocoding of high resolution imagery and open-loop altimeter operation. For comparison, a 0.5 m accuracy (3D rms) is presently achieved by the DORIS tracking system onboard Jason-1 using the DIODE real-time navigation function. In case of spaceborne GPS, ionospheric errors can well be eliminated through the use of dual-frequency tracking or the GRAPHIC combination of code and phase data in single-frequency receivers [16]. This leaves the GPS broadcast ephemeris errors with a representative Signal-In-Space-Error (SISRE) of 1–1.5 m as the limiting factor. Even though a 0.5 m real-time position accuracy is within reach of a GPS based navigation system, this performance has so far only been validated in lab experiments and flight demonstrations are still pending. As a major step forward, JPL and NASA have implemented a service for transmitting real-time corrections to the GPS broadcast ephemerides via the TDRSS satellites. In combination with the Real-Time GIPSY navigation software, these corrections should enable decimeter position accuracies onboard a LEO satellite [25].

In terms of robustness, the long cold-start time (typically 10–15 min) of many spaceborne GPS receivers represents a limiting factor. In particular, GPS receivers presently don't lend themselves as safe-mode sensors that can deliver immediate position and/or attitude information after being switched on. GPS tracking is hardly feasible today on heavily tumbling spacecraft. Among others, fast signal acquisition techniques will be required to extend the application range of GPS receivers for these purposes.

4.3 New Signals

The prospect of new GPS signals (L2C, L5, L1C) and the build-up of the Galileo Constellation causes great attention by terrestrial and spaceborne GNSS users alike [26]. Key benefits include the larger number of satellites transmitting navigation signals and the improved signal characteristics. The larger number of satellites improves

- the geometric dilution of precision,
- the redundancy and data screening capabilities, and
- the number of occultation and reflection events for scientific applications.

The new signals and navigations data in turn offer

- direct (versus-semi-codeless) tracking of dual-frequency signals,
- lower tracking noise and enhanced multipath suppression,
- data & pilot codes and an moderate increase in total signal power,
- tri-carrier ambiguity resolution,
- more accurate broadcast ephemerides,
- integrity information.

It remains to be seen, which of these advantages can ultimately be materialized in future space missions. The improved multipath reduction, for example, applies only for reflecting objects more than several meters from the antenna and is thus primarily of interest for GNSS navigation in the vicinity of the International Space Station (ISS). On the other hand, radio occultation measurements will clearly benefit from the unencrypted ranging codes that enable improved signal-to-noise ratios and dual-frequency tracking down to very low tangent point altitudes.

Most other benefits come at a notable increase in hardware cost and complexity. Compatibility with the new signals and the increased number of visible satellites will trigger the demand (even though not necessarily a serious need) for a 2–3 times increase in the processing power of correlators and micro-processors. With a total of four frequency bands (L1, L2, E5, E6) and an “inflationary” number of different signals, a variety of different receiver designs are possible. It remains to be seen, which types of spaceborne GNSS receivers will ultimately evolve and find a sufficiently large market. Likely candidates include an L1 single-frequency receiver as well as a L1+E5a dual-frequency receiver for tracking open service signals from up to 24 GPS

and Galileo satellites. For an intermediate transition time, the need to support L2 signals of the GPS constellation, might even result in tri-band receiver designs. Given the mass and power budgets of current space-grade GPS receivers, major efforts will, however, be required to keep the resulting receivers within reasonable limits.

4.4 Advanced Science Applications

LEO satellite-based Global Navigation Satellite System (GNSS) receivers for bistatic altimetry/reflectometry and radio occultation measurements are of great interest as a possible component of future tsunami and Earth observation systems [27]. The general idea is that densely spaced grids of sea surface heights with a few centimeters precision could be established fairly rapidly using multi-frequency GNSS receivers as add-on payload to independently planned Earth observation missions. The required performance of such a space-based monitoring system requires highly advanced GNSS receivers with improved algorithms and quasi real-time data processing capabilities to satisfy the needs of a future spacebased Tsunami Early Warning System. To support these activities, GFZ and DLR have recently launched a study for the development of a GNSS Occultation, Reflectometry and Scatterometry receiver (GORS) in the frame of GITEWS project [28]. A close cooperation between research organization and industry is considered as a key factor for a successful development of a cost effective science instruments. In view of limited projects budgets and the restricted technical capabilities of current space-grade receivers, the development activity and initial flight demonstrations will be based on the modification of a COTS based dual-frequency GNSS.

5 Summary

The status and prospects of GNSS receiver technology for space applications have been described. Miniaturization, increased performance and the support of new navigation signals have been identified as needs for future missions. GNSS reflectometry and scatterometry are considered as emerging scientific applications that deserve proper attention by receiver system designers.

References

1. Rush J.; *Current Issues in the Use of the Global Positioning System Aboard Satellites*; Acta Astronautica 47(2–9), 377–387 (2000). DOI 10.1016/S0094-5765(00)00079-5
2. Jäggi A., Hugentobler U., Bock H., Beutler G.; *Precise Orbit Determination for GRACE Using Undifferenced or Doubly Differenced GPS Data*; submitted to Advances in Space Research (2006).
3. Gill E., Montenbruck O., Kayal H.; *The BIRD Satellite Mission as a Milestone Towards GPS-based Autonomous Navigation*; Navigation – Journal of the Institute of Navigation 48(2), 69–75 (2001).

4. Lamy A., Charmeau M.-C., Laurichess D., Grondin M., Bertrand R. (CNES); *Experiment of Autonomous Orbit Control on the DEMETER Satellite*; 18th International Symposium on Space Flight Dynamics, 11–15 October 2004, Munich, Germany (2004).
5. Leung S., Montenbruck O.; *Real-Time Navigation of Formation-Flying Spacecraft Using Global Positioning System Measurements*; Journal of Guidance, Control and Dynamics 28(2): March-April 2005, 226–235 (2005).
6. Kroes R., Montenbruck O., Bertiger W., Visser P.; *Precise GRACE Baseline Determination Using GPS*; GPS Solutions 9, 21–31 (2005). DOI 10.1007/s10291-004-0123-5
7. Um J., Lightsey E. G., *GPS Attitude Determination for the SOAR Experiment*; Navigation – Journal of the Institute of Navigation 48(3), 181–194 (2001).
8. Purivigraipong S., Unwin M., Hashida Y.; *Demonstrating GPS Attitude Determination from UoSat-12 Flight Data*; ION-GPS-2000 conference, 19–22 September 2000, Salt Lake City (2000).
9. Yunck T. P.; *Spaceborne GPS for POD and Earth Science*. in: Reigber Ch., Lühr H., Schwintzer P., Wickert J. (eds.), *Earth Observation with CHAMP – Results from Three Years in Orbit*, Springer, Berlin, 25–30 (2004).
10. Reigber Ch., Jochmann H., Wünsch J., Petrovic S., Schwintzer P., Barthelmes F., Neumayer K.-H., König R., Förste Ch., Balmino G., Biancale R., Lemoine J.-M., Loyer S., Perosanz F.; *Earth Gravity Field and Seasonal Variability from CHAMP*. in: Reigber Ch., Lühr H., Schwintzer P., Wickert J. (eds.), *Earth Observation with CHAMP – Results from Three Years in Orbit*, Springer, Berlin (2004).
11. Heise S., Jakowski N., Wehrenpfennig A., Reigber C., Luehr H.; *Sounding of the Topside Ionosphere/Plasmasphere Based on GPS Measurements from CHAMP: Initial Results*; Geophysical Research Letters 29(14), (2002). DOI 10.1029/2002GL014738.
12. Loiselet M., Stricker N., Menard Y., Luntama J.-P.; *Metop's GPS Based Atmospheric Sounder*; ESA Bulletin 102, May (2000).
13. Beyerle G., Hocke K.; *Observation and Simulation of Direct and Reflected GPS Signals in Radio Occultation Experiments*; Geophysical Research Letters 28(9): 1895–1898 (2001).
14. Cardellach E., Ao C.O., Juarez M.D., Hajj G.A.; *Carrier Phase Delay Altimetry with GPS-Reflection/ Occultation Interferometry from Low Earth Orbiters*; Geophysical Research Letters 31(10): L10402 (2004).
15. Gleason S., Adjrad M., Unwin M.; *Processing Ocean Reflected signals from Space: Early Results from UK-DMC GPS Reflectometry Experiment*; ION-GNSS-2005, 14–16 September 2005, Long Beach (2005).
16. Montenbruck O., Gill E., Markgraf M.; *Phoenix-XNS - A Miniature Real-Time Navigation System for LEO Satellites*; NAVITEC'2006, 11–13 December 2006, Noordwijk (2006).
17. Fichter W., Bruder M., Gottzein E., Krauss P., Mittnacht M., Botchkovski A., Mikhailov N., Vasilyev M., *Design of an Embedded GPS Receiver for Space Applications*, Space Technology, IFAC (2001).
18. Zin A., Landenna S., Conti A., Marradi L., Di Raimondo M.S.; *ENEIDE: an Experiment of a Spaceborne, L1/L2 Integrated GPS/WAAS/EGNOS Receiver*; ENC 2006 (2006).
19. Montenbruck O., Garcia-Fernandez M., Williams J.; *Performance Comparison of Semi-Codeless GPS Receivers for LEO Satellites*; GPS Solutions 10, 249–261(2006).
20. Serre S., Mehlen C., Boyer C., Holsters P., Seco-Granados G., Garcia-Rodriguez A., Issler JL., Grondin M.; *A Dual Frequency GPS Receiver (L1/L2c) for Space Applications*; NAVITEC'2006, 11–13 December 2006, Noordwijk (2006).
21. Reichinger H., Griesauer F., Zangerl F., Consoli A., Piazza F., Garcia-Rodriguez A.; *A Highly Integrated Modular European Spaceborne Dual Frequency GPS-Receiver*; NAVITEC'2006, 11–13 December 2006, Noordwijk (2006).
22. Langley R.B., Montenbruck O., Markgraf M., Kang C.S., Kim D.; *Qualification of a Commercial Dual-frequency GPS Receiver for the e-POP Platform Onboard the Canadian CASSIOPE Spacecraft*; NAVITEC'2004, 8–10 December 2004, Noordwijk, The Netherlands (2004).
23. Saito H., Mizuno T., Kawahara K., Shinkai K., Sakai T., Hamada Y., Sakaki H.; *Development and On-Orbit Results of Miniature Space GPS Receiver by Means of Aoutmobile-Navigation*

- Technology; 25th International Symposium on Space Technology and Science, 4–11 June 2006, Kanazawa, Japan (2006).*
- 24. Jayles C. H., Vincent P., Rozo F., Balandraud F; *DORIS-DIODE: Jason-1 has a Navigator on Board*; Marine Geodesy 27, 753–771 (2004).
 - 25. Bar-Sever Y., Bell B., Dorsey A., Srinivasan, J.; *Space Applications of the NASA Global Differential GPS System*; ION-GPS-2003, Portland, OR, USA(2003).
 - 26. Rizos C.; *New GNSS Developments & the Impact on Providers & Users of Spatial Data Infrastructure*; IGS Workshop, 8–11 May 2006, Darmstadt, Germany (2006).
 - 27. Martin-Neira M., Buck C., Gleason S., Unwin M., Caparrini M., Farres E., Germain O., Runi G., Soulat F.; *Tsunami Detection Using the PARIS Concept*; GNSSR05 Workshop on Remote Sensing Using GNSS- Reflections, June 2005, University of Surrey, Guildford, UK (2005).
 - 28. Helm A., Stosius R., Beyerle G., Montenbruck O., Rothacher M.; *Status of GNSS Reflectometry Related Receiver Developments and Feasibility Studies in the Frame of the German Indonesian Tsunami Early Warning System*; IGARSS-07, 23–27 July 2007, Barcelona (2007).

On-the-Fly Merging of Attitude Solutions

Peter S. Jørgensen, John L. Jørgensen, and Troelz Denver

Abstract Recent advances in autonomous attitude determination instrumentation enable even small satellites flying fully autonomous multi head star trackers providing full accurate and robust attitude information. Each sensor provides the full attitude information but for robustness and optimal usage of the available information, i.e. optimal accuracy, methods for merging such data should be investigated. The need for and desirability of attitude merging depends on the mission objective and available resources. To enable real-time attitude control and reduce requirements on download budget, on-board merging of attitude data will often be advantageous. This should be weighted against the need for post observation reconstruction of attitudes, especially needed when end products are sensitive to optimal attitude reconstruction. Instrument integrated merging algorithms will reduce the complexity of on-board AOCS. Methods for attitude merging are many. Two examples of merging methods taking into consideration anisotropic noise distributions are presented and discussed.

1 Introduction

With the advances in development of sensor technology and onboard computational power, autonomous multi sensor attitude instruments are becoming the preferred choice even for small satellite missions. As an example, several small satellites (e.g. PROBA, SMART-1, PROBA-2, Flying Laptop and PRISMA) are now featuring autonomous multi-head star-trackers.

P.S. Jørgensen

Measurement and Instrumentation Systems, Danish National Space Center, Technical University of Denmark, Elektrovej, Building 327, 2800 Kgs Lyngby, Denmark
e-mail: psj@spacecenter.dk

J.L. Jørgensen

Measurement and Instrumentation Systems, Danish National Space Center, Technical University of Denmark, Elektrovej, Building 327, 2800 Kgs Lyngby, Denmark

T. Denver

Measurement and Instrumentation Systems, Danish National Space Center, Technical University of Denmark, Elektrovej, Building 327, 2800 Kgs Lyngby, Denmark

Merging the individual measurements from several attitude sensors on a spacecraft has classically been performed in the on-board AOCS and when higher attitude knowledge is required on ground. However, with the computational surplus of state of the art multi-head attitude sensors, it is now possible to perform the attitude merging in the attitude instrument itself, while still enabling further improvements by post-processing on the ground. Despite that the process appears simple, this task is not trivial, since the relative orientation between attitude-sensors will often be non-constant over time due to thermally induces deformations in the spacecraft structure. Applied methods will, for optimal performance, have to take this into account, and reliably report the estimation of such biases and their variability.

There are several advantages of merging multi sensor attitudes in the instrument itself. Primarily, it reduces the complexity of the on-board AOCS sensor fusion module, which especially for small satellites can be desirable. Secondly, solutions incorporating measurements from several sensors will be more robust towards dropout of individual sensors. This is of interest to any mission, but especially to missions with relatively high agility requirements; e.g. in Earth imaging and formation flying applications. Also, combining the measurement data will improve the accuracy of the solution output from the attitude instrument. In addition to the obvious \sqrt{n} -noise reduction from two or more measurement of the same physical quantity, anisotropic accuracy distributions can be improved. E.g. for a star tracker, the accuracy of the determination of the roll about the line-of-sight can be reduced by a factor in the range of 5–10 (depending on sensor geometry) by combining solutions from two or more heads.

This paper presents the rationales for instrument-integrated merging of attitude solutions and discusses the pitfalls of this strategy. Two methods for merging attitude solutions are presented. These apply regardless of whether the merging takes place in the instrument, in the AOCS on-ground. An example of attitude merging results is presented.

2 Why Instrument Integrated On-the-Fly Attitude Merging?

Merging of attitude sensor data can be performed on ground (post observation) or on-the-fly (real-time), either in the on board AOCS core or in the individual multi-sensor instrument. A number of parameters should be taken into account when evaluating pros and cons for either approach.

On-the-fly attitude merging is characterized by real-time response enabling real-time agile attitude control. This includes both improved accuracy from merging two or more says on the attitude and increased robustness from immunity towards outages of individual sensors (e.g. blindings). These characteristics will be crucial to the overall mission success when the quality of the mission primary observation, obtained by e.g. telescopes, antennas or gravimeter, will be negatively impacted by lack of high accuracy attitude knowledge and control.

Secondary benefits include reduced downlink budget requirements and reduced costs of ground support operations.

Table 1 Characteristics to be considered when evaluating on-the-fly vs. post observation merging of attitude data

| Characteristics | On-the-fly merging | | Post observation, on ground merging |
|---|--|--|-------------------------------------|
| | Instrument merging | AOSC merging | |
| <i>Response time</i> | Real-time | Real-time | Days to weeks |
| <i>Real time attitude control</i> | Yes | Yes | No |
| <i>Robustness</i> | High | High | Low |
| <i>Accuracy</i> | High | High | High |
| <i>Flexibility of merging method</i> | Medium | Medium | High |
| <i>Additional relative orientation model parameters available</i> | None-Few | Some | Many |
| <i>AOCS load</i> | Low | High | Low |
| <i>Bandwidth required</i> | Low | Low | High |
| <i>Science reconstruction possibilities</i> | Limited, requires download of all data | Limited, requires download of all data | High |

The main advantage of performing attitude merging within the individual instrument is the reduction of AOCS complexity and required AOCS processing capability as well as performing the merging at a stage where intimate knowledge of noise spectrum and distribution is well established. This is to be weighted against the benefits of performing the merging process in the AOCS, namely: Increased availability of additional parameters characterizing the S/C state, e.g. structure temperatures; full system level control over the merging process.

Post observation merging is on the other hand characterized by high flexibility and use-specific optimization of the merging method applied. This includes detailed modeling of internal S/C platform flexures. This is especially needed when very high accuracy attitude information over the full orbit (attitude and pose) and over many orbits (seasons and time) is essential to the mission end product but the primary observation is not impacted by less than optimal attitude control, e.g. geopotential mapping missions.

Depending on the mission attitude knowledge requirements and on-board processing resources, either strategy may be selected, but for some missions it may be necessary to have both the fast response of on-board merging and the possibility of post processing the full attitude information from all sensors. Table 1 summarizes the main characteristics.

3 Merging Methods

Merging of attitude information can be performed in numerous ways depending of the goal and available information. Here methods will be restricted to simultaneous measurements from two or more sensor heads providing the full attitude (all three

degrees of freedom) in each measurement, as it is the case for multi head star trackers.

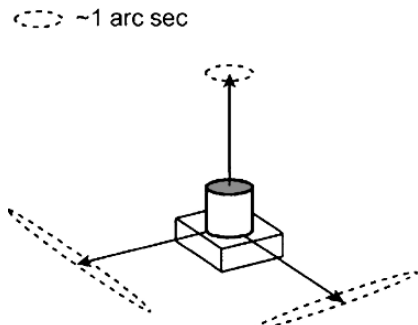
The attitude measurement gives the orientation of the sensor with respect to a reference frame (typically the inertial J2000 frame) and can be parameterized as e.g. a set of Euler angles, a quaternion or a direction cosines matrix.

Two important features characterize the merging method:

- Weighting. If weighting information in the form of noise estimates for the individual measurement is available this should be included in the merging. At least sensor specific information on anisotropic noise distribution should be used.
- Relative orientation of sensors. Either assumed to be constant or varying. If the relative orientation is assumed to be varying it may either be modeled against external information or simply filtered/traced.

When performing attitude merging it is essential to include knowledge about the relative sensor noise and the noise distribution properties. Relative sensor noise is normally specified as part of the measurement data in the form of e.g. a residual. Sensors will often have anisotropic noise distributions. For the star tracker example the direction of the boresight axis is determined with an accuracy, which is a factor 5–10 better than the accuracy of the rotation about the boresight axis. This is illustrated in Fig. 1.

Fig. 1 Example of anisotropic noise distribution for a star tracker. Dotted lines give the error ellipses for each of the three axis of the measurement frame. Since the pointing error typically is the same in all directions, the uncertainty of the pointing vector result in a small error circle. Since the roll noise is higher than the pointing noise, the error at lateral directions result in an error ellipse



When merging data with anisotropic noise distributions care must be taken to avoid worsening the overall noise. An example of this is shown in Fig. 2.

However including knowledge about the noise distribution can improve the accuracy of the merged solution relative to the two individual solutions. This is illustrated in Fig. 3.

For most S/C platforms the relative orientation between sensors will vary over time. This is a consequence of varying thermo-mechanical loads on the structure. Often a correlation with the orbit period is seen, an example of this is shown in Fig. 4. The magnitude of these variations will depend on the platform design, but

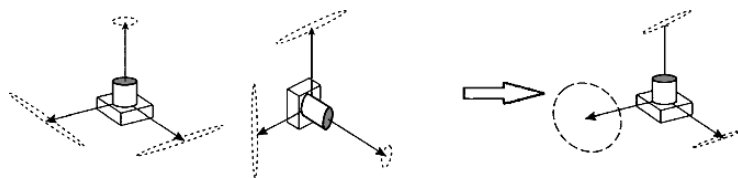


Fig. 2 Example of attitude merging of two orthogonal star trackers with anisotropic noise distribution. Simple averaging of the two independent attitude solutions will lead to less than optimal attitude knowledge. E.g. if simple addition of vectors is used, the error ellipse is added to the small error circle for two axes giving a new ellipse, and the two error ellipses will add to a large error circle in the last axis

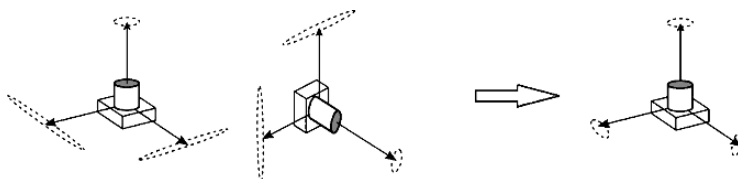


Fig. 3 Example of merging method where anisotropic noise distribution has been taken into account

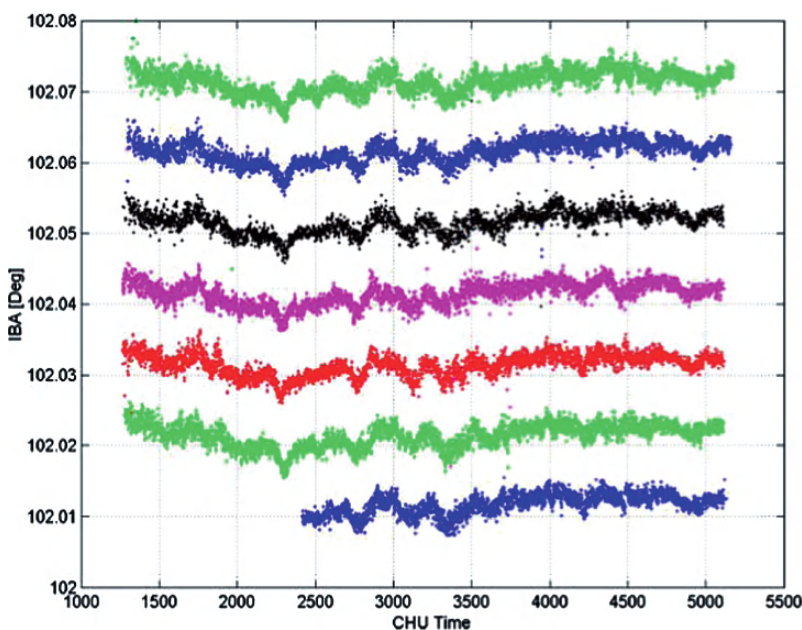


Fig. 4 Variation of relative orientation between two sensors over 6 consecutive orbits. The relative orientation is represented by the Inter Boresight Angle (IBA). IBA is offset 0.01 deg pr. orbit for clarity

will often be in the range of several tens of arc seconds for standard platform structures. Very stable platforms can be achieved by careful design, i.e. the SWARM optical bench carrying vector magnetometer and star trackers aims at a sub-arc second stability through the use of ultra low thermal expansion coefficient materials combined with thermal stability control [1].

Stability of the S/C structure shall be taken into account both when designing the mission and when selecting the method for attitude merging.

In the following, two examples of attitude merging methods for star tracker measurements are given.

3.1 Merging of Two Boresight Directions

A simple form of attitude merging of star tracker data is performed by merging the two line-of-sight directions into a single common reference frame [2]. This merging method utilizes the fact that for star trackers the boresight direction is more accurately determined than the rotation angle about this axis. The merging of the two boresight directions (v_1 and v_2) is performed by constructing:

$$\begin{aligned} v_a &= \frac{v_1 + v_2}{|v_1 + v_2|} \\ v_b &= \frac{v_1 - v_2}{|v_1 - v_2|} \\ v_c &= v_a \times v_b \end{aligned}$$

This orthogonal triad constitutes the merged common frame specifying the attitude and will carry the full accuracy in all three axes. Assuming a rigid support structure, the relative rotation (R_{i-C}) from each of the sensor frames ($i = 1, 2$) to the common (C) frame may be calculated for each attitude update. In case of dropout of one of the sensors, the common frame is constructed by offsetting the valid measurement with (R_{i-C}). In case of a non-rigid support structure filtering or parameterized modeling of (R_{i-C}) may be introduced.

This method does not support the introduction of variable weighting information but fixed weights may be incorporated if relevant.

Results obtained using this method is exemplified below. The example shows the merging for two sensor heads placed on a common bracket structure having an angle of 40 deg between the two boresights. The measurements were carried out on ground with two star trackers on a common mounting structure, operated at sea level, and thus show an elevated noise level relative to what is observed in space due to the influence of the atmosphere. Note the much smaller scale of the graphs showing the boresight direction (1st axis).

It is seen that the asymmetry in the noise distribution is significantly improved in the merged data, while maintaining the good overall performance.

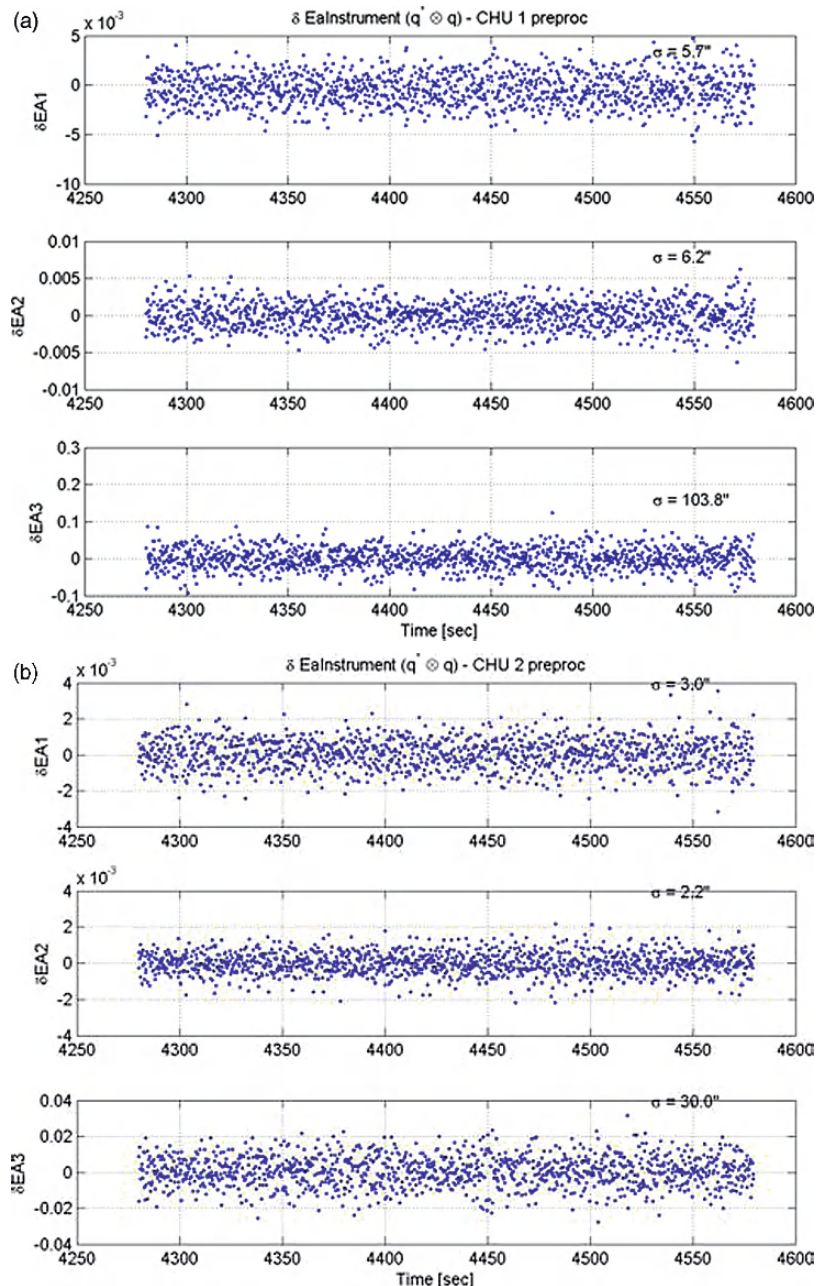


Fig. 5 Noise estimation in native star tracker frame for two sensor heads obtained from ground measurements. The anisotropic noise distribution is clearly seen

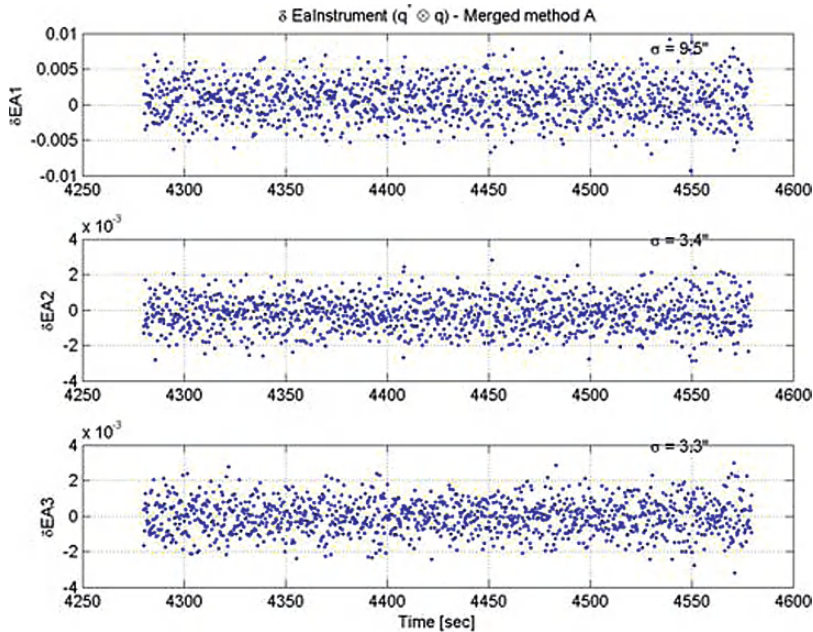


Fig. 6 Noise estimation for combined attitude solution obtained merging the two boresights. Please note that the three axes are not the same as for the individual sensors

3.2 Merging of the Full Attitude Information

Using the full attitude information from each sensor, any information on anisotropy in the measurement accuracy should be used in the merging process. A method achieving this is described in [3].

If the simultaneous attitudes measurements are represented by DC matrices (R_{REF-i}) and the orientation of the common frame (C) with respect to each sensor frame is R_{i-C} is assumed fixed. The sensor specific noise distribution matrix σ_i shall be transformed to the common frame resulting in σ_{Ci} .

$$\sigma_{Ci} = (R_{i-C}) \sigma_i (R_{i-C})^T$$

The noise distribution in the common frame is then applied as weights for merging the individual attitudes in the common frame $R_{REF-C,i}$.

$$R_{REF-C,i} = R_{i-C} R_{REF,i}$$

Also for this method the relative orientation between sensor and common frame can be modeled or filtered depending on available information and application.

4 Conclusion

Merging of individual attitude solutions from multi sensor head attitude instruments is important for obtaining the optimal performance with respect to accuracy and robustness. This merging can take place within the instrument, in on-board AOCS or on ground. Advantages and drawbacks of either approach have been discussed. On-the-fly attitude merging is crucial to missions where the primary observation will be influenced negatively by less than optimal attitude knowledge. Other missions may do as fine with on-ground post processing. When selecting merging method it is important to take into consideration weighting of the available attitude information, especially in the case of anisotropic noise distributions shall be included. Also platform stability shall be given consideration and if needed modeling or filtering of the relative attitude between sensors shall be included in the method.

References

1. J.M.G Merayo et al. (2007) The Swarm Magnetometry Package, Small Satellites for Earth Observation, 6th International Symposium of the IAA, Berlin, April 23–26, 2007.
2. This method has been developed and used by GeoForschungsZentrum Potsdam on the CHAMP satellite.
3. L. Romans (JPL 2003), Optimal combination of quaternions from multiple star cameras.

Design and On-Orbit Evaluation of Magnetic Attitude Control System for the “REIMEI” Microsatellite

Shin-Ichiro Sakai, Yosuke Fukushima, and Hirobumi Saito

Abstract Magnetic attitude control methods for the REIMEI microsatellite are presented. REIMEI is a 70 kg microsatellite and was launched in 2005. REIMEI achieved pointing accuracy of 0.05–0.1°, with three magnetic torquers (MTQs) and one moment wheel. With this configuration, the management of magnetic torque is important for attitude control. This paper proposes practical MTQs drive algorithm to generate required magnetic torque, maintaining undesirable disturbance torque to be low enough even in the neighborhood of singular points. Another key technology is in-orbit estimation of residual magnetic dipole and its feedforward cancellation. This method will contribute a lot, not only for a bias momentum satellite, but also for small/micro satellites with pure magnetic ACS. These proposed methods are demonstrated with in-orbit data of the REIMEI microsatellite.

1 Introduction

Recently, small or micro satellites attract interest, as a way to access space frequently with practical cost. Also in the field of space science, several small/micro satellites have achieved significant success. One typical example is the MOST satellite [1], and it indicates that the attitude control performance is important even for small/micro satellites. It should be also true for earth observation applications. Reaction wheel is the most commonly used actuators for usual attitude control system, however, reaction wheel is not suitable for some smaller spacecraft, from the view

S.-I. Sakai

Institute of Space and Astronautical Science / JAXA, 3-1-1, Yoshinodai, Sagamihara-shi, Kanagawa 229-8510, Japan
e-mail: sakai@isas.jaxa.jp

Y. Fukushima

Institute of Space and Astronautical Science / JAXA, 3-1-1, Yoshinodai, Sagamihara-shi, Kanagawa 229-8510, Japan

H. Saito

Institute of Space and Astronautical Science / JAXA, 3-1-1, Yoshinodai, Sagamihara-shi, Kanagawa 229-8510, Japan

point of size, weight and cost. Magnetic torquer (MTQ) seems to be more practical solution for micro satellites.

INDEX (INnovative-technology Demonstration EXperiment) is a 70 kg scientific microsatellite for aurora observation (Fig. 1). On August 2005, it was successfully released into a nearly sun-synchronous polar orbit by Dnepr rocket, and then renamed as REIMEI. Restricted mass budget allows only one reaction wheel for this satellite. Therefore, three magnetic torquers are the main actuators. Even with this configuration, the REIMEI satellite achieved attitude control capability with accuracy of $0.05\text{--}0.1^\circ$. This paper describes two key technologies for such magnetic attitude control system (ACS). One of them is the algorithm to calculate magnetic dipole, to generate required torque avoiding singularity problems. The other is in-orbit estimation of residual magnetic dipole.

2 REIMEI and its ACS Overview

This section briefly introduces the REIMEI satellite and its attitude control system. It will be helpful to understand following academic discussions.

REIMEI is about 70 kg in weight, and 50 cm cube in stowed configuration. For aurora observation, REIMEI payload consists of two main instruments:

- Multi channel auroral camera (MAC), high time/spatial resolution auroral imager with three CCD and interference filters.
- Electron/ion energy spectral analyzer (E/ISA), to analyze energy spectra of electrons and ions with a capability of high-time resolution.

One typical observation with these instruments is simultaneous observation of particle and image. E/ISA analyzes the energy spectra at the spacecraft, and MAC captures auroral image at magnetic line foot point, where aurora is energized by the particle E/ISA observed. Such observation requires spacecraft with three-axis stabilization and inertial pointing capability. The required accuracy of attitude determination is less than 0.05° , and the precision of attitude control is less than 0.5° .

One strong constraint on the ACS design is limited mass budget of microsatellite. Two or more wheels could not be accepted in this point. Therefore, REIMEI ACS consists of three orthogonal magnetic torquers (MTQs) and one momentum wheel (MW) as actuators. MW provides agility around roll axis, and MTQs generate attitude control torque around yaw and pitch axis. In this point, magnetic torque plays an important role.

Figure 1 shows the layout of spacecraft and its coordinate system. Momentum wheel axis is parallel to the z -body axis (roll axis), and provides gyroscopic rigidity. MAC and star tracker field-of-view are in $+x$ and $-x$ direction, respectively. IRU consists of three fiber optic gyros (FOGs), which are small COTS devices. REIMEI ACS also consists of two sun sensors and one three-axis magnetometer (MAG). Specifications of ACS sensors and actuators are listed in Table 1. Note that all computational tasks are executed on one integrated control unit (ICU) with SH-3 CPU.

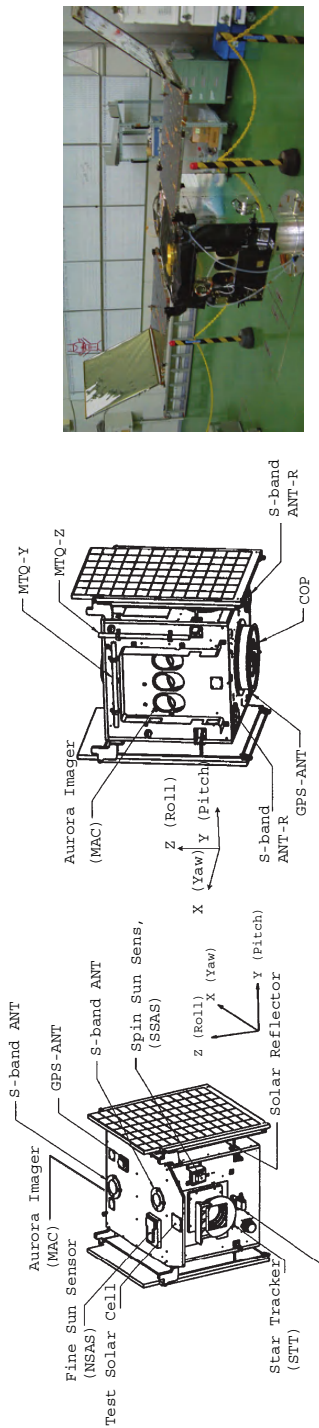


Fig. 1 The REIMEI Spacecraft layout and photo in deployed configuration

Table 1 Specification of REIMEI ACS sensors and actuators

| IRU (FOG × 3) | |
|----------------------------|--------------------------------|
| Weight | 0.14 kg @ 1-axis |
| Pulse Weight | 4.5 arcsec/pulse |
| Bias Stability | < 0.1°/h |
| Sun Sensor (NSAS) | |
| Weight | 0.9 kg |
| F.O.V | 50° |
| Accuracy | 0.05° |
| Random Noise | < 0.01° |
| Magnetometer (MAG) | |
| Weight | 0.5 kg |
| Range | ±1000 mG |
| Star Tracker (STT) | |
| Weight | 2.3 kg |
| F.O.V | 30° × 40° |
| Random Noise | < 3 arcmin(3σ) |
| Bias Error | < 1 arcmin(3σ) |
| Sampling Rate | 1 s |
| Momentum Wheel (MW) × 1 | |
| Weight | 2.45 kg |
| Ang. Momentum (Max.) | 1.0 Nms |
| Output Torque | > 0.01 Nm |
| Magnetic Torquer (MTQ) × 3 | |
| Weight | 0.3 kg @ 1-axis |
| Linear Dipole | > 6.0 Am ² @ 1-axis |

One important algorithm of REIMEI attitude control system is for management of magnetic torque, which determines magnetic dipole on MTQs to generate required control torque. In the following section, algorithm of magnetic torque control is discussed.

3 Magnetic Torque Control Low

3.1 Formulation

Attitude feedback controller requires certain amount of torque, which is a vector of three components. One of three components can be managed by momentum wheel, and remaining two components should be generated with MTQs. The issue to solve is to find magnetic dipole $\mathbf{M} = [M_x, M_y, M_z]^t$ which generates required torque on two axis, in geomagnetic field $\mathbf{B} = [B_x, B_y, B_z]^t$. If MW axis is parallel to z-body axis, required torque can be described as

$$\mathbf{T}^* = [T_x^* \ T_y^*]^t. \quad (1)$$

Since \mathbf{M} generates magnetic torque $\mathbf{T} = \mathbf{M} \times \mathbf{B}$, equation of \mathbf{T}^* and \mathbf{M} can be described as

$$\begin{bmatrix} T_x & T_y \end{bmatrix}^t = \mathbf{Bm}_2 \mathbf{M}, \quad (2)$$

where

$$\mathbf{Bm}_2 = \begin{bmatrix} 0 & B_z & -B_y \\ -B_z & 0 & B_x \end{bmatrix}. \quad (3)$$

Usually \mathbf{Bm}_2 is rank=2 matrix, therefore, magnetic dipole \mathbf{M} for \mathbf{T}^* can be calculated with pseudoinverse matrix,

$$\mathbf{M} = \mathbf{B}_{\mathbf{m}_2}^\# \mathbf{T}^*, \quad (4)$$

where $\mathbf{B}_{\mathbf{m}_2}^\#$ is a pseudoinverse matrix of \mathbf{Bm}_2 . Note that eq. 2 is underdetermined system, with three equations for two variables. As commonly known, pseudoinverse matrix finds out solution of minimum norm among all solutions. In other words, eq. 4 finds out the most efficient \mathbf{M} .

However, problem of this calculation occurs when $B_z = 0$, since it is a singular point of eq. 2. M_x and M_y have no contribution on magnetic torque, i.e., eq. 4 comes to be overdetermined, with two equations for one variables. Pseudoinverse matrix for overdetermined system outputs error minimum solution, and in this case, results huge magnetic dipole \mathbf{M} . The MTQs are saturated with this solution and generate large disturbance torque on z-body axis. This disturbance magnetic torque can be suppressed by momentum wheel torque, however, results large bias momentum fluctuation. Finally, it requires frequent unloading control and deteriorates attitude control performance.

To improve this behavior, novel algorithm is proposed in this paper, which is based on singularity robust inverse (SR-inverse) method. SR-inverse is proposed in the field of robotics [4], and also frequently used in CMG torque steering law. SR-inverse of \mathbf{Bm}_2 is

$$\mathbf{B}_{\mathbf{m}_2}^* = \mathbf{B}_{\mathbf{m}_2}' (\mathbf{Bm}_2 \mathbf{B}_{\mathbf{m}_2}' + kI)^{-1}, \quad (5)$$

where k is a parameter called scale factor. The solution of SR-inverse is determined “by evaluating the exactness and the feasibility simultaneously” [4], and k is a weighting factor to tune this balance. SR-inverse provides same \mathbf{M} as pseudoinverse when $k = 0$.

Important design to use SR-inverse is the automatic adjustment law of scale factor k . Generally speaking, k should have large value in the neighborhood of singular points. This paper proposes k adjustment to maintain T_z within a limitation. The difficulty of this adjustment exists in \mathbf{M} saturation with MTQ capability, and in proposed algorithm, k is adjusted in step-by-step manner as follows.

1. First, calculate M_z with SR-inverse,

$$M_z = \frac{B_x T_y^* - B_y T_x^*}{B_x^2 + B_y^2 + k_z}, \quad (6)$$

then limit M_z with MTQ capability.

2. Calculate M_x , M_y with SR-inverse and above M_z , as

$$M_x = \alpha (-T_y^* + B_x M_z), \quad M_y = \alpha (T_x^* + B_y M_z), \quad \alpha = \frac{B_z}{B_z^2 + k}, \quad (7)$$

then limit M_x , M_y with MTQ capability.

3. Calculate T_z which this \mathbf{M} will generate,

$$T_z = B_y M_x - B_x M_y, \quad (8)$$

then adjust scale factor k with

$$k_{j+1} = \begin{cases} k_j + a \Delta k_j & |T_{zj}| \geq T_{z0} \\ b \Delta k_j & |T_{zj}| < T_{z0} \end{cases} \quad (9)$$

$$\Delta k = \frac{dk}{dT_z} (|T_{zj}| - T_{z0}),$$

where a and b are the gain to tune the time response ($a > 0, 0 < b < 1$).

In eq. 6, k_z is another scale factor to avoid singular point of $B_x^2 + B_y^2 = 0$. It is necessary since we apply SR-inverse with small modification such that $|M_x^2 + M_y^2|$ is minimized instead of $\|\mathbf{M}\|$. Note that the computational complexity of this sequence is practical enough. Actually, it was implemented in REIMEI ACS.

Figure 2 shows the simulation results of proposed method, comparing with pseudoinverse solution. Even in the neighborhood of singular points, $B_z = 0$, proposed method generates moderate magnetic dipole. Scale factor k is automatically adjusted to limit disturbance T_z , and Fig. 2 shows this effect clearly. Therefore, disturbance T_z is much smaller than the pseudoinverse case.

3.2 Time-Sharing Unloading Control

As discussed above, $B_z = 0$ is the singular point for control torque generation. In contrast, larger B_x and B_y provides larger T_z . Since z -body axis is a bias momentum axis, period when $B_z \simeq 0$ is suitable for bias momentum unloading. Such time-sharing unloading control system was applied for REIMEI ACS.

3.3 Feedback Controller Design

Figure 3 shows the sensitivity function of the Euler angle feedback controller [6]. Since design target is a bias momentum satellite, whose bias momentum axis is z -body axis, attitude around x - and y - body axis are controlled with torque of y - and x - body axis, respectively.

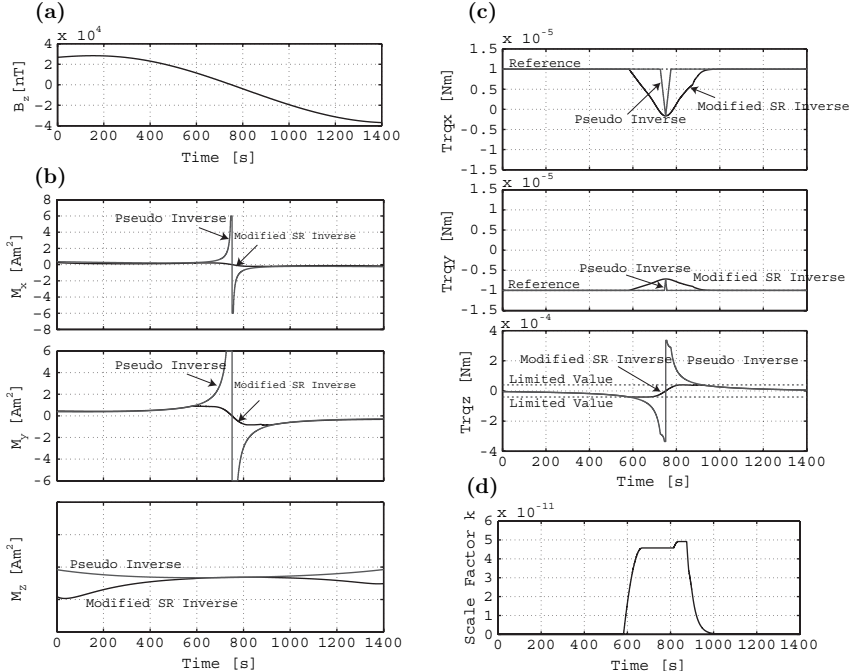


Fig. 2 Magnetic torque generation in magnetic field \mathbf{B} (a), Magnetic dipole \mathbf{M} to generate required T_x and T_y are calculated with two methods (b), Since proposed method provides \mathbf{M} with limitation of $T_z < T_{z01}$, disturbance torque T_z is much smaller than the pseudoinverse case (c), To limit the value of T_z , proposed method adjust the scale factor k dynamically (d)

4 Residual Magnetic Moment Observer

Generally, dominant attitude disturbance source for LEO microsatellite is residual magnetic dipole. Other disturbance sources, such as gravity gradient, solar radiation pressure or air drag, have relatively small effect for small spacecraft.

One approach to suppress disturbance is to enhance the feedback controller. This is an orthodox way, however, it depends on several conditions such as sensor noise, computational performance or plant model accuracy. Another approach is feedforward cancellation of residual magnetic dipole. In this case, performance depends on the accuracy of residual magnetic moment estimation. To estimate it with in-orbit attitude data, this paper proposes residual magnetic moment observer.

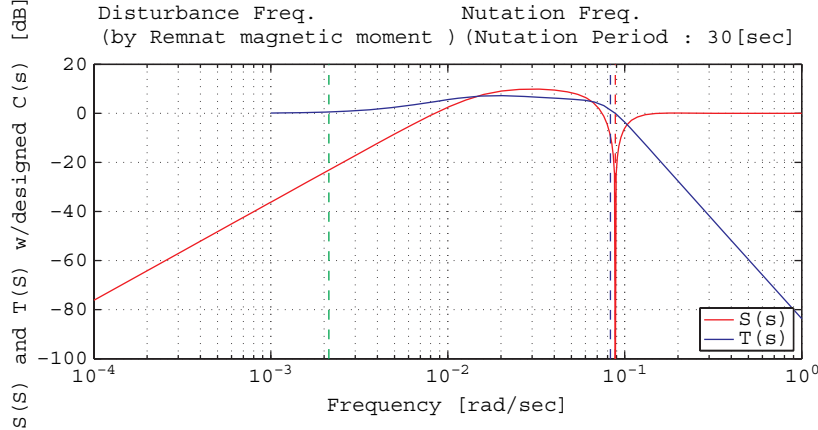


Fig. 3 Sensitivity function of closed loop system

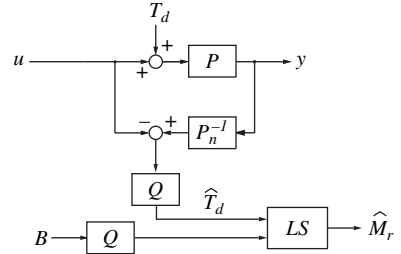


Fig. 4 Block diagram of residual magnetic moment observer

Figure 4 shows the block diagram of proposed residual magnetic moment observer. First thing to do is to estimate disturbance torque \hat{T}_d with disturbance observer (DOB) [7]. In Fig. 4, $P(s)$ is a plant model for spacecraft with bias momentum. $Q(s)$ should be low pass filter, and its order must be equal or higher than that of plant model. Input for DOB is s/c attitude $y(t)$ and control torque $u(t)$. Note that $u(t)$ can be calculated easily with MTQ output value and measured geomagnetic field data, and MW torque value.

The other part of proposed observer is least square (LS) estimation of residual magnetic dipole \hat{M}_r , with observed disturbance torque \hat{T}_d and measured geomagnetic field B . Estimated value of M_r will be found, when LS method is applied for equation of

$$\hat{T}_d = B_{m3} M_r, \quad (10)$$

where

$$B_{m3} = \begin{bmatrix} 0 & B_z & -B_y \\ -B_z & 0 & B_x \\ B_y & -B_x & 0 \end{bmatrix}. \quad (11)$$

Example of concrete implementation is described here for REIMEI case. The Q filter of DOB is designed as $Q(s) = 1/(\tau s + 1)^3$, where $\tau = 600$ s. Since observed $T_d(t)$ has time delay of τ , therefore, geomagnetic field data is also filtered with $Q(s)$ before LS estimation. With eq. 10, \mathbf{M}_r is estimated based on $\hat{\mathbf{T}}_d$'s three components. However, it is also possible to estimate \mathbf{M}_r with only $[\hat{T}_x, \hat{T}_y]$, eq. 2 and eq. 3. With N sample data, the equation for LS method comes to be

$$\begin{bmatrix} \hat{T}_{dx_1} \\ \hat{T}_{dy_1} \\ \dots \\ \hat{T}_{dx_N} \\ \hat{T}_{dy_N} \end{bmatrix} = \begin{bmatrix} 0 & B_{z1} & -B_{y1} \\ -B_{z1} & 0 & B_{x1} \\ \dots & & \dots \\ 0 & B_{zN} & -B_{yN} \\ -B_{zN} & 0 & B_{xN} \end{bmatrix} \mathbf{M}_r. \quad (12)$$

Since these matrices are usually huge, it is calculated as off-line calculation on ground for REIMEI case. However, recursive LS method is also available for such estimation, and it will enable on-board real-time estimation.

5 Evaluation of In-Orbit Performance

5.1 Residual Magnetic Moment Estimation with In-Orbit Data

Proposed residual magnetic moment observer was applied for in-orbit attitude data as off-line calculation. Figure 5 shows the estimated disturbance torque, which is the output of disturbance observer. This graph clearly shows that the period of disturbance torque is about half of orbital period. With these \hat{T}_{dx} , \hat{T}_{dy} and measured geomagnetic field \mathbf{B} , residual magnetic dipole \mathbf{M}_r was estimated with least square method, resulted to be $[-0.51, 0.042, 0.11] \text{ Am}^2$. Torque values which is calculated with \mathbf{B} and this $\hat{\mathbf{M}}_r$ are also plotted in Fig. 5 for comparison.

5.2 Performance Enhancement with Observed Residual Magnetic Moment

Finally, this estimated $\hat{\mathbf{M}}_r$ was uploaded to spacecraft, and used as feedforward value, to cancel residual magnetic dipole. It means that this $\hat{\mathbf{M}}_r$ is subtracted from \mathbf{M} , which is the output of magnetic torque controller. Figure 6 shows the effect of this feedforward cancellation. This graph consists of four periods. In the first period, attitude is controlled with only feedback controller. In the second period, feedforward cancellation was applied with 50% intensity. Then the intensity was increased up to 75% of $\hat{\mathbf{M}}_r$, and at last, full amount of estimated value was applied. These gradual steps clearly show the effect of \mathbf{M}_r cancellation. It indicates the validity of proposed \mathbf{M}_r estimation method. Figure 7 shows the detailed response with

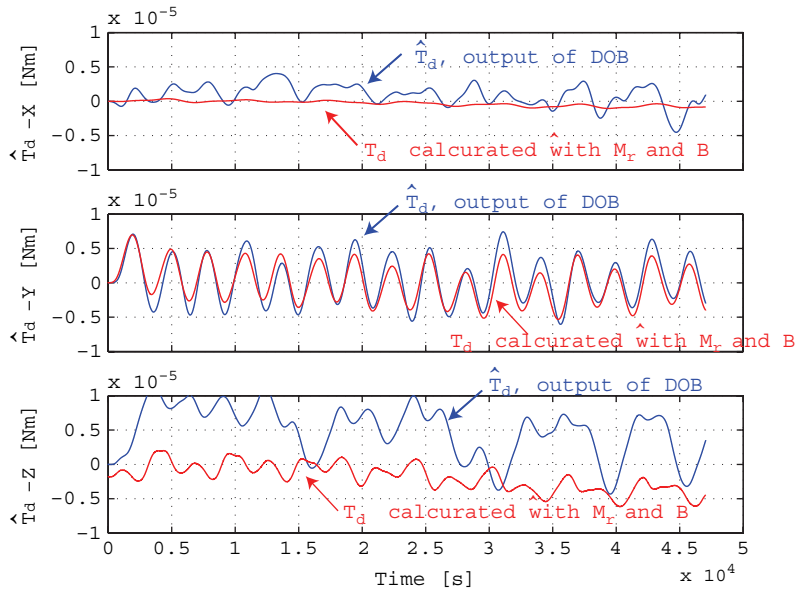


Fig. 5 Observed disturbance torque \hat{T}_d

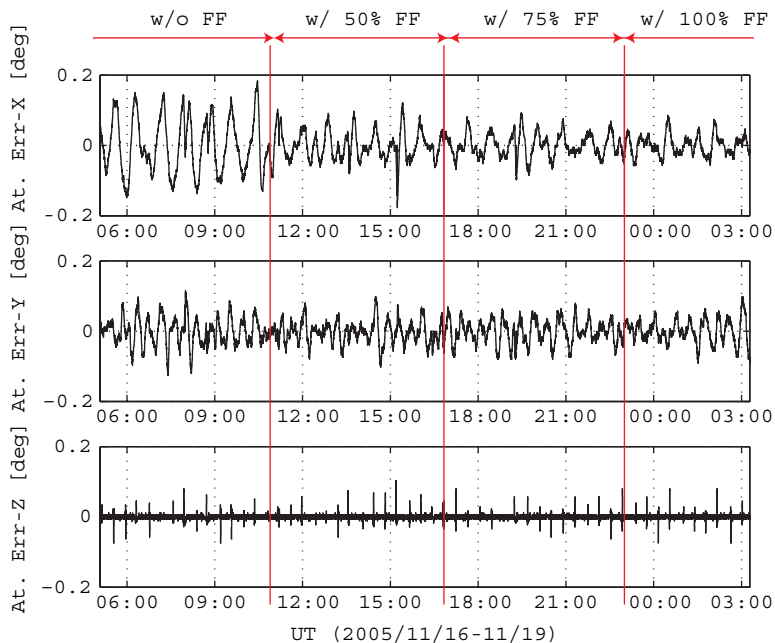


Fig. 6 Effect of feedforward M_r cancellation, with various intensity

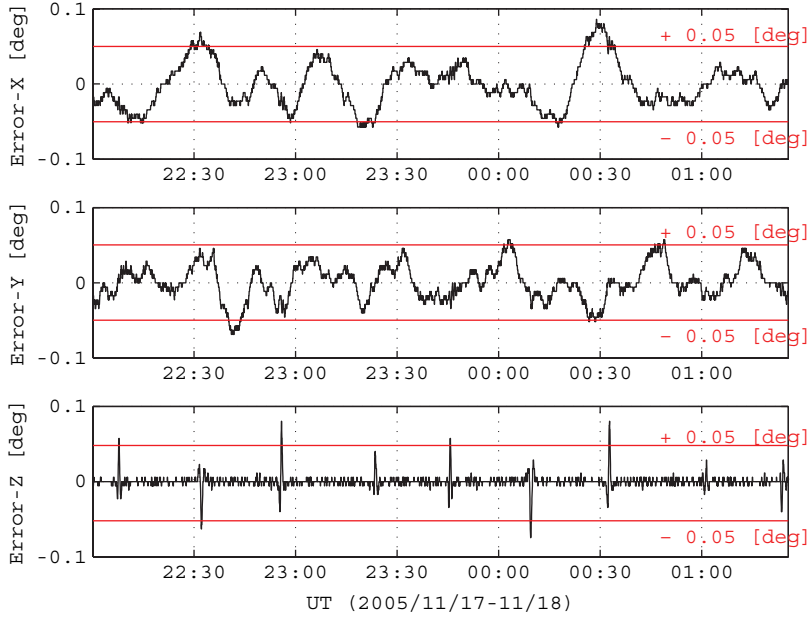


Fig. 7 Effect of 100% feedforward $\hat{\mathbf{M}}_r$ cancellation

100% intensity of feedforward cancellation. It is revealed that with $\hat{\mathbf{M}}_r$ feedforward cancellation, the pointing error decreased to 25–30%.

Such in-orbit \mathbf{M}_r estimation is necessary even if it is measured on ground? We suppose so. Just before the launch, \mathbf{M}_r was measured in magnetic shielding chambers for REIMEI in the final flight configuration. Measurements were carried out for several situations, e.g., with stowed or deployed solar panel, power off or on with batteries, etc. Then it was concluded that the residual magnetic moment of the REIMEI satellite is $[-0.054, -0.039, -0.069] \text{ Am}^2$. This measured value was also applied for feedforward cancellation, however, it did not improve the performance at all. It suggests that the residual magnetic moment was varied after the measurement, however, the reason is still a mystery.

5.3 Statistics of In-Orbit Performance

At the end of this section, statistical evaluations are described. During July 2006, REIMEI carried out about 90 aurora imaging observations. Worst attitude feedback error during each observation was evaluated for each case, then summarized in Fig. 8. This histogram indicates that worst-of-worst feedback error is about 0.1° . Attitude determination error has been evaluated to be less than 0.05° . Pointing accuracy is also confirmed with aurora imager, and this end-to-end absolute pointing accuracy was revealed to be $0.05\text{--}0.1^\circ$, typically. These evaluations clearly indicate that the achieved performance meets the requirements, as shown in Table 2.

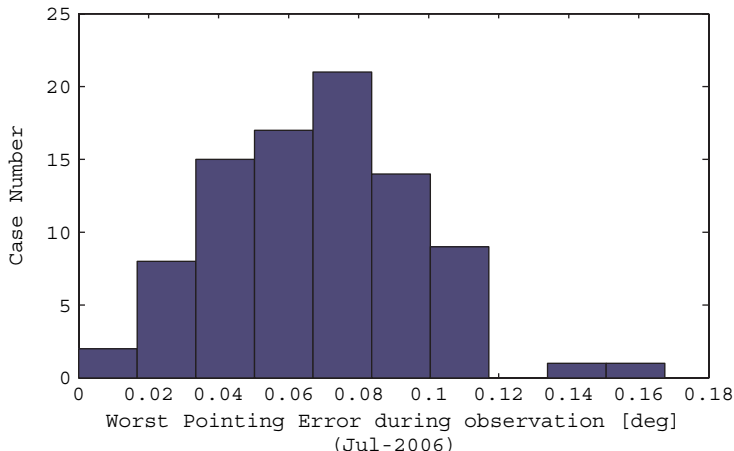


Fig. 8 Histogram of worst feedback error

Table 2 Requirement and Achievement

| | Requirement | Achieved |
|-------------------------|-----------------------|------------------------|
| Absolute Pointing Error | 0.5° | $< 0.2^\circ$ |
| Determination Error | 0.06° | 0.05° |
| Feedback Error | | 0.1° |
| Attitude Stability | $0.03^\circ/\text{s}$ | $0.004^\circ/\text{s}$ |

6 Summary and Conclusion

This paper studies on magnetic based attitude control system for small or micro satellites. Proposed methods are demonstrated with the REIMEI microsatellite, which was launched in 2005. One of our proposals is magnetic torque control law, for a spacecraft with three MTQs and one MW. This method manages the magnetic torque, according to the torque value required by attitude controller. Algorithm based on SR-inverse matrix prevents undesirable disturbance torque in the neighborhood of singular points. Advantage of the proposed method is described with simulations in comparison with usual pseudoinverse matrix. This algorithm was actually applied in the REIMEI satellite, and contributes to achieve required ACS performance.

Residual magnetic moment observer is also proposed in this paper. This method can estimate residual magnetic moment with in-orbit attitude and geomagnetic field data. It is also applied for REIMEI satellite, and the estimated value was actually applied in the feedforward controller, to cancel disturbance torque by residual magnetic dipole. Compared to the performance without this feedforward, the attitude control accuracy was significantly improved, such as 2–4 times better. In REIMEI case, this estimation was carried out on ground as off-line calculation, however, on-line estimation will also practical with recursive least square method. Such real-time

estimation will be valuable when residual magnetic moment varies dynamically, i.e., affected by solar cell current.

Note that the proposed residual magnetic moment observer should be also useful for a small or micro satellite with pure magnetic attitude control system. Recently, numbers of small/micro satellites are planned and launched. Magnetic based attitude control system should be one attractive solution, with limited cost and mass budget of small/micro satellites. The problem is the limited direction of magnetic torque, which is always orthogonal to geomagnetic field. Several studies are carried out [3], however, the control bandwidth is theoretically limited. Dominant source of disturbance torque for small/micro satellites is residual magnetic moments in many cases, therefore, feedforward cancellation with proposed observer will enhance the attitude control performance. The authors now estimate that pure magnetic attitude control will achieve pointing accuracy of 1.0° , if proposed magnetic moment observer is applied.

Acknowledgement This research was supported by all the members of INDEX/REIMEI team in ISAS/JAXA, including many students from several universities.

References

1. C. Simon and O. Grocott, "The MOST microsatellite Mission: One Year In Orbit," in *Proceedings of the 18th AIAA/USU Conference on Small Satellites*, Utah, USA, 2004.
2. B.S. Leonard, "NPSAT1 Magnetic Attitude Control System," in *Proceedings of the 16th AIAA/USU Conference on Small Satellites*, Utah, USA, 2002.
3. M. Lovera, E. De Marchi and S. Bittani, "Periodic Attitude Control Techniques for Small Satellites With Magnetic Actuators," *IEEE translation on control system technology*, Vol. 10, No. 1, 2002, pp. 90–95.
4. Y. Nakamura and H. Hanafusa, "Inverse Kinematic Solutions With Singularity Robustness for Robot Manipulator Control," *Journal of Dynamic Systems, Measurement, and Control*, Vol. 108, 1986, pp. 163–171.
5. S. Manabe, "The Coefficient diagram method," *14th IFAC Symposium on Automatic Control in Aerospace*, Seoul, Korea, 1998, pp. 199–210.
6. S. Sakai, Y. Fukushima and H. Saito, "Attitude controller design for small satellite taking account of gyro sensor noise," *Proceedings of International Astronautical Congress*, Vancouver, Canada, 2004, pp. IAC-04-A.3.09.
7. K. Ohishi et al., "Microprocessor-controlled DC motor for load-insensitive position servo system," *IEEE Trans. Ind. Electron.*, Vol. IE-34, 1987, pp. 44–49.

Session 6

Students Session

GPS and Low Cost Sensors in Navigation

Nasrin Bourghani Farahani and Nader Pouryaie

Abstract In this paper, we present our work on integrated navigation for low speed vehicles at low altitudes, using Global Positioning Satellites (GPS).

The commercial GPS systems are used for determination of speed and location of low speed objects on Earth or airborne objects, with acceptable accuracy. On the other hand, low cost Inertial Navigation System (INS) is suited for similar applications. These systems are self-contained, non-interrupted and do not need external signals. However, GPS errors result in constant drifts in position. These errors in position grow with time, or are unlimited.

The INS and GPS systems have complementary characteristics, and hence, can be selected for integrated navigation.

To determine the flight position, the INS system operates uninterrupted in an independent mode. Whenever, the GPS system determines the position (usually at lower rate than the INS system), the INS system corrects the speed and position.

The commercial GPS systems can not produce the required altitude estimations independently. Therefore, pressure sensor has been used to determine the errors in vertical channel. Kalman filter has been used to integrate all the measurements.

1 Introduction

We have used off the shelf low cost sensors, and obtained the required integrity and reliability using an efficient algorithm. Integrity means these can judge the health of input data.

N.B. Farahani

Iranian Research Organization for Science & Technology (IROST), Faculty Member of Electrical & Computer Department of IROST

e-mail: farahani@irost.org

N. Pouryaie

Iranian Research Organization for Science & Technology (IROST), Electrical Expert of Electrical & Computer Department of IROST

2 INS & Magnetometers

Inertial navigation system is composed of three accelerometers & three gyros each on its three measuring axes. Before mission INS needs initial alignment & calibration to find out deterministic errors of sensors & initial attitude of vehicle. INS has also some stochastic or random errors. Random errors of gyros can be compensated by making an AHRS. If vehicle is stationary (no thrust acceleration & centripetal acceleration) then by using the direction of local gravity vector measured by accelerometer, INS can measure two angles *roll* & *pitch*. Gravitational acceleration is always downwards & can be transformed in body frame (as sensed by accelerometers) according to following relationship.

$$\begin{bmatrix} g_x \\ g_y \\ g_z \end{bmatrix} = \begin{bmatrix} -g \sin \theta \\ g \cos \theta \sin \varphi \\ g \cos \theta \cos \varphi \end{bmatrix} \quad (1)$$

where θ is the pitch angle & φ is the roll angle with these relations a rough estimate of *roll* & *pitch* can be made as under:

$$\begin{aligned} \varphi &= \tan^{-1} \left(\frac{a_y}{a_z} \right) \\ \theta &= \sin^{-1} \left(\frac{a_x}{g} \right) \end{aligned} \quad (2)$$

The third angle or heading angle Ψ comes from magnetometer, with three magnetometers, we calculate magnetic field horizontal & vertical component in x & y direction of inertial frame using frame transformation (body to inertial) as M_x , M_y & ultimately our heading angle is:

$$\psi = -\tan^{-1} \left(\frac{M_y}{M_x} \right) \quad (3)$$

The difference between geographic north & magnetic north is compensated each time during navigation Gyros also give three angles, combining this information with the above estimated angles we can estimate the day to day random biases of gyros, which can be compensated later during the mission. Random errors in accelerometers (which accumulate errors in position & velocity) are corrected using GPS data.

3 GPS & Errors in GPS Data

Four satellites are used to position the object on earth, three satellites determine the position & fourth one is used to synchronize the clock of receiver with atomic clock of satellite. The GPS gives the position in geographic frame Latitude, Longitude,

Altitude & velocities in North, East, down (local geographic) frame. Every satellite emits a signal which has following information:

Information about status of satellite, Data Acquisition, precision of satellite, ionosphere delay, Ephemeris of satellite.

The precision of system depends upon six classes of errors:

Ephemeris data, Satellite clock, Ionosphere, Troposphere, Multipath

Receiver. noise, software accuracy, and inter-channel biases

Geometry of satellite with respect to user (Geometric Dilution of precision)

Error of Position = GDOP.UERE

Table 1 Standard error model - L1 C/A (no SA), (One-sigma error, m)

| Error source | Bias | Random | Total | DGPS |
|---|------|--------|-------------|------------|
| Ephemeris data | 2.1 | 0.0 | 2.1 | 0.0 |
| Satellite clock | 2.0 | 0.7 | 2.1 | 0.0 |
| Ionosphere | 4.0 | 0.5 | 4.0 | 0.4 |
| Troposphere | 0.5 | 0.5 | 0.7 | 0.2 |
| Multipath | 1.0 | 1.0 | 1.4 | 1.4 |
| Receiver measurement | 0.5 | 0.2 | 0.5 | 0.5 |
| User equivalent range | | | | |
| Error (UERE), rms | 5.1 | 1.4 | 5.3 | 1.6 |
| Filtered UERE, rms | 5.1 | 0.4 | 5.1 | 1.5 |
| Vertical one-sigma errors – VDOP = 2.5 | | | 12.8 | 3.9 |
| Horizontal one-sigma errors – HDOP = 2.0 | | | 10.2 | 3.1 |

Taking account of all these errors PPS service (with out selective availability) contribute to following errors in position: 22 meter of incertitude in horizontal position, 23 meter of incertitude in vertical position.

4 Navigation Algorithm & Quaternion

In navigation different reference frames are used, for applications close to the surface of earth, earth centered inertial frame is used. The velocity of vehicle in inertial frame can be given as

$$v_i = v_e + \omega_e^i \times r \quad (4)$$

Differentiating above equation gives:

$$a_{i/i} = \underbrace{a_{e/i}}_{\text{measured acceleration}} + \underbrace{\omega_e^i \times v_e}_{\text{coriolis acceleration}} + \underbrace{\omega_e^i \times \omega_e^i \times r}_{\text{centripetal acceleration}} \quad (5)$$

v_e = velocity of vehicle w.r.t earth frame

ω_e^i = rotation rate of earth w.r.t inertial frame

r = position vector of vehicle

a = acceleration in respective frame

As the accelerations are acquired in body frame, a transformation is required between body to inertial frame. Usually this is done using quaternion approach for less computation & no singularity.

The transformation or direction cosine matrix in form of quaternion can be represented as:

$$T_b^i = \begin{bmatrix} q_3^2 + q_0^2 - q_1^2 - q_2^2 & 2(q_0q_1 - q_2q_3) & 2(q_0q_2 + q_1q_3) \\ 2(q_0q_1 + q_2q_3) & q_3^2 + q_1^2 - q_0^2 - q_2^2 & 2(q_1q_2 - q_0q_3) \\ 2(q_0q_2 - q_1q_3) & 2(q_1q_2 + q_0q_3) & q_3^2 + q_2^2 - q_0^2 - q_1^2 \end{bmatrix} \quad (6)$$

The rate of change of quaternion can be represented as follows with out using trigonometric identities & avoiding singularities. This relation is used at a very fast rate for updating attitude matrix at the acquisition rate of INS

$$\begin{bmatrix} \dot{q}_0 \\ \dot{q}_1 \\ \dot{q}_2 \\ \dot{q}_3 \end{bmatrix} = \frac{1}{2} \begin{bmatrix} 0 & -p & -q & -r \\ p & 0 & r & -q \\ q & -r & 0 & p \\ r & q & -p & 0 \end{bmatrix} \cdot \begin{bmatrix} q_0 \\ q_1 \\ q_2 \\ q_3 \end{bmatrix} \quad (7)$$

$$\dot{q} = \frac{1}{2} \Omega \cdot q$$

Ultimately we always need Euler angles as output because they are more realizable &, it is also possible to represent Euler angles in the form of quaternion & vice versa:

$$eul(q) = \begin{bmatrix} \varphi \\ \theta \\ \psi \end{bmatrix} = \begin{bmatrix} \tan^{-1} \left(\frac{2(q_2q_3 + q_0q_1)}{1 - 2(q_1^2 + q_2^2)} \right) \\ \sin^{-1} \left(-2(q_1q_3 - q_0q_2) \right) \\ \tan^{-1} \left(\frac{2(q_1q_2 + q_0q_3)}{1 - 2(q_2^2 + q_3^2)} \right) \end{bmatrix} \quad (8)$$

$$\begin{bmatrix} q_0 \\ q_1 \\ q_2 \\ q_3 \end{bmatrix} = \begin{bmatrix} \cos \left(\frac{\varphi}{2} \right) \cos \left(\frac{\theta}{2} \right) \cos \left(\frac{\psi}{2} \right) + \sin \left(\frac{\varphi}{2} \right) \sin \left(\frac{\theta}{2} \right) \sin \left(\frac{\psi}{2} \right) \\ \sin \left(\frac{\varphi}{2} \right) \cos \left(\frac{\theta}{2} \right) \cos \left(\frac{\psi}{2} \right) - \cos \left(\frac{\varphi}{2} \right) \sin \left(\frac{\theta}{2} \right) \sin \left(\frac{\psi}{2} \right) \\ \cos \left(\frac{\varphi}{2} \right) \sin \left(\frac{\theta}{2} \right) \cos \left(\frac{\psi}{2} \right) + \sin \left(\frac{\varphi}{2} \right) \cos \left(\frac{\theta}{2} \right) \sin \left(\frac{\psi}{2} \right) \\ \cos \left(\frac{\varphi}{2} \right) \cos \left(\frac{\theta}{2} \right) \sin \left(\frac{\psi}{2} \right) - \sin \left(\frac{\varphi}{2} \right) \sin \left(\frac{\theta}{2} \right) \sin \left(\frac{\psi}{2} \right) \end{bmatrix} \quad (9)$$

Accelerations are then g-compensated (accelerometer measure only specific force)

$$a_l = \mathbf{T}_b^l a_b + \mathbf{T}_l^l g_l \quad (10)$$

Where gravitational force is assumed to be in the direction of Z_1 (spherical earth), and is given in local geographic frame as

$$g_l = \begin{bmatrix} 0 \\ 0 \\ g \end{bmatrix} \quad (11)$$

$$g = \Gamma/r^2$$

Γ = Gravitational Constant

τ = position vector

These accelerations are integrated twice using trapezoidal rule to achieve velocity & position. Vehicle position is transformed first from inertial coordinate system to geocentric one:

$$\begin{bmatrix} X_G \\ Y_G \\ Z_G \end{bmatrix} = \mathbf{T}_I^G \begin{bmatrix} X \\ Y \\ Z \end{bmatrix} \quad (12)$$

$$\mathbf{T}_I^G = \begin{bmatrix} \cos(\Omega t) & \sin(\Omega t) & 0 \\ -\sin(\Omega t) & \cos(\Omega t) & 0 \\ 0 & 0 & 1 \end{bmatrix}$$

And finally to geographic coordinate system

$$\begin{aligned} h &= R - R_E \\ \alpha_G &= \tan^{-1}(Y_G/X_G) \\ d_G &= \sin^{-1} \left(\sqrt{X_G^2 + Y_G^2}/R \right) \\ R &= \sqrt{X_G^2 + Y_G^2 + Z_G^2} \end{aligned} \quad (13)$$

Here b , i , l & G denote body, Inertial, local geographic & geographic frame respectively & T shows transformation (from subscript to superscript frame). h is mean sea level height, α_G is longitude, d_G is latitude, R is position vector & Ω is earth rotation rate. GPS positions are transformed from geographic to inertial frame & velocities are transformed from local geographic to inertial frame before integration with INS calculated results.

5 Error Model of Inertial Sensors

Accelerometers & gyros all posses some deterministic as well as stochastic errors. The error model of accelerometers & gyros is given as (IEEE standard)

$$\begin{aligned} d_{\omega x} &= b + s_f \omega_x + m_y \omega_y + m_z \omega_z + \eta \\ d_{fx} &= b + s_f a_x + m_y a_y + m_z a_z + \eta \end{aligned} \quad (14)$$

b = bias component

s_f = scale factor

η = random noise

m_y, m_z = misalignment coefficient ω_{xyz} = Gyro rates

a_{xyz} = Acceleration

The deterministic errors in model can be compensated in Navigation algorithm. The stochastic components of errors in sensors give unbounded errors, when integrated & are called random walk. These random errors need to be estimated & compensated in real time.

6 Integration Techniques

GPS & INS in our particular case are integrated in loosely coupled mode. In this mode Integration Kalman filter treats both GPS & INS as separate navigation systems. It takes their outputs as measurements in navigation solution & only INS errors are estimated explicitly. It means dynamic errors of gyros are ignored. There are other integration techniques like, tightly coupled & ultra tightly coupled integrations but for our application loosely coupled mode was found to be suitable

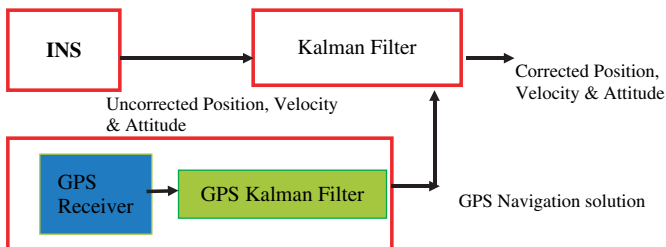


Fig. 1 Loosely coupled INS/GPS intégration

6.1 Kalman Filtering

In navigation Kalman filtering is used to optimally combine information from different sensors. Kalman filter uses Kinematics equations of vehicle which are fed by INS measurements. To converge the output of this filter absolute sensor (GPS) correction is used. Since the equations of system are highly non-linear we use Kalman filter in extended mode. Extended Kalman filter line arises the equation at small instant of time taking partial derivatives. General formulization of extended Kalman filter can be given as:

$$\begin{cases} \hat{x}_{k+1} = f(\hat{x}_k, u_k, 0) \\ \hat{z}_k = h(\hat{x}_k, 0) \end{cases} \quad (15)$$

(\hat{x}_k is an estimation states calculated using k iterations)

The linearization is realized by introducing the Jacobean matrix

$$A = \left[\frac{\partial f}{\partial x} \right] H = \left[\frac{\partial h}{\partial x} \right] \quad (16)$$

There are two stages of Kalman filter algorithm, Prediction & Correction

6.1.1 Prediction

This step is evaluated at the frequency of quantization of filter (1/Ts). In this step matrix of covariance & states are predicted as follows

$$\begin{aligned} \hat{x}_{k+1}^- &= f_k(\hat{x}_k, u_k, 0) \\ P_{k+1}^- &= P_k + T_s (A_k P_k + P_k A_k^t + Q) \end{aligned} \quad (17)$$

6.1.2 Correction

This step is evaluated when new measurements are available. Measurements are used to correct the state vector & the matrix of covariance as follows:

$$\begin{aligned} K_k &= P_k^- H_k^t [H_k P_k^- H_k^t + R]^{-1} \\ \hat{x}_k &= \hat{x}_k^- + K_k (z_k - H_k \hat{x}_k^-) \\ P_k &= (I - K_k H_k) P_k^- \end{aligned} \quad (18)$$

Where:

P_k = covariance matrix

K_k = Kalman gain

H_k = Observation matrix

R = covariance of measurement noise

Q = covariance of system noise

\hat{x}_k = Estimated state vector

A = state transition matrix

For our particular case the state vector & output vector are

$$\begin{aligned} x^{(14)} &= (xyz^{(3)}, uvw^{(3)}, q^{(4)}, g^{(1)}, \delta_{pqr}^{(3)})^t \\ z^{(9)} &= (xyz^{(3)}, uvw^{(3)}, \varphi, \theta, \psi)^t \end{aligned} \quad (19)$$

Where:

- xyz : Positions local NED frame
- uvw : Velocity in body frame
- q : Quaternion
- g : Acceleration of gravity
- δ_{pqr} : Bias of gyros
- $\phi\theta\psi$: Euler angles

We estimate gravity to correct the bias of vertical accelerations. For proper tuning of filters several test were made in order to reach a suitable value of R , Q & P matrices

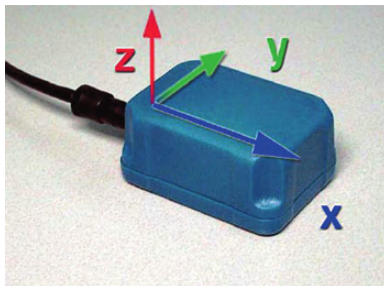
7 Experimental Setup

The components of hybrid INS used for this experiment are as follows

❖ MEM type INS

- Three Accelerometer (a triad orthogonal, measure acceleration vector in body frame)
- Three gyros (a triad orthogonal, measure attitude of system in Body frame)
- Three Magnetometer (measure magnetic heading of system)
- Thermometer

❖ GPS receiver



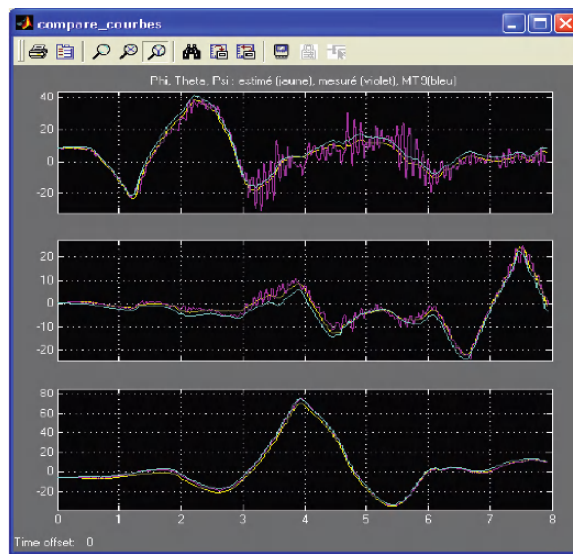
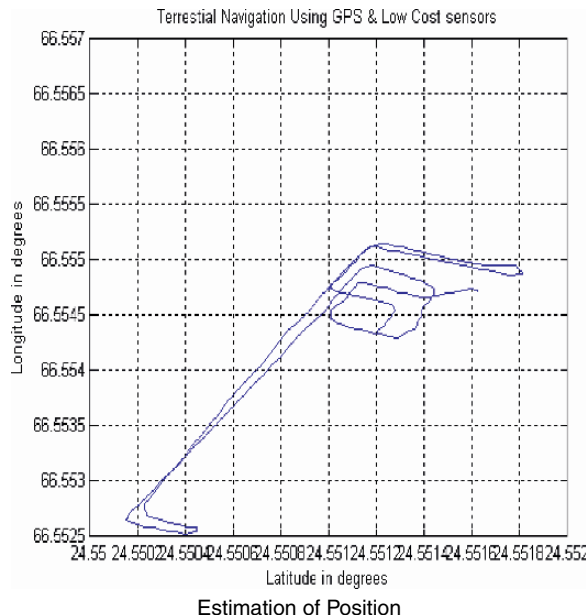
MEM Type Ins



Hand held GPS receiver

8 Results & Verification

A terrestrial navigation system is built & tested using different trajectories & velocities. An accuracy of 10–20 m in position & 2–5° in attitude is achieved.



References

1. R.M. Rogers, Applied Mathematics in Integrated Navigation System, AIAA Education series, 2nd ed., 2003
2. J. Tithertron & C. Weston, Strap down inertial navigation, AIAA Education series, 2nd Rev. Ed., 2004
3. M.S. Grewal et al., GPS Inertial Navigation & Integration, John Wiley & Sons, 2001
4. S.C. Bose, Multisensor Navigation & Fault Isolation, Technalytics, 2004
5. http://edu-observatory.org/gps/gps_accuracy.html

GPS Based Attitude Determination for the Flying Laptop Satellite

André Hauschild, Georg Grillmayer, Oliver Montenbruck,
Markus Markgraf, and Peter Vörsman

Abstract This paper introduces the GPS based attitude determination system (GENIUS) onboard the university small satellite Flying Laptop. The attitude determination algorithm which is based on a Kalman Filter and processes single differences of the C/A-code and carrier phase measurements is shortly described. The algorithm uses the LAMBDA-method to resolve the integer ambiguities of the double differences of the carrier phase measurements. These resolved ambiguities are then used to fix the single difference ambiguities in the filter. The results of ground based tests and numerical simulations are introduced and the accuracy of the attitude determination algorithm is assessed.

1 GENIUS Experiment on the Flying Laptop

The micro-satellite Flying Laptop is currently under development at the Institute of Space Systems, Universität Stuttgart [1]. The satellite has a mass of about 100 kg, is three-axis stabilized and will be launched in a polar, sun-synchronous, low earth orbit.

GENIUS (Gps Enhanced Navigation Instrument for the Universität Stuttgart micro-satellite) is an experiment for GPS based determination of the spacecraft attitude which is developed in cooperation with the German Space Operation Center

A. Hauschild

DLR/GSOC, Oberpfaffenhofen, Germany

Institute of Aerospace Systems, Technical University Brunswick, Germany

e-mail: andre.hauschild@dlr.de

G. Grillmayer

Institute of Space Systems, Universität Stuttgart, Germany

O. Montenbruck

DLR/GSOC, Oberpfaffenhofen, Germany

M. Markgraf

DLR/GSOC, Oberpfaffenhofen, Germany

P. Vörsman

Institute of Aerospace Systems, Technical University Brunswick, Germany

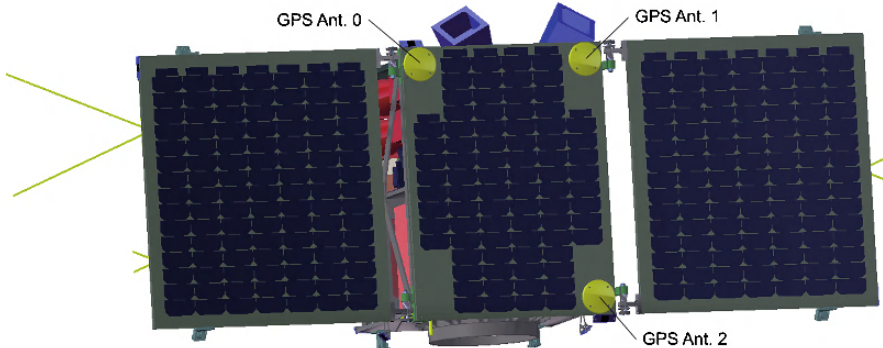


Fig. 1 GPS satellite antennas in L-shaped arrangement

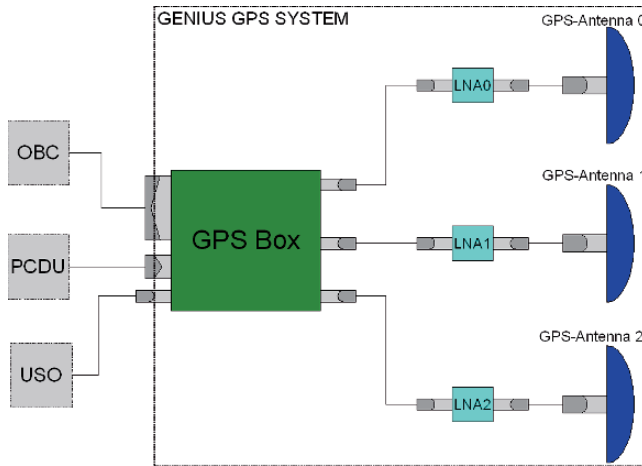


Fig. 2 GENIUS system overview

(DLR/GSOC). It also supplies the standard real-time position and velocity needed by the attitude control system for the nadir and target pointing mode. The GENIUS GPS system consists of three independent GPS receiver boards, each connected to a separate antenna and low noise amplifier (LNA) as shown in Fig. 2. The GPS Box is connected to the on-board computer (OBC), the power control and distribution unit (PCDU) and the ultra stable oscillator (USO). The used Phoenix boards are commercial 12-channel GPS L1 receivers with a DLR/GSOC developed firmware for space and high dynamics applications [4]. Three GPS antennas are mounted on the middle solar panel in an L-shaped arrangement, creating two baselines with a length of 440 mm and 610 mm respectively (Fig. 1). The antennas are pointing in the opposite direction of the payload cameras and therefore have optimum visibility of the GPS constellation during Earth observation. The three GPS receivers are integrated in a single $100 \times 80 \times 67$ mm box together with an interface board for RS-422

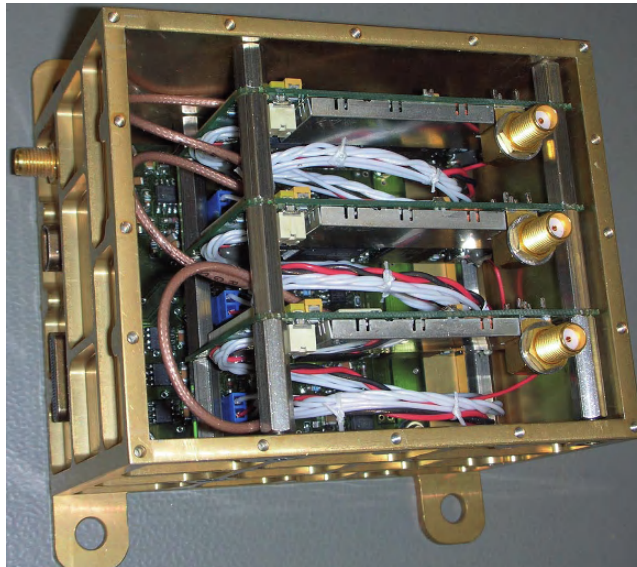


Fig. 3 GPS Box hardware assembly (opened)

conversion, the USO signal distributor and a latch-up protection for each receiver (Fig. 3). To achieve a high level of redundancy, each receiver can be switched on/off independently varying the system input power from 0.9 W for 1 receiver to 2.6 W for all 3 receivers according to measurements at the testing model. Among other hardware modifications to prepare the receiver boards for space usage, the oscillators were removed to synchronize all receivers to the central 10 MHz USO. This external oven controlled crystal oscillator with a high accuracy of 10^{-13} over a period of 1000 s drives the clocks of the receivers and also eliminates variations between individual receiver clocks.

GPS position and velocity are sent to the OBC every second, while the raw carrier phase measurements are recorded every 10 s and will be dumped during ground station contacts. With the algorithm described below, the satellites's attitude is calculated post facto and can be compared to the star tracker reference data for accuracy assessment.

2 Attitude Determination Algorithm

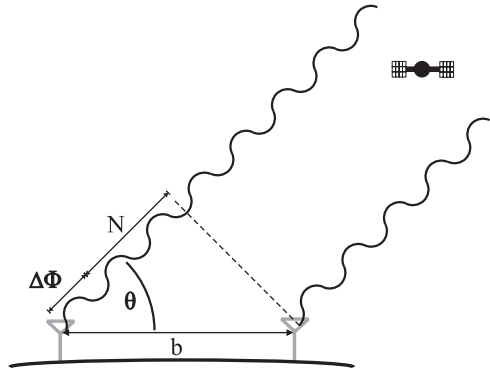
GPS attitude determination with carrier phase measurements is based on the principle of interferometry. Figure 4 depicts a carrier phase signal from a GPS satellite arriving at two antennas separated by the distance b . The differential range from the antennas to the GPS satellite consists of the fractional wavelength $\Delta\Phi$ which can be measured by the receiver and the number N of complete cycles, which is

unknown and therefore called integer ambiguity. If N is known, the angle θ between the baseline and the line-of-sight vector to the GPS satellite can be determined via

$$\cos \theta = \frac{\Delta\Phi + N}{b}$$

Having four or more measurements from different GPS satellites, the differential antenna vector (baseline) and the differential clock offset of the receivers can be determined [3]. Thus, GPS based attitude determination can be separated into two different problems: First, the ambiguities of the carrier phase measurements must be resolved prior to be able to use these measurements as precise range measurements. Secondly, a filter algorithm must be implemented to improve the accuracy of the attitude solution. In this section the filter algorithm shall be explained first and afterwards the ambiguity resolution procedure shall be introduced.

Fig. 4 Single baseline GPS interferometry for attitude determination



The attitude determination algorithm used for GPS based attitude determination of the small-satellite Flying Laptop is based on a Kalman Filter. The filter state consists of two baseline vectors, which are the relative position vectors between the GPS antennas. Since the GENIUS experiment employs three independent Phoenix GPS receivers, the differential receiver clock offset between two receivers involved in each baseline must be estimated. Finally the angular velocity vector of the satellite is estimated along with the ambiguities of the carrier phase measurements for each baseline. The propagation of the relative antenna motion is based on a simple kinematic model, which assumes a rotation of the satellite body with a constant angular velocity vector. The differential clock offset and the ambiguities are assumed to be constant over time. Note that no differential equations must be solved in this case, since the change in the baseline can be propagated using a simple rotation matrix computed from the angular velocity vector. Since this simplified system model is only an approximation of the truth, process noise is included in the filter to avoid a filter divergence due to unmodelled effects. In this case, variations of the satellite's angular velocity vector are compensated by angular accelerations, which are modelled as Gaussian noise with zero mean. Variations in the differential receiver clock offset are modelled as a clock drift which consists of Gaussian noise with zero

mean. No process noise is added to the ambiguity estimates, since their values do not change as long as the satellite is tracked continuously.

The filter processes inter-receiver single differences of the C/A-code and carrier phase measurements. The advantage of using differential measurements is that errors common to both measurements cancel out. In this case the GPS satellites' clock offset and all error which originate at the signal transmission path are eliminated. The remaining errors are due to receiver noise, multiple signal reception at the GPS antenna and antenna phase center variations. The angular velocity is not directly observable through the measurements and must therefore be estimated by the Kalman Filter.

As already mentioned previously, the ambiguities of the carrier phase measurements must be resolved before these observables can be used for attitude determination. There exists a great variety of ambiguity resolution methods in the literature. One of the most powerful methods is the LAMBDA-method [5], which can resolve the integer ambiguities of carrier phase double differences based on a float estimate of these ambiguities and their corresponding covariance matrix. The attitude determination algorithm performs a check for unresolved ambiguities after each propagation step. If unresolved ambiguities exist, the estimates of the single differences from the filter state are transformed to double differences using a common reference satellite. These float estimates of the double difference ambiguities are passed to the LAMBDA-method, which tries to resolve the integer values. If the solution of the integer ambiguities passes a validation scheme, they are used to fix the single difference ambiguities in the filter state with a second measurement update. During this update, the integer double differences are used as "pseudo"-measurements of the single difference ambiguities. Since the double difference ambiguities are known exactly from the LAMBDA-method, their standard deviation is set to zero during the measurement update. As a result, the entries in the filter covariance matrix for the ambiguities are reduced to zero, which prevents the filter from updating the ambiguities during the following epochs. Thus the "pseudo"-measurement update allows to constrain the single difference ambiguities in the filter efficiently.

Finally, the attitude information must be computed from the baseline vectors. The Kalman filter estimates the baseline vectors in the earth-fixed earth-centered frame. Additionally, the vector components of both baseline vectors in the satellite's body-fixed frame are known from pre-flight evaluations. The Triad-Method or the QUEST-Method are used to process the information to attitude coordinates parametrized as a rotation matrix or quaternions.

Figure 5 depicts the complete attitude determination procedure. The algorithm starts at each epoch with an editing of the available GPS satellites. At this point satellites below a certain elevation threshold or below a minimum signal-to-noise ratio are excluded. In the next two steps newly acquired and lost GPS satellites are included or excluded from the filter state. Then, a residual check of the carrier phase measurements is performed for the satellite with already resolved ambiguities to detect if the ambiguities of individual satellites have changed by cycle slips. If the residual check fails, the ambiguity of the affected satellite is reset and marked as unresolved to ensure that the ambiguity resolution procedure is repeated for this

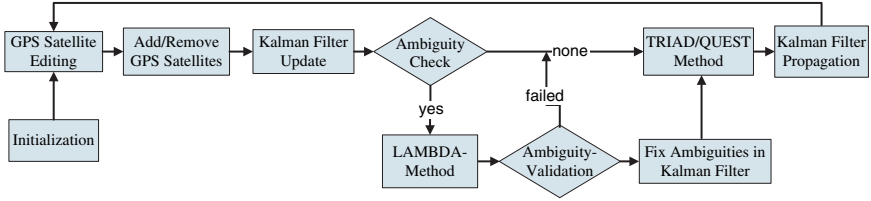


Fig. 5 Flowchart of the GPS Attitude Determination Algorithm

satellite. After the measurement update of the Kalman Filter, the ambiguity resolution branch described previously is entered if necessary. Finally, after the baseline vectors are been transformed to attitude parameters, the state vector and the state covariance matrix are propagated to the next epoch and the complete procedure is iterated.

3 Performance Evaluation

The verification and performance evaluation of the attitude determination algorithm has been accomplished with test data, collected during a field experiment. For this experiment, three GPS antennas have been mounted to an aluminum rack in a comparable arrangement to the antenna system on the Flying Laptop satellite. The two baseline vectors had a lengths of 0.4 m and 0.6 m. The aluminum rack has been placed on a turntable in order to simulate the rotation of the satellite. The turntable allows a rotation of the antenna array around the vertical axis with a constant rate. The antennas were connected to three Phoenix GPS receivers. The plots in Fig. 6 show the Euler angles yaw, pitch and roll over time for measurements taken over an interval of one hour with a rotation rate of $1^\circ/\text{s}$. The angles describe the rotation of the antenna array with respect to the local horizontal coordinate system. The upper plot for the yaw angle clearly shows the rotation rate of the platform. The plots for the roll and pitch angle in the lower plot represent the tilt of the platform with respect to the local horizon. Ideally, both angles should be zero at all times. Instead, both pitch and roll angle show variations with a standard deviation of about 1° . The maximum variations are in the order of 2° . The deviations of the roll and pitch angle are caused by errors in the horizontal components of the differential antenna positions. These positioning errors can be of different origin. The dominating error source are multipath errors on the carrier phase measurements, which are caused by multiple signal receptions at the antenna due to reflections of the electromagnetic wave at objects in the vicinity of the antenna array. During the field experiments, the carrier phase multipath errors of low elevation satellites reached magnitudes of up to 2.5 cm [2], which corresponds to the observed deviations of the Euler angles. In contrast to the measurement errors causes by the receiver noise, the assumption of a Gaussian distribution does not hold for multipath errors. Therefore these errors are more difficult to be filtered out using a Kalman Filter. Additionally, systematic

errors like antenna phase center variations and mounting offsets introduce errors in the solution for the Euler angles. A rigor assessment of the magnitude of the different error sources cannot be provided for the experiment, since no reference attitude from a more accurate sensor is available.

It can be stated from the results of the experiment that the algorithm provides reasonable results for the attitude solution. The noise on the measurements can be filtered out effectively by the Kalman Filter, but systematic errors cause deviations of the attitude solution from the true solution. The single difference carrier phase ambiguities for new satellites could be resolved within several seconds using the LAMBDA-method.

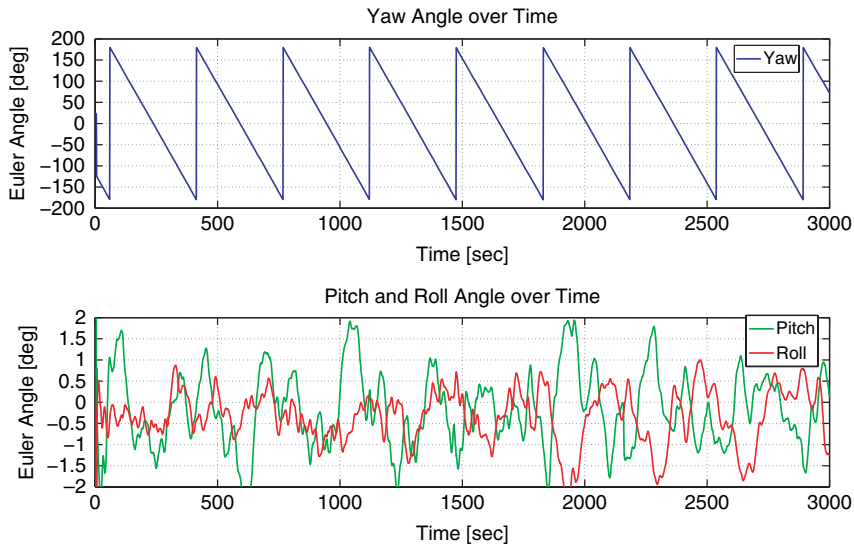


Fig. 6 Yaw, pitch and roll angle with respect to the local coordinate frame for the dual baseline experiment with a rotation rate of $1^\circ/\text{s}$

In order to prove that the algorithm can also handle the frequent changes of the GPS satellite constellation typical for space-borne applications, numerical simulations have been executed. During these simulations, the C/A-code and carrier-phase measurements of the GPS system on the Flying Laptop satellite have been created using realistic attitude scenarios. In the first attitude scenario, the nadir-pointing-mode, the satellite orbits the earth with a constant angular velocity vector in nadir orientation. In this attitude mode, the assumed system model for the Kalman Filter comes close to the real world dynamics, thus the filter does not suffer performance problems. The second attitude mode is the target pointing mode. During this mode, the satellite is pointed to a target fixed on the earth's surface and thus continuously controlled by the attitude control system, which applies control torques to keep the satellite aligned with the reference frame during its pass over the ground target. Due to the applied torques, the angular velocity vector of the satellite changes and the assumption made for the system model in the Kalman filter is no longer true.

The plots in Fig. 7 show the errors in the Euler angles between the reference attitude solution and the estimated attitude from the Kalman filter for the target pointing mode. For the upper plot in the figure a process noise of $\sigma_{\omega} = 0.5^{\circ}/\text{sec}^2$ has been selected. It is obvious that the errors in the yaw, pitch and roll angles are close to zero over the complete simulation interval. For the middle plot the Kalman filter has been executed with the same settings as before, only the process noise of the system model has been reduced by one order of magnitude to $\sigma_{\omega} = 0.05^{\circ}/\text{sec}^2$. In this plot, the error for the pitch angle shows deviations of approximately 2° with respect to the nominal attitude. The yaw angle also shows deviations from the nominal attitude, which are much smaller and hardly recognizable in the plot. These deviations appear during the transitions between nadir pointing and target pointing mode. Reducing the process noise by another order of magnitude leads to the Euler angle errors as shown in the lower plot of Fig. 7. Obviously, the pitch error shows larger deviations compared to the nominal attitude with a maximum error of 10° during the transitions between the two attitude modes. Additionally, the yaw and roll angle deviate from the reference attitude in the same interval.

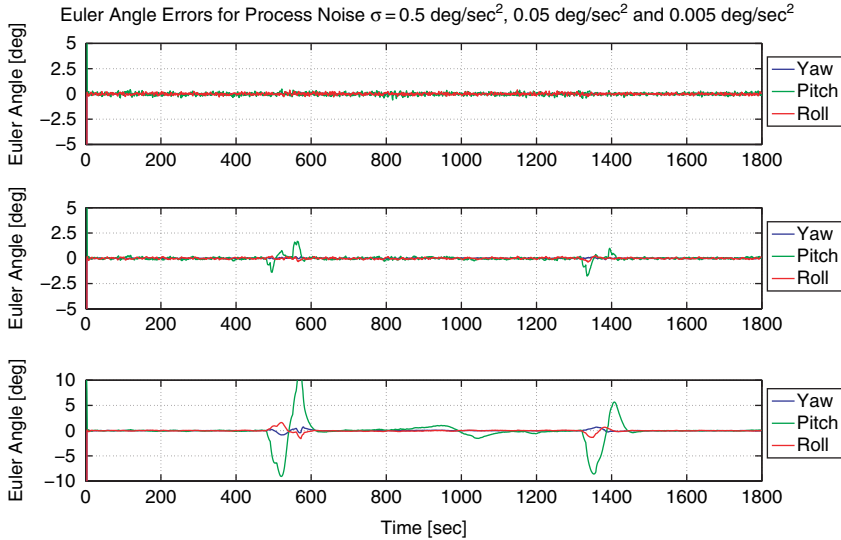


Fig. 7 Euler Angle Errors for the target pointing mode from PEM simulations, the figure shows the errors with different setting for the process noise σ_{ω} of $0.5^{\circ}/\text{s}^2$, $0.05^{\circ}/\text{s}^2$ and $0.005^{\circ}/\text{s}^2$ (from top to bottom)

It becomes obvious from the plot that choosing a comparably large amount of process noise avoids the deviation of the Euler angles from the true solution. This is a reasonable results, since the Kalman Filter assigns a higher weight to the measurements than to the propagated system model during the state update. Decreasing the process noise leads to deviations in the attitude solution since the filter relies more and more on the (incorrectly) propagated system model, which does not take the applied control torques into account. Thus parts of the information from the

measurements are ignored by the filter and the corrections applied to the baseline vectors and the angular velocity vector are too small. According to the previous discussion the necessary process noise for a satisfying filter performance is determined by the target pointing mode, which is the worst case scenario for the filter. The standard deviations of the Euler angles errors for the process noise of $\sigma_{\dot{\omega}} = 0.5^\circ/\text{s}^2$ are $\sigma_\psi = 0.0445^\circ$, $\sigma_\theta = 0.1385^\circ$ and $\sigma_\phi = 0.0972^\circ$. Thus an attitude determination with approximately $\sigma = 0.1^\circ$ appears to be possible, which is one order of magnitude smaller than the accuracy reached for the ground based experiments. It must be noted though, that the numerical simulation does only contain the C/A-code and carrier phase measurement errors due to receiver noise. Multipath errors are difficult to model and are thus not included in the simulation. Fortunately, signal reflections in space can only result from the satellite body itself. Since the three GPS antenna are mounted the panel with the solar generators, no objects which could cause strong signal reflections are in the vicinity of the antennas. Though the multipath errors had a comparably large impact on the filter performance during the ground based experiment, their influence on the accuracy for the space-borne scenario can be expected to be much smaller.

4 Summary, Conclusions and Future Work

In this paper the GPS based attitude determination system of university small satellite Flying Laptop has been introduced. An algorithm based on a Kalman Filter is used to process the measurement data and produce an offline attitude solution which will be compared to the attitude information available from the satellite's star camera. The algorithm uses the LAMBDA-method to resolve the integer ambiguities of the double differences of the carrier phase measurements. These resolved double difference ambiguities are then used to fix the single difference ambiguities in the filter. Thus the algorithm provides a seamless transition from the ambiguity resolution to the attitude determination. The algorithm can be initialized without any a priori knowledge about the ambiguities or the initial attitude of the satellite. Ground based tests and numerical simulation are used to validate the algorithm and assess its accuracy. It has been found that the attitude can be determined with a standard deviation of about 1° for ground based tests under the influence of multipath and about 0.1° for the space-borne application without multipath errors. The accuracy of the algorithm in current form can be expected to be between 0.1° and 1° depending on the magnitude of the systematic measurement errors in space.

During target pointing mode, the changes in the angular velocity vector lead to a divergence between the dynamics of the real system and the modelled system in the Kalman filter. Though large deviations in the attitude solution can be avoided by increasing the process noise, the suppression of measurement noise is less effective in this case. To overcome this drawback, a more sophisticated system model must be used for the Kalman Filter which reflects the real system more closely. Additionally, measurements from a rate gyro system can be used in addition to the GPS measurements

References

1. Georg Grillmayer, Albert Falke, and Hans-Peter Röser. Technology Demonstration with the Micro-Satellite Flying Laptop. In *Small Satellites for Earth Observation – Selected Proceedings of the 5th International Symposium of the International Academy of Astronautics*, pages 419–427, Berlin, Germany, 2005. ISBN 978-3-11-018851-6.
2. André Hauschild. Attitude Determination of a Small Satellite Using GPS Carrier Phase Measurements. Master's thesis, Technische Universität Braunschweig, 2007.
3. Pratap Misra and Per Enge. *Global Positioning System Signals, Measurements, and Performance*. Ganga-Jamuna Press, Lincoln, Massachusetts 01773, 2001.
4. Oliver Montenbruck and Markus Markgraf. User's Manual for the Phoenix GPS Receiver. Technical Report GTN-MAN-0120, Rev. 1.7a, German Space Operations Center, 15. Sep. 2006.
5. P.J.G. Teunissen, P.J. de Jonge, and C.C.J.M. Tiberius. The LAMBDA method for fast GPS surveying. In *Proceedings of International Symposium 'GPS technology applications'*, pages 203–210, Bucharest, Romania, September 1995.

Electromagnetic Formation Flight System Design

Daniel W. Kwon

Abstract Electromagnetic Formation Flight (EMFF) is a proposed method of actuating multiple spacecraft in relative degrees of freedom using electromagnetic forces and reaction wheels. The electromagnetic dipole is created by running current through high temperature superconducting wire. One of the challenges of EMFF is maintaining the cold temperatures necessary for superconducting. The current thermal design uses cryogenic coolers and multilayer insulation. This paper investigates models of the thermal design developed in Matlab and Sinda. The temperature distribution is simulated first using a simplistic 1-D model and then a 3-D model for the coil. The discrete solution procedure involves differencing Laplace's equations and includes the effects of a material with anisotropic thermal conductivity and multiple layers of insulating material. These results are then compared to experimental data, which are conducted using a copper test article in a vacuum chamber. Work done on the Matlab model to match the experimental environment includes modeling the free-molecular flow and accounting for the variation of parameters as a function of temperature. The Matlab model, Sinda and experimental results correlate well ensuring that the EMFF thermal design will operate successful on a satellite.

1 Motivation

An increasing number of missions are using multiple spacecraft flying in close proximity to replace traditional large monolithic space systems. Formation flying space interferometers are an example of this application. A method of providing actuation for these formation flight satellites is the use of electromagnetic forces and reactions wheels. This method has several advantages over traditional propellant-based thrusters such as the replacement of consumables to extend mission lifetime, elimination of impinging thruster plumes, and the enabling of high ΔV formation flight

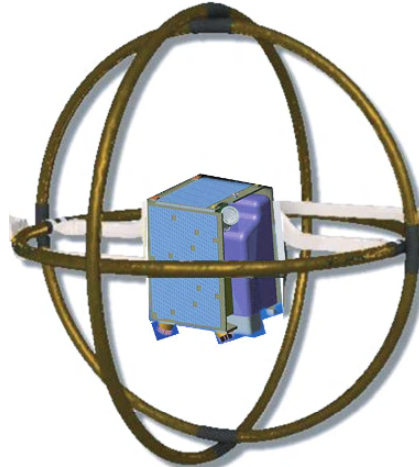
D.W. Kwon

Massachusetts Institute of Technology, Space Systems Laboratory, Cambridge, Massachusetts 02139, USA

e-mail: dankwon@mit.edu

missions [1]. A large steerable electromagnetic (EM) dipole can be created by running current through three orthogonal coils made of high temperature superconducting (HTS) wire. The EM dipole creates coupled forces and torques on nearby satellites with electromagnetic formation flight coils. Using a reaction wheel, one can de-couple the forces and torques to provide all the necessary actuation in relative degrees of freedom for a formation flight array [2]. Figure 1 shows a conceptual drawing of a small EMFF satellite which could be used for Earth observation missions.

Fig. 1 Conceptual drawing of a small EMFF satellite



The HTS wire is an enabling technology for EMFF because it allows the creation of a large dipole field. One of the challenges of using HTS is maintaining the temperature necessary for operation. The entire length of the superconducting wire must be maintained below a critical temperature in order for it to operate at superconducting levels. Commercial off-the-shelf (COTS) wire from American Superconductor used by the EMFF testbed has a critical temperature, T_c , of 110 K. For EMFF satellites in the proximity of Earth, LEO or GEO, heat from the sun and Earth need to be rejected in order to maintain temperatures below T_c . This can be accomplished using cryocoolers and various types of insulation such as Multilayer Insulation (MLI). One characteristic of the HTS wire is that at colder temperatures more current can be driven through the wires creating a larger dipole field and thus improving the performance of EMFF. However, this benefit comes at the expense of additional power and mass required by the thermal system. The unique problem investigated in this research is the topic of cooling large space structures.

The coil thermal system design is critical for the operation of EMFF in space. On the MIT-Space Systems Lab EMFF testbed, the coils are immersed in a bath of liquid nitrogen to maintain a continuous temperature of 77 K [3]. The use of liquid nitrogen on the testbed does not migrate into a flight design because the liquid nitrogen is a consumable. Since one of the benefits of EMFF is to replace consumables the design of the thermal system must be self-sufficient. The first task to accomplish the objective is to model the thermal performance of the design in simulation using

Matlab. Operation of the design or a scaled model in a vacuum chamber, which simulates the space environment, is then used to validate the Matlab models. Once the cooling methods, heat distribution, and heat rejection methods are modeled and experimentally verified, the thermal design can be migrated to a flight version with high confidence.

2 Design Overview

The design of the coil thermal system is shown in Fig. 2 for a single coil. The HTS wire stack is wrapped around a thermally conductive jacket, which provides structure for the wire stack and electrical isolation. Around this is MLI, which provides good insulation from the outside environment reducing the heat load into the coil. The thermally conductive jacket also functions to provide a uniform temperature distribution circumferentially around the coil, to serve as an attachment point for cooling, and as structure for the coil system and spacecraft. Heat is extracted from the coil by a cryocooler.

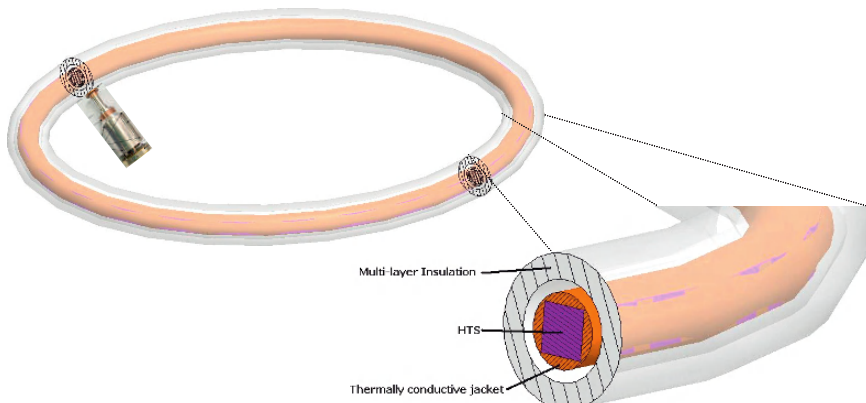


Fig. 2 Design of an EMFF coil thermal system

System trades have been performed to analyze the cost benefits of operating more than one cryocooler. These analyses assumed steady state bulk heat flow with a uniform temperature and heat flux distribution. It was determined that using multiple cryocoolers operating at different temperatures results in a minimum total power consumption point. This is because a cryocooler requires less power when operating at warmer temperatures, given a constant thermal load. Also, given a constant cold tip temperature, a cryocooler requires less power at lower thermal loads. By implementing one cryocooler on the outside of the insulation system, where the thermal load is high, but at a warmer temperature, and implementing one cryocooler right at the coil working at a low temperature and low thermal load, an optimum operating power can be achieved. Here a system of two cryocoolers was analyzed. Figure 3

shows that when the outer cryocooler is operating at 78 Watts and extracting 21 thermal watts, the optimum total cryocooler power is approximately 200 Watts. This is for a large EMFF system with a one meter radius coil using a single vacuum gap for insulation. The thermal environment analyzed the worst case heating from the sun for a single coil in steady-state. Given a smaller sized coil using the insulation system in Fig. 2, the heat extraction required by the cryocooler(s) is significantly reduced and the power needed could be lower than 50 Watts.

The current plan of approach is to utilize three types of models to reach confidence on developing a flight-like thermal system. The nature of these models is analytic, discrete, and analog or experimental and is summarized in Table 1. For experimental validation it is sufficient to analyze a single HTS coil. The coil shown in Fig. 2 will be enclosed in a vacuum chamber with cooling provided by liquid nitrogen since a liquid nitrogen feedthrough is simpler and more cost effective than a cryocooler. Uniform heating due to radiation from the wall provides the heating environment for the coil. The coil is in contact with a thermal conductor and wrapped in MLI. The current model uses a copper tube as the thermally conductive jacket. A more complex design can be analyzed once this simpler system is modeled in simulation and its performance, i.e. the time-vary temperature distribution, is verified experimentally. The models described in the following section details the chamber model.

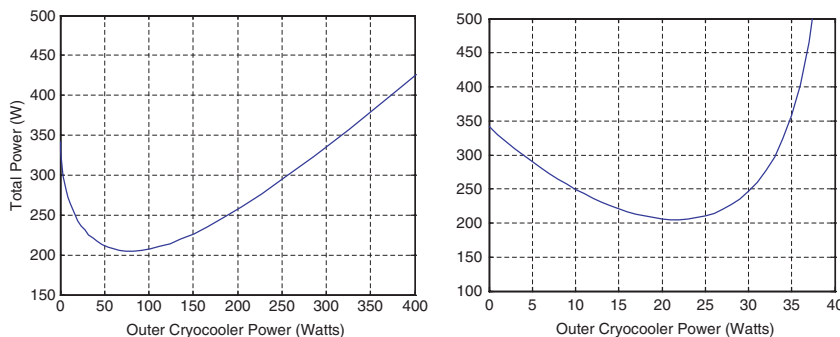


Fig. 3 Total power requirements using two cryocoolers

Table 1 Plan for current approach

| | Analytic | Discrete | Analog |
|-------------|--|--|--|
| Purpose | Mathematical model of temperature distribution based on first principles | Finite difference model simulates temperature distribution | Experimental verification of analytic and discrete models |
| Benefits | High fidelity and strong understanding | Ability to add non-uniform parameters and well used codes | Final verification of model, increases TRL of EMFF |
| Limitations | Nonlinear Radiation term makes solution complex | Large models are computationally expensive | Implementing model & environment accurately is challenging |

2.1 Analytic Model

A 3-D analytic model in cylindrical coordinates (r, θ, z) has been developed for the temperature distribution for the coil system shown in Fig. 2. Both the thermally conductive jacket and the MLI are modeled forming a two-layer model for a coil with length, l . The function for the temperature distribution has the following form consisting for Bessel functions (I_n, K_n) and sinusoids:

$$\begin{aligned} T(r, \theta, z) = & \sum_{m=1}^{\infty} \sum_{n=1}^{\infty} \left(A_{mn} I_n \left(\frac{m\pi}{l} r \right) + B_{mn} K_n \left(\frac{m\pi}{l} r \right) \right) \cos n\theta \cos \left(\frac{m\pi}{l} z \right) \\ & + \sum_{m=1}^{\infty} \left(C_m I_n \left(\frac{m\pi}{l} r \right) + D_m K_n \left(\frac{m\pi}{l} r \right) \right) \cos \left(\frac{m\pi}{l} z \right) \\ & + \sum_{n=1}^{\infty} \left(E_n r^n + F_n r^{-n} \right) \cos n\theta + G \log r + H \end{aligned} \quad (1)$$

where the constants (A through H) are solved for by applying orthogonality and the boundary conditions. The boundary condition given at the outer MLI layer is a linearized form of the radiation from the chamber wall and from the coil itself radiating outwards. At the inner copper layer, the cryocooler was modeled to extract heat from a small segment of the coil. The analytic model determined that MLI is a promising insulation material. It also showed that a simple conductor may not be sufficient as the thermal jacket around the HTS, because it exhibits a large temperature spread away from the cryocooler. Placing multiple cryocoolers along the coil is a possible solution, but comes with mass and power penalties. The limitations of the analytic model were that it contained a linearized radiation approximation and did not model the anisotropic properties of the MLI. For these properties, the finite difference model was used.

2.2 Finite Difference Model (FDM)

The discrete model of the thermal system finite differences the coil in three dimensions. A time-varying implicit model has been constructed for the thermally conductive jacket. This is an improvement over the analytic model, which was a steady-state model. This time-varying FDM can be used to examine the transient cooling response of the coil. The anisotropic property of the MLI has also been modeled. There is a thermal conductivity perpendicular to the radiation shields, K_r , which acts through the MLI layers, and a thermal conductivity parallel to the radiation shields, K_θ , acting along a MLI layer. The heat diffusion equation is used as a starting point and is finite differenced so that the temperature at each node can be solved by Gaussian Elimination.

Figure 4 illustrates the general procedure used by the FDM for a one dimensional model. The FDM can use either a fixed temperature boundary condition or flux boundary condition at the cold point where the cryocooler is located. A control

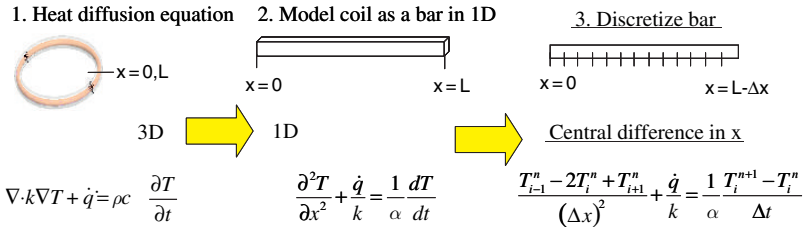


Fig. 4 Methodology for finite difference model for a 1-D system

volume approach is used at the boundary conditions to determine the temperature at the outside and inside surfaces. Similar to the analytic model the FDM consists of the inner copper jacket layer and the outer MLI layer, which is the EMFF thermal design from Fig. 2. The outer boundary accounts for the radiation from the chamber walls (or deep space) and from the coil body, which is a function of temperature to the fourth power. The volumetric heat input into each node for a simplified 1-D model is expressed by:

$$\dot{q} = \begin{cases} \frac{q_{cryo}}{\text{Volume Element}}, & x = 0 \\ \frac{\varepsilon_t \sigma [T_w^4 - (T_i^n)^4] A_c}{\text{Volume Element}}, & x > 0 \end{cases} \quad (2)$$

where q_{cryo} is the heat extracted by the cryocooler (or liquid nitrogen) located at the origin, and T_i^n is the temperature of the coil at a location i at time n . The effective emissivity, ε_t , accounts for the emissivity of both the chamber walls and the test article and their view factor. In addition, the model captures the effect of free-molecular flow in the chamber and also the variation of thermal diffusivity, $\alpha (T_i^n)$, as a function of temperature. The heat flux into the coil due to free-molecular flow is given by:

$$q [w/m^2] = F_a G p (T_2 - T_1) = h_{eff} (T_{CU} - T_w) \quad (3)$$

where the effective convection coefficient, h_{eff} , is largely a function of p , the system pressure. It was found that the free-molecular flow is a very low order effect on the system.

For comparison with the Matlab models, a simple 1-D model of the copper tube consisting of 19 nodes was constructed in a commercially available thermal code called Sinda. The Sinda model represented the experimental setup used in the chamber.

2.3 Experimental Model

A toroidal vacuum chamber was designed and built by MIT and Payload Systems Inc. as a testing facility for the thermal design and is shown in Fig. 5. The chamber, constructed out of COTS Polyvinyl Chloride (PVC) tubes, has a major radius of

1 m, minor radius of 12.5 cm, and holds a high vacuum (10^{-5} Torr). Currently a copper tube is used as the test article to represent the thermally conductive jacket. A liquid nitrogen feedthrough enters the chamber and wraps around the copper article so that conduction with the liquid nitrogen tubing provides cooling for the entire article and acts as the cryocooler. Three plastic spacers support the copper tube. Ten thermocouples are inside the chamber via two instrumentation feedthroughs. It has been shown that the experiment is repeatable. A single tank of liquid nitrogen allows for approximately 3 hours of cooling time. The transient cooling data of the copper tube was used for comparison with the simulation models.

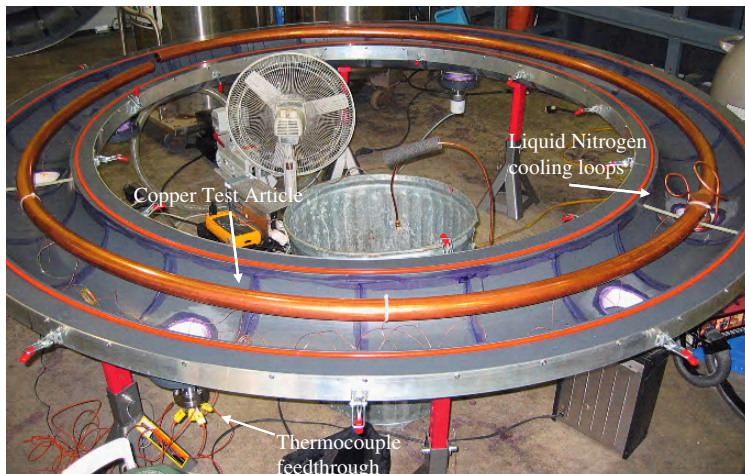


Fig. 5 Experimental vacuum chamber (opened) for EMFF thermal system

2.4 Model Comparison

Simulation models that were created include a 1-D FDM, 3-D FDM, and Sinda model. It has been shown in Fig. 6a that all three of these models match each other for a one meter coil (modeled as the copper test article) in the experimental vacuum chamber. The boundary condition used at the cryogenic cold finger was a fixed temperature of 100 K. The temperature increases as distance along the coil circumferentially (z-direction) increases and the maximum temperature is located opposite the coil, as expected.

To match the experimental model, the 3-D FDM was expanded to use the experimental data for the wall temperature and cold point temperature at the liquid nitrogen feedthrough. Overall, the experimental data had a faster transient cooling rate than predicted by models, however the FDM matched the experimental data to within 10 K at the end of the data run (approximately 3 hours), which is shown in Fig. 6b. The figure shows the temperature along the coil according to the model (solid line) and at nine thermocouple locations. Discrepancies between the model

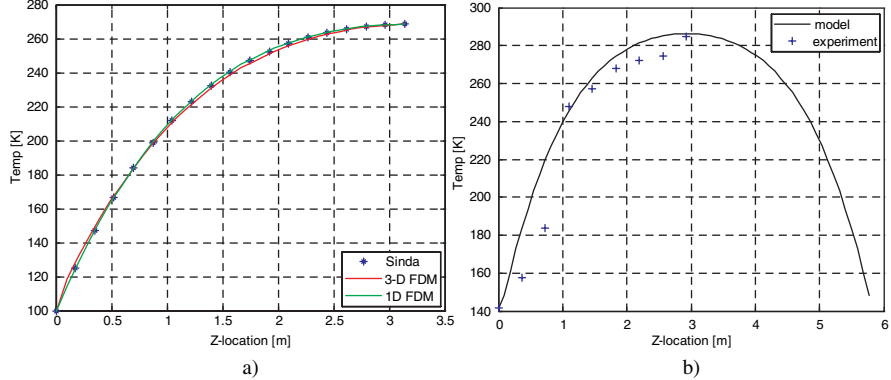


Fig. 6 (a) Comparison of finite difference models (1-D, 3-D) and Sinda, (b) Comparison of experimental results with FDM

and the data are due to the film layer formed in the liquid nitrogen cooling loops which give unsteady cooling. Also heat introduction from the spacers holding up the test article and through the thermocouple wires are not incorporated in the model. While the maximum temperature of the design with just the thermally conductive jacket is higher than T_c , the Matlab models can now be run with the MLI incorporated in the design. Current results indicate that even with MLI the maximum temperature is greater than T_c . In order to obtain a more uniform temperature distribution around the coil, a heat pipe operating at cryogenic temperatures can be used. The heat pipe acts as the thermal conductive jacket and the HTS wire stack is located inside the pipe in the vapor space. Preliminary design of the heat pipe using multiple screen mesh layers as the wicking structure and using nitrogen as the working gas allows for a heat pipe with sufficient power capacity, in the tens of Watts, to cool the entire coil. Implementation of the cryogenic heat pipe is currently underway.

3 Conclusions

Electromagnetic formation flight is a unique and promising method of actuation for formation flight systems. The thermal system is a critical aspect of the design for an EMFF system since constant low temperature control of the superconducting coils is required despite a large variation of heating environments possible in low Earth orbit. The current thermal system design consisting of multilayer insulation and a thermally conductive jacket to maintain uniform temperatures around the coil has been modeled analytically and using finite difference models. These models correlate well in an experimental chamber set up for testing the thermal design. Additional work done on modeling include accounting for possible heat losses due to structural connections in a flight design and including the time-vary effects of the heating environment while in orbit. Future tests with MLI and the integration of the heat pipe with the HTS wire stack need to be conducted. For final validation, it

is proposed to use a thermal vacuum chamber, to incorporate a sun and earth heat source and include the radiator in the EMFF thermal system.

References

1. Kong, E. M. C., Kwon, D. W., Schweighart, S. A., Elias, L. M., Sedwick, R. J., Miller, D. W., "Electromagnetic Formation Flight for Multisatellite Arrays," *AIAA Journal of Spacecraft and Rockets*, Vol. 41, No. 4, pp. 659–666, July–August 2004.
2. Elias, Laila M., Kwon, Daniel W., Sedwick, Raymond J., and Miller, David W., "Electromagnetic Formation Flight Dynamics including Reaction Wheel Gyroscopic Stiffening Effects," *AIAA Journal of Guidance, Control, and Dynamics*, Vol. 30, No. 2, pp. 499–511, Mar–Apr. 2007.
3. Kwon, Daniel W., and Miller, David W., "Electromagnetic Formation Flight of Satellite Arrays," S.M. Thesis, MIT SSL #02–05, January 2005.

Preliminary System Simulation Environment of the University Micro-Satellite *Flying Laptop*

Alexander Brandt, Ivan Kossev, Albert Falke, Jens Eickhoff,
and Hans-Peter Roeser

Abstract The Institute of Space Systems at the Universität Stuttgart builds a micro-satellite for the purpose of technology evaluation and scientific experiments. The complexity of the project and its limited human resources require efficient modern development and engineering techniques. To support the satellite development process, EADS Astrium Friedrichshafen has sponsored a Model-based Development and Verification Environment infrastructure, to be used for test and design verification. This paper focuses on the set-up of the Model-based Development and Verification Environment simulator, in particular on the configuration of the simulated satellite environment, the creation of equipment models and operational facilities to control the simulated satellite and the simulator. Orbit and thermal simulations were conducted to demonstrate the functionality of the environment setup under consideration.

1 Introduction

Since 2003 the Institute of Space Systems of the Universität Stuttgart carries out the Stuttgart Small Satellite Program whose first spacecraft is the *Flying Laptop* (Fig. 1). The *Flying Laptop* project's objectives are technology demonstration and Earth observation [1, 2]. The complexity of the project requires efficient modern

A. Brandt
Universität Stuttgart, Pfaffenwaldring 31, 70569 Stuttgart, Germany

I. Kossev
Universität Stuttgart, Pfaffenwaldring 31, 70569 Stuttgart, Germany

A. Falke
Universität Stuttgart, Pfaffenwaldring 31, 70569 Stuttgart, Germany
e-mail: falke@irs.uni-stuttgart.de

Jens Eickhoff
EADS Astrium GmbH, 88039 Friedrichshafen, Germany

H-P. Roeser
Universität Stuttgart, Pfaffenwaldring 31, 70569 Stuttgart, Germany

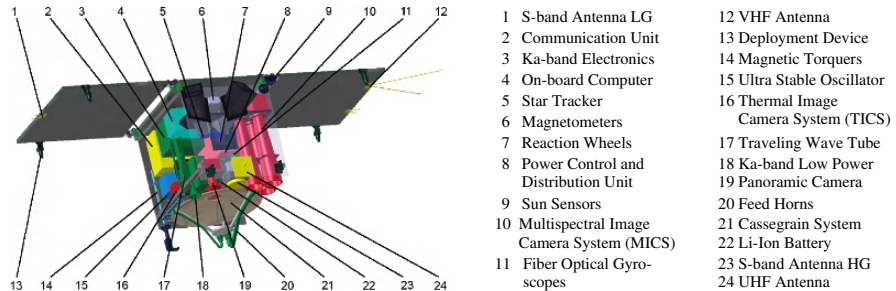


Fig. 1 Design of the *Flying Laptop*

development and verification techniques. To support the satellite development process, EADS Astrium Friedrichshafen has sponsored a Real-time Simulator (RTS) infrastructure, which is used for test and design verification.

The Real-time Simulator is part of Astrium's Model-based Development and Verification Environment (MDVE) [3, 4], which is a real-time capable functional simulation environment. The MDVE configuration used at the Institute of Space Systems includes a Real-time Simulator and a Core Electrical Ground Support Equipment (EGSE). The latter is required to command the RTS and the simulated satellite. In the current MDVE implementation the Core EGSE is substituted by the Mission Control System (MCS). The Real-time Simulator consists of four parts (Fig. 2):

- the On-board Computer (OBC) Simulator,
- the satellite equipment models,
- physical models, which simulate the spacecraft dynamics or thermal aspects,
- and the simulator kernel, which includes important low-level simulator functions like the scheduler, the numerical solver and the Telemetry (TM)/Telecommand (TC) handler.

Prior to this work, the Real-time Simulator at the Institute of Space Systems consisted of an

- initial version of the OBC and Power Subsystem models,
- as well as of most of the Attitude Control System (ACS) sensors.

This paper discusses the extension of the existing MDVE RTS to a first functional state. This includes the following steps:

- As a basis for the integration of ACS control loops, ACS actuator models must be created and the Environment and Dynamics Physical Models must be verified.
- For conducting thermal simulations, a S/C thermal model must be created and verified. Additionally, thermal control system hardware models must be implemented.
- To enable simulation data processing and evaluation, the RTS as well as the simulated S/C must be connected to a MCS.

In this paper the implementation of these steps is presented.

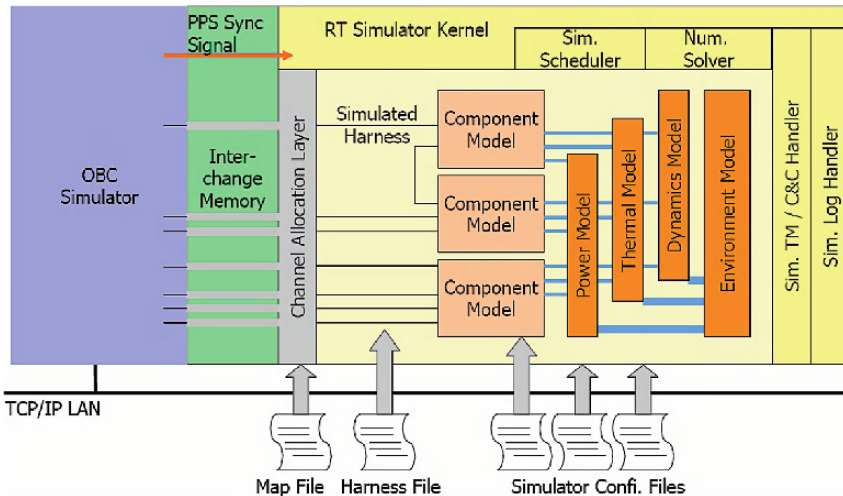


Fig. 2 The Real-time Simulator structure

2 Implementation

2.1 Integration of the Environment and Dynamics Propagator into the RTS

The environment and dynamics models have been sponsored by EADS Astrium Friedrichshafen and implement the RTS Environment and Dynamics Propagator. Quantities, which are calculated by the propagator, are accessible for all RTS models via an environment and dynamics interface. For example a sensor equipment model is interconnected to the propagator via this interface to acquire data which is then transmitted to the OBSW as measured sensor data. The ACS actuator models report their induced forces, torques and angular momentum to the propagator as input for the integration of the S/C equations of motion. Figure 3 shows which propagator quantities are exchanged with the magnetic torquer and reaction wheel models. The Environment and Dynamics Propagator implements the environment models given in Table 1. These models may be enabled or disabled (except for the sun and moon gravitational effects) providing comparable functionality as the High Precision Orbit Propagator (HPOP) of the Satellite Tool Kit (STK) [5].

At simulator initialization, the propagator is characterized by data from the RTS configuration files as follows:

- The environment models from Table 1 are initialized.
- The simulation start time is set.
- Initial position, velocity and attitude are set.
- Satellite parameters like mass, moment of inertia matrix and geometry parameters are set.

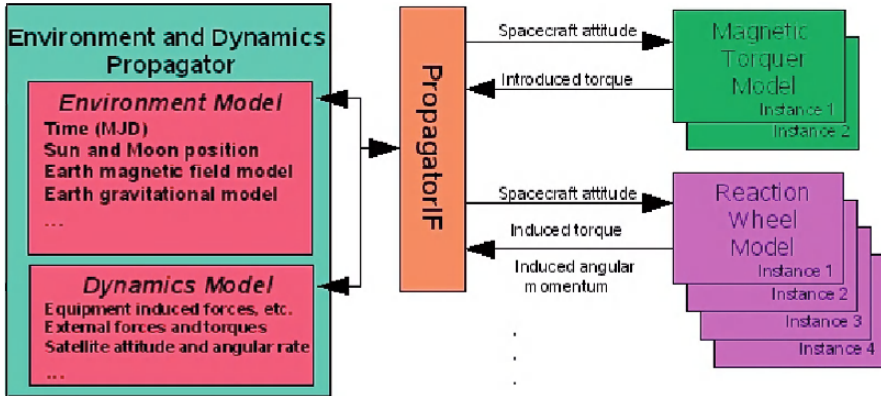


Fig. 3 Environment and dynamics infrastructure

Table 1 Environment and Dynamics Propagator environment models

| Model type | Model name |
|-----------------------------------|---|
| Earth atmospheric model | fixed density or interpolation table data |
| Solar and albedo flux models | interpolation table data |
| Earth magnetic field model | IGRF10 |
| Earth gravitational field model | JGM3 |
| Sun and moon gravitational effect | no model name |

The position and velocity accuracy of the Environment and Dynamics Propagator has been verified by comparing simulated orbits with data acquired by STK [6]. The simulations show that the propagator's accuracy agrees well with the accuracy of STK's HPOP. Figure 4 illustrates the time dependency of the Longitude of Ascending Node acquired by an STK and an MDVE simulation. Data has been logged in 10s intervals, which affects the calculation precision.

Figures 5 and 6 represent a comparison of the orbit inclination and altitude acquired by both simulation environments. These show good agreement, which certifies the Environment and Dynamics Propagator as suitable for ACS and orbit propagation within this project.

2.2 Integration of the Thermal Propagator into the RTS

The Thermal Propagator consists of a thermal integrator, sponsored by EADS Astrium, and a nodal thermal model. The propagator interacts with the equipment models via a special Thermal Interface and integrates a system of energy conservation equations whose inputs are the solar, Earth infra-red and albedo heat fluxes as well as the dissipated power provided by the equipment models. The current implementation of the Thermal Propagator supports only orbit-averaged solar, Earth infra-red and albedo heat fluxes, which are invariant with respect to the S/C attitude. The propagator's outputs are the nodal temperatures.

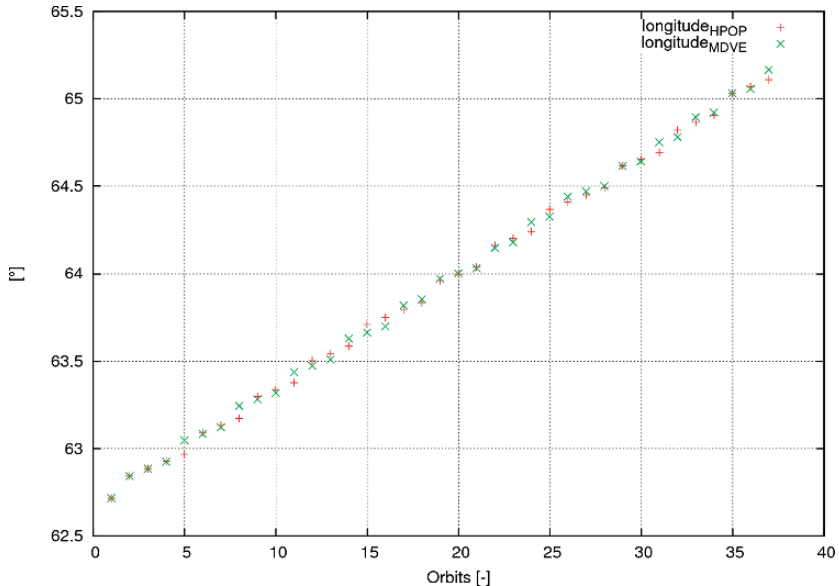


Fig. 4 Time dependency of the orbits longitude of the ascending node for the Flying Laptop nominal orbit. Comparison between the HPOP and the MDVE simulations

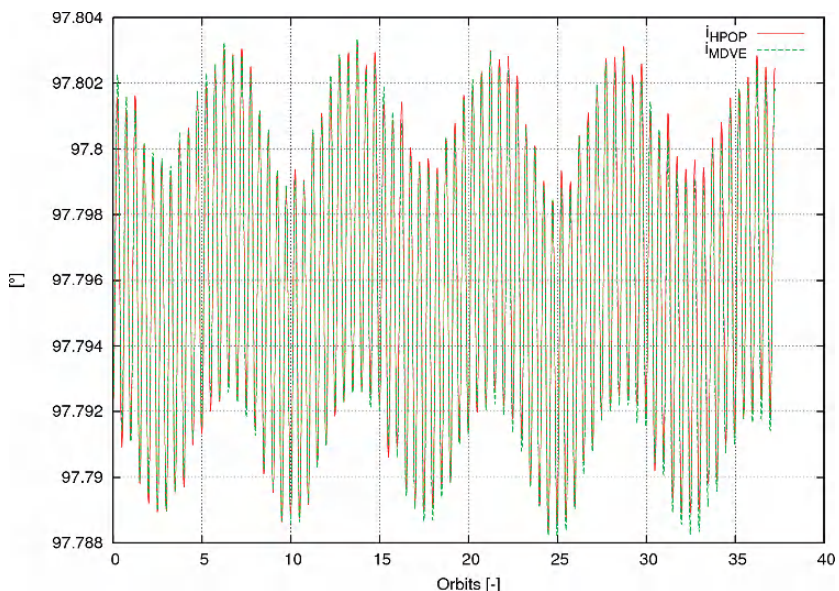


Fig. 5 Orbit inclination time dependency for the *Flying Laptop* nominal orbit. Comparison between the HPOP and the MDVE simulations ($i_{\text{NOM}} = 97.79^\circ$)

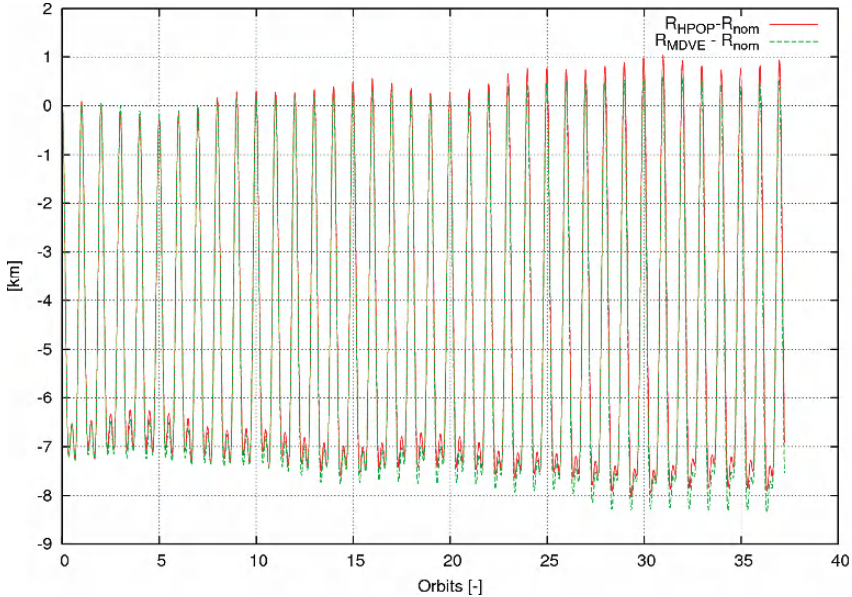


Fig. 6 Time dependency of the orbit altitude deviation for the *Flying Laptop* nominal orbit. Comparison between the HPOP and the MDVE simulations

2.2.1 Thermal Model

The thermal model describes the thermal properties of the S/C and is therefore the coupling between the general purpose Thermal Propagator and the S/C under consideration. The thermal model is of a nodal type and consists of a reduced number of nodes to ensure low numerical complexity and thus the real-time capability of the RTS. In case of the *Flying Laptop*, 33 of these nodes model the S/C's equipment and structure and one node represents the space environment [7]. The reduced number of nodes is achieved by assigning more than one piece of equipment to one thermal node. To reduce modeling errors, attention has been paid that this node assignment is done for adjacent equipment. The node coupling network of the *Flying Laptop* MDVE thermal model is depicted in Fig. 7 for a constant sun-oriented S/C attitude. The nodal discretization of the S/C causes that the resulting thermal conductive couplings are lower than the real ones [8]. Since the propagator is invariant with respect to the S/C's attitude, the nodal network cannot be adjusted to attitude changes during simulation. The solid lines represent conduction couplings and the dashed ones represent radiation couplings. The couplings' values are calculated using analytical approximation expressions [8]. Only radiation conductors, which model incoming or outgoing heat fluxes, are shown. The internal radiation couplings are omitted to keep the illustration concise. The incoming solar (S), earth infra-red (E) and albedo (A) heat fluxes are represented by three virtual nodes, which are not part of the nodal thermal model but are displayed for reasons of clarity. In contrast, node 34 absorbs the outgoing heat fluxes and is part of the nodal model. Thermal simulations are

conducted and verified by comparison with I-deas NX software simulations [9]. Figure 8 shows the temperature time dependency of the Payload, Core, and Service Modules. The following differences can be observed:

- The temperatures in the MDVE simulation are higher than in the I-deas NX simulation, because of the MDVE thermal model's lower resulting thermal conductive couplings.

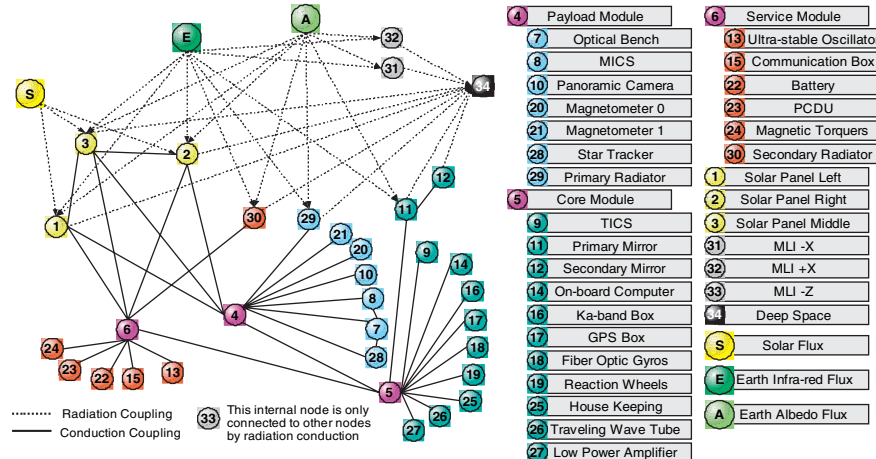


Fig. 7 The Flying Laptop nodal thermal model

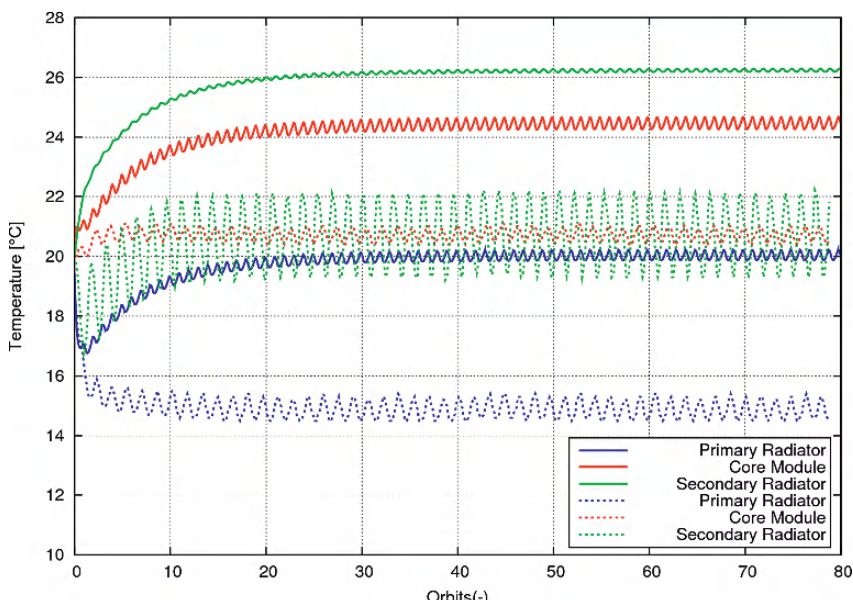


Fig. 8 Propagation of a temperature throughout the RTS to the MCS

- Generally, the MDVE features lower temperature amplitudes due to the orbit-averaged thermal loads in this simulation.
- The temperature amplitude of the Secondary Radiator in the I-deas NX simulation is much larger than the one in the MDVE simulation. It is assumed that this is also caused by the orbit-averaged thermal loads.
- A gap between the temperatures of the MDVE Secondary Radiator and the temperatures of the Core Module can be observed, which is absent in the I-deas NX simulation. It is assumed that this is caused by the lower resulting thermal conductive couplings.

Since the main objective of MDVE is system simulation and not detailed thermal analysis, the results of the conducted simulations confirm the validity of the created thermal model despite the temperature differences.

2.3 Equipment Models

The S/C is represented in the RTS by a number of equipment models, each of them modeling specific equipment hardware. Each piece of hardware is implemented by a single C++ class with a number of instances corresponding to the equipment's occurrence in the S/C. Initially, a Unified Modeling Language class diagram of the hardware equipment is created. This diagram contains information about the number of instances to be created from this class, about the number and type of the lines of the simulated hardware harness as well as information about the model's monitoring variables, which will later be accessible for monitoring and manipulation. From this UML diagram an automatic source code generation tool creates the hardware model class framework. This equipment modeling approach results in identically organized and functioning class instances, representing multiple equipments of a certain type. For example, in the *Flying Laptop* there are four identical momentum wheels, mounted in a tetrahedral configuration. From a modeling point of view, the wheels' functionality is identical and the only difference between them is their orientation and state at a certain point of time. By using a base class, the equipment's behavior is implemented only once, while each instance is characterized at simulator initialization via Extensible Markup Language (XML) configuration files. The XML files contain mission scenario data, which is acquired from the project's database.

The model's operation consists in the execution of the equipment functional model and interaction with the remaining equipment and physical models, as well as with the RTS kernel (Fig. 9). The simulator kernel has direct access to the model's system variables (e.g. the model's clock) and is responsible for the logging of model specific data. The equipment's functional model is executed by a fixed-increment time advance mechanism (the simulator scheduler), whereby the model's state is propagated. The functional model consists of the discrete and the continuous models parts, the first one modeling the equipment's mode transitions and the second one calculating continuous quantities. Signals (TM/TC, power supply) are transmitted via the simulated model harness and data is exchanged with the propagators via their

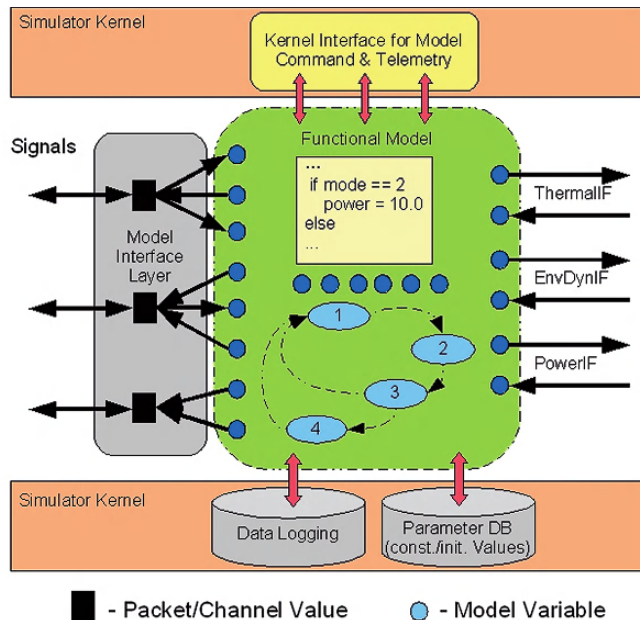


Fig. 9 Equipment model diagram

corresponding interfaces. As an example of how an equipment model operates, the operation of the reaction wheel model is explained in the following.

2.3.1 Reaction Wheel Operation

The Reaction Wheel model class [6] is instantiated four times to realize the four reaction wheels mounted in the *Flying Laptop*. At simulator initialization, the model is characterized by parameters for:

- the wheel momentum of inertia,
- the nominal supply voltage,
- the maximal motor current, torque and speed,
- the wheel orientation in S/C body frame,
- time constants,
- and the model's initial operational mode.

The Reaction Wheel's functional model is realized by a discrete model part, which models the equipment's hardware and software states as well as by a continuous part, which models the Reaction Wheel's dynamics. Each time the model is invoked, its discrete model part acquires the model's input:

- the supply voltage provided via two power lines by the Power Control and Distribution Unit,

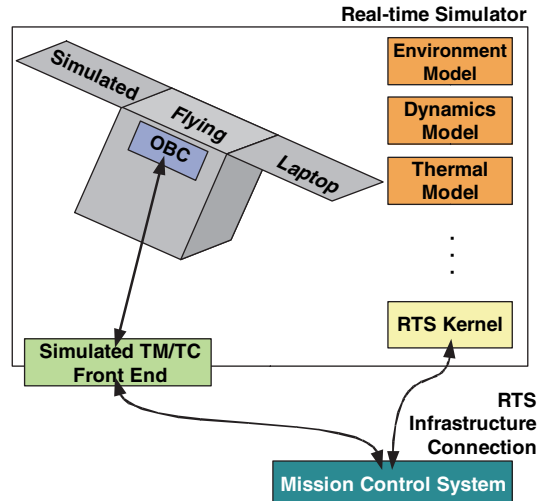
- the equipment's temperature,
- and the induced failure modes.

Having completed this procedure, enough data is available to determine the equipment operational mode. The model's communication reception line is read out and the received commands are processed. Telemetry is sent to the OBC upon request via the model's transmission line and then the model's continuous part is executed. The latter integrates an adapted discretized Reaction Wheel SIMULINK model, developed during Phase A of the project. This model calculates, among others, the wheel momentum, the induced torque and the consumed power, which are finally reported to the Environment and Dynamics Propagator and the Thermal Propagator respectively. This sequence of operations (except for the model's initialization) is cyclically initiated by the scheduler to implement the models state propagation in time.

2.4 Communication

The communication between the system simulator and the MCS consists of two main aspects: a connection between the simulated satellite and the MCS making the communication with the spacecraft possible during simulation, and a second connection between the RTS and the MCS, which is used to command the RTS. Thus the MCS is able to both operate the simulated satellite and to control the RTS (Fig. 10). The RTS allows failures to be induced into the simulation to test the On-board Software (OBSW) performance in case of malfunctions [4].

Fig. 10 Data links between the MDVE simulation and the MCS



In conventional Software Verification Facility (SVF) implementations a dedicated OBC simulator exists [3], which features an integrated TM/TC front end for

communication with the MCS. The front end directly reads TM from and writes TC into the registers of the emulated OBC [4]. Since the Field Programmable Gate Array (FPGA) OBC of the *Flying Laptop* prevents Direct Memory Access (DMA), a qualitatively different approach for the TM/TC front end integration is developed [7]. The TM/TC will be transferred between the OBC model and a special equipment model, called “TM/TC adapter”. Together with a separate TM/TC task, running parallel to the equipment simulation, the simulated TM/TC front end of the *Flying Laptop* RTS is realized. For commanding and telemetry processing, the European Space Agency’s SCOS 2000 software is used. SCOS’s capability of handling packets according to the Consultative Committee for Space Data Systems (CCSDS) standard requires at present the simulated TM/TC front end to encapsulate the *Flying Laptop* TM/TC packets using the Packet Utilization Standard (PUS). For interfacing the MCS with the RTS and the simulated TM/TC front end, a program called SCOS RTS Proxy is used. It translates pure PUS packets into a format understandable for SCOS-2000. The proxy’s functions consist in:

- TM encapsulation
 - TM PUS packets into TM Transfer Frames
 - TM Transfer Frames into Network Controller and Telemetry Router System (NCTRS) TM Data Units
- TC extraction
 - TC Transfer Frames from NCTRS TC Data Units
 - TC PUS packets from TC Transfer Frames
- Routing of TC PUS packets to either the RTS kernel or to the simulated TM/TC front end.

Since the creation of the simulated TM/TC front end, the RTS is capable of handling PUS packets. The creation of the SCOS RTS Proxy enables the communication between the simulator (RTS kernel, simulated TM/TC front end) and SCOS-2000. The following example demonstrates the simulator data flow from the OBC to the MCS.

2.5 Simulator Data Flow

As stated above, the OBC interfaces with the simulated TM/TC front end similarly to an equipment model. The resulting data flow is illustrated by the propagation of temperature data to the MCS (Fig. 11). For each scheduled time step, the temperature of a thermal model’s node is calculated by the Thermal Propagator and exposed within the Thermal Interface. The House Keeping (HK) unit, an equipment model which interfaces with the temperature sensors, queries the temperature from the Thermal Interface and converts it into a measured voltage, since the real temperature sensors on-board the *Flying Laptop* will also output voltages. Then the HK sends these cyclically to the OBC, which analyzes this data, creates the housekeeping

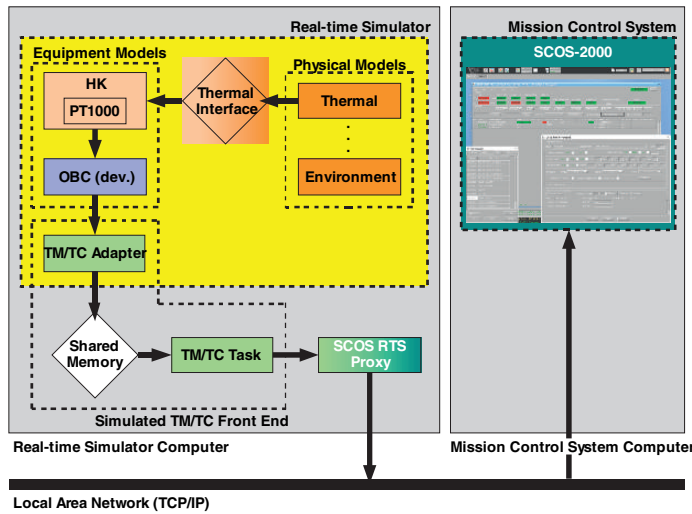


Fig. 11 Propagation of a temperature throughout the RTS to the MCS

TM packets, and sends them to the TM/TC adapter where they are written into a shared memory area. From the shared memory they are instantly read out by the TM/TC task, which forwards them to the SCOS RTS Proxy. The TM PUS packets are encapsulated into NCTRS TM Data Units by the proxy and sent via the Local Area Network from the Simulation Computer to the SCOS-2000 Packetizer, running on the MCS Computer.

3 Conclusion

As a conclusion, it can be summed up that

- the creation of actuator models for the ACS, the communication equipment and the thermal control subsystems,
- as well as the integration of the environment, dynamics and thermal physical models,
- and the setup of the MCS and its connection to the simulator

has significantly contributed to the completion of the *Flying Laptop* MDVE first functional state and has paved the way to the Real-time Testbed simulator configuration.

References

1. Falke, A.; Grillmayer, G.; Walz, S.; Hesselbach, F.; Eickhoff, J.; Roeser, H.-P.: *LED in-flight calibration and model-based development of ACS algorithms for the university micro-satellite*

- Flying Laptop. Italy, Chia Laguna: Small Satellite Systems and Services – The 4S Symposium, September 25–29 2006.
- 2. Grillmayer, G.; Hirth, M.; Huber, F.; Wolter, V.: *Development of an FPGA Based Attitude Control System for a Micro-Satellite*. AIAA-2006-6522, USA, Keystone, CO; AIAA/AAS Astrodynamics Specialist Conference. August 21–24, 2006.
 - 3. Eickhoff, J.; Falke, A.; Roeser, H.-P.: *Model-based Design and Verification – State of the Art From Galileo Constellation Down to Small University Satellites*. Spain, Valencia: 57th International Astronautical Congress (IAC), October 2–6, 2006.
 - 4. Eickhoff, J.: *Systemsimulation in der Satellitenentwicklung I&II – (System simulation in Satellite Engineering I+II)*. Germany, Stuttgart: Annually lectures at Institute of Space Systems, Universität Stuttgart, 2007.
 - 5. AGI: Satellite Tool Kit. <http://www.stk.com/products/desktopApp/stkFamily/>, last visited on April 22 2007.
 - 6. Kossev, I.: Development of Functional Software Models of the ACS Actuators and Integration of an Environment and Dynamics Propagator into the Simulation Environment for the Micro-satellite Flying Laptop. Institute of Space Systems. Universität Stuttgart. Diplomarbeit. IRS-07-S03. 2007.
 - 7. Brandt, A.: Development of Functional Models for Communication and Thermal Hardware and a Thermal Model for the Flying Laptop Micro-satellite Simulation. Institute of Space Systems. Universität Stuttgart. Diplomarbeit. IRS-07-S-02. February 2007.
 - 8. Gilmore, D., Ed.: *Spacecraft Thermal Control Handbook*. Volume I.: Fundamental Technologies. 2nd Ed., AIAA, Reston, Virginia, 2002.
 - 9. Putze, U.: *Entwicklung des Thermalkonzeptes und Aufbau der analytischen Thermalmodelle für den Flying Laptop*. Institute of Space Systems. Universität Stuttgart. Diplomarbeit. IRS-06-S-04. January 2006.

A Miniaturised UV Imaging Spectrometer for Remote Sensing of Atmosphere: Volcanic Sulphur Dioxide, Ozone, and Aerosols

Juan A. Fernandez-Saldivar

Abstract A new compact and low-cost high spectral resolution imager for selected ultraviolet bands is proposed to operate in a micro-satellite constellation with the objective of monitoring important atmospheric constituents: sulphur dioxide (SO_2), ozone (O_3) and aerosols. The spectral resolution and imaging performance of the sampled spectra are studied, given the distortions observed from different angular fields to estimate the slit function. Radiative transfer simulations using MODTRAN with the derived resolution will show the differential radiances under various scenarios with SO_2 “clean” and “contaminated” atmospheres. The instrument design exploits the excellent response of new silicon carbide photodiodes in this region; its blindness to visible radiation provides for a relatively simple and compact optical design ($9 \times 13 \times 6$ cm). The use high-efficiency transmission gratings and 20-bit electronics (consuming less than 5 W) offer high sensitivity. Other wavelengths outside this region (331 nm and 360 nm) are sampled at a ground distance of 7×32 km, so that the presence of aerosols may be detected, and the background UV albedo can also be determined for retrieval algorithm purposes.

1 Introduction

Currently observations in the UV region are restricted to large platforms and instruments such as NASA’s Total Ozone Mapping Spectrometer (TOMS) and Ozone Monitoring Instrument (OMI) and ESA’s Global Ozone Monitoring Experiment (GOME) and Scanning Imaging Absorption Spectrometer for Atmospheric Cartography (SCIAMACHY). With the exception of TOMS, which was not designed to monitor SO_2 and still holds an unrivalled record in detecting volcanic activity [1], all the others face various trade-offs when observing the UV spectrum between 300 and 315 nm wavelength. Because of the wide dynamic range of backscatter

J.A. Fernandez-Saldivar

Surrey Space Centre, University of Surrey, Guildford, Surrey, GU2 7XH, UK

e-mail: j.fernandez@surrey.ac.uk

radiation observed, it is common to optically split this region in to two ranges and use detectors with differing sensitivity (Fig. 1 Left), thus degrading the signal to noise ratio. This split occurs precisely in a region where the SO_2 absorption features provide easier discrimination with respect to O_3 and this can lead to problems in the retrieval algorithms.

2 Spectral and Radiometric Analysis

The spectral range and resolution required to discriminate SO_2 from O_3 is defined by the absorption spectra of these trace gases. In the region between ~ 300 and 320 nm SO_2 absorption is greater than O_3 (Fig. 1 Right). However it is below ~ 313 nm, where the ozone absorption is smooth, that SO_2 features are more easily identifiable for discrimination. SO_2 shows a wave-like spectrum with peaks and troughs evenly spaced every ~ 1 nm (spectral sampling) and with an estimated Full Width Half Maximum (FWHM) of ~ 0.4 nm (spectral resolution). We can therefore use these peaks and troughs to obtain information on the ratio of SO_2 to O_3 (Fig. 1 Right inset). Above ~ 313 nm the features would require higher spectral sampling and resolution.

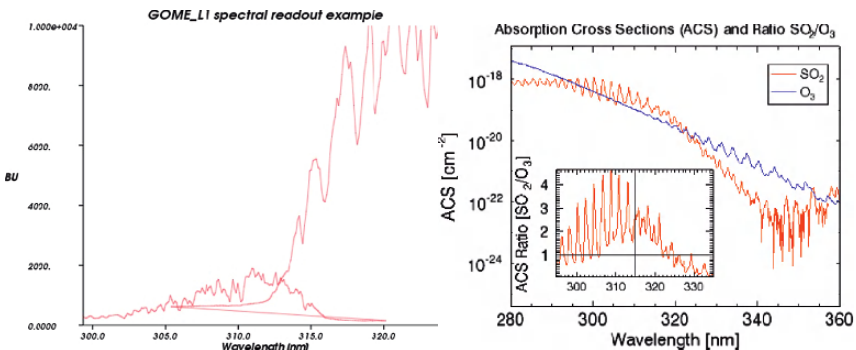


Fig. 1 (left) UV channel overlap for GOME [2]. (right) absorption cross sections for SO_2 at 243K [3] and O_3 at 241K [4]. (right Inset) ACS ratio of these constituents for discrimination

In order to estimate the radiometric resolutions required, a radiative transfer model was computed using MODTRAN [5] under these conditions: Tropical Atmospheric standard profiles, no aerosols, no clouds and solar angle of 25 degrees. Atmospheres with three ozone concentrations were analysed, each “contaminated” with an SO_2 layer of varying concentration at 4 km scale height (Fig. 2).

By taking the ratios of radiances obtained by from the atmosphere with varying amounts of SO_2 and O_3 with respect to those obtained from a standard no-clouds tropical atmosphere (no SO_2 , and 277 DU of Ozone), we can observe the different spectral signatures of these trace gases. As expected from its Absorption Cross Section we observe in Fig. 3 the jagged behaviour of SO_2 (Left) compared to the smooth

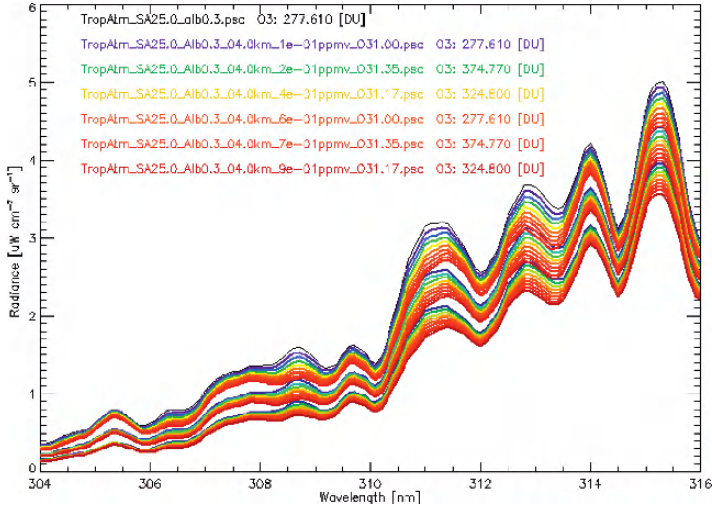


Fig. 2 Radiative transfer simulations for SO₂ contaminated atmospheres under 3 different O₃ conditions

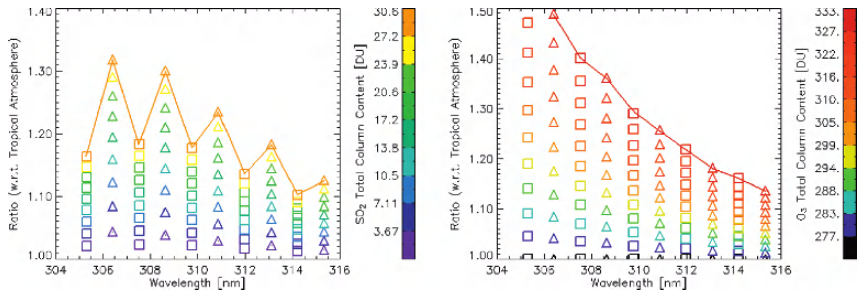


Fig. 3 Radiance ratio w.r.t. tropical atmosphere (left) atmosphere affected by SO₂ (right) affected by O₃

curves due to O₃ (Right). These features will allow the discrimination of these two gases using retrieval techniques such as the Band Residual Difference algorithm [6].

3 Instrument Design

The instrument was designed to obtain a ground sample distance at nadir of 4×30 km; this is considered useful according to the Disaster Management Support Group (DMSG) of the Committee on Earth Observation Satellites (CEOS) suggesting 10 to 20 km [7]. The calculated spatial resolution is half the area covered by a normal OMI pixel (12×24 km) and 20 times smaller than TOMS (50×50 km); it is expected to minimise cloud cover scenes and increase the sensitivity in detecting

SO_2 contaminated pixels. A medium swath ($\sim 300 \text{ km}$) for a single imager would require the use of two imagers in order to observe large drifting clouds and reduce the revisit time; it would also match the Disaster Monitoring Constellation of micro-satellites imager pair swath [8]. The challenging requirements of the application such as: wide dynamic range and low-noise demand an extremely low circuit noise matched to a highly sensitive detector to ultimately define the system sensitivity. For this purpose a low power ($< 5 \text{ W}$) electronic solution comprising a switched integrator and 20-bit Analog-to-Digital converter in a miniature device is proposed.

3.1 Optics

The optical layout was chosen to have minimum number of parts whilst maximising the optical throughput (etendue). It uses the largest commercially available holographic transmission grating, matching it with a custom-made area array of Silicon Carbide (SiC) photodiodes at the focal plane. The use of fused-silica lenses will provide good transmission and performance in the UV, and some optical surfaces have an aspherical design to minimise distortions. The optical design was optimised around the central wavelength at 310 nm because of the critical requirements in this region. The performance of auxiliary channels is not as critical because the spectral resolution needed in those channels is not as demanding as in the continuous region. The layout proposed is shown in Fig. 4 below. On top we observe the three main optical rays of the three wavelength regions, 360 nm , 331 nm and $305\text{--}315 \text{ nm}$ (left to right.)

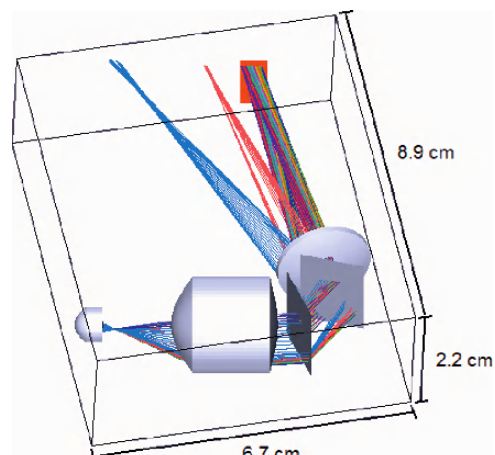


Fig. 4 Optical layout

3.2 Grating and Detector

Two key elements were the main drivers of the design: the transmission grating size ($15 \times 20 \text{ mm}$) and the pixel size of the photodiode array ($0.4 \times 0.6 \text{ mm}$). Transmission

gratings with high efficiency will provide the spectral dispersion required. An area array of Silicon Carbide (SiC) photodiodes is proposed because it is naturally blind to visible radiation. The combination of these two yields the spectral resolution and sampling required for the application. This is observed in Fig. 5, which shows the spectral imaging characteristics at the focal plane with its relative illumination and spectral resolution.

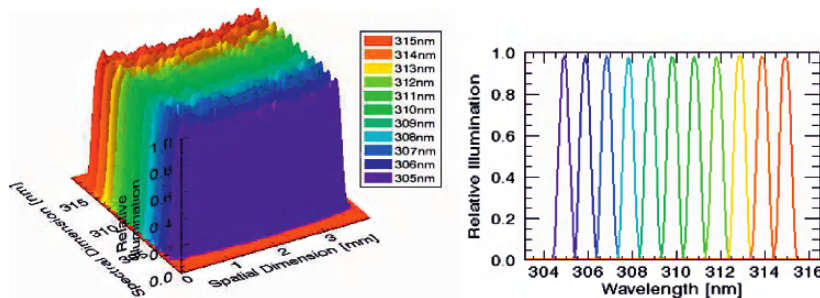


Fig. 5 (left) Spectral imaging at focal plane. (right) spectral resolution at 11 wavelengths

One area array of SiC photodiodes consisting of 10×10 pixels is proposed for the 10 contiguous channels (305–315 nm). Two linear arrays of 10×1 pixels will be used in the auxiliary channels 331-nm and 360-nm for determination of ozone products, aerosols and UV albedo.

The spectral imaging of all channels is shown in Fig. 6 below for the chief rays passing through the centre of the entrance pupil. A grid distortion is observed on all 3-wavelength ranges and a spectral “smile” causes the image to curve up as it approaches the edges of the detector arrays. However, this distortion is minimal for the chief rays.

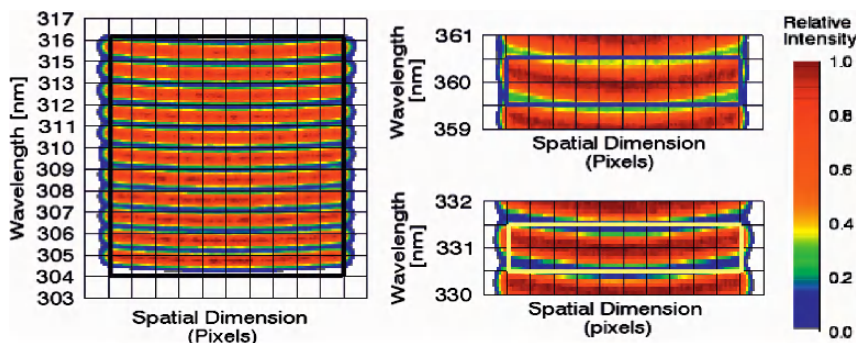


Fig. 6 Spectral imaging at focal plane. (left) detector array 305–315 nm (right) auxiliary channels 331 nm and 360 nm

The illumination on the focal plane is also analysed by considering the marginal rays passing through the entrance pupil from 2° to 14° . The real IFOV of the

spectrometer is 12.7° however a wider view is tested to test for influence on the spectral characteristics. This is shown in Fig. 7 for the chief rays (left) and for all rays including marginal rays (right).

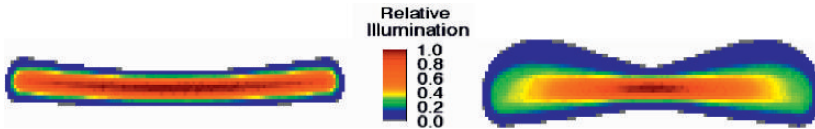


Fig. 7 Spectral imaging illumination @ 310 nm (*left*) $\pm 2^\circ$ fields. (*right*) $\pm 12.7^\circ$ fields

Slicing the above relative illumination images vertically at 10 different locations corresponding to the detector array columns, we obtain a Gaussian-like curve (Fig. 8).

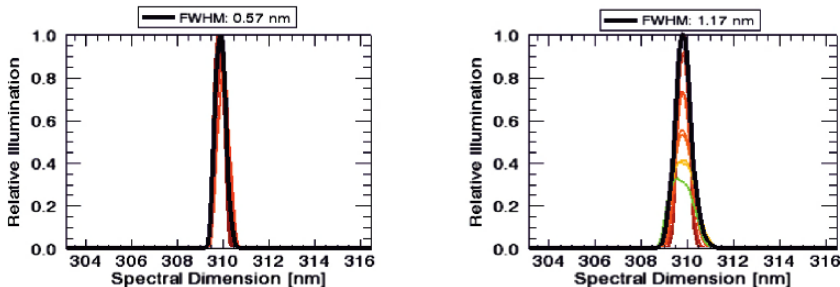


Fig. 8 Full width at half maximum (FWHM) @ 310 nm (*left*) $\pm 2^\circ$ fields. (*right*) $\pm 12.7^\circ$ fields

Once the real FWHM defined by the slit function has been obtained for all fields in the focal plane, the radiance ratios are computed by convoluting the spectral radiance with the appropriate slit function. The inclusion of marginal rays reaching the edge of the entrance pupil Fig. 9 (right) shows the reduction in the apparent “modulation” of the spectrum, with respect to that obtained with the chief rays alone (left). The Left graph is representative of the very best performance we could expect from the instrument on the optical axis, whereas the Right graph is representative of the overall instrument performance.

The marginal ray analysis allows determination of spectral and spatial distortions in terms of variations in the expected FWHM and the relative position of the wavelengths as the marginal rays reach the edge of the entrance pupil (Table 1).

The changes in relative intensity are a result of vignetting; however the absolute expected levels of radiance should still meet the optical signal requirements of the algorithm ($0.01 \mu\text{W cm}^{-2} \text{ sr}^{-1}$ threshold). The widening of the FWHM and the resulting offset will combine to degrade the sensitivity at the edges of the FOV. However, it is proposed to use two instruments in a similar way to the way the DMC imagers are operated, giving an optical axis which is tilted $\sim 12^\circ$ off-nadir. This counteracts the degradation to some extent over the central portion of the image. At the edge of the swath of the imaging pair, the lack of sensitivity will greatly reduce the performance.

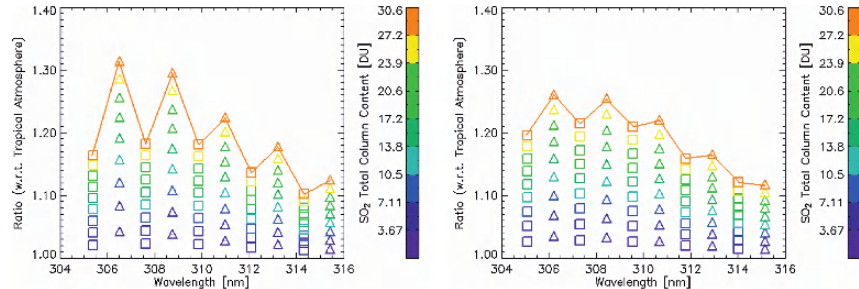


Fig. 9 Radiance ratio w.r.t. tropical atmosphere (*left*) $\pm 2^\circ$ fields with FWHM = 0.57 nm. (*right*) $\pm 12.7^\circ$ fields with FWHM = 1.17 nm

Table 1 Spectral and spatial changes in FWHM and position

| Field [degrees] | Relative Intensity | Spectral Position [nm] | Spectral FWHM [nm] | Spatial Position [mm] | Spatial FWHM [mm] | Abs. wav offset [nm] | Position offset [mm] |
|--------------------|-----------------------|------------------------------|--------------------------|-----------------------------|-------------------------|-------------------------------|----------------------------|
| 0 | 1 | 309.8746 | 0.5403 | 2.9388 | 0.2406 | 0.0000 | 0.0000 |
| 2 | 0.923396 | 309.8609 | 0.5712 | 2.9449 | 0.2544 | 0.0138 | 0.0061 |
| 4 | 0.761339 | 309.8235 | 0.6668 | 2.9616 | 0.2969 | 0.0511 | 0.0228 |
| 6 | 0.590644 | 309.7750 | 0.8132 | 2.9832 | 0.3621 | 0.0996 | 0.0444 |
| 8 | 0.469599 | 309.7188 | 0.9734 | 3.0082 | 0.4335 | 0.1559 | 0.0694 |
| 10 | 0.380238 | 309.6503 | 1.1038 | 3.0387 | 0.4915 | 0.2243 | 0.0999 |
| 12 | 0.315583 | 309.5621 | 1.1727 | 3.0780 | 0.5222 | 0.3125 | 0.1392 |

This is a condition all spectral imagers face to some extent and it is a design trade-off we cannot easily avoid without adding optical complexity to the instrument.

If we consider the variations in FWHM along the spectral dimension we observe these are a minimum in the detector array covering 305–315 nm. On the auxiliary channels (331 nm and 360 nm) the performance is degraded due to the widening of the slit function. This occurs because the optical design is aimed at producing the best optical performance at the shorter wavelengths which have lower radiances. However, despite this compromise, the overall instrument performance of the instrument meets the requirements of the application in mind. Table 2 below summarizes the results obtained for representative wavelengths.

Table 2 Spectral and spatial changes in FWHM and position

| Wavelength Band [nm] | Relative Intensity | Spectral Position [nm] | Spectral FWHM [nm] | Spatial Position [mm] | Spatial FWHM [mm] | Wavelength offset [nm] |
|----------------------------|-----------------------|------------------------------|--------------------------|-----------------------------|-------------------------|------------------------------|
| 305 | 0.962532 | 304.9648 | 0.5149 | 5.1252 | 0.2293 | 0.0353 |
| 310 | 0.957696 | 309.8746 | 0.5403 | 2.9388 | 0.2406 | 0.1254 |
| 315 | 0.969093 | 315.0067 | 0.5639 | 0.6534 | 0.2511 | -0.0067 |
| 331 | 1 | 330.9560 | 0.5397 | 2.9066 | 0.2909 | 0.0440 |
| 360 | 0.922996 | 359.9814 | 0.6851 | 2.8727 | 0.4817 | 0.0186 |

The expected instrument specifications are shown in Table 3 below.

Table 3 Instrument Specifications

| | |
|--|---|
| Field of View | 25.8° × 0.57° |
| Pixel Size | 0.4 × 0.6 nm |
| Pixel sample distance | 7 × 31.5 km [§] |
| Revisit Time | Daily * |
| Spectral Resolution | 0.5–1.1 nm/0°–12° |
| Slit | 6 × 0.100 mm |
| Grating | 2847 lines mm ⁻¹ |
| Etendue | 7.48 × 10 ⁻⁴ sr ⁻¹ cm ⁻² |
| S/N @ 0.1 uW sr ⁻¹ cm ⁻² | ~244 (on axis) |
| Entrance Pupil Diameter | 4 mm |
| Back Focal Length | 60.17 mm |
| Working F/# | 6.33 |

[§]single imager

*dual UV-Imager on DMC-type constellation

4 Conclusions

The instrument is designed in order to meet the rapid response and dynamic requirements of demanding applications such as volcanic activity monitoring. The demanding requirements to consider when designing such a system were shown indicating the potential of such instruments to successfully detect and discriminate two important trace gases: SO₂ and O₃. The auxiliary channels may also be used to determine the concentration of aerosols.

The optical design and its spectral imaging properties across its field-of-view were discussed together with the requirements of various atmospheric scenarios and imaging characteristics. The instrument imaging performance fulfils the application needs according to radiative transfer simulations of realistic atmospheric scenarios. The detection limits, based on the expected detector performance, are aimed ideally to observe minor concentrations of SO₂ produced by passively outgassing volcanoes ≤5 DU and certainly should be capable of monitoring volcanic events releasing >10 DU. However, the real detectivity will be defined once the noise performance of the electronics have been tested and verified.

The relatively low-cost and small size of the instrument proposed makes it a suitable instrument for a micro-satellite-based atmospheric remote sensing mission.

References

- Carn, S.A., Krueger, A.J., Bluth, G.J.S., Schaefer, S.J., Krotkov, N.A., Watson, I.M., Datta, S., *Volcanic eruption detection by the Total Ozone Mapping Spectrometer (TOMS) instruments: a 22-year record of sulfur dioxide and ash emissions*, in *Volcanic Degassing*, C. Oppenheimer, Pyle, D. M., Barclay, J., (Eds.) 2003, Geological Society: London, pp. 177–202.

2. ESA, *Basic ENVISAT Atmospheric Toolbox (BEAT)*. 2006, European Space Agency.
3. Bogumil, K., Orphal, J., Burrows, J.P., *SO₂ Absorption Cross Sections at 243K – version1.0*. 2000, Institute of Environmental Physics – University of Bremen: Bremen, Germany.
4. Burrows, J.P., Richter, A., Dehn, A., Deters, B., Himmelmann, S., Voigt, S., Orphal, J., *Atmospheric remote-sensing reference data from GOME. Part 2. Temperature dependent ACS of O₂ in the 231–794 nm range*. Journal of quantitative spectroscopy and radiative transfer, 1999. **61**: pp. 509–517.
5. Berk, A., Anderson, G.P., Acharaya, P.K., Hoke, M.L., Chetwynd, J.H., Bernstein, L.S., Shettle, E.P., Matthew, M.W., Adler-Golden, S.M., *MODTRAN 4 Version 3 Revision 1 User's Manual*. 2003, Air Force Research Laboratory.
6. Krotkov, N.A., Carn, S., Krueger, A. J., Bhartia, P. K., Yang, K., *Band residual difference algorithm for retrieval of OS₂ from the Aura Ozone Monitoring Instrument (OMI)*. IEEE transactions on geoscience and remote sensing, 2006. **44**(5): pp. 1259–1266.
7. CEOS, *Team Report: VOLCANO (Final Report)*, C.D.M.S. Group, Editor. 2001.
8. Underwood, C.I., Mackin, S., Stephens, P., Hodgson, D., Da Silva Curiel, A., Sweeting, M., *Evaluation of the utility of the Disaster Monitoring Constellation in support of Earth Observation Applications*. in *Small Satellites for Earth Observation*. 2005, Berlin, Germany: Walter de Gruyter.

Session 7

Special Aspects

BeeSat Attitude Determination and Control System

Martin Herfort, Marco Berlin, Hans-Peter Geile, and Zizung Yoon

Abstract Berlin Experimental and Educational Satellite (BeeSat [1]) is a highly innovative pico satellite project of the Department of Astronautics at Berlin Technical University. Main objective of BeeSat is the on-orbit verification of miniaturized reaction wheels suitable for pico satellites which have been developed with our main industrial partner Astro- und Feinwerktechnik Adlershof GmbH [2]. Work is done to provide a number of additional pico satellite technologies. This paper outlines motivations for equipping a pico satellite with an attitude determination and control system (ADCS) based on reaction wheels. BeeSat's ADCS is exposed briefly alongside some of the solutions the research team at TU Berlin developed. A sun sensor system based on Position Sensitive Detectors is introduced, a new design principle for magnetic coils is explained and the Microwheel system is displayed.

1 Introducing Pico Satellites

At TU Berlin good experiences with micro satellites have been made. The series of TUBSAT [3] micro satellites has shown remarkable results and provided students with hands-on experience ever since the micro satellite TUBSAT-A was

M. Herfort

Berlin Technical University, Institute of Aeronautics and Astronautics, Department of
Astronautics, Marchstr. 12, 10587 Berlin
e-mail: Martin.Herfort@ILR.TU-Berlin.de

M. Berlin,

Berlin Technical University, Institute of Aeronautics and Astronautics, Department of
Astronautics, Marchstr. 12, 10587 Berlin

H.-P. Geile

Berlin Technical University, Institute of Aeronautics and Astronautics, Department of
Astronautics, Marchstr. 12, 10587 Berlin

Z. Yoon

Berlin Technical University, Institute of Aeronautics and Astronautics, Department of
Astronautics, Marchstr. 12, 10587 Berlin

launched in 1991. Regarding the overall increase in capability, performance and efficiency of electronics pico satellites become a more and more serious subject to research.

CubeSats [4] are pico satellites, which means, that their total mass may not exceed 1kg. They have a cubic shape and standardized outer dimensions of $10 \times 10 \times 11.3\text{cm}^3$. Furthermore they have to meet special requirements to ensure the safety of launch vehicle and primary payload. Those limitations make it hard to realize features already taken for granted on larger satellites but on the other hand offer universities cheap and easy access to space.

Technologies for pico satellites can be used on larger satellites as well, one example being the reaction wheel developed for BeeSat which can easily be equipped with a larger flywheel mass and then meet the needs of nano satellites.

2 Beesat's Goals

The goals of the BeeSat project can be divided into three different groups:

2.1 Technology Demonstration

First and foremost BeeSat is a technology demonstration and evaluation satellite platform. The main goal is the on-orbit verification of newly developed reaction wheels for pico satellites. On the side of the ADCS also a new design principle for magnetic coils is evaluated as well as a sun sensor system based on Position Sensitive Detectors (PSD). Technologies tested on BeeSat also include: An in-house developed on-board computer, modified transceivers, a power control and distribution unit. The dependable operating system and middleware TinyBoss [5] developed for BeeSat eases programming and adds to overall security.

2.2 Widening the Field of Possible Pico Satellite Applications

Due to limited technological resources only few applications are suitable for the current generation of pico satellites. Acquiring technologies for pico satellites also means enabling them to fulfill the more demanding missions already envisaged at TU Berlin [6]. Possible applications and capabilities include:

- Occultation measurement
- Remote sensing and target pointing with one or more satellites
- High bandwidth communications
- Constellations
- Formation flight

2.3 Student Education

During numerous seminar papers and diploma theses students already have gained valuable experiences regarding mission analysis and satellite design. Once launched BeeSat will also serve as a means of teaching satellite operation.

3 Design Principles

Building a CubeSat means that a number of limitations will be encountered during satellite development. Outer dimensions of $10 \times 10 \times 11.3\text{cm}^3$ limit the room available within the spacecraft and put harsh limits on the overall energy consumption of the satellite. The mass limit of 1kg has also shown to cause many difficulties. In order to fulfill BeeSat's goals under the limitations of the CubeSat standard a couple of design principals have shown to be useful.

3.1 Use of Commercial of the Shelf Parts

Latest commercial of the shelf (COTS) parts often have better electrical, mechanical and monetary properties than their already space-proven counterparts. Due to their usually short life cycles (BeeSat is designed for one year of operation) and limited resources in space and energy, pico satellites can and have to take use of COTS components. Often they have to be adapted and always be qualified before being flown within the satellite. Another advantage of this strategy is that this valuable possibility for on-orbit verification of small parts can also help funding the satellite mission. BeeSat's sun sensor system (see Section 4.3) is a good example of a COTS part adapted to fulfill important tasks during a pico satellite mission.

3.2 Functional Integration Rather than Subsystem Separation

Enabling one assembly unit to fulfill a number of tasks means saving manpower during development as well as valuable mass and volume on the satellite. Due to its thin (1 mm) outer structure with many cut-outs BeeSat needs a structural fortification altering the natural frequency and adding to overall rigidity. This fortification also holds and isolates batteries so that they do not suffer from space conditions. Furthermore it serves as shielding for radiation sensitive parts of the on-board computer and provides various mounting points.

The printed circuit boards (PCB) (see Fig. 4) on each side of the satellite also fulfill a number of tasks within different subsystems. The magnetic coils for attitude control are printed within those boards; they also hold sun sensors and their aperture plates and electronics. Furthermore each PCB also holds solar cells for energy generation.

4 Attitude Determination

BeeSat will be equipped with a unique ADCS. Most of its parts were newly designed in order to provide future missions with the necessary hardware to fulfill more demanding tasks. During the TUPEX [7] experiment BeeSat's attitude sensors have all been successfully tested on a suborbital flight of the Rexus sounding rocket. Figure 1 shows TUPEX' main board and outboard plate containing sun sensor system and solar cell.



Fig. 1 TUPEX Experiment main board and outboard plate after recovery

4.1 Magnetic Field Sensor System

Two magneto-resistive magnetic field sensors, each measuring in three axes, will be used on BeeSat. An applied magnetic field changes resistivity within the sensor so that output voltage is proportional to the magnetic field. Once measured the magnetic field vector can be compared with the output of a reference model (IGRF10-13) calculated on-board the satellite in order to derive the satellites attitude.

4.2 Gyros

Gyros of appropriate size, weight and power consumption for pico satellites with a measurement range suitable for satellite operations are not available yet. Gyros used for BeeSat have a range of $\pm 150^\circ/\text{s}$ while the predicted angular rates do not exceed $5^\circ/\text{s}$. They will be used as additional reference and for tests at high rotation rates necessary for verification of the Microwheel system.

4.3 Sun Sensor System

The sun sensor system developed for BeeSat consists of six Position Sensitive Detectors (PSD) each covered with an aperture plate. One is placed on each side of the satellite in order to calculate the sun vector in body-fixed frame.

Incident sunlight passes through the aperture plate and shows up as a spot on the surface of the PSD. A photo current is generated and split up to each side of the sensor, the magnitude depending on the distance between spot of incident sunlight and each side contact. The currents are transformed to voltages, amplified and measured. Through combination of all sun sensor measurements the direction of incident sunlight with respect to the satellite is derived. The on-board navigation system (ONS) delivers a sun vector in inertial reference frame. Both vectors can be compared in order to obtain attitude information. Figure 2 shows a sectional view of the aperture plate with subjacent sensor and sunspot.

Fig. 2 Sun sensor and aperture plate

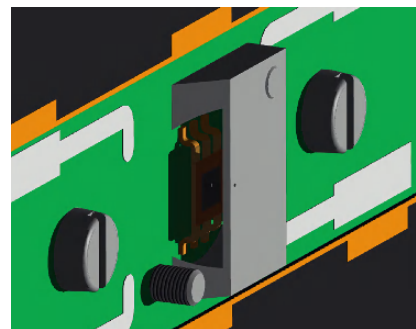
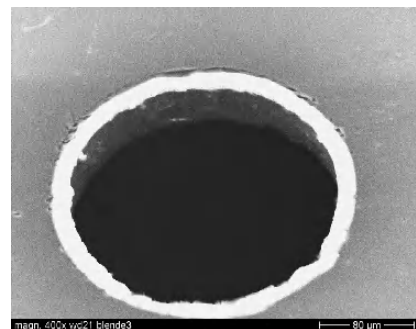


Fig. 3 Pinhole in aperture plate



During tests an accuracy of 1.5° has been reached after calibration. In order to reach better results a new aperture plate has been built. Other than the first version which had only a drilled hole here the aperture is angled at 120° and fabricated much more precisely. The outside of the aperture plate is polished while the inside is anodized in order to prevent scattered light. A scanning electron microscope image of the pinhole can bee seen in Fig. 3.

Table 1 Technical properties of attitude sensors

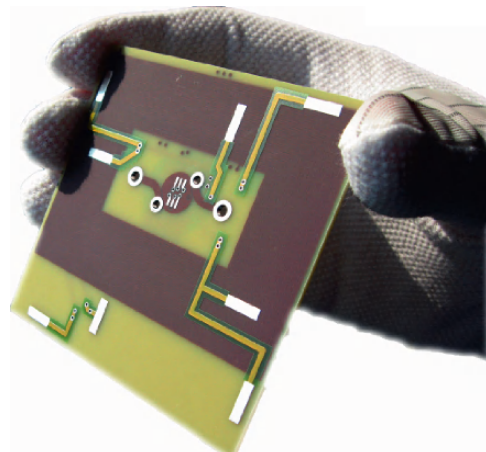
| | Magnetic field sensor | Gyro | Sun sensor |
|-------------------------------------|-----------------------|-----------------|-----------------|
| Manufacturer | Honeywell | Analog Devices | Hamamatsu |
| Outer dimensions [mm ³] | 7.4 × 7.4 × 2.8 | 7.0 × 7.0 × 3.0 | 7.0 × 4.8 × 1.8 |
| Power consumption [mW] | 30 | 30 | 1.5 |
| Range | ± 6 Gauss | ± 150°/s | 2 × 2mm |

5 Magnetic Coil System

The magnetic coil system which induces an external torque on the satellite bus due to the Lorentz force, consists of totally six coils. A pair of two coils is mounted in each axis to allow redundant operation. The main tasks of the coil system are coarse three-axis stabilization of the satellite body and the desaturation of accumulated angular momentum within the reaction wheels.

5.1 Hardware Design

The coil is embedded within a printed circuit board of seven layers, instead of winding the wire into a coil. One coil is able to generate a magnetic dipole moment of 0.03Am^2 , which corresponds to a maximum torque of approximately $1 \cdot 10^{-6}\text{Nm}$ at a power consumption level of 0.2 W. This innovative design approach seen in Fig. 4 makes the mounting devices conventionally needed to patch the wined coil on the bus frame, unnecessary. Furthermore this design is cost reducing for the coil can be manufactured at once with the other circuits. Also this design method prevents the coil from shortcuts because the windings are not insulated by epoxy enamel but are fixed in the circuit board with a defined distance and is therefore more robust. One drawback may some loss of the inducible dipole moment due to the spiral form of the circuit path, which has to be compensated by an increased number of windings.

**Fig. 4** Magnetic coil on PCB

5.2 Coil Control Algorithms

Bdot controller

The well known \dot{B} algorithm (1) has been implemented for detumbling and attitude stabilization as well as for desaturation of reaction wheels. The \dot{B} algorithm only requires knowledge of the current magnetic field and its derivative to dissipate the rotational energy stored in satellite bus or reaction wheels.

$${}^R m_{Coil} = -K \cdot {}^R \dot{B} - m_c \quad (1)$$

With ${}^R m_{Coil}$ being the generated dipole moment in body frame, K the scalar gain factor, ${}^R \dot{B}$ the time derivate of magnetic dipole in body frame and m_c the constant dipole offset for steady state orientation.

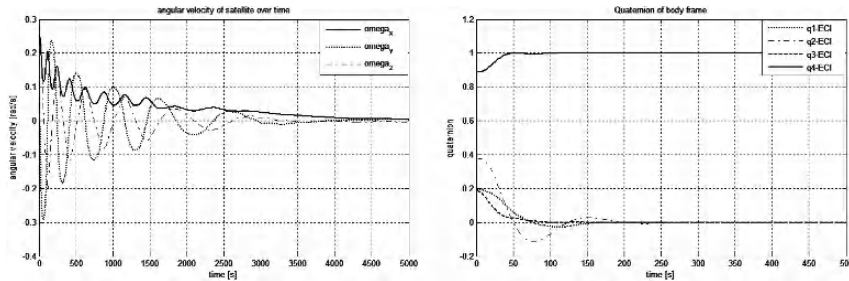


Fig. 5 Simulation results of Bdot controller (*left*) and PD controller (*right*)

PD Controller

Due to the fact that force cannot be generated alongside the earth's magnetic field vector the coil system is not able to perform full three-axis attitude control. A PD controller [8] has been implemented to overcome this limitation. Using one reaction wheel and at least two coils in the remaining axes three-axis attitude control can be performed even if one wheel loses functionality.

$$\begin{aligned} {}^R m_{Coil,X} &= \frac{1}{\kappa B_y} (K_z \cdot \psi_{error} + K_{zd} \cdot \dot{\psi}_{error}) \\ {}^R m_{Coil,Y} &= 0 \\ {}^R m_{Coil,Z} &= -\frac{1}{\kappa B_y} (K_x \cdot \phi_{error} + K_{xd} \cdot \dot{\phi}_{error}) \end{aligned} \quad (2)$$

$${}^R \tau_{Wheel,y} = -({}^R m_{Coil,Z} {}^R B_x - {}^R m_{Coil,X} {}^R B_z) + (K_y \cdot \theta_{error} + K_{yd} \cdot \dot{\theta}_{error}) \quad (3)$$

Here K_x , K_{xd} , K_z , K_{zd} are scalar gain factors, ${}^R B$ stands for the earth's magnetic field in body frame, ψ_{error} , $\dot{\psi}_{error}$, ϕ_{error} , $\dot{\phi}_{error}$ represent the current error angles and ${}^R \tau_{Wheel}$ is the torque generated by a reaction wheel.

6 Microwheel System

BeeSat's important task is the on-orbit verification of newly developed reaction wheels. In a partnership with Astro- und Feinwerktechnik Adlershof GmbH and funded by the DLR (FKZ 50JR0552), reaction wheels with brushless motors have been developed especially to the needs of pico satellite developers.

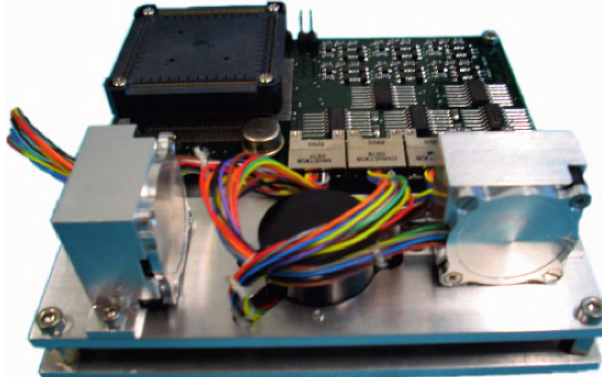


Fig. 6 Laboratory model of the Microwheel system

6.1 Technical Properties

Brushless motors and a special bearing system are used for the Microwheels.

With a total mass of 114.5 g , a torque of $4 \cdot 10^{-5}\text{ Nm}$ per wheel and a maximum power consumption of 1 W for the complete Microwheel system including the wheel drive electronics the qualification model of the reaction wheels exceeds the characteristics reached by the development model of Astro and TU Berlin. The small moment of inertia ($1.17 \cdot 10^{-5}\text{ kg} \cdot \text{m}^2$) is sufficient for pico satellites, it adds to overall accuracy while the high revolution speed of up to 16000 RPM still allows absorption of an angular momentum that equals BeeSat rotating at $7^\circ/\text{s}$. To allow easy adaptability for different missions or larger satellites the flywheel mass can be exchanged. A laboratory model of the Microwheel system including the wheel drive electronics can be seen in Fig. 6.

6.2 Microwheel Control Algorithms

The Microwheel system is controlled through a number of different linear single input/single output controllers for inertial pointing, earth pointing and large angle maneuvers. They consist of a state regulator and integrator as seen in equation (4). State variables are reconstructed through the state observer seen in Fig. 7.

$$\dot{\omega}_{MW} = -\underline{K} \cdot \hat{x}(t) + K_i \int e(t) dt \quad (4)$$

Controller output is the desired wheel acceleration and its integral the target wheel speed. Matrix K is the state space control and $\hat{x}(t)$ are reconstructed state variables. K_i is the integrator gain, $e(t)$ is the control error.

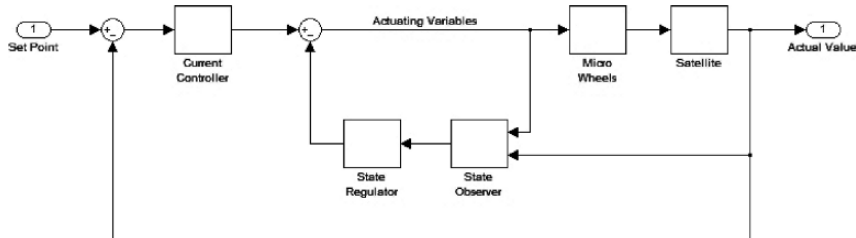


Fig. 7 Control loop

Figure 8 shows a simulated large angle maneuver over 60° in all three axes at the same time with a constant disturbance of $1.85 \cdot 10^{-7}$ Nm. Oscillation during ascent and overshooting can be attributed mainly to coupling effects.

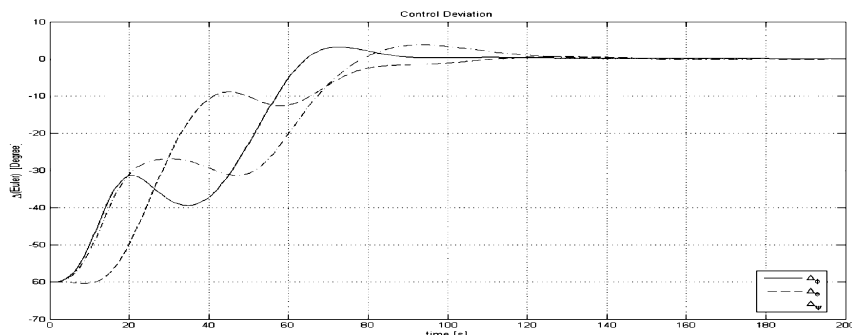


Fig. 8 Simulated large angle maneuver

7 Summary

Within the BeeSat project a number of components and strategies are evaluated in order to acquire pico satellite technologies. It's ADCS contains reaction wheels developed for pico satellites, a sun sensor system based on PSDs as well as a magnetic coil system on PCBs.

References

1. BeeSat project: <http://www.beesat.de>
2. Astro- und Feinwerktechnik GmbH: <http://www.astrofein.com>
3. TUBSAT micro satellites project: <http://www.ilr.tu-berlin.de/RFA>

4. Cubesat community: <http://cubesat.atl.calpoly.edu>
5. S. Montenegro, K. Brieß and H. Kayal, Dependable Software (BOSS) for the BEESAT pico satellite, *DAta Systems In Aerospace - DASIA 2006*, Berlin (2006)
6. H. Kayal and K. Brieß, Pico Satellite Concept of TU-Berlin, *Small Satellites for Earth Observation*, IAA-B5-1401, Berlin (2005)
7. S. Trowitzsch et al, *An Experimental Sounding Rocket Payload for Evaluation of Pico Satellite Technologies*, Space Technology Education Conference, Braunschweig (2006)
8. Z. Fan, S. Hua, M. Chundi, and L. Yuchang, An optimal attitude control of small satellite with momentum wheel and magnetic torqrods, *Proceedings of the 4th World Congress on Intelligent Control and Automation*, Shanghai (2002)

Initial SPHERES Operations Aboard the International Space Station

Alvar Saenz-Otero and David W. Miller

Abstract The Satellite Position Hold Engage Reorient Experimental Satellites (SPHERES) program, developed by the MIT Space Systems Laboratory, began operations aboard the International Space Station (ISS) on May 2006. SPHERES was designed as a research facility to demonstrate metrology, control, and autonomy algorithms for distributed satellites systems. By operating in the risk-tolerant environment of the ISS, SPHERES allows researchers to push the limits of their algorithms. Five test sessions, conducted during 2006, achieved multiple objectives for the different areas under study. The first test session was dedicated to hardware checkout. The second test session demonstrated basic 6DOF closed-loop control of the satellites. Fault detection and isolation algorithms were also tested, successfully using the inertial measurement system to detect simulated faults in space. Formation flight tests during the fourth and fifth session demonstrated two types of control architectures. Following the principle of incremental algorithm development, demonstrations of multiple scenarios of spacecraft docking occurred during test sessions one through four; the last session demonstrated docking to a tumbling spacecraft. The results of these test sessions are the basis upon which substantial more research will be conducted in the following years.

1 Introduction

The MIT Space Systems Laboratory developed the Synchronized Position Hold Engage and Reorient Experimental Satellites (SPHERES) program to incrementally mature algorithms for Distributed Satellite Systems (DSS) in a microgravity environment. SPHERES was specifically designed to help develop algorithms relevant to guidance, navigation, and control of the spacecraft of distributed satellite systems. By operating inside the ISS, SPHERES exploits the microgravity environment

A. Saenz-Otero
MIT Space Systems Laboratory, Cambridge, MA, 02139 USA
e-mail: alvarso@mit.edu

D.W. Miller
MIT Space Systems Laboratory, Cambridge, MA, 02139 USA

to represent the dynamics of complex missions while operating in a risk-tolerant environment. As such, SPHERES allows scientists to push the algorithms to their limits in various realistic mission scenarios, learning about both their theoretical and physical limitations.

1.1 Motivation

The motivation for SPHERES arises from the need to mature estimation, control, and autonomy algorithms for upcoming distributed satellite systems programs. Distributed satellite systems utilize multiple small satellites to achieve the same goals as a single larger satellite would. DSS trades control complexity with the expense and limitations of launch vehicles to send large single satellites to space. DSS includes proposals to use multiple spacecraft to implement reconfigurable space-based radar [1], autonomous docking of spacecraft for re-supply (e.g. Orbital Express [2]) and/or assembly (e.g. the Vision for Space Exploration inter-planetary stacks[3]), and the use of separated spacecraft telescopes (e.g. ESA's Darwin [4] and NASA's TPF [5]) to capture the light of distant planets.

The transition from theory to application has been shown to be a challenging process, but one that is necessary[6]. Traditional algorithm development methods which use simulations or ground-based facilities (see [7] for a complete review) do not provide either the fidelity or time necessary to mature an algorithm. While some of the upcoming missions are termed as “demonstration mission”, their cost prohibits scientists from actually *testing* algorithms on them. Therefore, a need exists to provide scientists with a development facility which closely simulates the operational environment without having the risks associated with the planned high-cost missions.

1.2 Design Principles

Based on substantial previous experience in the development of space technology maturation laboratories [8], the MIT Space Systems Laboratory created a design philosophy [4] which was followed in the design of the SPHERES program. The design of the project was based on the need to *support the incremental maturation of a wide range of algorithms that encompass a field of study in a risk-tolerant and representative environment*.

The principle of incremental algorithm maturation prescribes that algorithm development should consist of multiple steps that grow upon each other. This requires planning a set of tests which will demonstrate separate parts of an algorithm and then bring them together to demonstrate the whole. In the case of autonomous control for DSS, it calls for the demonstration of individual maneuvers during initial tests, followed by larger tests that combine the maneuvers for a high-level goal. The long-term life and reprogramming capabilities of the SPHERES facilities enable scientists to run individual tests as necessary and combine the resulting algorithms in subsequent test sessions.

The principle to encompass a field of study calls for a facility to support enough research so that all the areas necessary to demonstrate a complex task can be demonstrated. For example, fields of study such as formation flight or autonomous rendezvous require the study of areas such as estimation, controls, and autonomy. The availability of standard modules for these areas and reprogramming capabilities of SPHERES enables scientists to concentrate on their specific area within DSS.

The requirement to allow testing in a risk-tolerant environment exists in order to enable scientists to push the limits of their algorithms. A practical algorithm development facility does not restrict the user due to the potential of permanent damage/failure of the facility due to an algorithm. Rather, the facility allows scientists to push their algorithms to the limits in such a way that a failure of the algorithm can be clearly observed and evaluated. By operating under human supervision in the controlled environment of the ISS, SPHERES enables scientists an unprecedented level of risk-tolerance.

Lastly, the goal for operating in a representative environment arises from the desire to mature algorithms to ever-higher technology readiness levels (TRLs, [9]). In order to demonstrate that an algorithm has reached readiness, TRLs emphasize the need to operate in a “relevant environment” – for space applications this means operations in 6DOF. SPHERES enables operations in true micro-gravity, allowing the maturation of algorithms to TRL 6 or even 7.

2 Overview

The SPHERES laboratory for Distributed Satellite Systems [10] consists of a set of tools and hardware developed for use aboard the ISS and in ground based tests. Three micro-satellites, a custom “global metrology” system (based on ultrasound time-of-flight measurements which simulates GPS inside the testing volume), communications hardware (two RF channels), consumables (tanks and batteries), and an astronaut interface are aboard the ISS. Figure 1 shows the SPHERES satellites

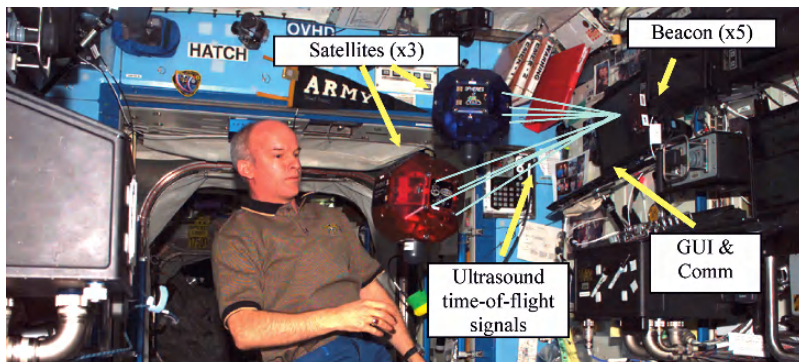


Fig. 1 SPHERES hardware components operating aboard the ISS (Picture courtesy of NASA)

being operated aboard the ISS and identifies the different elements of the facility. The ground-based setup consist of another set of micro-satellites, a research oriented GUI, and the guest scientist program to allow multiple researchers to use the facility.

The SPHERES satellites were designed to provide the best traceability to proposed formation flight missions by implementing all the features of a standard thruster-based satellite bus. The satellites have fully functional propulsion, guidance, communications, and power sub-systems. These enable the satellites to maneuver in 6-DOF, to communicate with each other and with the laptop control station, and to identify their position with respect to each other and to the experiment reference frame. The laptop control station is used to collect and store data as well as to upload control algorithms to the satellites.

3 ISS Test Sessions

Five test sessions were conducted aboard the ISS during 2006: May 18, May 20, August 12, August 19, and November 11. Table 1 presents the primary objectives for the first five test sessions. The following sections describe each test session in further detail to illustrate the ability of SPHERES to both meet its design principles and help advance our understanding of algorithms required for successful future DSS programs.

Table 1 Test sessions 1–5 objectives

| Session | Objectives |
|---------|---|
| 1 | <ul style="list-style-type: none"> • Hardware checkout • Open-loop control, 3DOF closed-loop rotations, and basic maneuvers towards docking |
| 2 | <ul style="list-style-type: none"> • Firmware fix (from session 1) • DOF closed loop rotations; fault detection and isolation (FDI) of simulated thruster failures; position hold, and autonomous docking translation maneuvers |
| 3 | <ul style="list-style-type: none"> • Autonomous docking to a fixed beacon • On-line calculation of the mass and inertia of the satellite (Mass-ID) • Two satellite initial tests: formation flight (3DOF slave/master) and docking |
| 4 | <ul style="list-style-type: none"> • Global metrology system checkout • Show “avoidance” trajectories • Two satellite formation flight: 6DOF slave/master • Initial tests of two satellites docking |
| 5 | <ul style="list-style-type: none"> • Continue tests for Mass-ID • Cooperative and uncooperative docking and “safe docking” • Peer-to-peer formation flight maneuver |

3.1 First Test Session

The SPHERES First ISS Test Session took place on 18-May-2006. The hardware checkout objectives were successful as all the SPHERES hardware (satellite, beacon, beacon tester, laptop transmitter and consumables) was located, installed and operated. Data was collected during open-loop tests to evaluate the performance differences between two different mixer algorithms that convert force and torque outputs by control algorithms into thruster on/off time commands. Enough data was collected to validate the operation of the global metrology system. The primary obstacle during the first test session was a corrupted FLASH memory space on the satellite which stored the IMU bias and scale factors. The corrupted FLASH prevented closed-loop tests from performing correctly. Despite this issue, the successful operation of the hardware and interfaces, as well as the collection of a substantial amount of data resulted in an overall successful test session. Table 2 presents a chronological list of all the tests performed during the first Test Session. The table shows the inability to complete closed loop tests during this test session. It also shows how the SPHERES team planned the incremental collection of data to validate the system in such a way that future test sessions will benefit from the tests on this session. Further, the ability to recover from these issues demonstrates the risk-tolerant nature of SPHERES.

Table 2 First test session tests

| Test | Description | Result |
|----------|---------------------------------------|--------------------------------|
| T 1 (2×) | Quick checkout with IMU data download | Success |
| T 2 | Open-loop rotations, old mixer | Success (low gas pressure) |
| T 3 | Open-loop rotations, new mixer | Success (low gas pressure) |
| T 4 | Beacon track attitude PD | Metrology data collection only |
| T 6 (4×) | Closed-loop XYZ rotation | FLASH corruption error |
| T 8 (2×) | Dock Free Short S#1 PD | Metrology data collection only |
| T 2 | Open-loop rotations, old mixer | Success (full gas pressure) |
| T 3 | Open-loop rotations, new mixer | Stopped inadvertently by crew |
| T 3 | Open-loop rotations, new mixer | Success (full gas pressure) |
| T 8.3 | Dock Range only S#1 | FLASH corruption error |

3.2 Second Test Session

The SPHERES Second ISS Test Session took place on Saturday 20-May-2006. The session successfully accomplished a majority of its objectives. The FLASH memory corruption exhibited during the first test session was fixed. Furthermore, several tests involving closed-loop control using the gyroscopes and the ultrasonic navigation system were successful. The data show the ability of the SPHERES satellite to perform closed-loop 3D rotations, to estimate its 6DOF position with respect to a SPHERES beacon, and to detect faults online using fault detection and isolation (FDI)

algorithms. The tests which had estimator divergence during this session provided enough data to overcome the issue in future sessions. This test session demonstrated the risk-tolerance of SPHERES by simulating thruster failures without any doubt on the ability of the satellites to continue operations after such failures. Further, it showed the ability to run tests in multiple research areas by showing both control (closed loop 6DOF), estimation (using a single beacon) and autonomous FDI.

Table 3 Second test session tests

| Program | Test | Description | Results |
|-------------------------|--------------|------------------------------|--|
| P101 (NASA Ames) | T 1.1 (6×) | Flash Memory Test | Communications initialization problem |
| | T 6 (4×) | Closed-loop XYZ rotation | Communications initialization problem |
| | T 1.1 | Flash Memory Test | FLASH fixed |
| | T 6 | Closed-loop XYZ rotation | Success |
| | T 14 (2×) | De-Tumble, Track, and Dock | Estimator diverged |
| | T 16b | Dock Fixed Long S#2 PD | Partial success (wrong initial conditions) |
| P112 | T 1 | Failed-on thruster FDI | Lost communications |
| | T 1 | Failed-on thruster FDI | Success |
| | T 2 | Failed-off thruster FDI | Success |
| | T 3 (2×) | Multiple thruster FDI | Lost communications |
| | T 3 | Multiple thruster FDI | Success |
| | T 4 | Closed-loop attitude control | Success |
| | T 5 | FDI with attitude control | Success |
| P113 | T 1 | Quick checkout | Lost communications |
| | T 2 | Basic Position Hold | Lost communications |
| | T 2 | Basic Position Hold | Success |
| | T 15 | Attitude path following | Success |
| | T 3 | Stationkeeping 3D – 1 | Success |
| | T 8/8.1 (3×) | De-tumble, Track, & Dock | Reset due to low battery (good start) |

3.3 Third Test Session

The SPHERES Third ISS Test Session, on Saturday 12-Aug-2006, demonstrated multiple steps towards autonomous docking, collected initial formation flight data, and taught the SPHERES team about important environmental noise factor. As shown in Table 4, tests were not repeated as often as before. On the other hand, many tests were affected by infrared noise; this issue was corrected for future sessions. The first set of tests demonstrated individual maneuvers towards autonomous docking and path-based trajectory following. The second set began the use of two satellites for formation flight and docking. Throughout these tests, state information was successfully transmitted between satellites.

Table 4 Third test session tests

| Program | Test | Description | Results |
|---------|------|-----------------------------------|-------------------------------------|
| P124 | T1 | Quick Checkout | IR Noise |
| MIT | T2 | 3D Position Hold with Disturbance | IR Noise |
| Docking | T2 | 3D Position Hold with Disturbance | Good estimation, but IR Noise |
| | T3 | Docking PD (1.5 m) | Success |
| | T4 | De-tumble, Track, & Dock Set 1 | Success |
| | T5 | Trajectory 3 (Safety w/rotation) | Good control |
| | T6 | 3D Position Hold (Robust) | Started well, estimator diverged |
| P126 | T1 | ID all axes | Stuck thrusters |
| Mass ID | T2 | ID all axes, proof mass | No “proof mass” attached |
| | T2 | ID all axes, proof mass | Stuck thrusters |
| | T3 | Single-thruster, proof mass | IR Noise |
| | T4 | Single-thruster firings | IR Noise & stuck thrusters |
| | T4 | Single-thruster firings | Partial success |
| | T5 | Fuel slosh | Partial success |
| | T5 | Fuel slosh | Partial success |
| | T6 | Roll-Pitch-axis spin | Success |
| | T7 | Pitch-Yaw-axis spin | Stuck thruster |
| | T8 | Yaw-Roll-axis spin | Partial success |
| P125 | T1 | Quick Checkout | IR Noise |
| MIT | T2 | Twin Rotations: Independent | SN2: success / SN3: low battery |
| 2 Sat | T2 | Twin Rotations: Independent | Success |
| Initial | T3 | Twin Rotations: Formation | Success |
| Tests | T4 | Twin Position Hold: Formation | Estimator diverged (IR Noise) |
| | T5 | Two Satellite Docking – Set 1 | Drifting “target” prevented docking |

Of special interest in this session were the results of multi-satellite operations. Figure 2 shows the attitude of independent rotations (left side) and formation flight rotations (right side, “leader” on top). During independent rotations the satellites did not react to disturbances (in this case IR noise) on the other satellite. During formation flight reaction to external disturbances by the crew (green spike) can be seen at the end of the formation flight tests.

3.4 Fourth Test Session

The fourth Test Session, on 19-Aug-2006, was dedicated primarily to testing the global metrology system. Table 5 shows the two main groups of tests conducted during this session. The tests in the first group collected all the data necessary to develop the robust estimators later used in the fifth and subsequent test sessions; although a configuration problem prevented online estimation from succeeding. The second set of tests (once the configuration problem was corrected) was highly successful, and provided important demonstrations. Algorithms for both formation

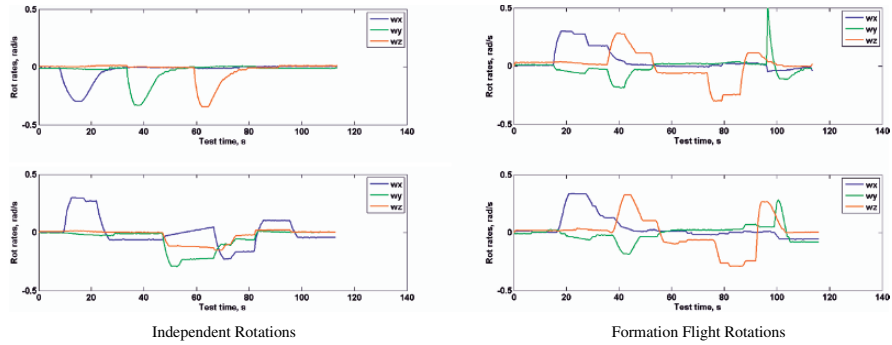


Fig. 2 Formation flight test results during test session 3

Table 5 Fourth test session tests

| Program | Test | Description | Results |
|-----------|--------------|---|--|
| P131 | T1 | Quick Checkout | IR Noise |
| MIT 4a: | T2-7 (8 tot) | Global Sys ID | Valid data collected, invalid beacons loc. |
| Global | T8 (2×) | 3D Position Hold with Disturbance | Valid data collected, invalid beacons loc. |
| Sys-ID | T9 (4×) | Trajectory: 3D Avoidance | Valid data collected, invalid beacons loc. |
| | T10 | Trajectory: Avoidance w/Rotation | Incomplete (stopped by crew) |
| P132 | T1 | Quick Checkout | Success |
| MIT 4b: | T2 | Ultrasound Shadow: 1.5 m | Success |
| Global | T3 | Ultrasound Shadow: 0.5 m | Success |
| Metrology | T4 | Ultrasound Shadow: 0.2 m | Success |
| | T5 | Gyroscope Calibration | Success |
| MultiSat | T6 | 2 Sat. Position Hold – Independent | Success |
| | T7 | 2 Sat. Leader, Follower | Success |
| | T8 | 2 Sat. Docking: Target Hold | Estimator diverged after contact |
| | T8 | 2 Sat. Docking: Target Hold | Success |
| | T9 | 3D Formation | Success |
| | T10 | 2 Sat. De-tumble, track, & dock | Success |
| | T11 | 2 Sat. Docking: Plume Impingement Check | Success |

flight and docking tests were validated during this session, so as to be used with high confidence in future sessions.

3.5 Fifth Test Session

The fifth Test Session was accentuated by the successful demonstration of autonomous docking to a tumbling target. Figure 3 presents the trajectory followed

by the chaser (blue) satellite while the target (red) satellite maintained a constant rotation and actively held its position with respect to the global frame (ISS frame). One can see a spiral forming in the path of the blue satellite. This success is the result of the incremental development and maturation of algorithms throughout the previous sessions. While only a few tests were run during this session (shown in Table 6), each of the tests is of high complexity. The tests demonstrated complete docking algorithms and full formation flight operations. These tests clearly demonstrate the ability to incrementally mature algorithms and to cover a field of study by developing multiple areas (specifically controls, estimation, autonomy, and new to this session communications). Further, the risk tolerant nature of SPHERES enabled the team to test these complex algorithms after just four prior test sessions in microgravity (less than 12 hours/seven months of microgravity experience).

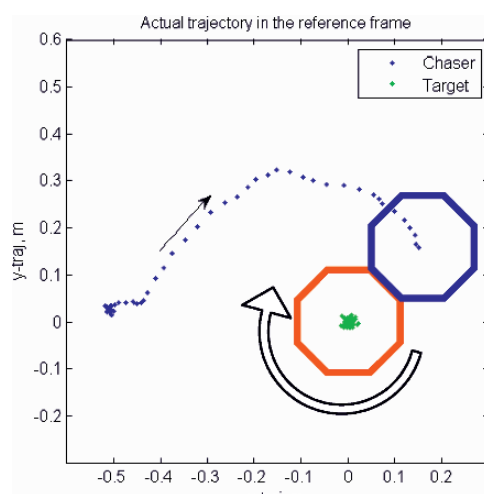


Fig. 3 Results of docking to a tumbling target

Table 6 Fifth test session tests in chronological order

| Program | Test | Description | Results |
|-----------|---------------|----------------------------|---|
| P142 | T1-12 | Multiple tests for Mass ID | Partial – stuck thrusters were not fully identified from previous session |
| Mass ID 2 | (15 runs tot) | | |
| P141 | T1 (3×) | Quick Checkout | Incorrect battery installation |
| MIT 5: | T1 | Quick Checkout | Success |
| Docking | T2 | Docking to Fixed Target | Success |
| Multi-Sat | T6 | Docking to Tumbling Target | Success |
| | T6 | Docking to Tumbling Target | Success |
| | T5 | Safe Docking w/fault | Success |
| | T4 | Safe Docking | Success |
| | T12 | Circular Formation Flight | Success |

4 Conclusions

SPHERES has demonstrated its ability to create a laboratory environment aboard the space station for the incremental maturation of DSS algorithms. The first four sessions helped the SPHERES team achieve steady-state operations, having fully understood the microgravity capabilities and behavior of the facilities and the ISS. Using the data collected from each test session, the SPHERES team incrementally matured formation flight and docking algorithms resulting in multiple “space firsts”. SPHERES was the first free-flyer to operate aboard the ISS. On the second test session it was the first space program to intentionally simulate failures of thrusters in space in order to test fault detection algorithms. During the fifth session SPHERES was the first to demonstrate docking to a tumbling target in a microgravity environment. The circular formation flight was another first (demonstrate covering an optical field in a micro-gravity environment with separated spacecraft), although there were synchronization problems that prevented the test from being fully successful, so it requires further research. SPHERES is expected to operate aboard the station for multiple years to complete these tasks and more.

References

1. A. Das, R. Cobb, M. Stallard, “Techsat 21 – A revolutionary concept in distributed space based sensing”, *AIAA Defense and Civil Space Programs Conference and Exhibit*, Huntsville, AL (1998)
2. J. Shoemaker, and M. Wright, “Orbital express space operations architecture program,” *Spacecraft Platforms and Infrastructure*, Vol. 5419 SPIE, 57–65 (2004)
3. W. Hofstetter, O. de Weck, E. Crawley, “Modular Building Blocks for Manned Spacecraft: A Case Study for Moon and Mars Landing Systems”, *INCOSE 2005 – Systems Engineering Symposium*, Rochester , NY (2005)
4. C. V. M. Fridlund, “Darwin – The Infrared Space Interferometry Mission”, *ESA Bulletin 103*, Noordwijk, The Netherlands (2000)
5. C. A. Beichman, N. J. Woolf, C.A. Lindensmith, C. A., “The Terrestrial Planet Finder (TPF) : a NASA Origins Program to search for habitable planets”, *TPF Science Working Group*; National Aeronautics and Space Administration ; Pasadena, Calif.: Jet Propulsion Laboratory, California Institute of Technology, JPL publication; 99–3 (1999)
6. D. W. Miller, G. J. W. Mallory, “Control Testbeds and Flight Demonstrations: Transitioning Theory to Application”, *American Control Conference (Vol. 2)*, Philadelphia, PA (1998)
7. Saenz-Otero, A, “Design Principles for the Development of Space Technology Maturation Laboratories Aboard the International Space Station”, Massachusetts Institute of Technology, Department of Aeronautics and Astronautics, Ph.D. Thesis, Cambridge, MA (2005)
8. D. W. Miller, J. de Luis, “Using the Shuttle, MIR and ISS for Operating Micro-Gravity Engineering Research Laboratories”, *AIAA-2001-4648*, Albuquerque, NM (2001)
9. J. Mankins, “Technology Readiness Levels”, Advanced Concepts Office, Office of Space Access and Technology, NASA, April 1995
10. A. Saenz-Otero, A. Chen, et al, “SPHERES: Development of an ISS Laboratory for Formation Flight and Docking Research”, *2002 IEEE Aerospace Conference, #081*, (2002)

BIRD Microsatellite Thermal Control System – 5 Years of Operation in Space

F. Lura, B. Biering, H.G. Lötzke, H. Studemund, and V. Baturkin

Abstract Microsatellite BIRD (*Bispectral InfraRed Detection*) with mass 92 kg and overall sizes $0.55 \times 0.61 \times 0.62$ m operates in a sun-synchronous orbit more than 5 years. The temperature range $-10 \dots +30^\circ\text{C}$ for payload with average power about 35 W and peak power of 200 W in observation mode, continuing 10–20 min, is provided by passive thermal control system (TCS). Operation of TCS foresees a thermal stability of payload structure by use of heat transfer elements – conductors and grooved heat pipes, thermally jointing the satellites segments. Two radiators, multilayer insulation (MLI) and low-conductive stand-offs provide the required temperature level. Review of TCS performance is based on an analysis of daily telemetric data, collected by 33 temperature sensors and power consumption. The analysis includes the definition of minimal, maximal and averaged temperatures of satellite main units and comparison with designed parameters. TCS successfully supports the required temperature level of satellite components during the whole period of exploitation.

1 Introduction

The main features of BIRD (*Bispectral InfraRed Detection*), having launched on 22nd October 2001 by PSLV-C3 Indian rocket and operating till now (nominal operation time is 1 year) in the sun-synchronous 568 km orbit, are presented in [1],

F. Lura

German Aerospace Center, Berlin, Rutherfordstr. 2, D-12484, Berlin, Germany
e-mail: Franz.Lura@dlr.de

B. Biering

German Aerospace Center, Berlin, Rutherfordstr. 2, D-12484, Berlin, Germany

H.G. Lötzke

German Aerospace Center, Berlin, Rutherfordstr. 2, D-12484, Berlin, Germany

H. Studemund

German Aerospace Center, Berlin, Rutherfordstr. 2, D-12484, Berlin, Germany

V. Baturkin

National Technical University of Ukraine “Kyiv Polytechnic Institute”, Kyiv, Ukraine
Pr. Peremogy, 37, 03056, Kyiv, Ukraine

and the description of thermocontrol system and some summaries – in [2, 3]. This satellite is intended to demonstrate in space new compact infrared imaging sensor technologies and the approach to modular design of a microsatellite. The BIRD microsatellite is a cubic shaped, 3-axis stabilized microsatellite without a propulsion system. The mechanical structure (satellite bus) is designed as a three-boxes cubic main body, and consists of the service segment, the electronic segment and the payload platform (Fig. 1). The main body is covered with MLI except the instruments windows and 2 radiators. One fixed and two deployable solar panels as well as the reject mechanism are mounted to the body.

The payload is mounted to the special payload platform, which makes about 1/2 of the body volume and 1/3 of the total mass of the spacecraft. To keep the line of sights of the instruments very stable, the payload platform is connected deformation free with the lower satellite segments. The heat transfer from (or to) the payload platform to (from) the main radiator on the bottom side of the service segment in +Y – direction is realized by two heat pipes [4]. The heat removal from the IR instrumentation is realized to the separate IR – radiator, positioned in –Y direction. BIRD TCS is designed as a passive, when a heat rejected by radiators, through MLI and devices windows is compensated by inner heat generation. The temperature limits of major satellite units are typical for space components [3]. The solar panels generate about 40 W each and 8 NiH₂-cells can accumulate 240 W*h to supply up to 200 W in peak power during 20 min observation.

2 BIRD Thermal Regime in Flight

The temperature measurements are performed by 33 temperature sensors of the type AD590 (by Analog Devices, USA). The sensors have been spread over the satellite structure, payload instruments, housekeeping equipments and solar panels (see Fig. 1).

The temperature telemetry covers the most of satellite operation time (about 98%). Figure 2 illustrates the volume of a daily collected thermal telemetry (in DOS format) during 2001–2006 years, where daily averaged telemetry is 4.2 Mb. The typical period of temperature data gathering is 30 sec with the storage period of 24 hours (near 15 orbits). During the day the temperatures of satellite units have the evident periodic character similar to the radiator (see Fig. 3) that deals with non-uniform external condition for the main radiator along the orbit and tight thermal contact between radiator and other units, which are thermally connected by two heat pipes.

The on-orbit temperature variation for radiator is about 1–3.5°C, for payload platform less than 1°C. Sometimes the radiator has the rise of the temperature due to satellite manoeuvres as shown in Fig. 3 after 12:00. Solar panels, which have essentially less thermal mass, are directly illuminated by sun flux, and therefore they have the widest range of temperature excursions. The central panel, which is cooled from one side, has the maximal temperature 75...90°C and minimal –20...–40°C in shadow (Fig. 3). The side panels –X and +X (two sides radiate) have

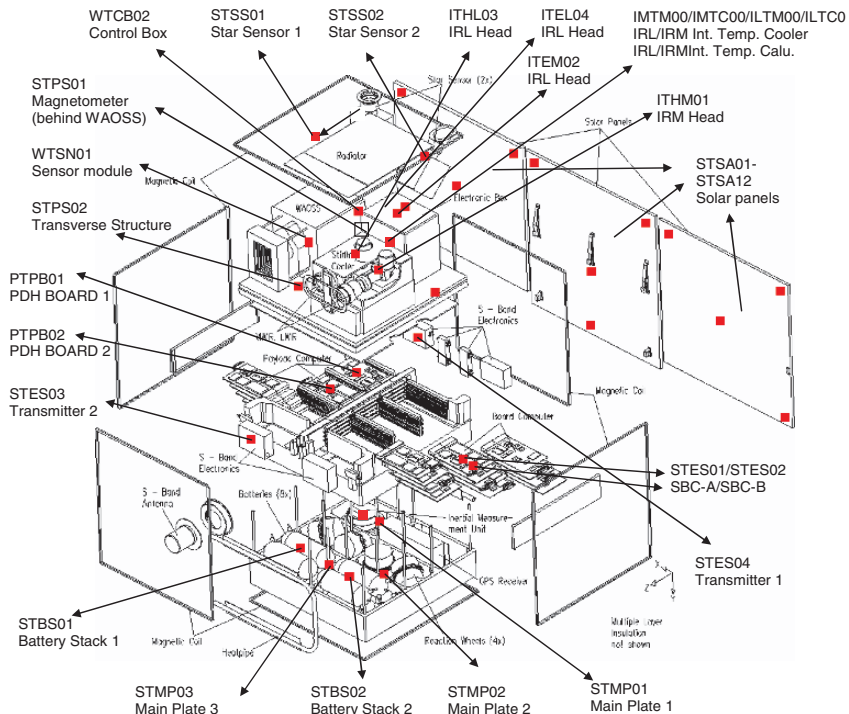


Fig. 1 Scheme of temperature sensors layout on satellite BIRD

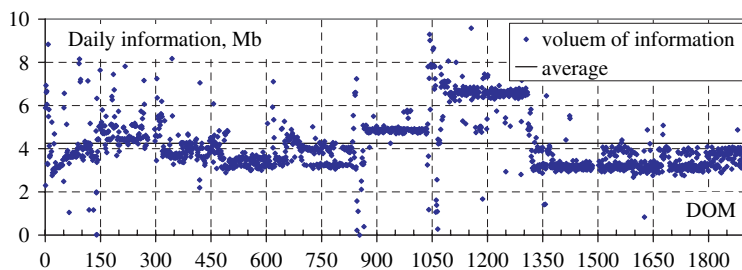


Fig. 2 Variation of daily downloaded thermal information

the maximum temperature $65 \dots 70^\circ\text{C}$ and minimum -70°C and less. The period between maximums is about 96 min.

There is a certain interest to review the satellite temperature during the whole period of its exploitation, as every daily telemetry reflects events partly. Simple summarizing of each daily information will produce extremely large file, which is inconvenient in processing by commonly used software such as EXCEL. In order to reduce the volume of summarized file, having saved the most important features of thermal performance during each day, presenting by the values of temperature and

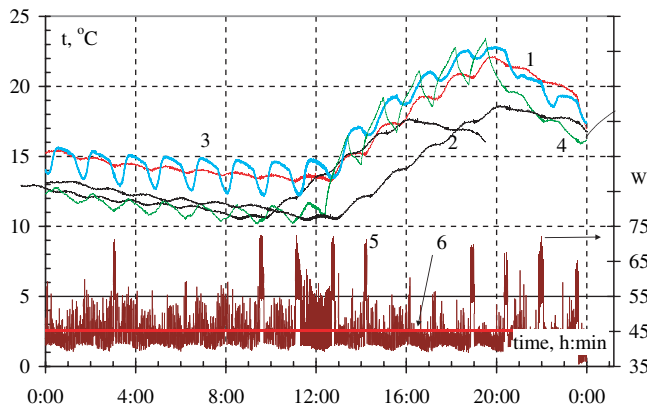


Fig. 3 Daily temperature (03.07.2003) for star sensors (1), payload platform (2), battery stacks (3), radiator (4) and consumed power (5 – instant, 6 – averaged)

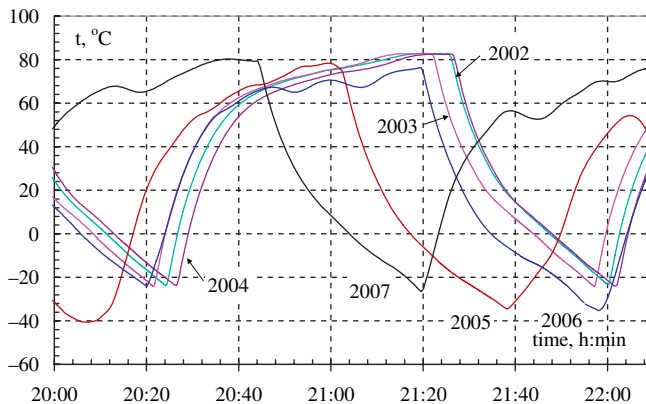


Fig. 4 Averaged temperature (for 4 sensors) of central panel for 01.01.2002–2007

power: maximal $T_{\max} = \max(T_{\tau 1} : T_{\tau 2})$, minimal $T_{\min} = \min(T_{\tau 1} : T_{\tau 2})$ and mean integral for the certain period, the algorithm of reading and processing of initial daily telemetry has been proposed. Figures 5–10 present the overview of most important temperatures for period till day of mission (DOM) 1897. Averaged daily power lays within the range of 40–50 W during DOM 1 ... 846, reducing to 20 W for the period DOM 846 ... 1037 and 30–35 W for 1040 ... 1897. The radiator temperature is always within the planned limits $-10 \dots +25^\circ\text{C}$, except DOM 1000 ... 1037. The rise of the temperature within DOM 846 ... 1037 deals with the loss of sun-pointed orientation due to the failures of 2 reaction wheels. After a new attitude control scheme was introduced (DOM 1037), the orientation on the Sun was recovered.

Satisfied main radiator temperature provides the temperature limits for other units, as it is the reference one for most of them. Variation of the radiator temperature is caused by changing of daily power consumption (variation in 1 W causes the

temperature changing in 1°C) and by orientation with respect to the Sun and Earth during maneuvers. The level of electronics maximal temperature (Fig. 8, 9) is less than 40°C at power generation of 5–10 W per units. Solar arrays maximal temperature has evident oscillation of function with the period in 365 days that deals with variation of solar intensity during the year.

Comparison of thermal requirements with the results obtained on the base of telemetry has shown that minimal and maximal temperatures, which were met during the BIRD flight performance lay within the design temperature limits. The table 1 shows the correspondence of obtained maximal and minimal temperatures with design limits. An analysis of flight temperature data during five years of BIRD microsatellite exploitation (10. 2001–12. 2006 years) confirms the correctness of

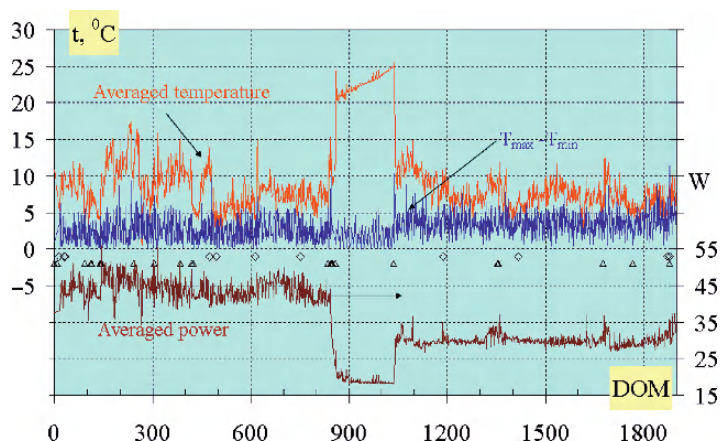


Fig. 5 Radiator averaged temperature its maximal temperature change during each day within 2001–2007 1 – solar storms, 2 – technical events on satellite

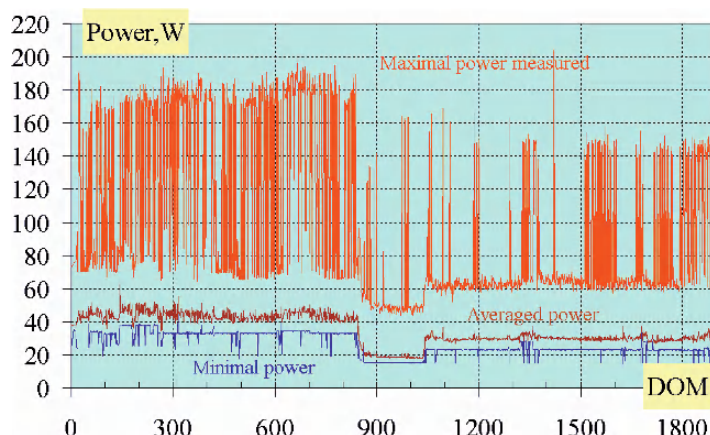


Fig. 6 Averaged per day, minimal and maximal consumed electrical power during 2001–2007

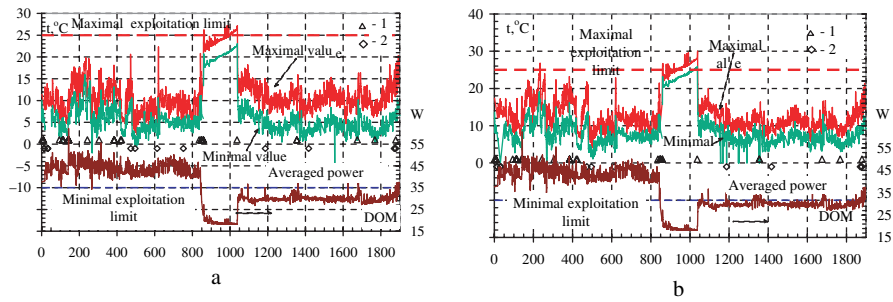


Fig. 7 Telemetry statistics – radiator and battery stacks temperature extremes within 2001–2006. Starting point – 22. 10. 2001, proceeded data – till 31.12.2006: **a** radiator; **b** battery stacks; 1 – solar storms, 2 – technical events on satellite

Fig. 8 Telemetry statistics – board processors 1 and 2, temperature extremes within 2001–2006: 1 – solar storms, 2 – technical events on satellite

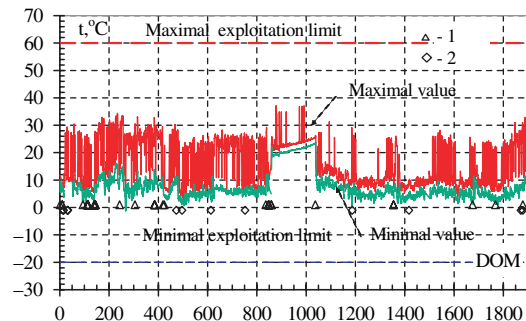
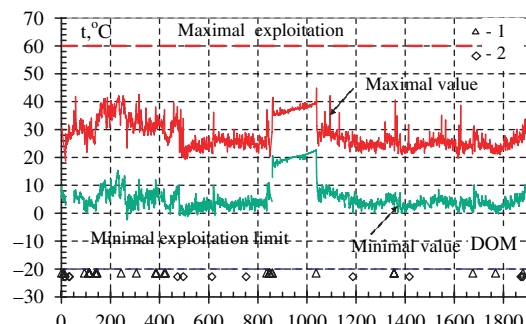


Fig. 9 Telemetry statistics – transmitters 1 and 2; temperature extremes within 2001–2006: 1 – solar storms, 2 – technical events on satellite



accepted thermal control conception for this microsatellite mission with multifunctional payloads and reliability of used components of thermal control system. Collected database will be applied for thermal performance forecasting of the similar equipment for future missions realized by microsatellites.

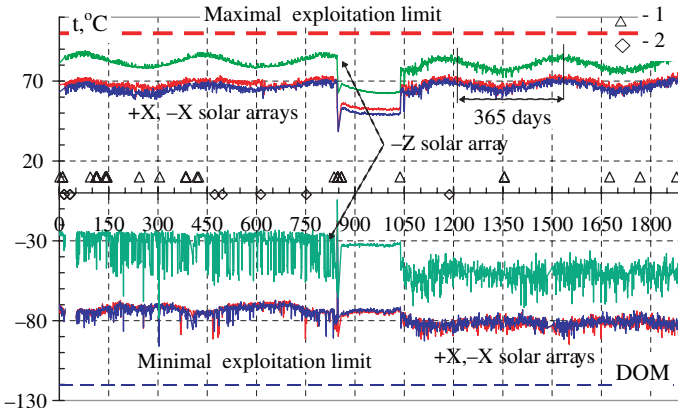


Fig. 10 Telemetry statistics – solar arrays, $-Z$, $+X$, $-X$, temperature extremes within 2001–2006: 1 – solar storms; 2 – technical events on satellite

Table 1 Comparison of designed temperature limits for operation of satellite units and obtained temperature variation during the BIRD microsatellite flight in 2001–2006

| Description of unit | Q Low N op | HL | HH | Q. high N op | HL/HH obtained DOM 1-845 | HL/HH obtained DOM 1-1897 |
|--------------------------------------|---------------|------|-----|-----------------|-----------------------------------|------------------------------------|
| IR Head, Channels M, L | -35 | -15 | 15 | 50 | -8,4/8,9 | -8,4/8,9 |
| Battery Stacks 1, 2 | -15 | -10 | 25 | 35 | 0,0/26,8 | 0,0/30,0 |
| Control Sensor Module | -50 | -15 | 30 | 60 | -10,0/26,1 | -10,0/26,1 |
| Control Connector Box | -50 | -15 | 30 | 60 | -10,0/26,1 | -10,0/26,1 |
| Main radiator | -30 | -15 | 35 | 60 | 0,0/22,8 | 0,0/27,2 |
| Payload Platform | -30 | -20 | 30 | 60 | -2,7/18,8 | -2,7/23,7 |
| Star Sensors 1 and 2 | -30 | -25 | 30 | 60 | -4,2/28,0 | -4,2/28,0 |
| Processors boards SBC_A and SBC_B | -30 | -15 | 40 | 60 | 10,0/34,0 | 10,0/38,5 |
| Processor Boards 1 and 2 | -30 | -20 | 60 | 60 | 1,0/33,8 | 0,0/37,1 |
| S-B-Transmitters 1 and 2 | -30 | -20 | 60 | 60 | -1,5/42,6 | -1,5/44,8 |
| Electronic Unit, IR Channel M, L | -50 | -40 | 45 | 50 | -1,4/40,2 | -1,4/44,3 |
| Solar Panel $+X$ | -180 | -120 | 100 | 130 | -91,6/73,4 | -94,7/75,1 |
| Solar Panel $-X$ | -180 | -120 | 100 | 130 | -96,0/70,9 | -96,0/72,3 |
| Solar Panel $-Z$ | -180 | -120 | 100 | 130 | -69,5/88,7 | -71,8/88,7 |

Remark: HL and HH – low and high design temperature limits, Q Low N op and Q High N op – qualification non-operational temperature limits

3 Conclusions

1. BIRD thermal conception, foreseeing the combination of active thermal control and deep cooling of IR sensors with the passive thermal control for all

other devices and housekeeping components, has proved itself during on-orbit exploitation from October 2001 – till now

2. Thermal unification of geometrically stable and thermal conductive payload plate and main radiator by heat pipes allows to minimize the influence of a displacement of satellite shell and reduce the on-orbit temperature variations due to increase of the thermal mass. This principle may be useful for design of satellites equipped with precision optical devices
3. The NiH₂ batteries have not individual cooling system and have been thermally attached to the main radiator. This approach has greatly simplified the design of thermal control and makes it cheaper
4. The passive thermal concept is sensitive to values of heat generation, MLI performance and external heat fluxes. The shifting of temperature level in the case of necessity can be realized by changing of on-board power, positioning of radiator with respect to the Earth and Sun.

Contacts

Authors are interested in exchanging of information in the field of small satellite thermal design/ modeling/ on-ground verification. The person for contact: Dr. Franz Lura, affiliation is presented at the beginning of the paper, <http://www.dlr.de/Berlin>

References

1. K. Brieß, W. Bärwald et al. The BIRD mission is completed for launch with the PSLV-C3 in 2001. *Digest of the 3rd IAA International Symposium “Small Satellites for Earth Observation”*. Berlin, April 2–6, 2001/Berlin: Wissenschaft und Technic Verl. ISBN 3-89685-566-2, pp. 323–326 (2001)
2. B. Biering, F. Lura, H. G. Lötzke et al. TCS design of the microsatellite BIRD for infrared earth observation. *28th International Conference on Environmental Systems*, Danvers, Massachusetts, USA, report No. 981639 (1998)
3. F. Lura, B. Biering, H.-G. Lötzke, H. Studemund, V. Baturkin. Thermal performance of BIRD microsatellite thermal control system – 3 years of operation in space. *35th International Conference on Environmental Systems and 8th ESSECS*, Rome, Italy, report No. 2005-01-2986 (2005)
4. V. Baturkin, D. Olefirenko. Research of axially grooved heat pipe heat transfer characteristics in ground tests. *31st International Conference on Environmental Systems*, Orlando, Florida, USA, report No. 2001-01-2237 (2001)

The “Mailbox Ground Station” – A Procedure to Improve the Operational Key Requirements of Earth Observation Systems

Bernd Brand and Tino Zehetbauer

Abstract The performance of small satellite constellations used for security relevant Earth observation like crisis/catastrophe monitoring and reconnaissance are mainly characterized by the operational key requirements called system response time and image information age. Both parameters are driven by the satellite orbit, the number of satellites within the constellation and the number and location of the ground stations. Regular larger time gaps between imaging and data download to the ground station occur for such satellite systems and are unacceptable for both parameters in terms of security relevant Earth observation. This behaviour can be improved by increasing number of satellites or the usage of data relay satellites, however both solutions are expansive ones. Therefore a patent pending procedure was developed as a low cost possibility to improve the operational performance. The procedure is called “Mailbox Ground Station”.

The procedure uses a dedicated additional ground station, optimized located to the satellite constellation. Normally the polar region will be preferred for constellations with polar orbits. The Mailbox ground station will be used as an intermediate data download, storage and upload facility. The presentation will demonstrate and explain easily the Mailbox ground station system using a fictional satellite constellation used for Earth observation purposes.

1 Operational Key Requirements

In the use of satellites for earth observation, users frequently wish to have the fastest possible access to image data residing in a satellite. Especially for security relevant Earth observation like crisis/catastrophe monitoring and reconnaissance the length

B. Brand

German Aerospace Centre (DLR), Microwave and Radar Institute, Department Reconnaissance and Security, Oberpfaffenhofen, D-82234 Wessling, Germany
e-mail: Bernd.Brand@dlr.de

T. Zehetbauer

German Aerospace Centre (DLR), Microwave and Radar Institute, Department Reconnaissance and Security, Oberpfaffenhofen, D-82234 Wessling, Germany

of time between satellite commanding respectively the pick-up of the image data and availability of image product is a key requirement for these missions.

The length of time between the pick-up of the image data and the availability of the image product is referred to as the “age of information”. Together with the system response time the image information age is a key requirement for these missions. Figure 1 shows the definition of these important parameters.

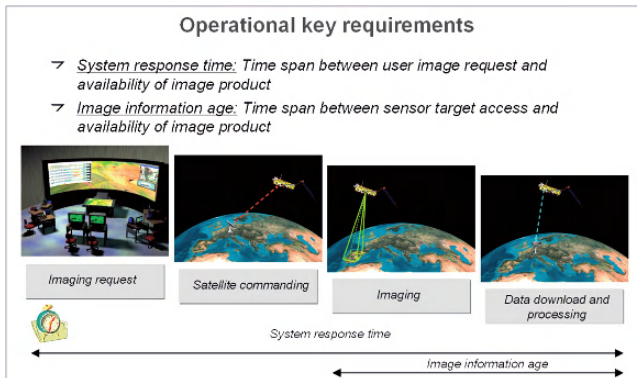


Fig. 1 Definition of system response time and image information age

2 Operational Performance Driver

In many satellite missions, it has up to now been customary that the user is located in the data receiving station of the respective satellite and has to wait until the satellite has moved into the receiving range of the antenna. Since the possibility to contact the satellite will exist only during the period when the latter is flying over the ground station, a disadvantage of this method resides in the large time gaps in which no contact is possible between the ground station and the satellite and the data age is adversely affected thereby.

Another presently available method for quicker access to image data residing in a satellite consists in the use of existing ground station receiving networks. In this method use can be made of antenna installations distributed worldwide. An example hereof is the “IGS (International Ground Stations) – Network” for the Landsat 5 and Landsat 7 satellites, which network makes it possible to receive image data on many places worldwide.

The purpose of such networks is the in-situ reception of data by geographically widely distributed users, also with the possibility of data transfers between the participating stations. The onward conveyance of the satellite data between a reception site and a user is performed by data transmission via terrestrial data lines or by communication satellites.

The disadvantages of using ground station networks of the above type become apparent in cases where no geographically widespread user groups are involved or

when classified, safety-relevant (military) data have to be transmitted. The establishing of such a geographically widespread data receiving network for individual user will, however, entail considerable costs. This applies particularly to safety-relevant data of earth observation satellites wherein a tap-proof, access-protected onward transmission between a receiver station and a user must be safeguarded.

When considering, at the same time, the high data quantities which may be in the order of magnitude of several gigabits per image product, the use of public networks (Internet) has to be excluded. As a consequence, an expensive installation of terrestrial data routes or the use of high-cost data channels via communication satellites will be necessary.

High expenses for the establishing of suitable terrestrial data connections are to be expected particularly if, due to marginal conditions related to the mechanics of satellite routes, the satellite receiving system is located at sites on the surface of the earth which are problematic regarding their geographic accessibility.

The above is true particularly of the near-pole regions in the area of the north and south poles which are considered as particularly suitable locations for the placement of receiving antennae for earth observation satellites since there, due to the inclination of the orbit normally provided for this type of satellites, a contact possibility exists virtually during each orbit cycle around the earth.

3 Mailbox Ground Station

In the following a new method for reducing information age will be presented avoiding the disadvantages of the data transfer concepts mentioned before. For reaching this aim a special way of using a dedicated ground station called Mailbox ground station is proposed. Preferably the method can be applied to satellite constellations on high inclined orbits.

There will be required orbits arranged in close proximity to the poles to thus make it possible to determine a smallest possible geographic region which all of the satellites of the constellation can fly over at the smallest possible intervals, i.e. – if possible – during each orbit cycle around the earth. In case of satellites on near-pole orbits, i.e. on orbit planes with an inclination of about 90° relative to the earth's equator, such regions can be determined as sections delimited by near-pole circles of latitudes, with the north or south pole each time forming the centre.

The size of these surfaces will depend on the extent to which the inclination of the satellite orbit planes deviates from 90° . In the ideal case of a polar orbit having an orbit inclination of 90° , the region flown over by all earth observation satellites on each of their orbits around the earth will be reduced to a point, notably the north and south poles. For a constellation wherein all earth observation satellites have the same orbit inclination, differing from 90° , the geometric shape which is flown over by each earth observation satellite during each orbit cycle will be a circle (circle of latitudes). If the constellation consists of earth observation satellites having different inclinations, the corresponding above-mentioned region will be a spherical segment of the earth's surface delimited by two circles of latitudes.

Regarding the definition of the above described regions (point, circle, spherical segment), what is to be observed is always the normal projection of the satellites onto the rotating surface of the earth. Additionally, as an effect of minor influence, it is to be noted that the orbit plane of satellite orbits will over time tend to rotate about the north/south pole axis relative to a reference system fixed in space, which effect is caused by the uneven mass distribution within the earth's globe.

A feature resides in the arrangement, additionally to the user ground station, of a further ground station, referred to hereunder as Mailbox ground station, for data connection to the earth observation satellites in the above described region which is flown over by preferably all earth observation satellites at brief intervals. By this special arrangement of the Mailbox ground station, it is now made possible to establish a connection to virtually each earth observation satellite of the constellation during each orbit cycle.

In case that, for technical and/or financial reasons, it should not be possible to arrange the Mailbox ground station in the described region which is flown over by all earth observation satellites at brief intervals, also other regions can be selected for the Mailbox ground station. This, however, has the disadvantage that in this case not each orbit cycle performed by the earth observation satellites can be utilized for a data connection. Thus, there should always be selected a region which is suitable to be flown over by as many earth observation satellites as possible and at intervals as short as possible. For the near-pole satellite orbits as commonly used for earth observation missions, these regions are located in geographic areas with preferably high altitudes.

The Mailbox ground station is positioned in such a manner that, during fly-over by one or a plurality of earth observation satellites, it will be possible both to receive the image data residing in the earth observation satellite(s) and to transmit the data temporality stored in the Mailbox ground station to selected earth observation satellites of the constellation. By the arrangement of only one Mailbox ground station in a region which is flown over preferably by all earth observation satellites of the constellation at brief intervals, there is no need anymore for the above-described expensive use of ground stations distributed world-wide, nor will there be the requirement to perform a likewise expensive and technically complex data transfer from these stations to the user.

Further there are preferably required different node positions of the individual satellite orbit planes. A node position describes the position of the virtual piercing points of the satellite orbits through the equator plane and, in combination with the above-described inclination, describes the position of the satellite orbit plane in space. By suitable selection of the node position when designing a satellite route, it can be determined at which times certain regions on the earth's surface will be flown over.

A further problem resides in the sometimes very long connection gaps between an earth observation satellite and the user ground station, which can be in the range of ten hours and more. These gaps are largely caused by the relative movement between the earth observation satellite on its orbit plane and the surface of the earth which due to the earth's rotation is turning under the satellite.

In case of the above described contact gaps, it may happen that, under the effect of the earth's rotation, the user ground station and consequently the spatial receiving range of this station have moved into such a far distance from the satellite orbit plane that the earth observation satellite is not capable anymore during its orbiting to get into the receiving range of the user ground station.

The influence of the drift of the satellite orbit plane caused by the uneven mass distribution of the earth's globe, which drift is relatively small in comparison to the earth's rotation, is negligible with regard to the subsequent considerations because, during the time periods of relevance here, it will lead to merely insignificant shifting between an earth observation satellite and a receiving range of the ground station.

By suitable selection of the orbit nodes for the individual earth observation satellites of the constellation, the individual orbit planes can be arranged to the effect that, provided that the number of satellites is sufficient, in the ideal case there will at all times one or a plurality of earth observation satellites flying through the receiving range of the user ground station during their orbiting movement. Should the number of satellites be too small, it is at least possible to reduce the time periods during which none of the earth observation satellites in orbit can contact the user ground station.

The Mailbox ground station will be used for intermediate storage of the image data of an earth observation satellite of the constellation which currently has a reduced possibility to contact the user ground station; thus, these image data can then be transmitted to another earth observation satellite of the constellation which, when next having the occasion to contact the user ground station, will provide an image whose data age is satisfactory to the user.

Figure 2 is a schematic representation of the geometric conditions and the participating components for a constellation comprising three earth observation satellites on different orbit planes, a user ground station and the Mailbox ground station. In four steps the sequence of target access by satellite 1 and data download to the user by satellite 2 is shown. Dependent on target coordinates a significant improvement of image information age can be achieved by using this procedure.

A central component is the Mailbox ground station which is located on the surface of the earth and serves for intermediate storage of the data received from earth observation satellites flying across the respective region. The intermediate storage of the data has to be maintained until the earth observation satellite selected for onward transmission of the data will fly over the Mailbox ground station.

Apart from the data store, there is provided a data receiving unit and a data transmission unit, consisting of receiving hardware and transmission hardware, respectively, and preferably a common antenna. The receiving and the transmitting of the data is started respectively in response to commands predetermined for use between the Mailbox ground station and the earth observation satellites and can be realized in a fully automated manner, thus offering also the option to use an unmanned and thus economically advantageous Mailbox ground station. To avoid costs for setting up the Mailbox ground station particularly in polar regions, one can use the existing infrastructure of ground stations in these geographic regions.

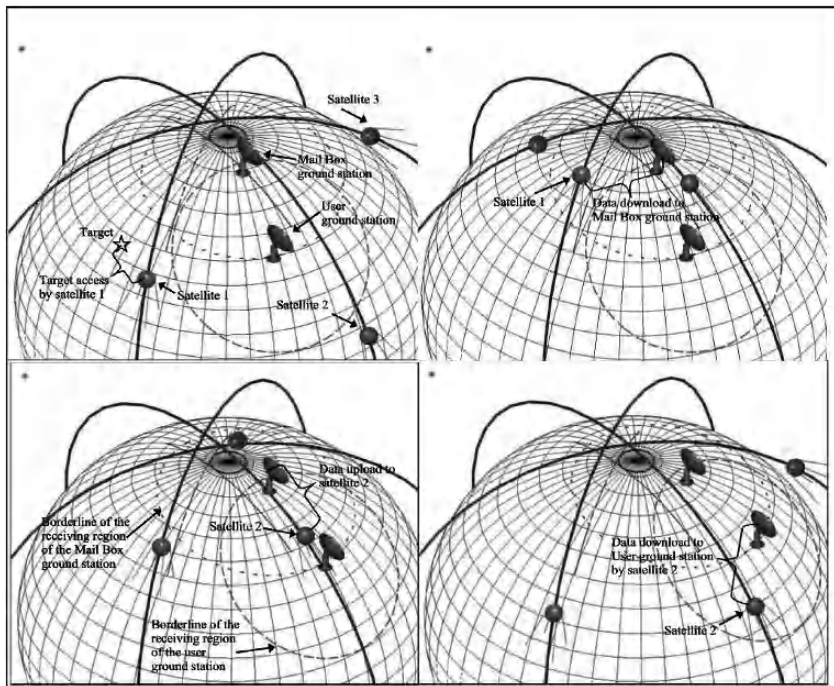


Fig. 2 Geometric conditions for Mailbox ground station concept

In case that, for technical or financial reasons, it should not be possible to arrange the Mailbox ground station in the described region which is flown over by all earth observation satellites at brief intervals, also other regions can be selected for the Mailbox ground station. This, however, has the disadvantage that in this case not each orbit cycle performed by the earth observation satellites can be utilized for a data connection. Thus, there should always be selected a region which is suitable to be flown over by as many earth observation satellites as possible and at intervals as short as possible. For the near-pole satellite orbits as commonly used for earth observation missions, these regions are located in geographic areas with preferably high altitudes.

4 Simulation

For demonstration the effect of improvement for image information age which can be achieved by using the Mailbox ground station procedure a simulation result is presented here. The scenario selected is determined by a 6-satellite constellation with an inclination of 98.1° and an orbit altitude of 681 km (IKONOS orbit parameters). Figure 3 presents the scenario start configuration including the data receiving

areas of the user- and the Mailbox ground station. In this simulation Svalbard is selected for Mailbox ground station and the user ground station will be located at Weilheim (DLR).

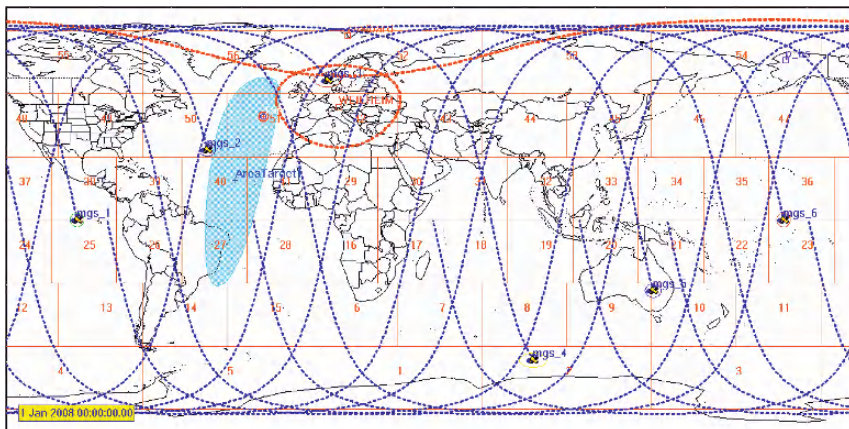


Fig. 3 Scenario start configuration for simulation

The result for image information age reduction which will be realized for a selected target is shown in Fig. 4. It should be mentioned that the influence of the Mailbox station on image information age reduction strongly depends on the image target location. For a given scenario defined by satellite constellation and ground stations those geographical areas can be determined which will profit from Mailbox station procedure.

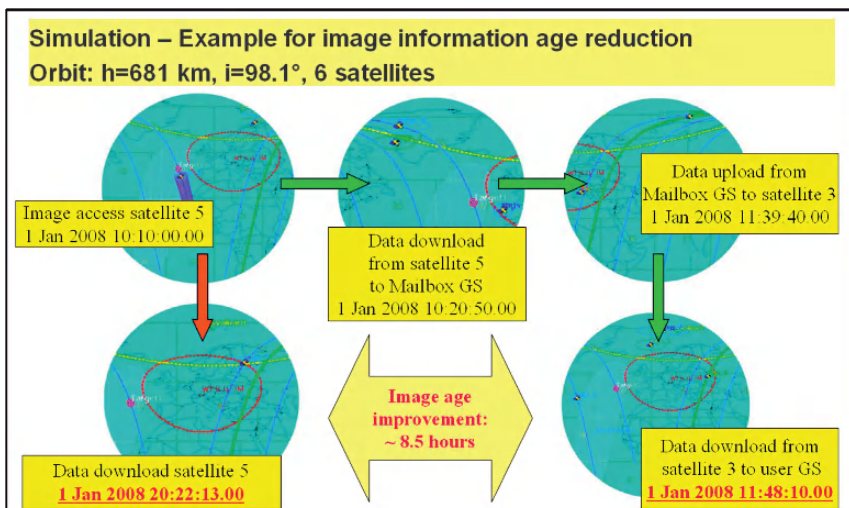


Fig. 4 Example for image age reduction

5 Conclusion

In contrast to previously employed methods performed by using only one (user) ground station or using worldwide networks of ground stations, the long connection gaps occurring are avoided along with their negative influence on the age of the image information. Besides improvement for image information age the Mailbox ground station can also be used for reducing the command time.

Further, the need for relay stations or special terrestrial data connections between the ground stations or the worldwide network and the user ground station is obviated and also the confidentiality of the data is safeguarded because the data do not have to be transmitted via public networks. About this the usage of easy adaptable and commercial available hardware is possible and there is no need for expensive space-hardware like dedicated (high data rate) communication satellites or data-interlink systems.

A Software-Defined Radio Approach for the Implementation of Ground Station Receivers

Jyh-Ching Juang, Chiu-Teng Tsai, and Jiun-Jih Miau

Abstract As many pico-esats will be released in one launch, the closeness in spatial and spectral separation between different pico-sats may render problems for ground stations in satellite tracking. We implement a ground station receiver with software defined radio (SDR) approach to solve this problem. In the SDR, bandpass sampling is used to down convert RF signal. Single antenna interference cancellation (SAIC) technique with Maximum-Likelihood Sequence Estimator (MLSE) algorithm is used to cancel interference. Doppler shift for transmitter is estimated based on received signals. The SDR-based ground station provides a receiver capable of receiving multi-channel, flexible data rate, flexible modulation type, with co-channel interference (CCI) cancellation capability.

1 Introduction

Recently, many pico-sats and/or small satellites have been developed and planned to be launched to take advantage of short development time, miniature devices, standard launcher interfaces, and piggy-back launch opportunities. Many missions including collaborative earth observation can be realized through the design of pico-sats and their constellation. However, a problem associated with the pico-sat operations is that the communication frequencies, typically in the UHF/VHF band, are very close between two different pico-sats. As many pico-sats will be released in one launch, the closeness in spatial and spectral separation between different pico-sats may render problems for ground stations in satellite tracking, especially in the early orbit phase. Even when there is a contact, it may be difficult for a participating ground station to distinguish the satellite that is being pointed at by the ground

J.-C. Juang

Department of Electrical Engineering, National Cheng Kung University, Tainan, Taiwan
e-mail: juang@mail.ncku.edu.tw

C.-T. Tsai

Department of Electrical Engineering, National Cheng Kung University, Tainan, Taiwan

J.-J. Miau

Department of Aeronautics and Astronautics, National Cheng Kung University, Tainan, Taiwan

station antenna. The station may have to resolve the desired signal out of a class of near-by interferences. Also, the frequency overlap due to Doppler shift, clock drift and operation error aggravate the tracking problem. Indeed, if the contact with a satellite is interrupted by such errors, the station may have to search the signal again, which is highly time-consuming. Giving the very limited contact time of LEO satellites, the tracking of a cluster of satellites may be extremely challenging.

Traditional ground station receivers are typically implemented by commercial amateur radios. The signal received is down converted to intermediate frequency (IF) by mixers and demodulated by a TNC modem. Then, ground station PC deals with the digital signal to decode the telemetry information. The architecture's weakness is that the channel number is limited to be one or two channels per receiver. And the modulation method and data rate is often fixed. If a user wants to change the capability of a ground station, change of hardware, either through installation of new equipment or tuning of dials/buttons, is necessary. Such a hardware approach may be costly and inflexible to operate. These situations need to be improved in order to have better mission performance. A feasible strategy is to employ a software-defined radio (SDR) approach to implement the ground station receivers. In this paper, a SDR architecture is proposed and developed. The resulting ground station receiver constitutes an antenna, A/D converter and processing software to acquire, process, and decode radio signals. The key for the successful acquisition and tracking of multiple radio signals lies in the use of processing software. In the paper, the processing software is described and its performance against conventional receivers is assessed.

2 Architecture

2.1 Hardware

Figure 1 shows the architecture of the SDR-based receiver. One antenna receives the RF signals. Broadband selective antenna is suitable to receive several satellite bands and reject other bands. An antenna with amateur radio VHF/UHF and ISM 2.4GHz band is considered. Due to weak signal and system noise factor, an LNA is put near to the antenna output port as possible. Then, a filter is designed to suppress noise and prevent aliasing. The A/D converter digitizes the incoming signals into digital samples. This differs from the conventional approach in which mixers and down-converters are used to render IF signal. Conventional ground stations process intermediate frequency (IF) signal and decode by a TNC modem. The SDR-based receiver performs the remaining signal reception and processing tasks using software in a computer.

2.2 Signal Processing Procedure

The RF signal from satellites must be down converted to IF signal. Instead of using mixers, the SDR-based receiver utilizes A/D converter and band pass technique

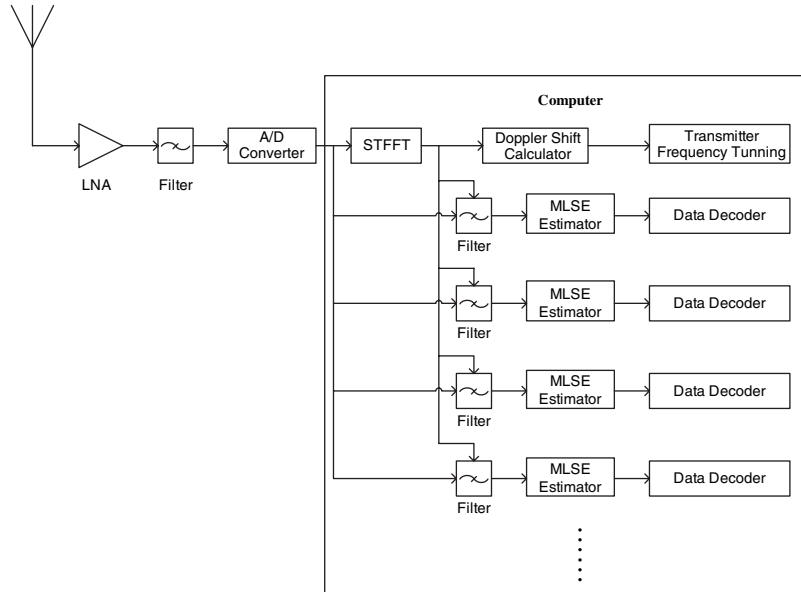


Fig. 1 Architecture of the SDR-based ground station receiver

[1, 6]. The latter allows the use of a low sampling rate device to process high frequency signals. In the approach, the sampling frequency is selected as 20 MHz so as to accommodate different frequency and the associated Doppler variation of different satellites with a communication frequency in the range of 140~150 MHz and 430~440 MHz.

The digitized IF samples that are available at the A/D converter output may consist of signals from a cluster of satellites together with noise and interferences. A software processing algorithm is needed to extract the signal from a certain pico-sat. Because the bandwidth is wider in SDR than that in traditional receivers, the noise effect in SDR is also more severe. For a certain signal, other pico-sats' signals and other illegal amateur radio users' signal are regarded as interferences. As a result, the interference issue can not be neglected.

A Short-Time FFT (STFFT) is used to track the variation of the frequency as a function of time. The width of the Short-Time FFT window needs to be well-considered to have a suitable frequency resolution and time resolution. STFFT with wider window has better frequency resolution and worse time resolution; in contrast, STFFT with narrower window has better time resolution and worse frequency resolution. As the Doppler shift due to satellites is not fast, the time resolution is specified as 10 second. The frequency resolution becomes 100 Hz, given the aforementioned sampling frequency. Through the STFFT, the spectrum can be obtained. If the strength of the signal at a certain frequency is greater than the threshold, a signal is detected. Consequently, the frequency information, includes the frequency variation of each working channel, can be utilized to form the digital window and

execute the tracking loop. In parallel, several digital filter windows are implemented to suppress the noise. The center frequency of each filter window is the same as every peak's frequency in the spectrum. And the bandwidth of every filter window is 20 kHz, the same as the bandwidth for the narrow frequency modulation communication in amateur radio band.

As a cluster of satellites are in presence, the frequencies of two or more channels may overlap occasionally. In addition, illegal ground-based users may interfere the channel. The co-channel interference (CCI) increases bit error rate (BER) significantly [3, 9]. CCI can be cancelled by the single antenna interference cancellation (SAIC) technique [5, 7] for ground stations with one antenna only, or by implementation multi-input multi-output (MIMO) technique [8] at ground stations with multi antennas. The Maximum-Likelihood Sequence Estimator (MLSE) algorithm [2] is known to be capable of handling CCI in SAIC. The desired signal under interferences can be represented as

$$r[k] = A_1[k]e^{j\theta_1[k]} + A_2[k]e^{j\theta_2[k]} + N[k] \quad (1)$$

where $A_i[k]$ and $\theta_i[k]$ is the amplitude and phase of the i -th signal at time kT_s , respectively. T_s is the sampling period. The Viterbi estimation method [4] is used to determine the maximum likelihood estimate of $(\theta_1[k], \theta_2[k])$. The computation trellis has 64 states, and the trace back depth is 32. Although this method cannot cancel the interference perfectly, the BER has been improved. Figure 2 depicts the successive CCI cancellation architecture.

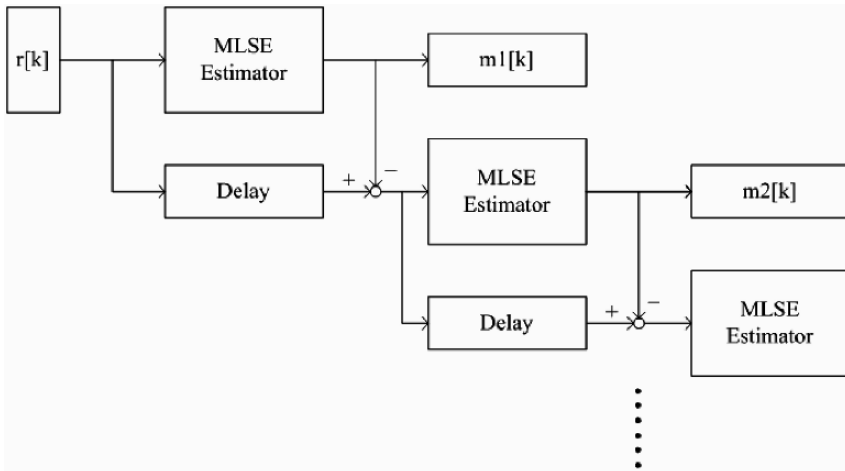


Fig. 2 Successive CCI cancellation architecture

After the interference cancellation stage, the signal output from the MLSE estimator is decoded as digital code, 1 or 0. The data stream from the satellite is then be obtained.

3 Simulation Result

To assess the interference cancellation performance, simulations are performed. The condition of the simulation assumes that the IF is 1 MHz with 1200 bps AFSK signal. Figure 3 shows the simulated BER at IF 1 MHz with 1200 bps AFSK signal, without Doppler shift. Figure 4 further shows the simulated BER at IF 1 MHz with 1200 bps AFSK signal and Doppler shift with variation 20 Hz per second. The Doppler shift condition is selected for usual pico-sat tracking condition.

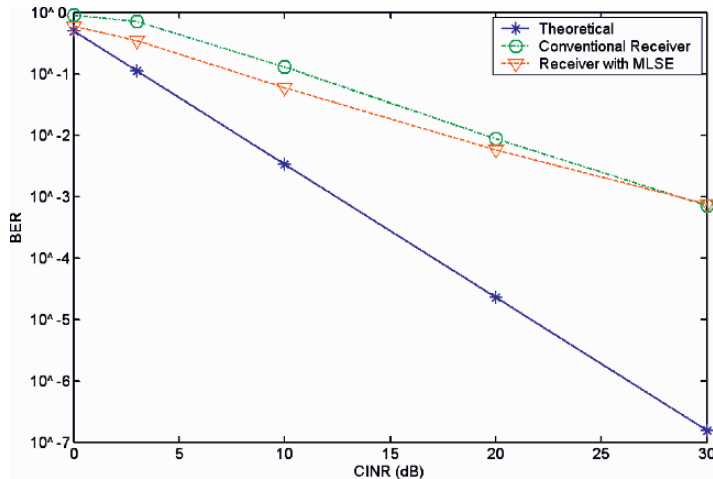


Fig. 3 Simulated BER without Doppler shift

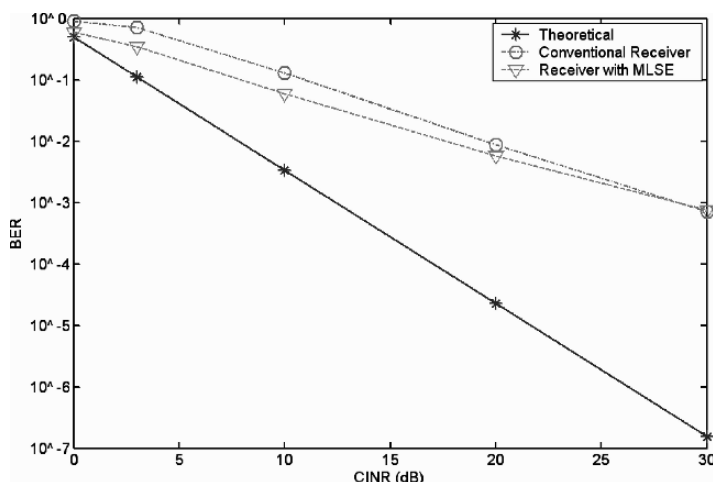


Fig. 4 Simulated BER with Doppler shift

The simulation results entail that the proposed CCI scheme running under as SDR architecture is capable of reducing the effect of interferences on signal reception in the presence or absence of Doppler shifts. The performance enhancement is more significant when the signal to noise and interference ratio is low.

4 Conclusion

The benefits of SDR in terms of programmability and flexibility are widely known. Indeed, SDR-based receivers can change channel number and modulation method by just changing the software. The communication band can be changed by tuning the sampling rate of SDR's A/D converter. SDR can also deal with several different bands at the same time. All these changes can be achieved without hardware modification. The paper has attempted to explore this advantage to build a SDR-based ground station receiver so that a cluster of pico-satellites can be successfully tracked especially in early orbit phase. In particular, an interference cancellation approach is adopted in the SDR to reflect the scenario when the frequency band is occupied with interferences. As a result, users can enjoy a ground station capable of multi channel, multi data rate, flexible architecture, low cost and lower BER.

Acknowledgement The research was supported by the National Space Organization, Taiwan under Grant 95-NSPO(B)-SE-FA09-01(II).

References

1. D. M. Akos, M. Stockmaster, J. B. Y. Tsui, J. Caschera, Direct Bandpass Sampling of Multiple Distinct RF Signals, *IEEE Trans. Commun.*, Vol. 47, No. 7, pp. 983–988, 1999.
2. W. Etten, Maximum Likelihood Receiver for Multiple Channel Transmission Systems, *IEEE Trans. Commun.*, Vol. 24, No. 2, pp. 276–283, 1976.
3. A. Goldsmith, *Wireless Communications*, Cambridge University Press, 2005.
4. J. Hamkins, A Joint Viterbi Algorithm to Separate Cochannel FM Signals, *Proc. IEEE ICASSP '98*, Vol. 6, pp. 3297–3300, 1998.
5. P. A. Hoeher, S. Badri-Hoeher, W. Xu, C. Krakowski, Single-Antenna Co-channel Interference Cancellation For TDMA Cellular Radio Systems, *IEEE Wireless Communications Magazine*, Vol. 12, No. 2, pp. 30–37, 2005.
6. P. B. Kenington, *RF and Baseband Techniques for Software Defined Radio*, Artech House, 2005.
7. A. Mostafa et al., Single Antenna Interference Cancellation (SAIC) for GSM Networks, *Proc. IEEE VTC*, pp. 1089–93, 2003.
8. P. A. Ranta, A. Hottinen, Z.-C. Honkasalo, Co-channel Interference Cancellation Receiver for TDMA Mobile Systems, *Proc. IEEE ICC*, pp. 17–21, 1999.
9. P. Stavroulakis, *Interference Analysis and Reduction for Wireless Systems*, Artech House, 2003.

Session 8

Missions (2)

Mission Requirements and Analysis of Indonesia's Second Generation Satellite to Support Food Security Program

S. Hardhienata, G. Prabowo, and F. Fitrianingsih

Abstract One of the main priority middle term programs of the Indonesian government is to provide food security to the country's population. Considering the Indonesian geographical condition and its position as a government institution, the Indonesian National Institute of Aeronautics and Space (LAPAN) decides to develop a second generation satellite to help the government achieving its food security program goals. This paper describes the mission requirements and analysis of Indonesia's second generation satellite (a remote sensing satellite) to support the food security program.

1 Introduction

Indonesia's geographical condition, namely consisting of thousands of Islands covering a vast area, is very suitable for adopting satellite technology to help the country solve several of its national goals. Among these goals is to succeed the food security program. Food security is a foundation for a nation's development; therefore it becomes one of the top research priorities for the country's research institutions. Based on the Government National Middle Term Plan (RPJM) 2004–2009, the research activities focuses on six priority sectors, namely food security, health care and medicine technology, new and renewable energy resource, transportation technology and management, information and communication technology, as well as defense and security.

As a government institution, the Indonesian National Institute of Aeronautics and Space (LAPAN) has the responsibility to support the government in meeting its national goals. With the successful launch and operation of the LAPAN-TUBSat

S. Hardhienata

National Institute of Aeronautics and Space (LAPAN) – Republic of Indonesia
e-mail: s-hardh@indo.net.id

G. Prabowo

National Institute of Aeronautics and Space (LAPAN) – Republic of Indonesia

F. Fitrianingsih

National Institute of Aeronautics and Space (LAPAN) – Republic of Indonesia

Surveillance Micro satellite in January 2007, LAPAN confidently moves to the next step namely developing a second generation satellite (a remote sensing satellite) whose mission direction is to support the national food security program. Its primary objective is to monitor the crop and harvest area as well as identify the plant growth phase.

2 Mission Requirements and User Needs

To fulfill the mission, goal criteria's has to be described clearly as mission objectives which describes what the satellites must do in order to achieve its objective. The satellite mission objective can be obtained through the user need's analysis by considering its technical limitations. After the mission objectives are defined, the next step is to define the mission requirements and the mission limitations. The mission requirements will be applied as a reference in the satellite design. Fig. 1 presents the mission definition.

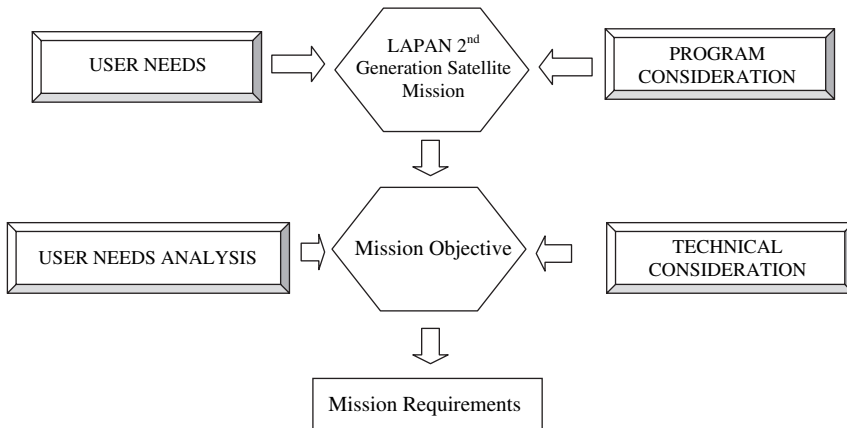


Fig. 1 Diagram of mission definition process

To obtain sufficient information about the user needs on remote sensing data, preparation has been made through seminars, workshops, and road shows. During the preparation process several government institutions have provided useful inputs namely the Agricultural Department, Marine and Fishery Department, and the Forestry Department. A significant input is the information that remote sensing satellite has been applied in Indonesia for a wide range of application ranging from agriculture, forestry, marine, disaster mitigation, and others. Table 1 describes the user needs in remote sensing satellite.

It can be seen from the table that the urgency and economical value of applying remote sensing satellite is very high. In the forestry sector, monitoring of fire points and fumes, which accounts for the destruction of hectares of forest area in Indonesia, can save the government more than \$ 9 Billion, whereas in the Marine and Fishery

Table 1 Government department user demand for remote sensing satellite

| No | Department | Utility | Urgency and Economical value |
|----|--------------------|--|--|
| 1. | Agriculture | 1. Delineation in the land utilization change 2. Crop growth monitoring 3. Identification of the River Current Water Damage 4. Identification of the field destruction due to tsunami disaster 5. Delineation of the agro climate zone 6. Delineation of the flood potential and drought zone | Revitalization of 15 million agricultural fields as well as flood disaster mitigation and its economical impact |
| 2. | Forestry | 1. Monitoring of fire point/forest burning 2. Monitoring of fog/cloud (fumes) 3. Detection of forest burning | Prevent loss due to forest destruction can reach \$ 9.7 billion. |
| 3. | Marine and Fishery | 1. Management and monitoring of the coastline space arrangement, conservation area determination, marine tourism planning. 2. Utilization of the coastline resources: fish cultivation, coral reef inventory, mangrove forest identification, ecotourism development. 3. Sea mapping, Exclusive Economical Zone and international border. 4. Fish potential zone identification. 5. Vessel Monitoring System. Environment monitoring program. | Support on the inventory and management of the natural resources with an economical value reaching \$ 6 billion. |

sector the utility implementation can support the natural resource inventory process which according to estimation has an economical value reaching \$ 6 Billion a year.

3 Remote Sensing Application in Food Security

According to the World Food Summit in 1996 Food Security occurs when “all people at all times have physical economic access to sufficient safe and nutritious food to meet their dietary needs and food preferences for an active health life”. This statement is not too different than the definition of food security stated in the Indonesian Law No 7 Year 1996, namely a condition where food needs are acquired for every household as indicated by the sufficient availability of food, both its quantity and quality, prevalent, and affordable.

The availability of primary food such as rice is an important indicator that describes whether food security has been met or not. The government strategy in meeting the food security is based on the availability of five primary food types for the community. To ensure community access on their primary food source accurate information and analysis on food demand and availability is necessary if the government wants to decide the best strategy. The food availability depends on the

food production, stock, and import. Meanwhile, the food demand is affected by the amount of population and their consumption rate. After both information are available food security analysis can be formulated to decide the best strategy. This process is presented in Fig. 2.

The application of satellite image to support food security in Indonesia has already been performed, such as the ASTI experimental project between the Agricultural Department and the Technology Application and Assessments Agency (BPPT) to predict rice harvest as well as cooperation between LAPAN and NASDA to apply remote sensing satellite from Japan, namely JERS-1, ADEAOS, and ALOS to map the rice crop field, monitor their growth phase, estimate rice harvest, and detect crop diseases.

Besides experimental project, the Agricultural Department has also applied remote sensing satellite for agricultural field area estimation in national levels, such as NOAA, Landsat TM, JERS, and SPOT. However not all of these satellites are suitable for high spatial resolution image remote sensing in the province level crop area estimation. In this case, Landsat TM can be applied.

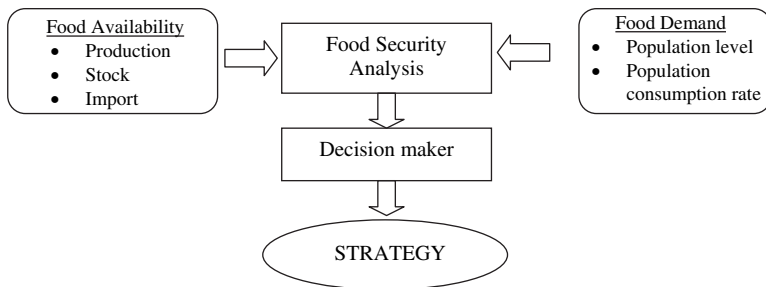


Fig. 2 Diagram of the food security analysis

Principally, all remote sensing devices can be used for crop monitoring. The choice depends on the desired specific application. Hyper spectral image satellites such as MODIS and TERRA-ASTER Satellites are optimal to identify the crop condition and discrimination, whereas the multi spectral image satellites (medium to high resolution) are optimal for crop area estimation, crop growth stage identification, and crop productivity. Ideally, hyper spectral image is applied to distinguish the food commodity because the hyper spectral sensor has more canals, thus the sensor sensitivity to distinguish color differences is better and therefore easier in detecting different food commodity. Less canal sensor requires multiple data if used for crop identification (called multi spectral sensors).

Compared to a conventional satellite, remote sensing satellites have the advantages in covering local and global areas with periodic and continuous observation, providing objective information, and has independent inputs for field verification, whereas conventional satellites are able provide more accurate information for crop identification. The disadvantages of the remote sensing satellite is the need for higher resolution due to higher accuracy however this statement is used for early

estimation and needs further verification. The conventional satellite has the disadvantage that it covers only small areas and thus takes longer time for global analysis.

4 Users Tendency in Remote Sensing Data

Although all remote sensing satellite are applicable for crop monitoring, the users tend to choose one or two satellite type because more satellite types requires different methods thus consumes more time and energy. Many users also prefer medium resolution for economical reason because higher resolution satellites are more expensive than the lower one.

Table 2 provides remote sensing data and the type of information provided by these satellites, whereas Table 3 displays the satellite image price. It can easily be seen that better spatial resolution result in an increased cost per square kilometer (compare the cost per km² of IKONOS and SPOT).

The user needs analyses for the development of LAPAN's second generation satellite comprises the demanded image resolution, time delivery, and crop data. The image resolution should be good enough to analyze province level images, which means it is able to provide images with a 1:25,000 to 1:100,000 ratios, thus provides detailed information for each regency. The time data delivery should range from 14 to 30 days for plant identification (especially rice) whereas the demanded

Table 2 Remote sensing data and type of information

| Satellite | Spatial Resolution | Equivalent with map scale | Type of Information |
|------------|--------------------|---------------------------|---------------------|
| NOAA-AVHRR | 1.1 km | 1,000,000–2,500,000 | Diagram |
| MODIS | 210 m | 500,000–1,000,000 | Exploration |
| Landsat TM | 30 m | 100,000–250,000 | Observation |
| SPOT 4 | 10–20 m | 50,000–100,000 | Deep Observation |
| SPOT 5 | 3–10 m | 25,000–50,000 | Semi detail |
| IKONOS | 1–4 m | 2,500–10,000 | Detail |

Source: Agriculture Department, 1999

Table 3 Satellite Image Price

| Type of Data | Spatial Resolution | Scene size | Unit cost | Cost per km2 |
|--------------|--------------------|---------------|------------|--------------|
| NOAA- AVHRR | 1,1 Km | 2300 × 2300km | USD 25 | Free data |
| Resours-O | 210 m | 500 × 500km | – | – |
| Modis | 250 | 1000 × 1000km | – | – |
| Landsat TM | 30 m | 180 × 180Km | USD 850 | USD 0,3/km |
| SPOT | 10–20 m | 60 × 60km | 17.000 FFr | USD 1,0/km |
| RADARSAT | 10–20 m | 40 × 40km | USD. 2000 | |
| IKONOS | 1–4 m | Min 10 × 10km | – | USD 34–44/km |

Source: Deputy for Remote Sensing LAPAN, 2002

type of information consists of the estimation of crop planting and harvesting area, growth stage identification, productivity, discrimination, and condition/plant stress.

The plant condition can be estimated using the reflectance spectral, whereas the plant stress level can be detected through infra red canal. A hyper spectral imager such as MODIS is more sensitive in detecting different wavelengths, thus can better detect plant stress. The full information regarding a plant condition can be obtained by combining hyper and multi spectral images. Table 4 provides the principal application of various spectral ranges:

Table 4 Application of Spectral Bands

| Spectral range (mm) | Principal application |
|------------------------|--|
| 0.45–0.52 | Sensitivity to chlorophyll, coastal water mapping, soil/vegetation discrimination, forest type mapping |
| 0.52–0.60 | Green reflectance for vegetation discrimination and vigor assessment |
| 0.63–0.69 | Sensitivity to chlorophyll, plant species identification, water type discrimination |
| 0.76–0.90 | Vegetation type, vigor, biomass determination, water body delineation, soil boundary and geological boundary mapping |
| 1.55–1.75 | Sensitivity to amount of water in plants, useful for drought studies and plant vigor studies |
| 2.08–2.35 | Sensitivity to hydroxyl ion in minerals, useful in discrimination of rock types, Effective in identifying zones of hydrothermal alteration in rocks. |
| 10.4–12.5 | Surface temperature mapping |

Source: An Introduction to Geographical Information System, Heywood, Cornelius & Carver

5 Technical Aspects and Constrains

As a remote sensing satellite with food security as its mission, LAPAN's second generation satellite should be able to meet the user requirements with its current technical achievements. This consideration should also match with LAPAN's satellite development program phases.

Besides achieving the mission objectives, the program also aims to increase the human resource capability and independence in satellite technology. To meet both objectives, an optimum point has to be searched. The result is a satellite with a weight between 50–300 kg and a performance like those given by Fig. 3.

The technical constrains can be classified into four points, namely the limitation of skill and experience, facility, manpower, and micro satellite constrains. The design of the satellite must be as simple as possible. The spatial resolution value of the satellite which consists of 3–4 canals will have a range between 10 and 30 or 3 and 10 m because these resolution are assumed to be sufficient for producing detailed regency level map with a scale between 1:50,000 to 1:100,000. This resolution is based on technical consideration, available human resources, demand level,

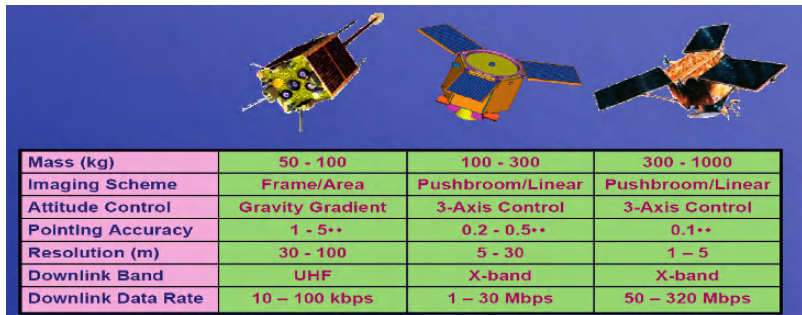


Fig. 3 Typical performance of several satellite model based on its weight (SATRECI)

and acceptable. Higher spatial resolution means more complex satellite system. The temporal resolution is between 2 weeks to one month. It is estimated that the satellite will be launched in 2010 using piggy back with a lifetime of about 3 to 5 years.

6 Conclusion

Food security becomes one of the main government programs in Indonesia and LAPAN as a government institution has the responsibility to support the success of the program by developing a second generation remote sensing satellite. Its primary objective is to monitor crop and harvest area as well as to identify plant growth phase in Indonesia. The satellite's mission requirements are obtained after considering the mission objectives which are obtained after analyzing the user needs, program considerations and user needs analysis as well as technical consideration. The technical constrains can be classified into four points, namely the limitation of skill and experience, facility, manpower, and micro satellite constrains. In addition, the design of the satellite must be as simple as possible.

References

1. Department of Agriculture, “*Annual Report of Pilot Project on the Use of Japanese Satellite Data in Indonesia*”, Jakarta – Indonesia, 2002.
2. Fitrianingsih, E., et al., “*Mission Design of Indonesian Second Generation Satellite*”, Proceedings of Small Satellite System and Services – 4s Symposium, Cagliari Sardinia – Italy, September 2006.
3. Hardhiyana, S., “*The Strategy of Indonesia Satellite Technology Development*”, Proceedings of ISNET International Seminar on Space Technology & Applications, Islamabad – Pakistan, September 2006.
4. Hardhiyana, S., “*Space Science and Technology Applications in Indonesia*”, Proceedings of Technology Summit and Technology Platform, New Delhi – India, November 2006.
5. Hardhiyana, S., Kadri. T. M., Briess, K., “*Remote Sensing Satellite to Support Food Sustainability Program in Indonesia*”, Proceedings SIPTEKGAN X-2006, ISBN: 979-8554-91-4, Jakarta – Indonesia, November 2006.
6. Heywood, I., Cornelius, S., and Carver, S., “*An Introduction to Geographical Information Systems*”, Prentice Hall, 3rd edition , 2006.

A Low-Cost Microsatellite Platform for Multispectral Earth Observation

A. Graziani, N. Melega, and P. Tortora

Abstract In the Microsatellite Laboratory of the University of Bologna a project was started in 2003, aimed at the development of a multipurpose microsatellite platform named ALMASat. The launch into orbit of the first prototype ALMASat-1 is currently foreseen by the end of 2008. One of the natural applications of the modular ALMASat platform is in the field of space-based Earth observation. At this aim, a spin-off company named ALMASpace was established in 2006, with the goal of designing and demonstrating the feasibility of a low-cost Earth observation mission based on the technological achievements obtained by the ALMASat project. This paper summarizes the main characteristics of the ALMASat-1 spacecraft and describes the current status of the design and development of the ALMASat-EO (Earth Observation) spacecraft bus and optical payload whose launch into orbit is currently scheduled at the end of 2010.

1 Introduction

ALMASpace is a new aerospace company, established in 2006 by a group of researchers of the II School of Engineering of the University of Bologna. ALMASpace represents the commercial development of a university project named ALMASat, started in 2003 in the Microsatellite Laboratory of the University of Bologna and aimed at the development of a multipurpose microsatellite platform.

The architecture of the ALMASat satellites has been selected in order to have a multipurpose bus, to be used with minor changes for several missions, accommodating payloads with different volume and power requirements. Many of the

A. Graziani

ALMASpace S.r.l., Via del Poggio n. 227, 47032 – Panighina, Bertinoro (FC), Italy
Università di Bologna, II Facoltà di Ingegneria, Via Fontanelle 40, 47100 – Forlì (FC), Italy

N. Melega

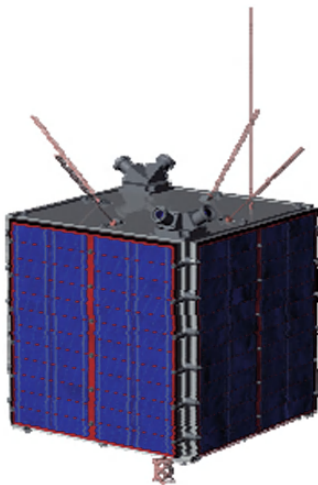
ALMASpace S.r.l., Via del Poggio n. 227, 47032 – Panighina, Bertinoro (FC), Italy
Università di Bologna, II Facoltà di Ingegneria, Via Fontanelle 40, 47100 – Forlì (FC), Italy
e-mail: nicola.melega@almasat.org

P. Tortora

Università di Bologna, II Facoltà di Ingegneria, Via Fontanelle 40, 47100 – Forlì (FC), Italy

ALMASat subsystems are assembled employing commercially-available technologies, thus guaranteeing low cost missions and a rapid response. The first microsatellite ALMASat-1 (Fig. 1) consists of a cubical prism, $300 \times 300 \times 300$ mm and 12 kg, with a modular structure consisting of shop-machined Al trays, and eight threaded bars, providing the necessary stiffness. The satellite is three-axis stabilized and makes use of a pitch momentum wheels and three orthogonal magnetic coils for attitude control; in addition, silicon-based cold-gas microthrusters will be carried on board as a technological payload, to be qualified for future missions. The attitude determination is provided by two (redundant) three-axis magnetometers and four sun sensors. The ADC System is controlled by a software that includes the dynamic model and the orbital model of the satellite. The communication system works at three different frequency bands: VHF (uplink) and UHF (downlink) are used for telecommands and telemetry while an S-band transmitter is used for higher data-rates in the downlink [1].

Fig. 1 ALMASat-1



The onboard power is provided by both silicon and triple junction solar cells; 48 series-connected Si cells are body mounted on each of the four lateral Al/Al honeycomb panels, while 30 series-connected Ga-As cells occupy a fifth panel on top the spacecraft. Power storage is guaranteed by three parallel connected battery packs made by four series-connected Li-Ion cells. To evaluate the platform performance, a possible orbit has been selected, referred to the selected launcher capabilities. The estimated orbit characteristics are reported in Table 1.

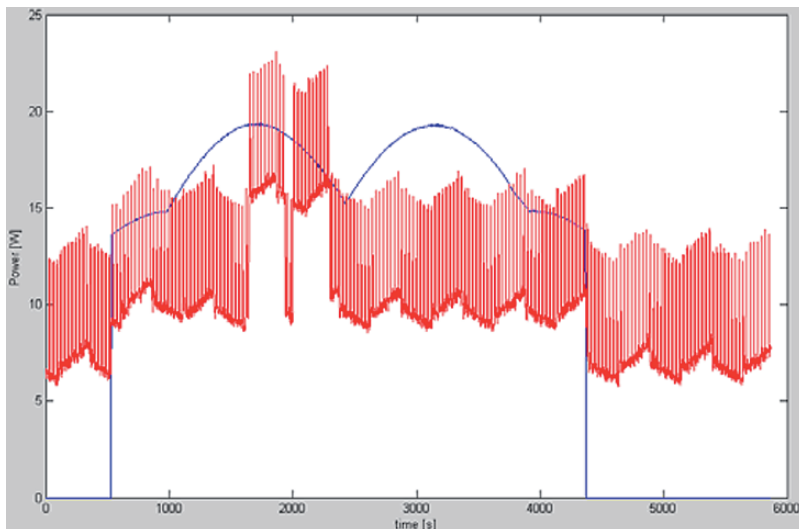
Based on the orbital characteristics, the power budget for ALMASat-1 was computed, defining different working configurations depending on the spacecraft orbit position. In particular, a power-saving configuration during the eclipse, and a fully operational configuration during the sunlight phase of the orbit were defined. The data obtained by the power budget are reported in Table 2.

Table 1 Orbit parameters

| Orbit parameters | Value |
|---------------------|------------|
| Semi-Major axis | 7028.17 km |
| Eccentricity | 0 |
| Inclination | 98 deg |
| Argument of Perigee | 0 deg |
| R.A.A.N. | 165.14 deg |
| Mean Anomaly | 0 deg |
| Orbit Period | 97.73 min |

Table 2 ALMASat-1 Power budget

| Power characteristic | Value |
|----------------------------|----------|
| Peak power produced | 19.38 W |
| Photovoltaic system Energy | 65322 J |
| Solar array power | 16.96 W |
| Energy margin | 4456.4 J |

**Fig. 2** ALMASat-1 instantaneous power generation and consumption

In Fig. 2 the instantaneous generated power (blue curve) and power consumption (red curve) along the orbit are shown.

2 Mission Target

A low-cost microsatellite Earth Observation mission is constrained by the overall spacecraft dimensions and the low-power generated on-board. A possible solution is the definition of a limited target represented by a specific portion of the Earth

surface. The limited dimensions of the target area reduce the costs per image and the time between the image request and delivery. This is a crucial aspect usually taken by the major image providers.

The possible cost budget for a small dedicated Earth observation mission is limited by the annual budget dedicated by regional-size administrations to environmental monitoring using traditional instruments, as aerial photogrammetry. Thus, local governments can be regarded as the typical customer for this kind of missions in order to obtain frequently updated images of their territory. For this reason, in the mission analysis phase it has been assumed that the mission target is the coverage of a limited portion of the Earth surface and, in particular, Italy.

3 Optical Payload

The development of the optical payload for an Earth observation microsatellite mission is always difficult due to the high number of constraints that have to be considered when dealing with the reduced dimensions and low-power available on the spacecraft. As a matter of fact, most of the widely available systems presently used to acquire Earth images, as *pushbroom* or *wiskhbroom* scanners, cannot be used onboard a microsatellite mainly because of the high power and data rate they require.

On the other hand, a common *still camera* with no moving parts and a *discrete* mode of operation instead of a *continuous* one (scanner), seems to be the right choice in order to reduce power consumption and complexity of the system; in particular, the main advantage of this system is that the linear sensor is replaced by a two-dimensional one able to acquire instantaneously an entire scene, thus preserving the correct geometry and reducing the number of frames necessary to acquire the target area. Moreover, a low frame rate allows the use of a *Full Frame* CCD ensuring the highest resolution and a 100% optical fill factor [2].

The camera has been designed in order to fit the available space dedicated to the payload, onboard the new ALMASat EO (see section 3); as explained below, it consists of an additional cube connected to the main spacecraft, with 300 mm side, which allows a maximum lens diameter of 200 mm.

The selected sensor is a monochrome DALSA FTF2020M full frame CCD with an active image area of 2048×2048 pixels (4 MPixels) and a spectral resolution of 12 bit. It has a square pixel structure ($12 \mu\text{m}$ side), antiblooming and it is capable of vertical and horizontal binning in order to obtain an increased sensibility during low-light exposures. To avoid excessive readout noise and high temperatures during operations, the sensor will be used in a single output mode with a maximum frame rate of 7.5 fps, thus avoiding the use of an active cooling system for the CCD.

Typically, in digital still cameras, multispectral capabilities are achieved by using mechanical wheels that rotate optical filters in front of the sensor. To avoid moving parts inside the instrument, which could compromise the success of the entire mission, a LCD continuous tuneable filter will be placed in-between the sensor and the optics, to provide better multispectral capabilities than the mechanical wheel [3].

Multispectral images will be generated overlapping single band images and creating arrays with a maximum of 10 spectral bands. The time the filter takes to switch between one wavelength to another is typically 50–150 ms depending on the value of λ .

CRI has already tested the correct operation of the filter in vacuum conditions; it was found that the filter did not experience mechanical damages or deformations during the test and that the optical tuning error is consistent with the one measured prior to the test. One of the main issues connected to the use of this kind of filter is the need of custom-designed optics instead of a commercial one; this is due to the filter causing a variation of the *B.F.L.* (*Back Focal Length*) which, in turn, results in a shift of the focus of the system.

The filter has an aperture of 35 mm, thus matching the dimensions of the CCD (main diagonal of 34.76 mm) and the wavelength can be varied between 400 and 720 nm (in the *visible spectrum*) with steps of 20 nm.

The number of bands and the value of the acquired wavelengths can be selected (both after launch, and during the whole mission lifetime) by storing appropriate palette onboard. This allows a flexible use of the instrument and enables a rapid response on specific targets, especially during disaster monitoring or for environmental and agricultural purposes.

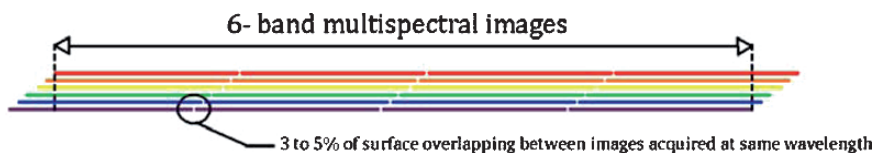


Fig. 3 Acquisition method, e.g 6 bands image

Diffractive optics have been designed in order to correct the 6 cm shift of the focal plane due to the filter housing, with a fixed focal length of 190 mm; six lenses are divided into two main groups and then inserted in a titanium case which will provide the necessary stiffness during the launch phase, and avoid misalignments between each lens.

The camera electronics is currently under development and a preliminary layout is shown in Fig. 4. The CCD will be controlled by a flexible FPGA that can be customized to use a variety of different sensors. The filter will be connected to a proprietary box linked to the FPGA via RS-232 interface.

The entire system will be managed by a platform based on an ARM7 microprocessor able to store images in a commercial flash memory drive and also send data via CAN BUS to the X-band transmitter.

Each image acquired by the sensor is currently in the order of 50 Mbit for a single band image, thus the use of an appropriate compression algorithm is necessary. One of the most flexible algorithms that can be used on-board to reduce the image dimensions is the JPEG2000, the new international standard for image data compression which uses latest compression techniques based on wavelet technology [4].

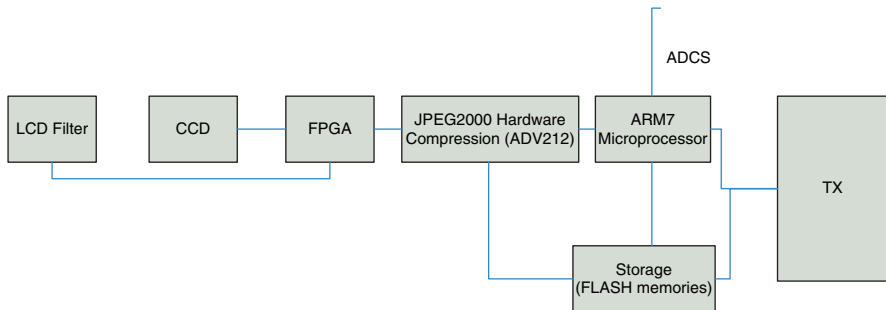


Fig. 4 Electronics Layout



Fig. 5 Rendered Optics

The JPEG2000 provides for both lossless or lossy compression in the same architecture with different compression ratios. Compression ratios usually vary between 2:1 in lossless mode to 15:1 in lossy mode with unnoticeable artefacts, allowing further use of the images for analysis.

The result is a 50 Mbit image reduced down to 3 Mbit. JPEG2000 also provides quality features like region of interest coding (ROI) and different types of progressive transmission [5].

The system weighs about 6 kg (including the filter) and is 290 mm long, with a maximum aperture of 155 mm, Fig. 4. The achieved ground resolution is about 40 m at 650 km and can be increased utilizing CCDs with different pixel size (26 m with 7.4 μm pixel side).

4 ALMASat-EO Bus

The bus and the main subsystems of the standard ALMASat microsatellite bus will be modified to fulfil the more stringent requirements of the optical payload. At a

first glance, it is clear that the overall dimensions of the ALMASat bus are not large enough to carry on-board the camera and the associated electronics. However, the modular structure of the bus allows adding other trays in order to reach the required dimensions. In particular, the ALMASat structure has been enlarged with six more stacked Al trays, thus doubling the original size, with the “bottom” side of the spacecraft hosting the camera payload.

The optical payloads needs a higher pointing accuracy in order to obtain good Earth-referenced images. The attitude determination and control system will be modified to satisfy this new requirements, by adding two reaction wheels, instead of just magnetic coils, to control the *yaw* and *roll* angles, so that the new set of attitude actuators will be made up by one momentum wheel (on the pitch axis), two reaction wheels and the three orthogonal magnetic coils. This solution offers a nominal pointing accuracy in the order of 0.1 degrees, fully compatible with the mission needs, as it has been already confirmed by numerical simulations.

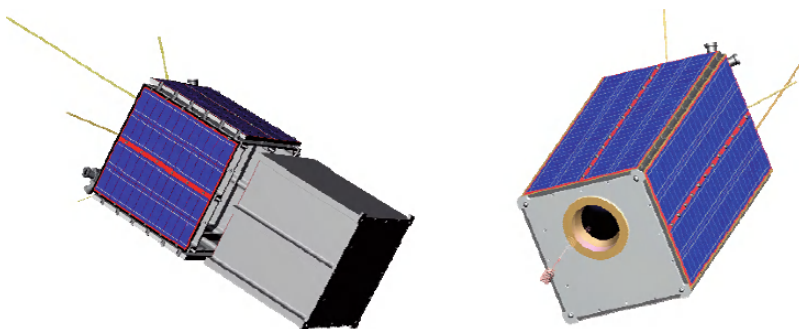


Fig. 6 Enlarged ALMASat bus and bottom view of the camera payload

Another enhancement in the ADCS system is the use of microthrusters for attitude control manoeuvres. During sun eclipse the pointing performance are worse than during the sunlight phase; thus, microthrusters have been proposed to be used to rapidly reacquire the nominal Earth-pointing mode attitude.

Another relevant improvement to the standard ALMASat bus will be made in the communication system architecture. The telemetry and telecommands will still be managed at VHF and UHF bands, while the payload data (the acquired images) will be transmitted to the ground through a X-band link whose ground and space segment components are currently under development. This system will allow data-rates up to 1 Mbit/s, thus guaranteeing to transmit to the ground at least one full image per orbit. The X-band communication system performance has been evaluated by computing a link budget, whose results are reported in Table 3.

The Link Budget was computed assuming the satellite with an elevation of 30 degrees above the ground station horizon. Due to the limited dimensions of the spacecraft, an on-board patch antenna was considered, while a high-gain parabolic antenna was hypothesized for the ground station.

Table 3 ALMA Space-EO
Link Budget

| Link data | Value |
|-----------------------------|----------------------|
| Transmitted frequency | 7.5 GHz |
| Transmitter power output | 9.5 W |
| Power consumption | 50 W |
| Spacecraft antenna gain | 6 dBiC |
| Ground station antenna gain | 35 dBiC |
| Data rate | 1 Mbps |
| BER | $1.00 \cdot 10^{-7}$ |
| System link margin | 1.3 dB |

Table 4 ALMA Space-EO
Power Budget

| Power characteristic | Value |
|----------------------------|-------------|
| Peak power produced | 67.30 W |
| Photovoltaic system Energy | 213583.22 J |
| Solar array power | 16.96 W |
| Energy margin | 91435.38 J |

The spacecraft power system will also be enhanced in order to satisfy the more stringent requirements in terms of on-board needed power. In particular, the larger area available for the solar panels, offered by the increased size of the spacecraft bus, will be entirely covered by triple junction Ga-As cells for a total peak power per panel of over 50 W.

Based on the orbital characteristics, assumed similar to those for ALMA Sat-1, the power budget was computed. Also in this case, a power-saving configuration during the eclipse, and a fully operational configuration during the sunlight phase of the orbit were defined. The results obtained from the power budget are reported in Table 4.

In Fig. 7 the on-board generated power for each panel is reported, printed in different colours, for a single orbit time span. The red curve, in particular, represents the total amount of power produced by the satellite, obtained as the sum of the power produced by each solar panel. The cyan and green curves represent the two lateral

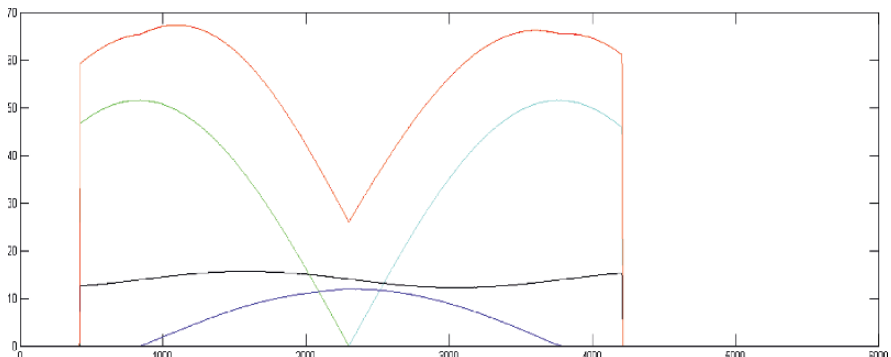


Fig. 7 Power generated by each panel

panels perpendicular to the sun. The black curve represents a lateral panel illuminated throughout the sunlight phase, while the blue curve represents the top panel.

In Fig. 8 the instantaneous generated power (blue curve) and power consumption (red curve) along the orbit are also shown. For the particular mission goal selected, the target area and the ground station are placed close on to each other; for this reason, Fig. 8 shows the corresponding, concurrent, peak power consumption for image acquisition and transmission to the ground.

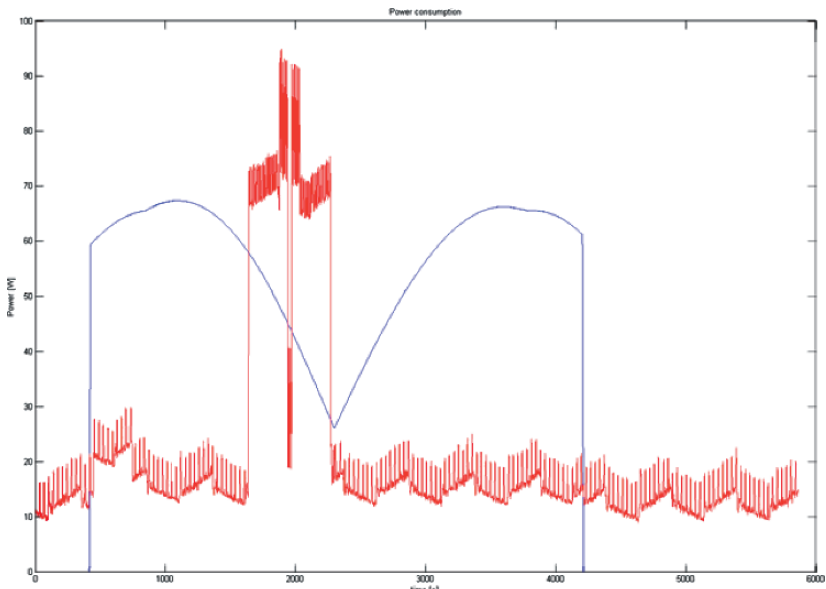


Fig. 8 ALMASat-EO instantaneous power generation and consumption during image acquisitions

5 Conclusions

This analysis demonstrates the versatility of the original ALMASat bus design that can be reused, with minor changes, also in Earth observation missions.

Further capabilities of the system, as multi-angle image acquisition, stereo imaging and onboard camera calibration will be investigated in next months to verify its possible future implementation. The optical payload, the X-band on-board transmitter and ground segment receiver and the on-board GNSS receiver are currently under development using COTS components, in order to reduce costs and realization time without affecting the subsystem reliability and lifetime. The expected launch date of the first ALMA Space-EO microsatellite is at the end of 2010 and its design and development has been funded by the Italian Ministry of Research (MIUR) for a total budget of ~ 900 kEuro.

References

1. Tortora P., Troiani E.: “*The Microsatellite Research Program at Università di Bologna*” – Acta Astronautica, Vol. 56, No 7, 2005, pp. 641–704.
2. Fouquet M., Sweeting M.N: “*Uo-SAT 12 Minisatellite for high performance Earth observation at low cost*” – IAF 1996
3. Fouquet M., Sweeting M.N: “*Remote sensing using the University of Surrey’s microsatellites*” – SRCRS Conference 1995
4. Kajfasz P., Nicholson D., Bonnot P.: “*Satellite onboard image coding using Piranha systematic DSP*” – DSP 2001
5. Rountree J., Webb B., Marcellin M.: “*Simulating onboard compression with JPEG2000*” – NASA Earth Science Technology Conference 2003

Nano-Satellites for Micro-Technology Pre-Qualification: The Delfi Program of Delft University of Technology

R.J. Hamann, C.J.M. Verhoeven, A.A. Vaartjes, and A.R. Bonnema

Abstract The Delfi program run at Delft University of Technology has the objective to provide a means of fast and affordable pre-qualification of new (micro-)technology in space. A second objective is to offer to MSc students the possibility to graduate on real hardware and software development for space missions. The first satellite in this program is Delfi-C3, a 3 kg CubeSat, which flies a new type of Thin Film Solar Cells, two Autonomous Wireless Sun Sensors and a miniaturized UHF-VHF transponder. Next in the series will be a Delfi-C3 successor, on which a more efficient power subsystem and a high efficiency Advanced Transceiver will be flown. Further missions are considered which will fly micro-technology now under development in the MISAT research program. The paper describes the Delfi-C3 mission and satellite with its payload. Emphasis is given to technical solutions and the way the project is implemented in the university's educational program. An overview is given of the current status of the project and plans for the future development of Delfi missions are outlined.

1 Introduction

Delfi-C³ [1] is the first in a series of nano-satellites of the Delft University of Technology. The satellite has been developed by students and staff of the faculties of

R.J. Hamann

Delft University of Technology, Faculty of Aerospace Engineering, Space Systems Engineering,
P.O.Box 5058, 2600 GB Delft, The Netherlands
e-mail: r.j.hamann@tudelft.nl, info@delfic3.nl

C.J.M. Verhoeven

Delft University of Technology, Faculty of Aerospace Engineering, Space Systems Engineering,
P.O.Box 5058, 2600 GB Delft, The Netherlands

A.A. Vaartjes

Delft University of Technology, Faculty of Aerospace Engineering, Space Systems Engineering,
P.O.Box 5058, 2600 GB Delft, The Netherlands

A.R. Bonnema

Delft University of Technology, Faculty of Aerospace Engineering, Space Systems Engineering,
P.O.Box 5058, 2600 GB Delft, The Netherlands

Aerospace Engineering and of Electrical Engineering, Mathematics and Computer Science. It will act as a technology test-bed for three payloads: Thin Film Solar Cells (TFSC), an Autonomous Wireless Sun Sensor (AWSS) and a radio-amateur, nano-satellite-based UHF/VHF linear transponder.

The project was initiated in November 2004. Based on a three-unit CubeSat, Delfi-C³ will be launched from a standard CubeSat deployer such as the X-POD. Delfi-C³ will make use of the amateur radio frequency bands for its telemetry down-link and tele-command uplink. Software will be made available to participating amateur radio operators, which will allow them to decode, display and send the telemetry to the central ground station in Delft. The satellite will not include an active attitude control system. A passive rotation rate damping will be used to limit its rotation rate. Furthermore, as the primary payloads do not require operations in eclipse a battery has been avoided, which simplifies the spacecraft design. A piggyback launch in September 2007 has been arranged on a Polar Satellite Launch Vehicle (PSLV) from India. It will be injected in a circular 98° inclination Sun-synchronous orbit at 630 km altitude. After launch and deployment, three months of gathering payload data is foreseen, after which the satellite will be switched into linear transponder mode. Figure 1 shows an exploded view of the Delfi-C³ satellite.

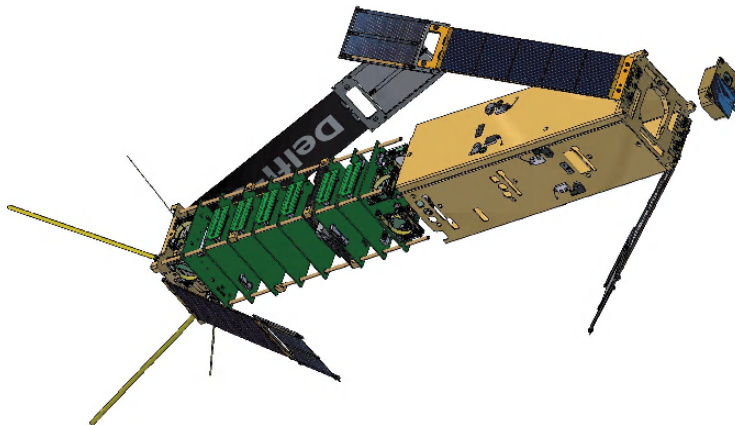


Fig. 1 Delfi-C³ satellite (exploded view)

At the date of writing Delfi-C³ subsystems have been produced and are under test. System integration has started and functional and environmental tests are scheduled for completion before July 2007.

2 Technology Payloads

The TFSC (Fig. 2) payload is based on the latest development in the area of photovoltaic cells by the company Dutch Space. The cells consist of a Copper Indium Gallium diSelenide (CIGS) photovoltaic layer, which is deposited by evaporation

on a titanium base layer of 25 micrometers. The cells will be integrated tile-wise, ensuring a minimal loss of active cell area. The aim of this new type of solar cell is to create a lightweight and low-cost product for future space applications. The target is a 50% cost reduction of solar arrays, while improving the power to mass performance with 50% compared to conventional solar cells. The efficiency will be more than 12%. Measuring the characteristic current-voltage curves and cell temperature under varying Sun input will test the performance of the TFSC payload. As the temperature of the thin foil cannot be measured directly, it will be measured by determining the electrical resistance of a dummy titanium cell mounted close to the actual TFSC's. The TFSC's cannot be body mounted because of their fragility, but also because of the high cell temperatures that would result from such a configuration. For this reason the four pairs of TFSC's are mounted at the tip of each deployable solar panel.

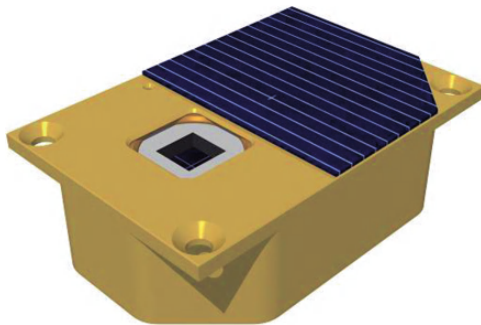
Fig. 2 TFSC payload



The AWSS (Fig. 3) is a development of TNO in the Netherlands [2] and is placed at the top and bottom of Delfi-C³. The sensors will have a half-sized GaAs solar cell as their own power supply, making them independent of the satellite's electrical power system. This autonomy is accompanied by a wireless radio frequency link, using an adapted commercial off-the-shelf transceiver.

The UHF/VHF transponder, which doubles as a transceiver in science mode, is of conventional design. It is however, for the first time that such a transponder, allowing five simultaneous users, will fly on a CubeSat.

Telemetry, both science and housekeeping data, is broadcasted continuously and may be received with a standard radio-amateur ground station. The satellite is

Fig. 3 AWSS payload

operated from the main ground station at the Delft University of Technology, and has a total of 25 minutes ground contact time in three passes per 24 hours.

To increase the amount of data received, a distributed ground network has been created composed of radio-amateurs worldwide. By means of software made available to them by the Delfi-C³ project they will be able to receive and decode the telemetry and to send the raw and decoded data to the operations center in Delft, where they are processed and made available to the users Dutch Space, TNO and, of course, the Delfi-C³ project itself.

3 Technical Constraints

Most important constraints for a nano-satellite are size, power and mass. The size limitation drives towards the application of surface mounted devices (SMD's) wherever possible and requires the implementation of deployment mechanisms for e.g. the eight antennae, which have in this case a maximum length of 0.5 m, which should be accommodated in an envelope with a maximum length of 0.3 m. So a dedicated design using a tape spring (measurement tape) that allows to store each antenna in a volume of 10 × 40 × 50 mm has been developed (see Fig. 4).

The Delfi-C³ architecture originally has been designed as a star architecture with one, single central computer. However, this led to a system bus of more than 120 wires running from top to bottom through the satellite, consuming 18% of the total mass budget. The transition to a decentralized Command and Data Handling Subsystem (CDHS), where each print is controlled by a dedicated microcontroller resulted in a mass saving of 11% (star architecture: 0.530 kg, 18% of total; decentralized architecture: 0.214 kg, 7% of total).

The transmitter uses most of the power (2 out of 3 Watts available). It then became obvious that conventional over-current protection (OCP) of the individual prints and subsystems would consume too large a part of the remaining power to allow satisfactory satellite operations. The solution was the introduction of a decentralized Electrical Power Subsystem (EPS), where a separate controller is used to protect and switch each print or subsystem. That way a power saving (exclud-

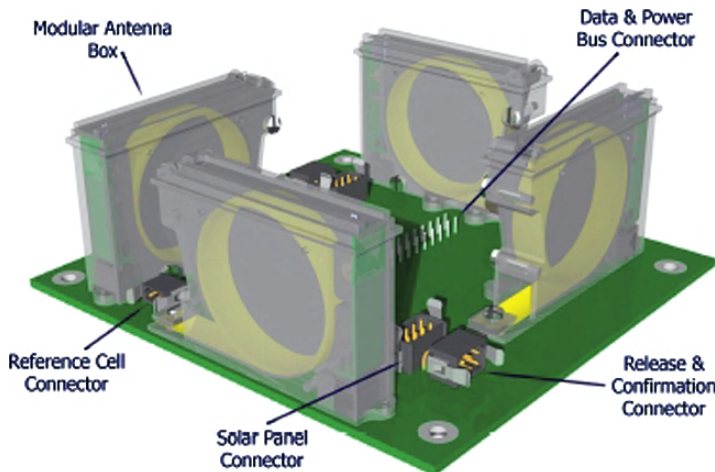


Fig. 4 Modular antenna box (MAB)

ing transmitter power) of 11% was achieved (conventional switch and OCP design: 0.182 Watt, 18% of total; decentralized “switching” micro-controllers: 0.073 Watt, 7% of total). The resulting architecture using no less than 18 micro-controllers is shown in Fig. 5.

4 Project Implementation in the Educational Program

The project team currently comprises about 25 students, who are in their last year of studies; half of them are in Aerospace Engineering, and half in Electrical and Computer Engineering. Although the project originally has been started with MSc students only, there is currently about equal participation of MSc and BEng students. It is felt that this is an ideal team composition in the later phases of the project. The work the students do on Delfi-C³ is part of their final thesis work. Six staff members are involved in the project for in average 50% of their time.

A “self-managed” student team has run the first year the project. As the students were very committed to building this first Dutch university satellite, this has worked very well. Also the fact that two well-known space companies are customers for the project was very stimulating and offered great learning opportunities for the students involved. However, the transition from a paper study to more serious hardware bread-boarding has been made too late and appeared to require more guidance by staff, in particular by staff with industrial experience. Student tasks need then to be specified more accurately, and achieving timely technology readiness and maintaining the schedule must get priority over the “learning by making mistakes”, which is the normal operating mode in a student run project.

This certainly is the case, when a commitment for a launch date has been made. In this phase students have to execute the tasks that are most urgent, even if they are normally considered to be too “menial” for MSc or BEng level graduation work or

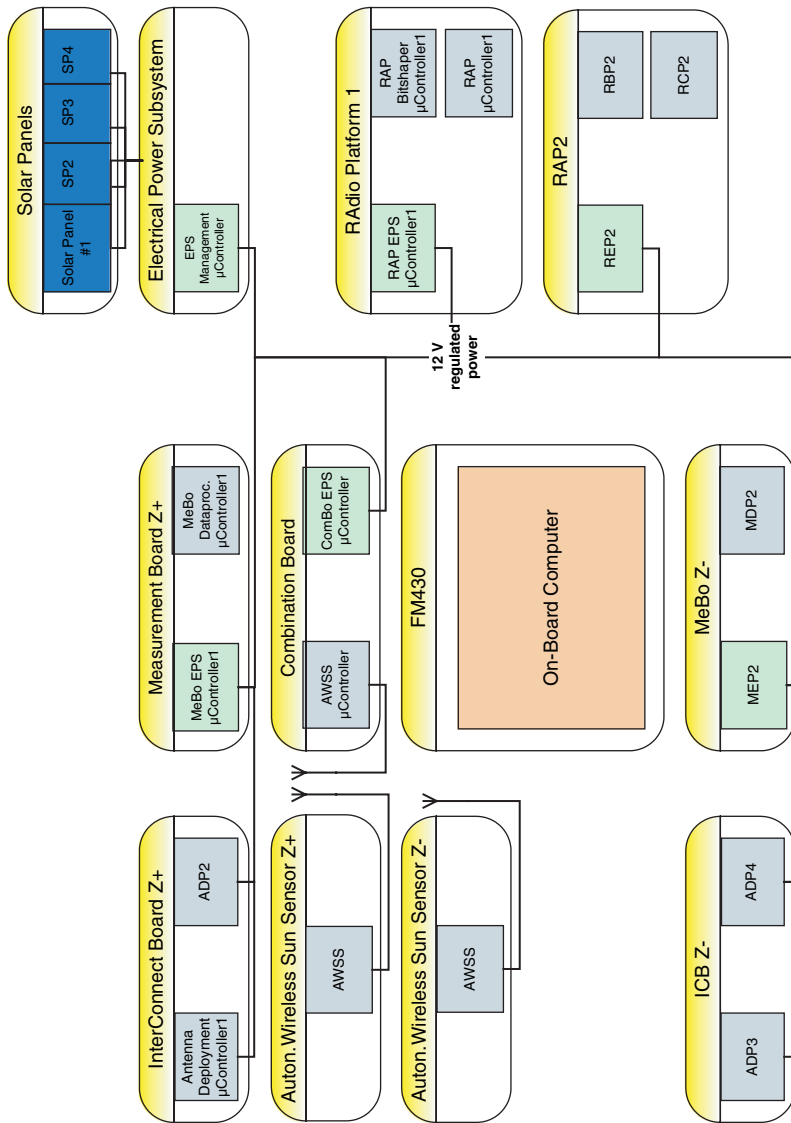


Fig. 5 Delfi-C³ controller architecture (light blue boxes: decentralized CDHS; green boxes: decentralized EPS)

if they are not directly in their field of expertise (it is, however, our firm opinion that this offers many unique learning moments to the students).

Also, the demands on the university's infrastructure increase in this phase: Workshop capacity, delivery times, fast design-to-test iteration cycles, specific production expertise are key requirements which are often difficult and sometimes even impossible to meet in an academic context. Good relations with established electronic and space industries are essential to achieve the technical project goals, and, for certain tasks, a direct use of their facilities and expertise should be made.

Finally, the use of Delfi-C³ for educational purposes is not limited to the higher education institutions directly involved in the project. Thanks to the mission architecture selected it is very well possible to equip secondary schools with a relatively simple and cheap ground station (kit), that allows the students to e.g. receive the satellite data, to make these visible and execute ground-based reference experiments, to carry out satellite ranging experiments and to explore the fundamentals of orbital mechanics. Activities in this sense have been started and help to rise the interest in engineering sciences with the younger generation.

5 Current Project Status

Delfi-C³ is currently in the test and verification phase. Subsystem testing has been completed for the most part and integration testing has also started.

Subsystem testing began in January 2007 with the Combination Board (ComBo). The ComBo is the interface of the FM430 On-Board Computer (OBC) board with the rest of the satellite and it houses the AWSS receiver. Problems discovered required repairs, which rendered the first ComBo as "non-flight". A second ComBo has been tested and will be flight hardware. The two InterConnect Boards (ICB's) house the antennae and its microcontrollers manage the deployable mechanisms: two solar panels and four antennae. Tact switches monitor the deployment status and a simulation board was made to simulate the mechanisms during functional testing (Fig. 6). For the moment, simulated deploy times have been used to test the functionality. Actual deployment times will be implemented following the deployment tests.

The two Measurement Boards (MeBo's) perform the measurements of TFSC payload. Initial problems with the circuits have been resolved and the board is now being functionally tested. Tests involving the Voltage Controlled Oscillator, which will be used as a back-up in case of OBC failure, are scheduled to be conducted anytime now.

Version 2.0 of the OBC software is almost completed and OBC – subsystem interface testing is underway.

Design and development of the Radio Amateur Platform (RAP) proved to be quite an effort, but an elegant breadboard of the RAP has been completed and the flight PCB is expected to come in soon.

Ground support equipment for the assembly, integration and test phase is being build. A stack dummy, for fit-checking subsystem boards, and the integration jig

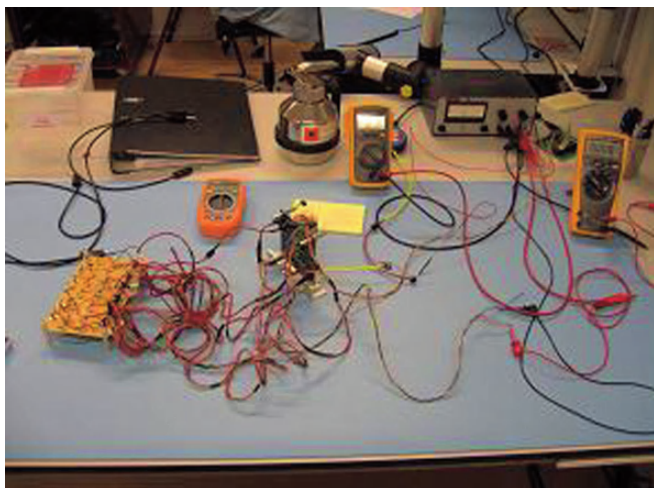


Fig. 6 ICB test setup

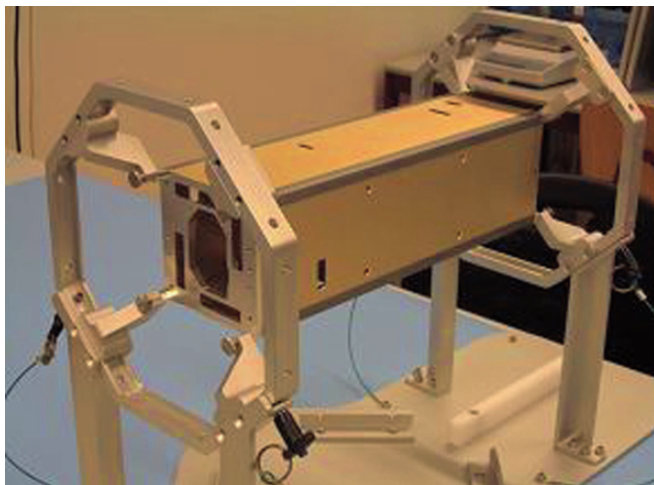


Fig. 7 Delfi-C3 chassis with *top* and *bottom* panel in integration and test jig

have just been completed. Figure 7 shows the integration jig that will also support the satellite during thermal-vacuum testing.

At this moment work is focused on the ground system. The first version of the telemetry decoding software has been produced and tested. Work on the science and housekeeping data post-processing system is progressing well. The User and Software Requirement Documents are being compiled and architectural and detailed design and coding will be started next month. The Delfi ground station has been used already for several other missions (e.g. SSETI Express) and is being upgraded to full redundancy (one of the lessons learned of that mission).

Much has been learned from the test and verification phase so far. Originally the idea was to have a “proto-flight” approach, but the problems encountered during the first subsystem tests of the Combination Board in January quickly proved that was not feasible, even for a small project like Delfi-C³. The test and verification phase was for Delfi-C³ the first moment during the project in which the design was properly confronted with real life practice and it became clear that (elegant) breadboards should have been built earlier in the project, if short development times of about two years are targeted for. Getting concept and ideas out in practice could have reduced the number of problems that were encountered during the beginning of the test and verification phase considerably. This is something that definitely will have to be done in the projects that follow.

Another example of the failure of the proto-flight approach is the fact that the Modular Antenna Boxes had to go through five design and test cycles before a satisfactory performance was achieved. For more details on the verification program of Delfi-C³ see [3].

6 Delfi-C³ FOLLOW-ON Mission

The spare of the Delfi-C³ satellite possibly will be used for a follow-on mission. Modifications for this mission will be made in the Electrical Power Subsystem and the Communication Subsystem.

The DelfiC³ satellite has, like many other satellites, different operation modes that require different ways of signal coding and transmission. A specific transceiver optimal for one of the operation modes may be suboptimal for another mode. As CubeSats are too small to carry separate optimal transceivers for each mode, an elegant solution to this problem is the reconfigurable transceiver. In such a transceiver the OBC takes many decisions during the mission that are normally taken in design phase by the designer and remain fixed during the rest of the operational life. This means that, for example, the architecture of the transceiver is not fixed, but “designed and implemented” by the OBC based on the specific transmission needs, like data rate, modulation scheme and the environmental circumstances like available power and quality of the transmission path. Since it is possible to implement most of the transceiver as a system-in-a-package (SIP), which is a micro-electronic system consisting of several integrated circuits (IC’s) bonded together and put into a single IC-package, the volume and mass penalty for having such an Advanced Transceiver (ATRX) onboard is negligible. The power consumption is never more than exactly needed to offer the required quality of service, since the OBC can always implement the optimal transceiver architecture.

Delfi-C³ has transmission modes in which the amplitude of the transmitted signal carries information and modes in which the information is contained in phase or frequency of the signal only. A first step into the direction of a fully reconfigurable transceiver is the design and implementation of a reconfigurable power amplifier (PA). Due to the limited onboard resources, the efficiency of the PA is of extreme importance. The antennae should transmit the maximum power available in the satellite.

The core of the PA in the ATRX is a switching amplifier. The power from the solar panels is put directly to the antennas via high efficiency switches that can modulate the phase and the frequency of the transmitted power. This is a very high efficiency mode with efficiencies (theoretically) much better than 90%, but unfortunately without the possibility for amplitude modulation. In this mode the PA can only be used to transmit frequency/phase modulated telemetry data. In transponder mode, also amplitude modulation must be possible. To achieve this, a high efficiency DC/DC converter modulates the power from the solar panels with the information. This amplitude modulated power supply is then fed to the switching PA that puts it to the antennas at the right carrier frequency and that can add frequency or phase modulation if required.

When a very high linearity is required, negative feedback will be applied to the PA-DC/DC converter system. Negative feedback is the most powerful means to linearize a system. Normally the stability of the feedback loop around a complex amplifier system might be questionable, but in the (also electrically) small and well-defined SIP-module, stability can be guaranteed.

Figure 8 shows a diagram of the PA system of the ATRX. The mode-selection switches are used by the OBC to put the PA in the optimal mode for a specific transmission, varying from highly linear with still a very good efficiency to maximum power output without amplitude modulation at an extremely high efficiency.

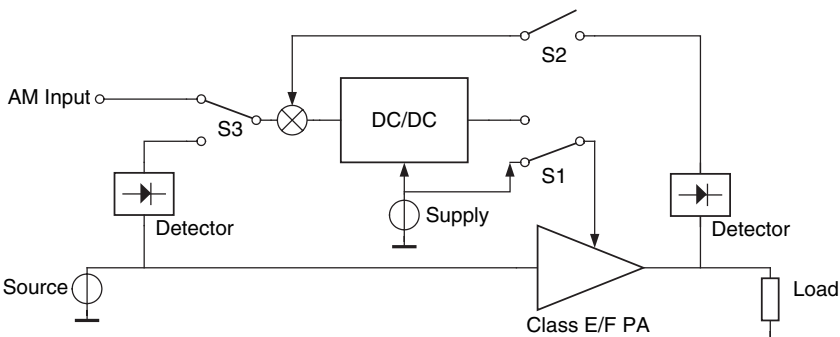


Fig. 8 Power amplifier system of ATRX

In this follow-on mission also a more advanced (maximum power point tracking) EPS will be flown, where the excess power will be used to maximize the transceiver performance. Actual realization of this mission depends on the success of the Delfi-C³ launch and operations and on the success of identifying candidate technologies from the MISAT program (see section 7) for a 2009 mission.

7 MISAT Derived Missions

Within the MISAT program [4], see Fig. 9, a number of micro-technologies are developed which are potential candidates for next Delfi missions. The AWSS is

already a pre-development of the Micro Sun Sensor, and the RF Front End and Smart Power technology will be incorporated in the Delfi-C³ follow-on mission.

For a next mission micro-propulsion and Micro Navigation System components may for example be combined in a simple formation-flying mission. Another possibility is to develop a nano-satellite attitude control system based on a micro-inertial platform. In the second half of 2007 a project will be started to identify candidate technologies for this third Delfi nano-satellite. Actual choice will depend the availability of flight-ready prototype technology end of 2009.

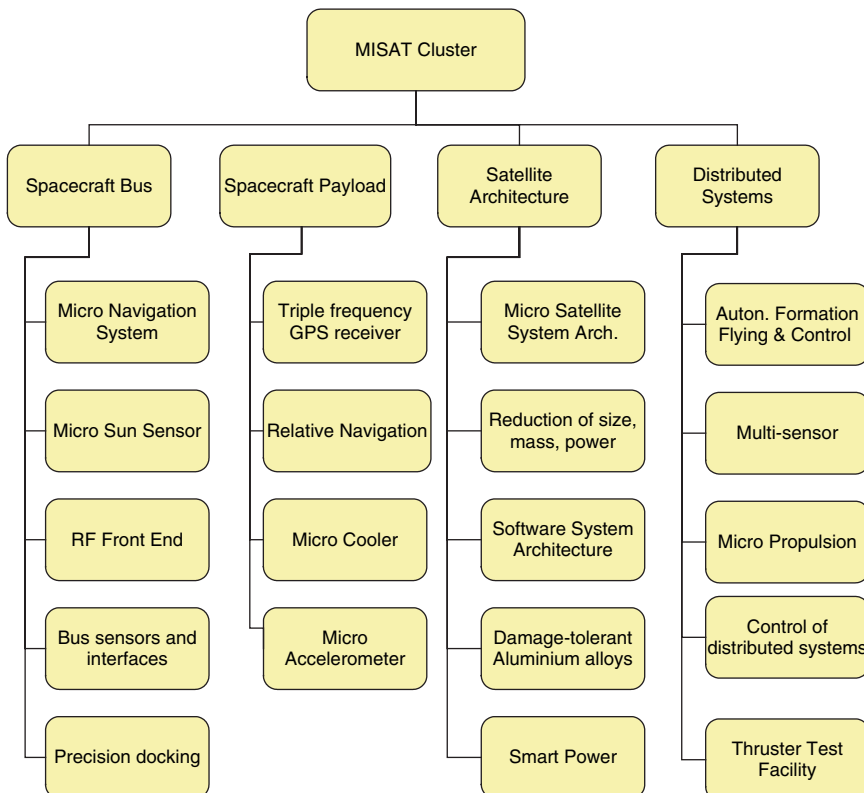


Fig. 9 Micro-technology development in the MISAT research program

References

1. W.J. Ubbels, F.A. Mubarak, C.J.M. Verhoeven, R.J. Hamann, G.L.E. Monna, The Delfi-C³ Student Nanosatellite – an Educational Test-Bed for New Space Technology, *Proceedings of the AMSAT UK 21th Annual Colloquium*, Guildford, UK (2006).
2. J. Leijtens, K. de Boom, Small sensors for small (and other) satellites, *Proceedings of the 6th IAA Symposium on Small Satellites for Earth Observation*, Berlin, Germany (2007).

3. A.A. Vaartjes, R.J. Hamann, R. Amini, Integration and Verification of a Command and Data Handling Subsystem for nano-satellite projects with critical time constraints: Delfi-C³, *Proceedings of the 58th International Astronautical Congress*, Hyderabad, (2007).
4. W. Jongkind, The Dutch MST Program MicroNed and its Cluster MISAT, *Proceedings of IC-MENS 2005*, Banff, Canada (2005).

Session 9

Spacecraft Bus

Development of the Method of the Creation of Micro-Satellite (~ 50 kg) Platforms for the Fundamental and Applied Research of the Earth and Near-Earth Outer Space

S.I. Klimov, V.G. Rodin, L.M. Zelenyi, and V.N. Angarov

Abstract The development of the method of the creation of micro-satellite (~ 50 kg) platforms for the fundamental and applied research of the Earth and near-earth outer space is complex problem both the scientific and technical plan, connected with development and use of contemporary spacecraft (SC) and with the scientific methods problems of conducting basic space research. All these problems are logically connected with the hierarchy of preparation and realization on board SC of experiments. At present in space physics and astrophysics is accumulated the significant observant material, obtained by SC. Great successes are achieved in the theoretical studies of near-earth space, atmosphere and lithosphere of the Earth. There are serious studies of laboratory and computer simulation. Examination from the united positions of entire complex of preparation and conducting of basic space research leads to the need of the association of the efforts of scientists and engineers, who carry out the study of each of the directions enumerated above.

1 Introduction

In the last decade because of the reduction of financing the entire space industry, presence of the conversion launch systems, qualitatively new achievements of microelectronics and micromechanics, accessibility of the elements of the space systems

S.I. Klimov
Space Research Institute (IKI), RAS, Profsoyuznaya 84/32, 117997 GSP-7 Moscow, Russia
e-mail: sklimov@iki.rssi.ru

V.G. Rodin
Space Research Institute (IKI), RAS, Profsoyuznaya 84/32, 117997 GSP-7 Moscow, Russia

L.M. Zelenyi
Space Research Institute (IKI), RAS, Profsoyuznaya 84/32, 117997 GSP-7 Moscow, Russia

V.N. Angarov
Space Research Institute (IKI), RAS, Profsoyuznaya 84/32, 117997 GSP-7 Moscow, Russia

much attention began to be given to the use of small space crafts: micro-satellite – MS (100–10 kg); nano-satellite – NS (10th kg) for conducting of scientific and applied research.

The analysis of the launching of small SC (mass to 300 kg), carry out in the period from 1986 through 2000, shows that this segment of space activity intensively commercialization. In Table 1 [2] is shown the distribution of the number launched small SC the categories: military, civil (budgetary), commercial.

The comparison of the periods of 1986–1990 and 1996–2000 demonstrates the clearly expressed tendency: a considerable increase in the portion of the starting of civil (2,5 times) and especially commercial (from 1% to 38%) SC occurred due to the sharp (four times) reduction of the share of the starting SC of military designation.

How this tendency it can influence conducting basic and applied space research?

At present in space physics and astrophysics is accumulated the significant observational material, obtained by SC. Great successes are achieved in the theoretical studies of near-earth space, atmosphere and lithosphere of the Earth. There are serious studies of laboratory and computer simulation. Examination from the united positions of entire complex of preparation and conducting of basic space research leads to the need of the association of the efforts of scientists, who carry out the study of each of the directions enumerated above. In this case it is necessary to carry out an integral approach to the solution of the problems presented by the way:

- the development of the methods of introducing the contemporary technological-design solutions in the process of creating of constructions and systems of micro-satellite platforms with the use of achievements of physical instrument manufacture, microelectronics and micromechanics;
- the development of the new methods of experimental studies of the Earth and near-earth outer space for their realization on contemporary highly effective SC;
- theoretical analysis method control onboard system micro- and nano- space platform with use achievement microelectronics and micromechanics for purposes guarantee high demand on their orientation and stabilization;
- conducting the laboratory and numerical simulation of control processes by onboard systems of micro-platform for the purpose of the determination of the critical elements of models.

Promising trends in development of experimental physics require of ever more precise and more highly informative scientific instruments. Moreover, situation is complicated by a constant reduction of financing scientific studies, even in the developed countries. This specifies the need for development and creating the new generation of scientific instruments with the light weight and the required power, the high level of the metrological parameters.

Since 2004 in the Space Research Institute of RAS is conducted the work on the theme “Creation of the onboard platform of the micro-satellite of applied and scientific designation on the basis of contemporary technologies and developments”,

included in the program of basic research of Presidium RAS "Changes in the environment and climate: natural catastrophes".

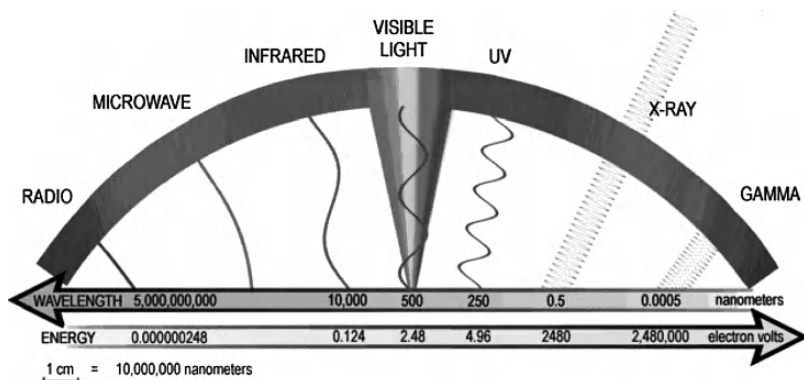


Fig. 1 Spectrum of electromagnetic radiation

At present micro-satellite sufficiently widely are used in the practice, including for warning and liquidation of extraordinary situations. In this case in practice is used the relatively narrow range of the electromagnetic radiations of the visible region – visible light (Fig. 1). Using a large experience of basic space research, SRI RAS in last 2 years studies the scientific programs with the use of micro-satellite, oriented to the study of infrared, ultraviolet – UV and X -ray ranges not only for basic space research, but also oriented to the tasks the study of some aspects of extraordinary situations.

The long-wave electromagnetic radiations (in Fig. 1 they must be represented on the left side of lower than the radio-frequency band overlap three orders in the frequency, from the portions MHz to first Hz), utilized for studies of plasma processes in space, they have the same value as seismic waves for studying the structure of the Earth. In comparison with the electromagnetic processes in other regions of physics, wave in the plasma they possess a number of specific special features. The fundamental value the resonance effects have from these special features: interaction of waves and particles, the transformation of waves, the formation of resonators and waveguides. Because of resonance effects, ULF-wave they transfer information about the dynamic phenomena in the near-earth space and the upper atmosphere, and they reach the amplitudes, sufficient in order to have an active effect on the flow of plasma processes and to effectively accelerate magnetosphere electrons. They determine some parameters of space weather thus. ULF disturbance accompany all geophysical phenomena, connected with the large release of energy – the magnetic storms, explosions, hurricanes and thunderstorms, earthquakes, and they are one of the basic agents, which connect in these periods different geophysical shells. Recorded by satellite and ground-based magnetometers ULF pulsations of the terrestrial magnetic field are the reflection of magnetohydrodynamic (MHD) waves in the near-earth medium.

2 Micro-Satellite Platform for Monitoring Greenhouse Gases (CO₂) and Catastrophic Phenomena on the Surface, in Atmosphere and Ionosphere of the Earth

Atmospheric carbonic acid, as basic greenhouse gas, plays the most important role in the climate of the Earth, absorbing the thermal radiation of the earth's surface, and preventing its emission into the space. Circulation CO₂ and generally carbon in the atmosphere, the ocean and the biosphere to the high degree is checked by natural factors, but it is known in also the time that 30% an increase of the concentration of this gas in the atmosphere occurred in the last 100 years [4]. The possible climatic consequences of this process are intensively studied by the leading scientific centers of entire peace and serve as the object of serious political discussions. In the last 40 years of the observations, which are led with the aid of the ground-based network, they show that only about half of the anthropogenic CO₂ remains in the atmosphere. Another half is absorbed by ocean and continental ecosystems. However, the measurements existing today ensure neither the necessary scope nor permission, necessary for the identification of drains CO₂. In particular, there are serious indications of the powerful drain CO₂ in the northern hemisphere, but it is not possible to divide the contributions of North American and Asian continents and oceans. For the verification of numerical models and forecasts comprised on their basis, for the evaluation of the role of different processes and reservoirs in the balance of carbon dioxide the very precise and localized measurements of its concentration in the atmosphere are necessary. Is well known the political aspect of this problem.

At the present moment in the world there are no satellites, which make it possible to solve this problem both globally, and it is regional [5]. Measurements with high spectral resolution in the broad spectral band in combination with the theoretical examination of the processes of the transfer of harmful substances will make it possible to make a serious contribution to the solution of this problem. Monitoring of low component and harmful impurities in the atmosphere is another most important task. Measurements by the method of solar radioscopy will make it possible to obtain the data about the scattered pollution due to the high sensitivity of equipment.

Comparatively recently appeared the new and extremely interesting data about the distribution in the atmosphere of the Earth of the greenhouse gases, connected with the processes in the Earth's atmosphere and on the Earth's surface. It was shown that methane CH₄ is one of the most important greenhouse gases of the Earth's atmosphere, in the essential measure, which determines radiation balance and the climate of planet. The effectiveness of absorption by methane of the thermal radiation of the earth's surface is 60 times higher than in CO₂. Ejections CH₄ into the atmosphere, according to the estimations of the reaching at present 500 megatons per year, and observing increase in its atmospheric content, can lead to a considerable increase in its temperature in the next decades. In this case the process of increasing the temperature is increasing, since its increase strengthens the isolation of methane into the atmosphere due to the melting of soils in the regions of permafrost.

Thus, the role of methane (concentration of which was doubled in comparison with the preindustrial period and it continues grow in connection with the tendencies of the warming up of climate) in the course of time grows and approaches a role of the strongest greenhouse gas – CO₂.

In the process of works according to the Program of basic research of the Presidium RAS “Changes in the environment and climate: natural catastrophes” we showed that measurements of reflected and scattered solar radiation in the UV- the neighbor IR ranges give the possibility of the remote sensing of basic greenhouse gases, such as CO₂ and CH₄, and also numerous atmospheric admixtures. In the case of catastrophic phenomena this method makes it possible to judge the course of the process, proceeding in the center of event, from the sufficiently large distances.

Measurements on the spacecraft make it possible to conduct the global monitoring of the distribution of greenhouse gases in the atmosphere of the Earth and plasma- wave effects in atmosphere and ionosphere of the Earth, that influence both the environment and the person himself and the different spheres of his activity.

Are most promising the spectroscopic observations in the neighbor IR range, which make it possible to conduct the precise measurements of the complete content CO₂ in the atmosphere with satisfaction of two conditions: high spectral resolution, which makes it possible to distinguish the separate unsaturated spectral lines in the weak strips CO₂ and a good knowledge of the optical path, which passes entire thickness of the atmosphere. Small overall sizes and mass of equipment play important role. The preparation of the compact spectrometer of high resolution for the Project Venus Express (14) makes it possible to propose for the micro-satellite “Chibis” the practically finished development of spectrometer ORACUL with resolving power of $\lambda/\Delta\lambda \approx 20000$ in the range 1.58 mkm. In the instrument the diffraction grating of the echelle grating, which works in the high orders of diffraction, is used.

Using, first of all, the experience, obtained in the implementation of projects “Venus- Halley”, “Phobos” and “Interball” on the technical tasks of the SRI RAS were carry out serious studies in the field of development and creating the sensors of the electromagnetic parameters of space plasma – the AC and DC magnetometers, the gauges of the tension of electric field and density of three-dimensional current. For the ferro-probe magnetometers (FZM) reduction in the weight and required power was achieved not only method of using the new electronic components, but also by development of new measurement procedure. Scientific and technological studies made it possible to reduce the internally-produced noise FZM, and now typical noise level our FZM it is about 10 pico-Tesla at the frequency of 1 Hz, and record value – is below 1 pico-Tesla.

As a result of prolonged studies the original super-lightweight version of induction magnetometers was created (IM). These new IM can have frequency range of approximately six decades with upper boundary ~ 1 MHz, noise level – several femtoTesla weight of approximately 75 grams, including electronics. The lightened model of electric probe for measuring the tension of electric field is created. Is developed new instrument – wave probe, which unites three sensors in one housing: the split Langmuir probe, IM and the gauge of electric potential. Its effectiveness is

confirmed by both the theoretical studies and by results of simulation experiments in the plasma chamber. These instruments underwent flight tests on board the satellite “Sich-1M” [15].

3 Study of the New Physical Mechanisms of the Electrical Discharges in the Atmosphere

A number of the physical phenomena in the atmosphere, which fundamentally changed our idea about the lightning discharges, are discovered in recent years.

1. In the observations from automatic spacecraft COMPTON and RHESSI are discovered the exceptionally powerful pulses of the gamma emission, which go from the Earth. Energy of pulses reaches tens of kJ, i.e., to 10^{17} – 10^{18} of radiation quanta with the energy 100 keV and above [18]. At present these phenomena in detail are investigated. It is experimentally proven that these pulses it is generated during 2–3 ms before the basic lightning discharge. COMPTON and RHESSI they were not intended especially for thunderstorm studies. Therefore, the measurements carried out on them do not bear complex nature and do not possess a sufficient time resolution.
2. Is discovered the generation of the short (\sim 1 s) single radio bursts, which lead to the emission of the radio-frequency pulses of the super high power (to 100 GW and above) [6]. Pulses are generated in the thunderstorm clouds at the large heights of 13–20 km such pulses create the radio emission in the very wide frequency band, observed at the distances to several 1000 km.
3. In the ground observations are discovered the flashes of the gamma emission, associated with the jumps of electric field, characteristic for the propagation of the stepped leader of lightning]. Gamma emission covers the area of 0.3–0.5 square kilometers, and possibly also more.

At the basis of the observed phenomena lies the theoretically forecast in the FIAN new physical phenomenon, which was called breakdown on the running away electrons [1]. The electrons of relativistic energies play the determining role in this process. The avalanche of the running away electrons being born in the course of the development of breakdown serves as the source of gamma emission. The special feature of this form of breakdown is the fact that it occurs in the low electric fields, but it requires for its initiation of the seeding particles of the high energy. The extremely large number of electrons of low energies simultaneously is born. The motion of these electrons in the electric field of thunderstorm gives birth to the powerful pulse of radio emission. Fundamental role in the development of breakdown on the running away electrons play the cosmic rays of high energies. Extensive air shower contains a large quantity of high-energy electrons, which serve as the required priming of breakdown. The development of extensive air shower with the particles of high energies at high altitudes occurs only if it is move at the angle, close to the horizon. In this case occurs strengthening breakdown on the running

away electrons and notable increase in its three-dimensional scale. For this very reason, according to theory, discharges at high altitudes bear so powerful a nature both in the radio and in the gamma emission.

The practical importance of the proposed studies is determined by the following circumstances.

1. Super-power gamma emission at the heights of 10–20 km is of significant interest from the point of view of safety of both the passengers and the aircraft of civil and military aviation.
2. Large areas, covered with intensive gamma emission on the Earth, can prove to be important both from the point of view of ecology and from the point of view of safety of people.
3. Super-power single radio-frequency pulses have powerful emission in practice in entire working range of the radio waves (to 3 GHz and above). They can serve as convenient natural radiation source for creating the global monitoring of radio communication.

4 Micro-Satellite Platform “CHIBIS”

4.1 Development of the Methods of Introducing the Contemporary Technological-Design Solutions in the Process of Creating of Constructions and Systems MP

In the last decade because of the reduction of financing the entire space industry, presence of the conversion starting systems, enormous achievements of microelectronics, accessibility of the elements of the space systems much attention began to be given to the use of small automatic spacecraft (micro-satellite) for conducting of scientific studies. In particular, SRI RAS in the cooperation with the Russian partners from the space industry was developed and with the support of the RSC “ENERGIA” was injected into orbit during March 2002 the micro-satellite “Kolibri-2000” [11]. The injection of the micro-satellite “Kolibri-2000” into orbit, close to the orbit of the ISS, is realized on 20 March, 2002, by separation from ship the “Progress M1-7”, redocked before this from ISS. Study program by “Kolibri-2000” included the following tasks: monitoring strong technogenic by action in the ionosphere; a study of ionosphere disturbances with the development of the magnetic storms in the terrestrial magnetosphere [12].

All systems and scientific instruments of the MS (mass in the equipped state – 20.5 kg, energy consumption 30 W) without the failures worked in entire period of its ballistic existence.

The basis of the technological-design solution of the “Kolibri-2000” was the thorough study of layout MS, on the basis of the main requirement, presented to the project, need for separation from that unjointed from the ISS, after the execution by cargo transport ship (CTS) “Progress” it of basic task,. This led to the need of

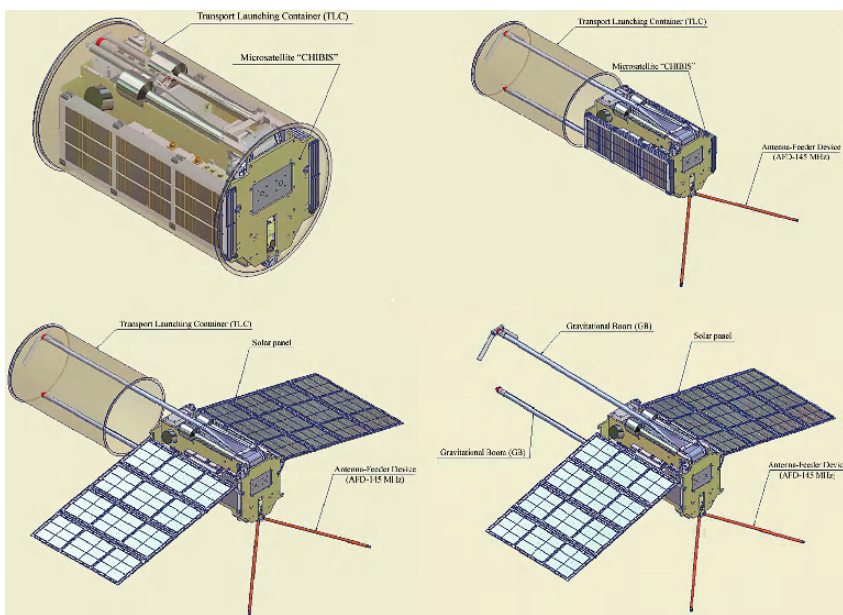


Fig. 2 Diagram of the separation (“launch”) of the microsatellite from TSC

using the specialized starter. Task was solved by developing the transport-starting container (TSC), intended also for the fixation MS inside the TSC during the injection the CTS into orbit and the jointing with the ISS. For the realization of the “starting” of the “Kolibri-2000”, the TSC were established by cosmonauts on the CTS “upper lid”, find even in docked configuration with the Service module (SM), i.e., inside the ISS.

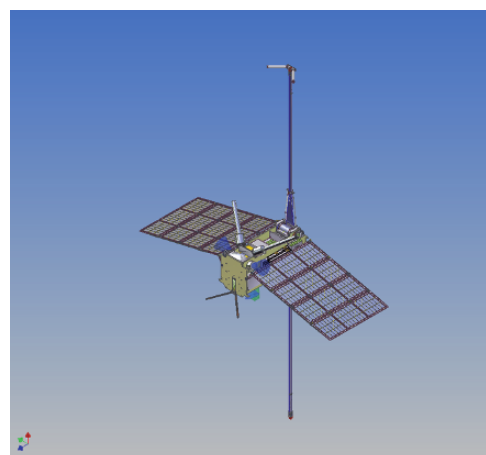


Fig. 3 Total view of microsatellite “Chibis”

In the course of creating the “academic” microsatellite “Chibis”, in which participate and acquire real experience young specialists, is used the contemporary concept of the “flying instrument”, which optimally combines the requirements of scientific instruments and micro-satellite platform. This makes it possible to conduct scientific space studies in Russia without the attraction of the expensive automatic spacecraft, developed by enterprises in the space field.

The development of the complex of scientific instruments proposed within the framework of project practically does not have an analog. For the first time is developed the complex of measuring equipment, oriented to the study of the lightning discharges, which entire overlapping practically spectrum of electromagnetic radiations and precisely under this task is created the design of small automatic spacecraft, its systems of the collection of information and support systems.

For the realization of the above-indicated projects, drawing on experience of development and use of a micro-satellite “Kolibri-2000”, is carry out the development of micro-satellite “Chibis” [19].

Main technical characteristics of the micro-satellite “Chibis”.

- Mass (total) –40 kg.
 - Scientific instruments –12.5 kg.
 - Service system –18.2 kg.
- Construction and temperature control system –9.3 kg.
 - Orbit –circular with the height \sim of 480 km.
- Orientation systems:
 - types: the electromechanical (electro flywheels); magneto dynamic (electromagnets); gravitational (boom);
 - accuracy of the determination of orientation from the sensors (starry, solar) and systems GPS – GLONASS –to 2- angle. deg.
 - accuracy of guidance $+/-$ 3–15 angle. deg.
- Data-transmission system:
 - S/C-Earth –1.2 Mbit/s
 - the capacity of onboard storage –100 Gbaytes
 - the volume of the adopted from the board information \sim 50 Mbayt/day
 - the radio frequency of command and telemetric links –145 MHz, 435 MHz. and 2.2 GHz
 - the system of onboard power supply –50 W:

Micro-satellite “Chibis” (Fig. 3) will be delivered onboard the ISS by cargo ship “Progress” analogous with the “Kolibri”. After separation from the ISS the orbit of the “Progress” will be raised to an altitude \sim of 500 km and the “Chibis” will be separated and it will begin to function in the working orbit.

5 Conclusion

In 2006 in SRI RAS is finished the phase “A”. Is developed the model composition of support and systems, construction of micro satellite “Chibis” and two complexes of scientific instruments.

The complex of scientific instruments #1:

- spectrometer for measuring the complete content CO₂ and CH₄,
- camera of optical range (spatial resolution 300 m),
- low-frequency flux-gate magnetometer (DC–64 Hz),
- high-frequency search-coil magnetometer (0.1–40 kHz),
- analyzer of the electromagnetic emissions (0.1–40 kHz),
- detector of ionosphere plasma (Ne and Ni in the range 1.10⁹–1.10¹³ m⁻³, Te 1000–6000 K).

The complex of scientific instruments #2:

- X-ray – gamma detector (range of X-ray and gamma emission – 50–500 keV),
- UV detector (range UV – emission – 300–450 nm),
- radiofrequency analyzer (20–50 MHz).
- camera of optical range (spatial resolution 300 m),

The results of space studies are used in many applications, including the education. Work with the schools is a natural method to inform the general public about the role of space studies for humanity. For this we are utilized radio amateur’s communication channels for the transmission of scientific information from the micro-satellite directly to the schools.

This work is executed with the partial support of the RFBR grants 06-02-08076 and 06-02-08244 and also within the framework of collaboration on basic space research between Russian Academy of Sciences and Bulgarian Academy of Sciences for “BalkanSat” project.

References

1. Gurevich A.V., K.P. Zybin, UFN 44 (2001) 1119.
2. Pyshnyi I.A., V.E. Chepiga, Launching of small artificial earth satellites with the use of carrier aircraft. M.: Mashinostroyeniye/Mashinostroyeniye – Polet, (2005) (in Russian) 168.
3. Chubenko A.P. et al., Phys. Lett. A 309 (2003) 90.
4. Cicerone R.J., E.J. Barron, R.E. Dickinson, I.Y. Fung, J.E. Hansen, T.R. Karl, R.S. Lindzen, J.C. McWilliams, F.S. Rowland, E.S. Sarachik, and J.M. Wallace., Climate change science: an analysis of some key questions, National Research Council, Washington DC (2001).
5. Dufour E., F.-M. Breon, Spaceborne estimate of atmospheric CO₂ column by use of the differential absorption method: error analysis. Appl. Opt. 42 (2000) 3595–3609.
6. Dwyer J.R. et al., GRL 32 (2005) L01803.
7. Fishman G.J., et al., Science 264 (1994) 1313.

8. Gurevich A.V., G.M. Milikh, R.A. Roussel-Dupre, Phys. Lett. A165 (1992) 463.
9. Gurevich A.V., K.P. Zybin, Physics Today, 58, May (2005) 37.
10. Jacobson A.R., JGR 108 (2003) D244778.
11. Klimov S.I., et al., Small Satellite for Eart Observation. 4th International Symposium of the International Academy of Astronautics (IAA) Berlin, April 7–11, 2003. Editors: H.P.Roser, R.Sandau, A.Valenzuela, (2003) pp. 95–98.
12. Klimov S.I., et al., Planet. Space Sci. 53 (2005) 349–356.
13. Koralev O.I., J.-L. Bertaux, I.I. Vinogradov, Compact high-resolution IR spectrometer for atmospheric studies //Proc. SPIE 4818, (2002) pp.272–280.
14. Koralev O.I., et al., ESA SP-554, Noordwijk, Netherlands: ESA Publications Division, ISBN 92-9092-865-4, (2004) pp. 73–80.
15. Korepanov V., et al., Adv. Space Res., 25(7/8) (2000) 1337–1342.
16. Nevejans D.E., et al., Applied Optics, Vol. 45, Issue 21, OSA, 5191–5206.
17. Smith D.A., et al., Radio Sci. 39(1) (2004) RS1010.
18. Smith D.M., et al., Science 307 (2005) 1085–1088.
19. Zelenyi L.M., et al., Proceedings of the 5th International Symposium of the International Academy of Astronautics, Berlin, April 4–8, 2005. Edited by Hans-Peter Roeser, Rainer Sandau, Arnoldo Valenzuela. Walter de Gruter, Berlin, NY (2005) pp. 443–451.

Session 10

Lessons Learned

Indigenous Mission of Satellite System Development Program in Taiwan

Shui-Lin Weng, Jer Ling, and Tung-Hung Tsai

Abstract Eight satellites were successfully launched in the first stage of three Taiwanese space programs. Among them, Formosat-2 launched in May 2004 with mission life of five years has performed an outstanding job in the field of disaster monitoring especially. Stepping into the second-stage long-term plan for the Taiwanese space development, the top priority for National Space Organization (NSPO) is to have an indigenous satellite on orbit. With the indigenous satellite on orbit in mind and appreciation of Formosat-2 performance, it is certainly essential for NSPO to launch another earth observation satellite as our next mission objective. In this paper, a brief description of mission definition with its associated payloads is presented and, then, following a satellite system design overview with its trade analyses is discussed. Note that the system design consideration is based on the fact that the mission is switched from former joining RapidEye constellation to the currently so-called Formosat-2 continuation mission due to unexpected surprise. Also, the satellite itself is composed of a bus platform of the intended heritage design with LEON-3 central processing unit (CPU) inside the on-board computer and accommodated with two categories of payloads for the remote-sensing application and various scientific missions. Commercial off the shelf (COTS) up-screening/qualification and validation/verification process is introduced to ensure their normal functions when operating in the severe space environments of the future flight.

S.-L. Weng

NSPO, Satellite System Development Program 8F, 9 Prosperity 1st Road, Hsinchu Science Park,
Hsinchu City 30078, Taiwan
e-mail: js.weng@nspo.org.tw

J. Ling

NSPO, Satellite System Development Program 8F, 9 Prosperity 1st Road, Hsinchu Science Park,
Hsinchu City 30078, Taiwan

T.-H. Tsai

NSPO, Satellite System Development Program 8F, 9 Prosperity 1st Road, Hsinchu Science Park,
Hsinchu City 30078, Taiwan

1 Introduction

Starting from 1991, three consecutive space missions were executed successfully by National Space Organization (NSPO) in Taiwan. Formosat-1, Formosat-2, and Formosat-3 are the names for those three that associated with different missions of science research, earth observation, and weather forecast, respectively. While each individual project was contracted to the corresponding satellite prime contractor accountable for the spacecraft development, many scientists, engineers, and managers from NSPO and other research institutes in Taiwan also earned hands-on experience by working with contractors side-by-side from the beginning to the end of the project. Seasoned skill has been built up and sound knowledge accumulated as well on every learner since then. Among them, Formosat-2 that was launched in May 2004 has performed an outstanding job in the field of disaster monitoring, such as earthquake, mud flood, land slide, tsunami flooding, typhoon/hurricane raid, and so on. By taking a look at the aforementioned remote-sensing images, we can certainly find that the earth environment is critical to everyone living in the world.

In this paper, a satellite system overview after the completion of preliminary design review (PDR) is presented. The satellite itself is composed of an intended heritage bus platform design with LEON-3 central processing unit (CPU) inside the on-board computer and accommodated with two categories of payloads for the remote-sensing application and various scientific missions. The earth observation instrument is designated as the primary payload, and the other five science payloads are attached on the bus external surface to perform both space and marine experiments. In addition, due to gaining export license permit from vendor-governed authority has been also an uncertainty to the program from the past experience, especially in such a complicated political environment. To overcome this restriction, use of commercial off the shelf (COTS) parts as many as we can, without shading the light of Taiwan first ever self-developed mission success is clearly a challenge to us. In attitude determination design, commercially available global positioning system receiver (GPSR) and a number of redundant fiber optic gyros are adopted with the star tracker for hardware implementation. COTS up-screening/qualification and validation/verification process is used to ensure their normal functions when operating in the severe space environments later on in the orbit.

2 Mission

The mission was originally intended for joining RapidEye constellation, becoming the 6th member of the family. The main purpose of the RapidEye mission, owned by RapidEye AG, Germany, is to establish a global monitoring service for agriculture, forest, disaster, and cartography while a constellation of five satellites deployed on a sun synchronous orbit will provide continuous observation of the earth. The polar orbit makes the global coverage possible and, with rolling spacecraft across 25 degrees each side, the global revisit time is within one day. A spacecraft preliminary

design review based on the RapidEye earth observation mission payload and satellite platform performances [1] has been passed [2] and then the work was conducted toward the critical design stage. However, the mission was terminated at this point unfortunately because the export permit, a required contractual document, had not been authorized to the mission support contractor. Thus the mission is revised to continue the Formosat-2 mission. Although different imaging payload will be used, it is still an earth observation satellite attached with original science instruments to tackle on the space research and application. As a Formosat-2 follow-on mission, the primary goals are remote sensing applications for natural disaster evaluation, agriculture application, urban planning, environmental monitoring and ocean surveillance over Taiwan area and its surrounding oceans.

3 Payloads

Two types of payloads, distinguished them from primary and secondary, are installed on the spacecraft bus to fulfill the mission. One optical remote sensing instrument is chosen as the primary to serve the purpose of civil application, and five science instruments are designed to perform space research and marine data collection.

3.1 *Remote Sensing Instrument*

The Remote Sensing Instrument (RSI) aboard of Formosat-2 spacecraft provides 2 m and 8 m Ground Sampling Distance (GSD) in Panchromatic band and Multispectral (MS) bands, respectively, over 24 km ground swath in the nadir direction. Similarly, the primary payload for the indigenous mission shall be targeting on the same performance level as, or even better than, what Formosat-2 possesses.

3.2 *Science Instruments*

The science instruments planned for the mission cover the research applications in both marine and space fields. One payload dedicated to the marine application and four payloads for space research are proposed and their introductions are described briefly in the following sections.

3.2.1 *Marine Science Application*

The traditional way to collect the ecosystem factors of Coral Reefs is mainly by ship. The frequency of data collection can range monthly to quarterly. An infrastructure that is composed of several segments of underwater sensors, floating platform, satellite communication payload, and ground station is introduced for the mission to efficiently collect the marine ecosystem factors with a higher frequency.

3.2.2 Space Science Application

“Living with a Star” is already an important topic of the space science research. To understand and model the space environment variation around the Earth, four payloads has been proposed to perform in-situ measurements, which includes magnetometer, electron spectrometer, ion mass and energy spectrometer, and neutral particle analyzer. With these four instruments operating simultaneously, one can get the full picture of space environment variations around the Earth.

4 Spacecraft Bus Design

As stated in the previous paragraph, the spacecraft is originally designed for joining the RapidEye constellation. However, the mission has been revised to be the NSPO self-developed remote sensing satellite for the continuation purpose of Formosat-2 mission. As a stand-alone remote sensing satellite, it is designed, with cost efficiency, to be capable of possessing multiple operation modes, including large field of regard, high agility for multi-tasking, mosaic, and stereo imaging, large duty cycle, and fine attitude control accuracy. The current design of spacecraft originally aiming at mission of RapidEye constellation, passing the PDR milestone, is octagonal shape with body mounted solar array. However, to be properly suited for the modified mission of increasing duty cycle, deployment of solar array(s) is considered as mandatory for the mission. To conquer the challenge of not making dramatic design change, several options have been studied to upgrade performance of the existing design.

4.1 Flight Scenario

After detailed mission analysis, 639 km altitude sun-synchronous orbit is selected as the mission orbit. It can provide mean 1.68-day revisit cycle for 45-degree field of regard at 24 degree latitude. The influence of orbit degradation to mean revisit cycle is pretty low, which implies low orbit maintenance frequency and effort. The spacecraft bus flying at lower altitude orbit can relieve the difficulty in the design of remote sensing instrument. Also, flying at lower altitude orbit can expand the availability of small launch vehicles for this class of small satellite. Imaging area will cover from +60 degrees North latitude to -40 degrees South latitude. The science mission will be allowed to perform experiment from eclipse until +70 degrees North latitude. The spacecraft will be always kept earth-oriented for the best operation for both imaging and science missions except for the period of changing to sun pointing after imaging in order to generate more solar power.

Fig. 1 Satellite ground track for 639 km sun synchronous orbit

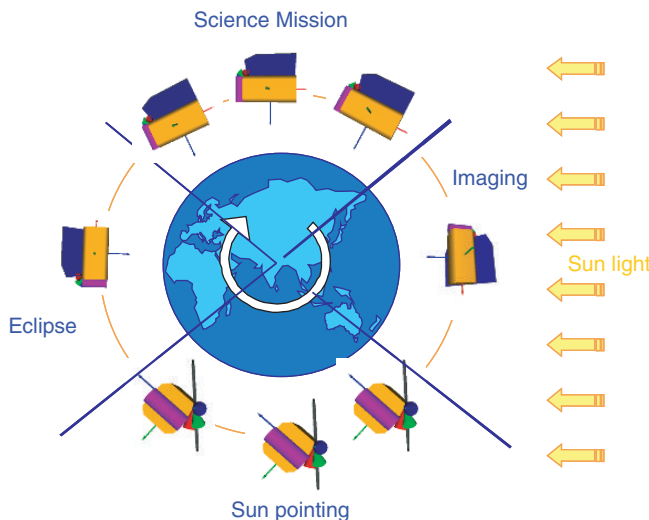
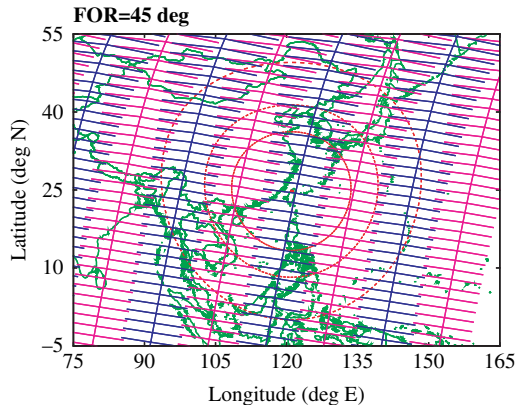


Fig. 2 Flight attitude in orbit

4.2 Configuration of Solar Array and Structure

Body configuration choices have been studied and trade analyses are given below.

Out of the above three options, the configuration of octagonal shape with two deployed solar arrays is selected as the best design currently. Although solar power generation will depend on the solar arrays configuration, shortage of power output of option 1 compared with options 2 and 3 is not likely to jeopardize a mission. Besides, we believe that the actual output power will surely be improved after the completion of critical design review stage. High agility capability is not a mandatory requirement for the RapidEye earth observation mission as Formosat-2 requires. In order to catch up with the Formosat-2 mission performance, reaction wheels adopted originally needs to be upgraded with higher torque output capacity to increase agility

Table 1 Comparison of different body configurations

| Options | Octagonal with two deployed solar arrays | Hexagonal with two deployed and one body-mounted solar arrays | Square box with one deployed and one fixed solar arrays |
|--|--|---|---|
| S/C configuration | | | |
| Solar power generation | 95% | 100% | 97% |
| Thermal control | Good. All bus panels can be used for heat dissipation. | Fair. Bus central panel is probably needed for thermal control. | Fair. Bus central panel is probably needed for thermal control. |
| Internal space for components installation | Good. Larger bus panel provides more flexibility. | Fair. Space utilization is not efficient. | Good. Larger bus panel provides more flexibility. |
| RSI accommodation | Good | Good | Good |
| Science payload accommodation | Good | Fair | Fair |
| X-axis Moment of Inertia | 100% | 93% | 93% |
| Cost impact | No | Yes. One more panel is needed. | No |

capability. In other words, larger reaction wheels will compensate the higher moment of inertia. Although the option selected does not provide the highest solar power generation and minimum moment of inertia, it possesses the highest flexibility to support any future earth-observation and space science mission for a small satellite development in Taiwan.

4.3 Shape Redesign of Solar Array

4.3.1 Influence on RSI Accommodation Volume

For intended RSI to be installed on the top panel, more space is needed compared with RapidEye payload. In original design, two tapered and symmetric solar arrays are used. To fully utilize space constraint imposed by the launch vehicle fairing, two un-symmetric, rectangular solar arrays are used. The shorter array is trying to leave more room for relieving the length constraint of telescope design. The taller array can compensate the reduced solar power from the small one and produce the same total solar power output.

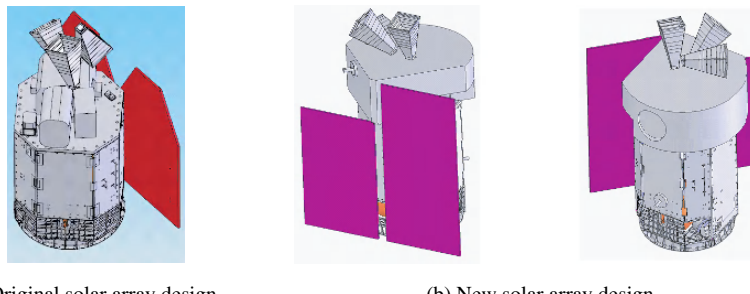
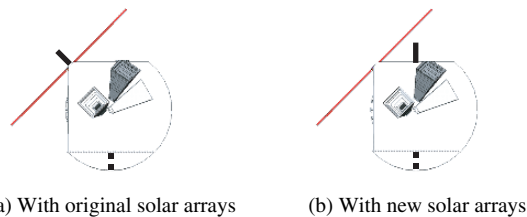


Fig. 3 Different solar arrays design (a) Original solar array design, (b) New solar array design

4.3.2 Influence on S-band Antenna Coverage

Original S-band antenna arrangement is the one facing the nadir and the other facing 45-degree off the zenith, which can produce about 87 % coverage. To enhance the reliability during contingency operation, if occurred, and also take advantage of created space resulting from the newly designed shorter solar array arrangement, the original 45-degree off zenith antenna is moved to face the zenith to increase the coverage ratio. The only blockage of this arrangement is from the shorter solar array. However, the best location will be adjusted after mock-up testing.

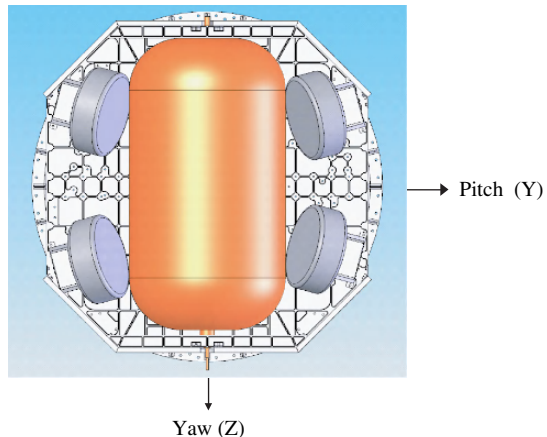
Fig. 4 S-band Antenna Installation



4.4 Upgrade of Agility Capability

As an earth-observation satellite, the agility capability in both roll and pitch axes is very important to the imaging performance. Larger reaction wheels are selected to replace the small ones for the new mission. Although the moment of inertia of roll and pitch axes deviates 100 %, the agility requirement for both axes is designed to maintain at the same level. In order to produce same agility capability in roll and pitch axes, the installation angle of reaction wheels has to be optimized to distribute more torque in pitch axis than in roll axis.

Fig. 5 Optimization of reaction wheels installation angles



4.5 Thermal Control of RSI

The thermal control of RapidEye payload is managed directly by the spacecraft bus. Since RSI is a very high precision instrument, the tolerance of thermal control is much smaller than spacecraft bus. To reduce impact to the spacecraft development when replacing RapidEye payload by RSI, the separation of thermal control philosophy of spacecraft bus and RSI has been enforced. Also, if future earth observation missions are taken into account, separate thermal control will make the spacecraft design more flexible to support different missions.

5 Leon 3 CPU Onboard Computer

The onboard computer, CDMU (Command & Data Management Unit), with LEON-3 CPU embedded has been indigenously developed for the current spacecraft bus and deemed, intended to be a heritage design for the future flight. It possesses capabilities of interface and control to all avionics by on board autonomy, of parameter change and application software exchange via telemetry/command contact, of provision of memory storage space for science instruments, and of onboard fault management control. The CDMU itself also has the capability of board-level redundancy control of another CDMU redundant unit. The LEON-3 CPU, by Gaisler Research, is a 32-bit synthesisable processor core based on the SPARC V8 architecture. It is chosen for its advantages over another such as its high level of configurability and fault immunity, the wide availability of the source code, a deeper pipeline and multi-processor support, and its suitability for the system-on-a-chip (SOC) design through its implementation in a flight qualified FPGA (Field Programmable Gate Array).

6 COTS Components

Flying the COTS components in space does not imply lower quality or poorer reliability. In order to ensure those adopted COTS components meeting the mission requirements, one needs to develop a verification approach to perform the task of up-screening or qualification to upgrade those COTS components toward higher level because the existing COTS components are not MIL or space qualified ones yet. Two COTS components, gyro and GPSR, intended to fly with the spacecraft have to go through the whole process of verification approach to confirm their functional capability. The μ FOR-6U gyro manufactured by LITEF, Germany, is a highly-integrated single-axis fiber optic rate sensor to measure the inertial rate of the spacecraft. It is designed for the commercial and military application. The Phoenix GPSR is developed by German Space Operation Center (GSOC) of DLR (German Aerospace Center) for highly dynamic and space applications. It employs a commercially available hardware platform based on MG5001 receiver hardware, which is developed and manufactured by Sigtec Navigation Pty, Australia. The MG5001 hardware is also originally designed for terrestrial application only and entirely based on COTS hardware.

7 Conclusion

The mission is the first program designed and developed indigenously by Taiwanese without introducing a prime contractor from a foreign country like we did before for Formosat-1, -2, and -3. An advanced LEON-3 CPU is aggressively chosen in the on-board computer trying to make the heritage design staying ahead and competitive for years to come. Flying with COTS components through sequence of verification approach provides a breakthrough in the space program development in Taiwan. Switching design concept and operation scenario from RapidEye constellation mission to Formosat-2 continuation mission, unwillingly scratching out part of PDR design accomplishment and still keeping procured components in use without hardware cost surge, has been accomplished by NSPO design team at the expense of the experience gained from the past space programs. A small satellite system has been developed through the execution of the indigenous mission. This satellite system is going to be capable of orbiting NSPO's future potential combination of earth observation and space science mission with necessary modification.

References

1. F. Doengi, et al., JSS Multispectral Imagers for Earth Observation Mission. *Proceedings of 5th IAA Symposium on Small Satellite for Earth Observation*, Berlin Germany (2005).
2. Chih-Li Chang and Fu-Feng Chen, Argo Mission: A New Remote Sensing Satellite Developed in Taiwan, *The 13th Australasian Remote Sensing and Photogrammetry Conference*, November 20–24, Canberra, Australia (2006).

First Year in Orbit – Results from the Beijing-1 Operational High Resolution Small Satellite

Alex da Silva Curiel, Luis Gomes, Dave Purl, Dave Hodgson, and Martin Sweeting

Abstract The Beijing-1 high-resolution spacecraft was launched in late 2005, and since its launch, the spacecraft has been commissioned and has started routine operations. The small spacecraft represents the highest GSD achieved for any spacecraft of such mass and size, yet is designed as a tool to provide high duty cycle commercial operational services.

The spacecraft provides a large data storage capacity with solid-state storage augmented by hard drives modified for use in space, allowing the instrument to map long 4000 km swaths. A software configurable image compressor and high speed X-band downlink permit both store and forward, as well as real-time downlinking. Finally, a high degree of agility permits the spacecraft to access a 600 km wide field-of-regard.

The mission addresses a range of applications in high-resolution mapping and disaster monitoring, including land cover analysis for the Chinese territories, precision agriculture, geological surveying, urban development.

1 Introduction

Small Earth Observation satellite missions have become increasingly sophisticated. For many years, SSTL has supplied small spacecraft carrying imaging instruments, and as the small satellite technology has matured, it has become possible to serve

A. da Silva Curiel

Surrey Satellite Technology Ltd, Surrey Space Centre, Guildford, Surrey, GU2, 7YE, UK
e-mail: A.da-Silva-Curiel@sstl.co.uk

L. Gomes

Surrey Satellite Technology Ltd, Surrey Space Centre, Guildford, Surrey, GU2, 7YE, UK

D. Purl

Surrey Satellite Technology Ltd, Surrey Space Centre, Guildford, Surrey, GU2, 7YE, UK

D. Hodgson

DMC International Imaging, Surrey Space Centre, Guildford, Surrey, GU2, 7YE, UK

M. Sweeting

Surrey Satellite Technology Ltd, Surrey Space Centre, Guildford, Surrey, GU2, 7YE, UK

the high resolution mapping and surveillance applications using microsatellites. The primary challenge for such missions is to provide sufficient utility in terms of system capacity.

State-of-the-art solutions can be identified by plotting the Ground Sampling Distance versus spacecraft mass for recently launched, and near-term missions (Fig. 1). Although metric class mission applications are well served by various commercial ventures, these missions are targeted at a multitude of applications, and are not well configured to provide a rapid response time, data freshness, synopticity (area captured per opportunity), or priority for any single particular user.

TOPSAT and Beijing-1 are aimed at providing some of these features specifically, and provide the best GSD achieved so far given their mass class. By ensuring the mission is affordable, each can provide a dedicated mission solution addressing the needs of a single customer and end-user. Beijing-1 in particular is configured as an operational, general-purpose mapping mission, with high on-board storage capacity and downlink rate. It also provides an exceptional degree of synopticity with over 4000 km mapping and downlinking capability every orbit.

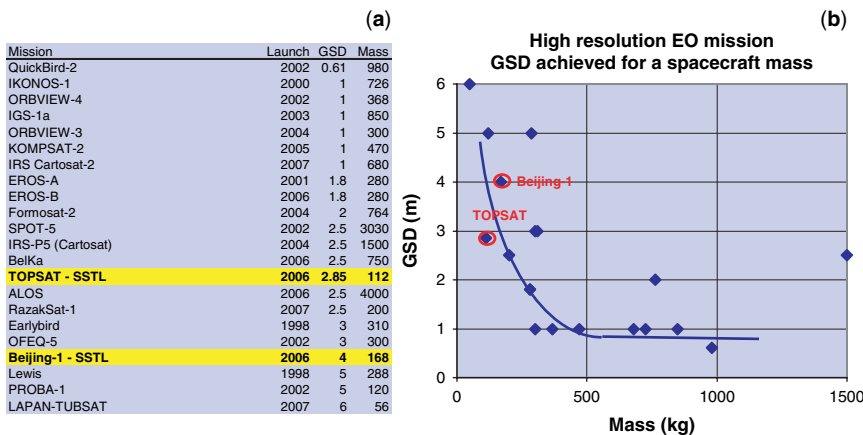


Fig. 1 (a) Summary of high-resolution EO missions and (b) plot of GSD vs spacecraft mass

2 The Beijing-1 Mission

The Beijing-1 mission is targeted at an operational mapping mission, with its subsystems and payload specified at providing the best data transfer for such a space-craft available over its lifetime, given its size and budget constraints.

Beijing-1, also known as China DMC +4, was designed and manufactured by Surrey Satellite Technology Limited (SSTL) of Guildford, United Kingdom, for the private company “Beijing LandView Mapping Information Technology Co”. (BLMIT), of Beijing, China, as the space segment of the Beijing-1 project. The space-craft was launched together with TOPSAT on a COSMOS launcher in October 2005.

The project comprised also the installation in Beijing of a Mission Control Centre, consisting of an S-band ground station and associated control systems, and the support to the customer payload data X-band ground station. Designed from the beginning as a pure mapping mission, the project aims at providing the Chinese market with yearly high resolution mapping of the Chinese territory. Special attention is being given to the large amount of building work being done for the Olympic Games in Beijing, since the mission allows re-mapping of the urban area every 3–4 days, at 4 meter ground sampling distance (GSD), a useful capacity in rapidly changing urban environments. The satellite was designed to map the entire Chinese territory every six month, at 4-meter resolution in Pan-chromatic mode.

3 Spacecraft Overview

Beijing-1 employs the SSTL-150 platform, with all the capabilities of the Disaster Monitoring Constellation (DMC) platform, plus a high performance 4-meter GSD imager with its own payload data processing, storage and transmission chain.

The small 168 kg satellite carries a panchromatic imaging instrument providing 4-metre Ground Sampling Distance (GSD) with 24 km swath. In addition it also carries an ultrawide swath with multi-spectral camera with 32-metre GSD and 600 km swath as carried by the other satellites within the Disaster Monitoring Constellation.

Although the standard platform capabilities can be tailored, for the Beijing-1 mission, these include a sophisticated and agile attitude control system that allows 30° off track roll maneuvers. It also includes an on-board hardware data compression, using a fully re-programmable high capability DSP unit, 4 Gbytes of volatile mass data storage, 240 Gbytes of non-volatile mass data storage (fully re-writable on demand), data encryption and the downlink, providing data transfer rates at 8 (in S-band), 20 and 40 Mbit/sec (in X-band). The 4-meter GSD imager is based on a lightweight mapping telescope with in-orbit focusing capability. It was developed by the Optical Payloads Group within SSTL.

The modular and configurable platform features make it a very powerful Earth observation tool, at a relatively very low cost. The mission can be operated in several different modes, each optimised for a specific objective. These modes are re-configurable from the ground, and new ones can be tailored as required by the operators.

The 4-metre instrument is a compact on-axis telescope, providing high quality mapping data. It is designed specifically so that it can be scaled and carried on a range of small satellites. It employs an athermal carbon fibre composite structure to provide good stability, and permits on-orbit adjustment of focus. These design choices for the telescope yield a cost effective solution and the ability to deal with a large temperature range without active thermal control, which significantly eases the satellite design and operating complexity.

The main points of the specification together with the parameters achieved are given in Table 1, and the reference conditions for these parameters in Table 2. This shows that all design goals were met or exceeded, and that in particular a high level of Signal To Noise level is achieved.

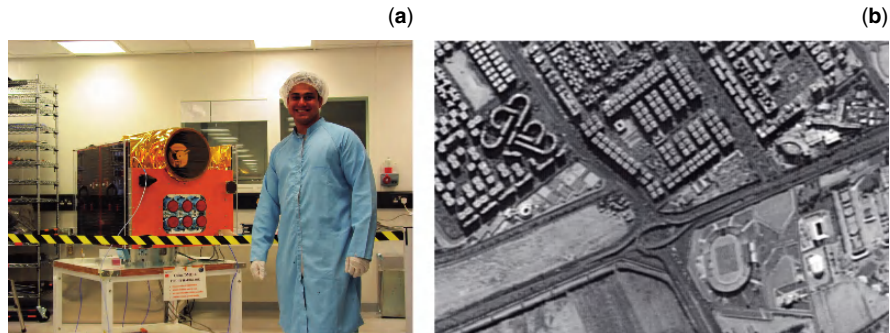


Fig. 2 (a) BEIJING-1 Microsatellite (b) Copied image of region near Cairo Airport, Egypt

Table 1 Main Points of the Specification

| Parameter | Required | Achieved |
|---|-----------------------------|-----------------------------|
| GSD (m) | 4 | 4 |
| Swath (km) | 24 | 24 |
| Band (nm) | 500–800 | 500–800 |
| Band edge accuracy across FoV (nm) | ± 30 | 2 |
| Energy in pass-band | $\geq 90\%$ | 98% |
| MTF at Nyquist: | | |
| centre | $\geq 15\%$ | $\geq 19.6\%$ |
| edge | $\geq 10\%$ | $\geq 13.6\%$ |
| Signal-to-noise ratio | ≥ 140 | 210 |
| Mass (kg) | ≤ 25 | 24 |
| Power (W) at 28V | ≤ 12 | 11.9 |
| Volume (mm^3) except mounting feet | $790 \times 400 \times 400$ | $790 \times 380 \times 378$ |

Table 2 Reference Conditions

| Parameter | Conditions |
|---------------|---|
| Orbit | 686 km, sun synchronous, 11:00 LTAN, nadir pointing |
| Signal | 0.3 albedo at 35° latitude at 11:00 on March 21st |
| Temperatures: | at imager mounting panel: |
| Performance | $10^\circ\text{C} \pm 10^\circ \pm 10^\circ$ uncertainty |
| Operational | -25°C to $+60^\circ\text{C}$ |
| Survival | -50°C to $+88^\circ\text{C}$ |
| Vibration | 21 grms random vibration |
| (qual) | $1 \text{ g}^2/\text{Hz}$ peak |

Typical test results for the most important property of the imager, the MTF, are given in Fig. 3 for the maximum field angle. The Nyquist limit is at 62.5 cycles/mm. These are end-to-end results including the optical system, detector and electronics, and were measured on the flight imager after environmental testing. The effect of satellite motion on the along-track results is not yet included.

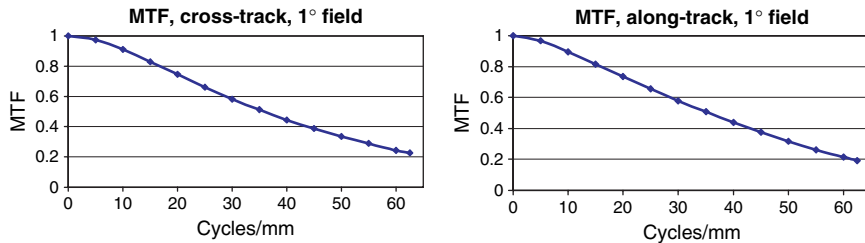


Fig. 3 Typical MTF curves

The measured spectral response of the imager is given in Fig. 4. The band edge cutoffs were achieved by a dielectric coating on the secondary mirror in combination with a glass blocking filter for the blue end.

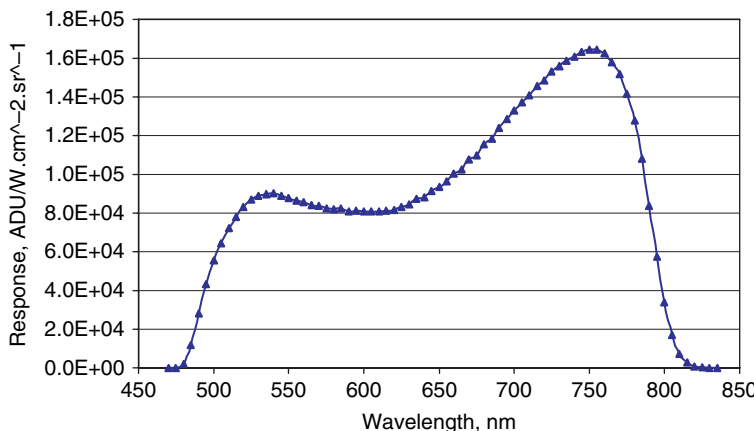


Fig. 4 Measured spectral response

Following a successful launch, the spacecraft platform was commissioned within weeks, allowing early payload characterization and calibration to commence.

The in-orbit imager performance was evaluated through the China Academy of Sciences and BLVMIT Ltd. A large ground target was prepared out as illustrated in Fig. 5. This was then imaged over a number passes, whilst the relevant ground reflectances and atmospheric conditions were monitored at the same time. Other features in the resulting images including water, soil, live vegetation, and dead vegetation were also utilized to provide a range of reflectances to measure the instrument linearity of response.

The results verified that the Ground Sampling Distance is 4 m as per the design, and that the linearity of response. Further campaigns were used to cross calibrate the multispectral sensors with the other DMC spacecraft.

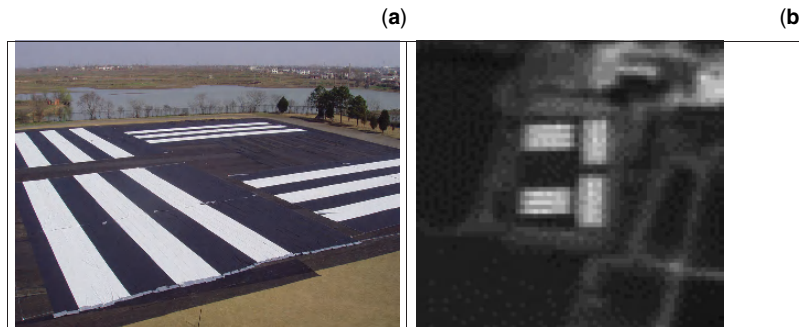


Fig. 5 (a) Ground reference target (b) as imaged by Beijing-1

With the instrument commissioned, the spacecraft has entered commercial operational service, addressing a diverse range of applications in high-resolution mapping and disaster monitoring, including land cover analysis for the Chinese territories, precision agriculture, geological surveying, urban development.

4 Applications and Service Segment

The spacecraft supports commercial on-demand tasking, across a range of applications including private, public and humanitarian. The spacecraft owner and operator is Beijing Landview Mapping Information Technology Co. Ltd. Provides commercial data sales of value added data products, but data products are also available through SSTL's subsidiary DMC International Imaging.

The image products are based on the two main sensors, with characteristics listed in Table 3. As Beijing-1 is coordinated within the Disaster Monitoring Constellation, daily revisit becomes possible through coordination with the other satellites within the constellation.

Table 3 Beijing-1 instrument characteristics

| Multispectral | Panchromatic |
|----------------------------|---------------------------------|
| 32 m GSD | 4 m GSD |
| 660 km swath | 24 km swath |
| 160–4100 km along track | 24–4100 km along track |
| daily revisit | 5 day revisit (30° offpointing) |
| < 10% radiometric accuracy | |
| < 25 m RMSE orthorectify | |

The data products supported by the mission are based on both of the instruments. data fusion products using both instruments are also supported with Digital Elevation Models (DEM), and using both instruments, and are listed in Table 4.

Based on the 240 Gbyte solid-state data store, it is possible to store image tracks over 4000 km in length, supporting systematic mapping of large areas. This has

Table 4 Data products

| Level | Description | Format |
|-------|---|---------|
| L1 | Radiometric Corrected Images | Raw |
| L2 | L1 Plus: Systematically Geometric Corrected Images | GeoTIFF |
| L3 | L2 Plus: Precision Geometric Corrected using GCPs | GeoTIFF |
| L4 | Ortho-Rectified Image using DEM Data | GeoTIFF |
| L5 | Stereo Image Product using DEM data | - |
| L6 | Fusion Image Product using 32 m GSD Multi-Spectral Image and 4 m GSD Panchromatic Image | GeoTIFF |

supported the development of a data products such as the mapping of the entire country of China every 6 months using the multispectral sensor.

Within China, the Beijing-1 data is used extensively in urban planning, in particular in preparation for the Beijing 2008 Olympics. For some products, the multi-spectral images are being combined with the panchromatic images providing pan-sharpened imagery. An example of such a data fusion product is provided in Fig. 6.



Fig. 6 Beijing-1 pan-sharpened multispectral image of Hefei City, Anhui Province, China

5 Conclusions

Increasingly sophisticated small Earth Observation satellite missions are becoming feasible. Affordable mission solutions now make it possible to target specific user groups and applications. For users this means higher priority service, and operational tools dedicated at their specific needs.

The Beijing-1 mission is providing an operational high resolution imaging service from orbit, with high frequency and capacity. The design philosophy that was employed is allowing both the platform and instrument to be scaled to address various different and emerging applications. Specifically, the use of such spacecraft solutions in constellations is highly promising to address high temporal resolution requirements. A wide range of applications are supported

References

1. Alex da Silva Curiel, Lee Boland, John Cooksley, Mohammed Bekhti, Paul Stephens, Wei Sun, Prof. Sir Martin Sweeting, “*First results from the disaster monitoring constellation*”, IAA-B4-1302, 4th IAA Symposium on Small Satellites for Earth Observation, Berlin, April 2003
2. Alex Wicks et al., “*An EO Constellation based on the TopSat Microsatellite: Global Daily Revisit at 2.5 metres*”, AIAA/USU conference on small satellites, Logan Utah USA, August 2001 SSC01-I-6
3. Dr. Peter Garner, Kevin Maynard, Dr. Stephen Hodgart, Martin Pointer, “*Flexible Low Cost X-Band Transmitter*”, ESOC TT&C conference, Darmstadt, September 2004
4. Andrew Cawthorne, Alex da Silva Curiel, Martin Sweeting “*The next generation DMC small satellite platform for high-resolution imaging*”, IAC05-B5.4.01, IAF, Fukuoka, Japan, October 2005
5. Alex da Silva Curiel, Andrew Cawthorne, Martin Sweeting, “*Progress in Small Satellite Technology for Earth Observation Missions*”, 5th IAA Symposium on small satellites for Earth Observation, IAA-B5-0301, Berlin, Germany, April 2005
6. Guglielmo S Aglietti, Luis Gomes, Alex da Silva Curiel, “*Hard disk drives for spacecraft application*”, IAC-06-B5.6.02, IAF, Valencia, Spain, October 2006

An Introduction to FORMOSAT-2's Global Effectiveness

Jeng-Shing Chern, An-Ming Wu, Yung-Nien Liu, and Lance Wu

Abstract FORMOSAT-2 (was called ROCSAT-2 formerly) of Taiwan's National Space Organization (NSPO) is a small satellite of 746 kg mass for two remote sensing missions. Its mission orbit is sun-synchronous of 891 km altitude for exactly 14 revolutions per day. For earth observation, the payload is an advanced high resolution remote sensing instrument (RSI) with ground sampling distance (GSD) 2 m in panchromatic (PAN) band and 8 m in four multi-spectral (MS) bands. For upward lightning observation, the payload is an imager of sprites and upper atmospheric lightning (ISUAL). Launch date of FORMOSAT-2 was on 20 May 2004. After nearly 3 years of mission operations in orbit, i.e., more than one half of the mission life of 5 years, it is a proper time to assess and evaluate its worldwide effectiveness in Earth observation. To evaluate the effectiveness of developing a satellite, especially to a country with very limited resources such as Taiwan, we need to include all aspects. This paper gives the global effectiveness of FORMOSAT-2 a rather detailed assessment from the following areas: public education in Taiwan, Earth science and ecological niche research, preservation of the world heritages, contribution to the International Charter: space and major disasters, observation of suspected north Korea and Iranian nuclear facilities, and scientific observation of the atmospheric transient luminous events (TLEs). It can be concluded that FORMOSAT-2's

J.-S. Chern

National Space Organization (NSPO) 8F, 9 Prosperity 1st Road, Science Park, Hsinchu, Taiwan 30078

e-mail: jschern@nspo.org.tw

A.-M. Wu

National Space Organization (NSPO) 8F, 9 Prosperity 1st Road, Science Park, Hsinchu, Taiwan 30078

Y.-N. Liu

National Space Organization (NSPO) 8F, 9 Prosperity 1st Road, Science Park, Hsinchu, Taiwan 30078

L. Wu

National Space Organization (NSPO) 8F, 9 Prosperity 1st Road, Science Park, Hsinchu, Taiwan 30078

global effectiveness is pronounced and definitely promised. The development of FORMOSAT-2 is very valuable, not only to Taiwan but also to the whole world.

1 Introduction

FORMOSAT-2 is the first remote sensing satellite (RSS) owned by the National Space Organization (NSPO) of Taiwan for the purposes of earth and upward lightning observation. It is a small satellite of 746 kg mass for two remote sensing missions. Its mission orbit is sun-synchronous of 891 km altitude for exactly 14 revolutions per day. For earth observation, the payload is an advanced high resolution remote sensing instrument (RSI) with ground sampling distance (GSD) 2 m in panchromatic (PAN) band and 8 m in four multi-spectral (MS) bands. For upward lightning observation, the payload is an imager of sprites and upper atmospheric lightning (ISUAL). [1-4]It was launched from Vandenberg, California on 20 May 2004. After nearly 3 years of mission operations (MO), it is a proper time to make an assessment of FORMOSAT-2's effectiveness to the world.

One of the ways to analyze the effectiveness of an RSS is simply to consider the cost. However, it can also be assessed and evaluated from both the direct and indirect effectiveness. In Reference 5, FORMOSAT-2's cost effectiveness to Taiwan had been discussed. In this paper, we try to investigate FORMOSAT-2's effectiveness to the world from the following five areas: public education in Taiwan, Earth science and ecological niche research, preservation of the world heritages, contribution to the International Charter: space and major disasters, observation of suspected north Korea and Iranian nuclear facilities, and scientific observation of the atmospheric transient luminous events (TLEs).

2 Public Education in Taiwan

2.1 Student Activities before FORMOSAT-2 Launch[6]

The student activities for celebrating FORMOSAT-2 launch were initiated by the Aerospace Science and Technology Research Center (ASTRC) of the National Cheng Kung University (NCKU) on 20 August 2003. All students of elementary, junior high and senior high schools were invited. There are four categories: call for "Name", "Painting", "Article" and "Plan". The "Name" must be simple but meaningful to represent FORMOSAT-2. Size of the "Painting" should be the A3 size, i.e., 29.5 cm × 42 cm. In the category of call for "Article", the students were requested to write a short paper about the development, missions, configuration, characteristics, etc. of FORMOSAT-2. Then in the category of call for plan, the students were encouraged to design a detailed plan for using the RSI or ISUAL observation results. The deadline of submission was 10 November 2003.

A total of 333 submissions had been received with the following distribution: call for name 122, call for painting 133, call for article 42 and call for plan 36.

The winning name is “Formosa #2” and the winning painting is shown in Fig. 1(a). This name leads to the change of the satellite from ROCSAT-2 to FORMOSAT-2. It is seen from Fig. 1(b) that the winning painting was painted on the fairing of the launch vehicle. This is another great honor to the winner.

2.2 Publication of Calendars for Children and General Public Educations[6]

Under the authorization of NSPO, the Newtonkids Book Company published calendars in both 2006 and 2007 for children education purpose. On the other hand, NSPO published calendar for the general public education purpose. NSPO selected 12 FORMOSAT-2 images captured in 2005 and 2006 to publish the calendars of 2006 and 2007, respectively.

2.3 URMAP (Your Map) System[6]

The OleMap Incorporation started to develop the URMAP system at about two years ago. It is already a very mature system and handy for application by the general public or the foreign travelers in Taiwan. There are three kinds of maps, satellite image, regular and electronic.

Fig. 1 First prize painting and its appearance on FORMOSAT-2 launch vehicle



3 Earth Science and Ecological Niche

3.1 Ice Crack Observed in Alert, Canada

In the Alert area of Canada, FORMOSAT-2 observed an ice crack in three consecutive days from 24 to 26 March 2006 in exact the same time everyday by using its daily revisit characteristics. As shown in Fig. 2, the width of the ice crack varied from about 600–800 m wide to narrower and then to even wider than the first day. NSPO provided this information to interested scientists for study and investigation. Figure 3 shows the same area after 1 year.

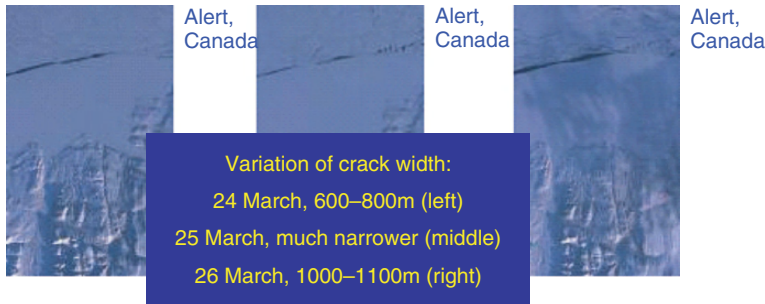


Fig. 2 Variation of ice crack in consecutive three days

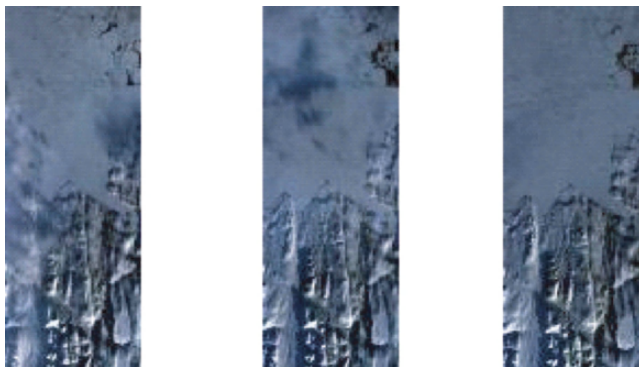


Fig. 3 Alert area imaged on 25 (left), 26 (middle) and 27 (right) March 2007

3.2 Coral Reef Near Taiwan Island and Ayers Rock in Australia

In Fig. 4(a), it shows a coral reef called the Dongsha Atoll. Dongsha Islands are to the east but not too far away from Taiwan Island. [5]The complete coral reef and abundant ecological environment have made Dongsha Atoll a fascinating place for researchers worldwide. The Ayers rock and its surrounding area had been imaged by FORMOSAT-2 as shown in Fig. 4(b). These two examples mean that NSPO also provides images related to ecological environment for the research and analysis of the ecological resources, and for the participation and promotion of the global ecological preservation and research activities.

4 Preservation of the World Heritages

Preservation and protection of the world heritages is one of the important jobs of the United Nations Educational, Scientific and Cultural Organization (UNESCO). With its high resolution, FORMOSAT-2 took the image of a castle named Jiayuguan (Fig. 5(a)) of the Great Wall in China. As we know, the Great Wall stretches from

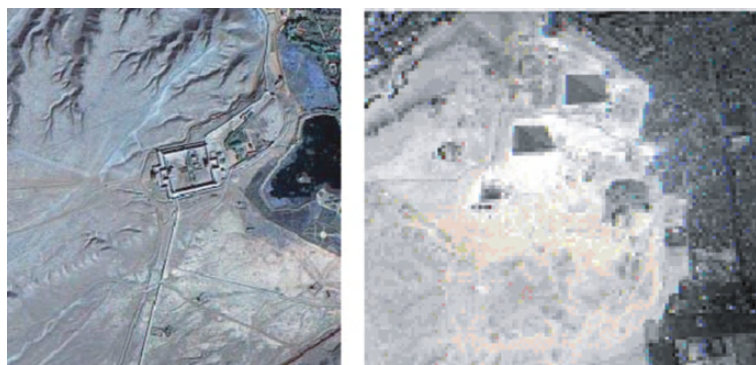


(a) Dongsha Atoll

(b) Ayers Rock

Fig. 4 FORMOSAT-2 images of Dongsha Atoll (Taiwan) and Ayers Rock (Australia) **(a)** Dongsha Atoll **(b)** Ayers Rock

Shanhaiguan Pass in the east to Jiayuguan Pass in the west. Actually, each “Guan” is a not only a pass and but also a castle where soldiers lived in the ancient dynasties. It had been enlisted in the World Heritages by UNESCO in 1987. Figure 5(b) shows three pyramids named Khufu (upper right), Khafre (upper middle) and Menkaure (middle left). The Sphinx of Giza can be identified clearly if we zoom into the detail of the image. Actually, FORMOSAT-2 has observed many World Heritages.



(a) Jiayuguan Pass

(b) Pyramids

Fig. 5 Jiayuguan pass of the great wall and pyramids khufu, khafre and menkaure **(a)** Jiayuguan Pass **(b)** Pyramids

5 International Charter: Space and Major Disasters

The International Charter is the “Charter On Cooperation To Achieve The Coordinated Use Of Space Facilities In The Event Of Natural Or Technological Disasters”. Charter’s purposes are “In promoting cooperation between space agencies and space

Table 1 FORMOSAT-2's effectiveness in contributing to International Charter Disasters

| No. | Charter ID | Place_name | International Charter Disaster | | | | | | | Charter Requester | Project Management | | |
|-----|------------------|------------|--------------------------------|-----------------------|--------------|-------------|------------|------------|---|-----------------------------|--------------------------|--|--|
| | | | Number of Scenes | | Request date | Ending date | SIFEM | CONAE | | | | | |
| | | | Notification (4/3) | Delivered | | | | Argentina | SIFEM | | | | |
| 1 | CHARTER ID 125-1 | Floods | ARGENTINE | CHOELE | 7 | 7 | 2006/07/29 | 2006/08/04 | SIFEM | CONAE | | | |
| 2 | CHARTER ID 125-2 | Floods | ARGENTINE | NEUQUEN CITY | 7 | 7 | 2006/07/29 | 2006/08/04 | SIFEM | CONAE | | | |
| 3 | CHARTER ID 125-3 | Floods | ARGENTINA | PIRAN | 5 | 7 | 2006/08/09 | 2006/08/18 | SIFEM | CONAE | | | |
| 4 | CHARTER ID 130 | Floods | SUDAN | FLOODS 1 AND FLOODS 2 | 7 | 7 | 2006/08/29 | 2006/09/05 | UNOOSA | UNOSAT | | | |
| 5 | CHARTER ID 131 | Floods | FRANCE | PONT A MOUSSON | 8 | 8 | 2006/10/05 | 2006/10/12 | French Civil Protection | CNES | | | |
| 6 | CHARTER ID 132 | Oil Slick | BULGARIE | BULGARIA | 5 | 5 | 2006/10/11 | 2006/10/17 | Civil protection of European Commission | Joint Research Centre (JRC) | | | |
| 7 | CHARTER ID 133 | Floods | SRI LANKA | SRI LANKA | 0 | 8 | 2006/11/03 | 2006/11/03 | UNOOSA | UNOSAT | | | |
| 8 | CHARTER ID 134 | Floods | ETHIOPIA | ETHIOPIA | 7 | 7 | 2006/11/06 | 2006/11/14 | UNOOSA | UNOSAT | | | |
| 9 | CHARTER ID 135-1 | Floods | SOMALIA | SOMALIA | 8 | 8 | 2006/11/14 | 2006/11/14 | UNOOSA | UNOSAT | | | |
| 10 | CHARTER ID 135-2 | Floods | SOMALIA | SOMALIA | 6 | 6 | 2006/11/17 | 2006/11/17 | UNOOSA | UNOSAT | | | |
| 11 | CHARTER ID 135-3 | Floods | SOMALIA | SOMALIA | 1 | 4 | 2006/12/02 | 2006/12/04 | UNOOSA | UNOSAT | | | |
| 12 | CHARTER ID 137 | Floods | KENYA | KENYA | 0 | 14 | 2006/11/20 | 2006/11/20 | United States | United States | Geological Survey (USGS) | | |

| No. | Charter ID | Place name | International Charter Disaster | | | | Charter Requester | Project Management | Pacific Disaster Center |
|-----|----------------|----------------------------|--------------------------------|--------------|-------------|------------|-------------------|--|--|
| | | | Notification (4/3) date | Request date | Ending date | Delivered | | | |
| 13 | CHARTER ID 139 | Typhoon PHILIPPINE | | 9 | 12 | 2006/12/02 | 2006/12/17 | UNOOSA | |
| 14 | CHARTER ID 140 | Floods INDONESIA | INDONESIA | 9 | 18 | 2006/12/29 | 2007/01/04 | UN-OCHA | UNOSAT |
| 15 | CHARTER ID 141 | Floods ARGENTINA | TUCUMAN PROVINCE | 5 | 5 | 2007/01/19 | 2007/01/25 | SIFEM | CONAE |
| 16 | CHARTER ID 143 | Floods ARGENTINA- PARAGUAY | PILCOMAYO RIVER | 7 | 7 | 2007/01/23 | 2007/01/29 | SIFEM | CONAE |
| 17 | CHARTER ID 145 | Floods MOZAMBIQUE | MUTARARA | 6 | 6 | 2007/02/09 | 2007/02/16 | UNOOSA | Argentina |
| 18 | CHARTER ID 145 | Floods MOZAMBIQUE | CAIA | 6 | 6 | 2007/02/09 | 2007/02/16 | UNOOSA | UNOSAT |
| 19 | CHARTER ID 151 | Tsunami SOLOMON ISLANDS | SOLOMON ISLANDS | 6 | 8 | 2007/04/04 | | UNOOSA | UNOSAT |
| 20 | CHARTER ID 152 | Earthquake AFGHANISTAN | AFGHANISTAN | 4 | 7 | 2007/04/05 | | United States Geological Survey (USGS) | United States Geological Survey (USGS) |
| | | | Total Images acquired | 113 | | | | | |

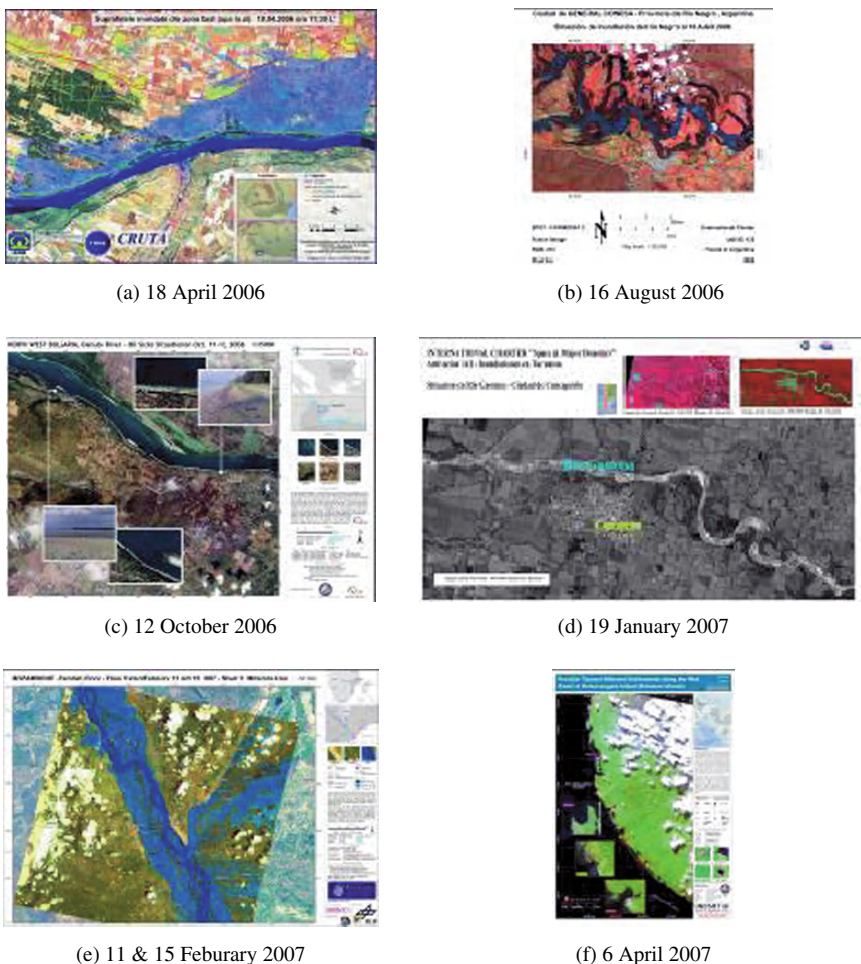


Fig. 6 Examples evidence FORMOSAT-2's effectiveness in International Charter: (a) floods in Romania, mid-April 2006, (b) floods in Argentine, 9–18 Aug 2006, (c) oil slick in Bulgaria, 11–17 Oct 2006, (d) floods in Argentine, 19–25 Jan 2007, (e) floods in Mozambique, 9–16 Feb 2007, and (f) earthquake in Afghanistan, 5 Apr 2007

system operators in the use of space facilities as a contribution to the management of crises arising from natural or technological disasters, the Charter seeks to pursue the following objectives: (1) supply during periods of crisis, to States or communities whose population, activities or property are exposed to an imminent risk, or are already victims, of natural or technological disasters, data providing a basis for critical information for the anticipation and management of potential crises; and (2) participation, by means of this data and of the information and services resulting from the exploitation of space facilities, in the organization of emergency assistance or reconstruction and subsequent operations.”

NSPO joined the International Charter in 2006. Because of NSPO is in cooperation with the Spot Image Company of France for the commercial promotion of FORMOSAT-2 images, the source of the images is shown as “Spot/Formosat-2” in the Charter’s website. Since NSPO joined the Charter, Spot/NSPO has provided images captured by FORMOSAT-2 in 20 events as listed in Table 1. Some of the images are presented in Fig. 6 for reference.

6 Suspected North Korea and Iranian Nuclear Facilities

Using the daily revisit advantage, FORMOSAT-2’s orbit 1 comes from north to south and passes over North Korea, South Korea, Taiwan, etc. at exactly the same time everyday. Therefore, it is very convenient for FORMOSAT-2 to take the image of North Korea’s nuclear facilities. Figure 7(a) shows the distribution of those facilities, and 7(b) is the suspected nuclear test site. The epicenter of the site predicted by US is as shown in the figure.

Another country tried to reestablish and reuse its nuclear facilities is Iran. The daily revisit and radiometric characteristics of FORMOSAT-2 make its observation so valuable for analysts to understand the status. As shown in Fig. 8, the reestablishment of the surfacing work and the construction of the reactor had been completed from 10 May to 1 July 2005.

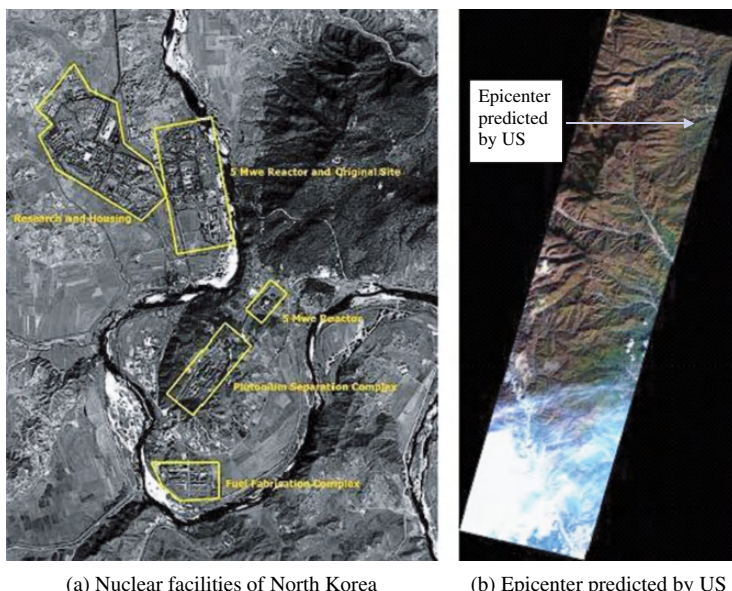


Fig. 7 North Korea’s nuclear facilities and suspected nuclear test site **(a)** Nuclear facilities of North Korea **(b)** Epicenter predicted by US (October 2006)

7 Atmospheric Transient Luminous Events (TLEs)

FORMOSAT-2's scientific payload ISUAL has captured 4219 emissions of light and VLF perturbation due to EMP sources (ELVES), 487 red sprites, 486 halos and 9 gigantic jets (GJ) (VLF = very low frequency, EMP = electromagnetic pulse). In other words, a total of 5201 TLEs have been observed within 2.5 years. [7] In order to protect the instrument, ISUAL is not operational when FORMOSAT-2 is passing the Southern Atlantic Anomaly (SAA) region. Since FORMOSAT-2 is the first satellite to observe TLEs from orbit, the results are very valuable. Space physics scientists are analyzing these natural phenomena.



Fig. 8 Establishment of Iranian heavy water production plant observed in 2005

8 Conclusions

FORMOSAT-2, the first Earth observation remote sensing satellite (RSS) of Taiwan, has been working on its mission orbit of 891 km for nearly 3 years. This paper gives the global effectiveness of FORMOSAT-2 a rather detailed assessment from the following areas: public education in Taiwan, Earth science and ecological niche research, preservation of the world heritages, contribution to the International Charter: space and major disasters, observation of suspected north Korea and Iranian nuclear facilities, and scientific observation of the atmospheric transient luminous events (TLEs). It can be concluded that FORMOSAT-2's global effectiveness is pronounced and definitely promised. The development of FORMOSAT-2 is very valuable, not only to Taiwan but also to the whole world.

References

1. J. S. Chern, J. Ling and Y. S. Chang, "ROCSAT-2, a Small Satellite for Two Remote Sensing Missions," Paper IAC-02-IAA.11.2.05, 53rd International Astronautical Congress, Houston, 10–19 October 2002
2. A. M. Wu, W. T. Shiau and J. S. Chern, "Ground Track Control of a Daily Repetitive Orbit," Paper IAC-04-IAF-A.7.05, 55th International Astronautical Congress, Vancouver, 4–8 October 2004
3. J. S. Chern, "Earth Observation Results of FORMOSAT-2 from June 2004 to February 2005," IAA-B5-0205P, 5th IAA Symposium on Small Satellites for Earth Observation, Berlin, 4–8 April 2005
4. J. S. Chern, Y. N. Liu and L. Wu, "Popularization of FORMOSAT-2 Images in Taiwan," Paper IAC-06-E5.P.4, 57th International Astronautical Congress, Valencia, 2–6 October 2006
5. J. S. Chern and L. Wu, "FORMOSAT-2's Cost Effectiveness to Taiwan," the Small Satellites Systems and Services Symposium (The 4S Symposium), Chia Laguna, Sardinia, Italy, 25–29 September 2006
6. J. S. Chern, S. S. Chen and L. Wu, "Student Activities before Formosa Satellites Launches," Paper IAC-06-E1.3.05, 57th International Astronautical Congress, Valencia, 2–6 October 2006
7. B. C. Chen, "Global Distribution of Transient Luminous Events," Department of Physics, National Cheng Kung University, January 2007

Session 11

Subsystems (2)

TopSat: Lessons Learned from a Small Satellite Mission

Elaine Baxter and Bill Levett

Abstract The UK's "TopSat" programme has been used to demonstrate the ability to build and operate a low-cost optical satellite capable of generating timely high quality imagery for a wide range of applications. Rapid end-to-end timeliness has been combined with a low-cost approach, leading to a world leading performance-to-cost ratio.

Historically, end-to-end timeliness has been a major constraint for space-based systems. During demonstrations using the TopSat spacecraft and RAPIDS mobile ground station, a total end-to-end timeliness (i.e. from image selection to image delivery) of less than 37 minutes was achieved.

TopSat and missions of this class are set to revolutionise the space remote sensing business, through reductions in costs and thus greater numbers of spacecraft. This will allow missions to be tailored much more exclusively to the requirements of major users.

1 Spacecraft

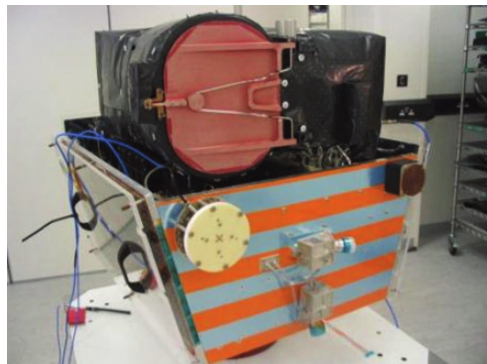
1.1 Overview

The TopSat satellite, built by a QinetiQ-led consortium, was launched on 27th October 2005. It has a mass of 108 kg and consists of a novel optical payload, which is integrated with a low-cost small satellite platform. It produces panchromatic imagery (17×17 km) with a spatial resolution of 2.8 m and overlapping multi-spectral imagery (12×18 km) with 5.6 m resolution. The panchromatic imagery can be georectified to better than 50 m absolute localisation using 4 GCPs [1].

E. Baxter
QinetiQ Space Division, A8 Building, Cody Technology Park, Ively Road, Farnborough GU14 0LX, UK
e-mail: ebaxter@qinetiq.com

B. Levett
QinetiQ Space Division, A8 Building, Cody Technology Park, Ively Road, Farnborough GU14 0LX, UK

Fig. 1 The TopSat spacecraft during final testing



Remarkably, the spacecraft (and operations) were developed and launched for under €20M, resulting in a world leading performance-to-cost-ratio. Although built as a technology demonstrator and not an operational system, TopSat has already



Fig. 2 TopSat image of Venice, Italy, 14th March 2007

sustained eighteen months of intensive use, routinely delivering 4 images per day. Images have been provided to the UK MoD, BNSC, academic community and commercial customers, as well as supporting a technical development programme sponsored by the TopSat Consortium.

1.2 Low-Cost Approach

The TopSat programme demonstrates a low-cost approach to responsive space missions. The spacecraft was developed with a design-to-cost approach, with appropriate re-use of existing technologies and facilities. The ground segment was based around COTS software and uses a high level of automation.

In addition, TopSat was launched on a shared launch vehicle – a Cosmos-3M rocket from Plesetsk, Russia. This was enabled by the size and low mass of the spacecraft, made possible by the innovative camera design.

2 Ground Segment

The spacecraft is operated from the Payload Operations Centre at Farnborough in the UK, often working in close communication with users to meet specialised requirements. During routine operations, imagery is downloaded to QinetiQ's ground station at West Freugh in Scotland. Imagery can also be rapidly down-linked through the mobile ground station, RAPIDS (see Section 3.2).

3 Rapid End-to-End Timeliness

TopSat's rapid end-to-end timeliness capability make it ideally suited to work within tight timescales; whether for disaster relief, news gathering or security applications. *Figure 3* shows an image of Kashmir taken for the Durham Landslide Centre, in



Fig. 3 TopSat image of a landslide in Kashmir, 27th September 2006

support of a study into the use of TopSat in the assessment of disaster impact. Additional imagery for the centre was used to provide casualty estimates from Typhoon Bilis [2].

3.1 Responsive Tasking

A key element of TopSat operations is the responsiveness of the image tasking process. Payload operations are scheduled using the TopSat Operations Management software (TOM) – developed by QinetiQ to work in conjunction with AGI's Satellite Tool Kit and Scheduler packages.

TOM allows the scheduling process to respond readily to space and ground segment constraints, in addition to varying imagery requirements. Payload command files can be generated for upload to the spacecraft in a matter of minutes, and the scheduling process can be readily extended to cope with larger task and image throughputs.

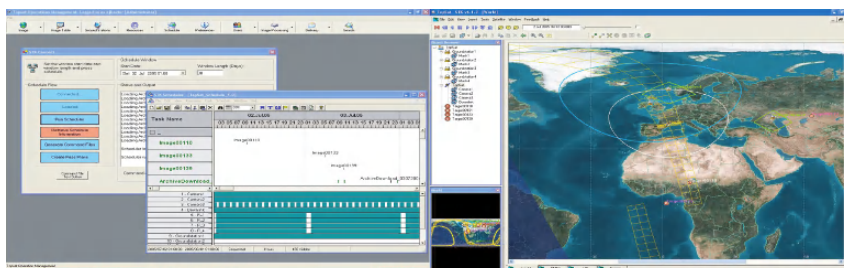


Fig. 4 The TOM software

Access to the TopSat imagery archive catalogue and co-ordination of requests between imagery users is encouraged through a web-based analysis tool. Users can view thumbnails of archive images, in addition to image details such as date of acquisition. Combining this with the TOM Software would make scheduling directly controllable by the end user, allowing a faster image tasking to delivery time and lower operations costs.

3.2 Direct-to User Down-Linking

TopSat imagery can be rapidly down-linked through the use of a mobile ground station, providing near real-time imagery directly to a field-based user. QinetiQ has enhanced the fully transportable RAPIDS ground station, with system electronics and image processing computers mounted in a customised Land Rover Defender.

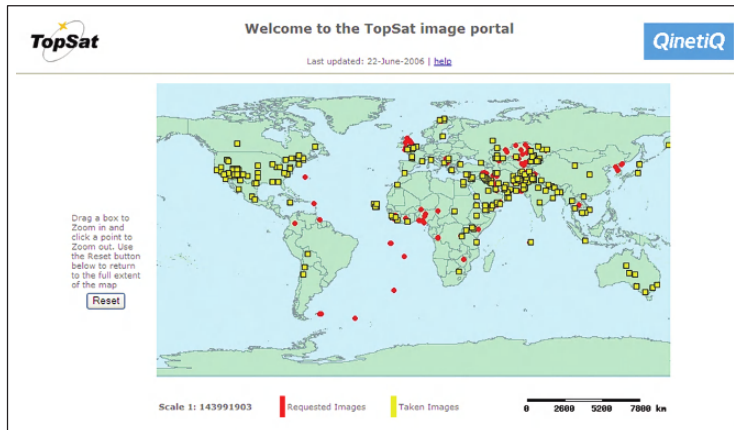


Fig. 5 TopSat image request analysis tool



Fig. 6 The RAPIDS mobile ground station

3.3 End-to-End Timeliness Demonstrations

In January 2007, several end-to-end timeliness demonstrations were conducted by the TopSat Consortium, emulating the tasking of the TopSat satellite directly with an uplink facility located within a theatre of operations, and the provision of fresh imagery into theatre through a deployed data ground station.

Imagery was commanded, acquired, down-linked and processed within a single image pass, achieving an end-to-end timeliness using the mobile ground station of less than 37 minutes.

3.4 Online Hosting of Imagery

In order to provide in-theatre access to the highest resolution image files even without the use of a mobile ground station, a web-based image browsing interface has

been developed for TopSat imagery, in which full resolution geo-rectified imagery is made available for viewing with relatively low-bandwidth.

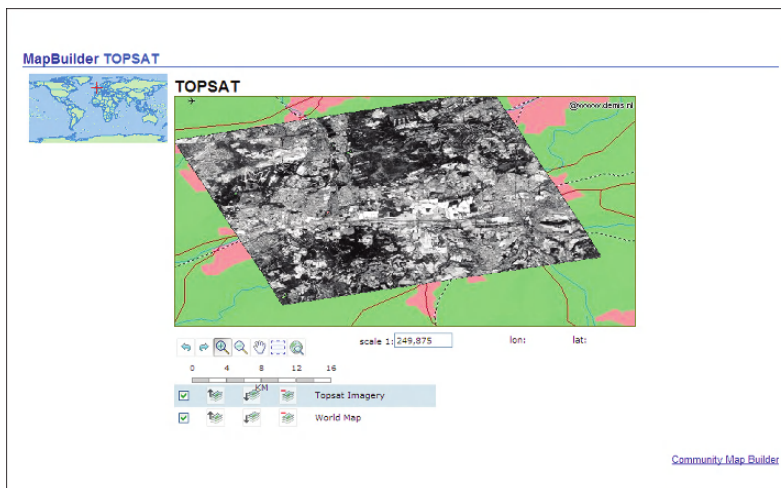
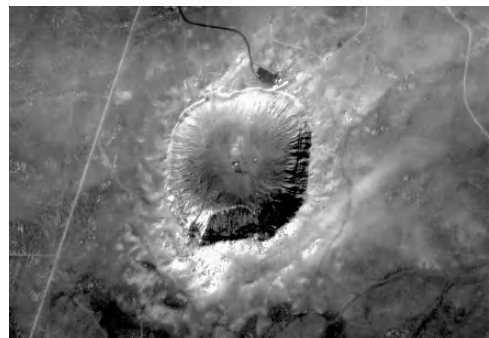


Fig. 7 Web browser tool

4 Mission Status

The TopSat Consortium consists of four UK partners: QinetiQ (who lead the mission, provide the on-board data handling unit, data down-links and Payload Operations Centre); the Rutherford Appleton Laboratory (RAL, who designed and built the onboard camera); Surrey Satellite Technology Limited (SSTL, who built the satellite platform and provide TT&C services); and Infoterra Ltd (who are responsible for the development of commercial data markets).

Fig. 8 TopSat image of a meteor crater in Arizona, 6th February 2007



The programme, originally funded by the British National Space Centre and the UK Ministry of Defence, has since become a commercial venture between the

TopSat consortium partners. During this time, the TopSat Consortium has embarked on a series of experiments to demonstrate the performance of the system, both in image timeliness and image quality.

5 Lessons Learned

The main lessons learned from the TopSat programme have been as follows:

- The challenges associated with developing an extremely compact, high performance camera can be overcome.
- Mounting a sensitive, high-performance optical payload on a micro-satellite platform is possible.
- Low-cost ground segment facilities can enable extremely fast data turnaround.
- A disparate consortium can be made to work without large administrative overheads, as long as significant face-to-face contact is maintained.

Fig. 9 TopSat image of Mt Fuji, Japan, 6th February 2007



6 Conclusions

The overriding achievement of the TopSat mission is the successful design, construction, launch and operation of a micro-satellite capable of sustaining routine tasking at a cost of less than €20M. The key to this was combining high quality imagery and rapid end-to-end timeliness with a low-cost approach. This required considerable technical and programmatic challenges to be overcome.

By virtue of its small size and low cost, TopSat-has opened the way for affordable constellations capable of launch on a single small launch vehicle. In the case of imaging spacecraft, this will reduce image costs and increase the availability of

data. The TopSat low-cost approach can be used in the future to develop even more capable missions, opening the door to an even wider community of users.

Fig. 10 TopSat image of the Great Pyramids, 18th January 2007



References

1. E. Baxter, J. Laycock, W.A. Levett, *TopSat: High quality imagery from a low-cost satellite* (ESA 4S Symposium 2006)
2. D. Petley, S. Dunning, N. Rosser, *On the application of TopSat for the rapid assessment of landslide impacts* (EGU General Assembly 2007)

High Data Rate X-Band Transmitter for Low Earth Orbit Satellites

Hacer K. Sunay, Neslin İsmailoglu, Tunahan Kirılmaz, Celal Dudak,
and Ozlem A. Sen

Abstract Main purpose of this study is to design a transmitter with data rates up to 100 Mbps, having QPSK/OQPSK modulation and 7 W (38.5 dBm) output power at 8.2 GHz. This output power satisfies the link budget for a low earth orbit (LEO) satellite at 700 km, utilizing required source-channel coding schemes in baseband for a BER performance of 10^{-6} . The modulation scheme of the transmitter can be selected as BPSK, QPSK or OQPSK. In addition to QPSK/OQPSK modulation scheme choice, the transmitter will have three different data rates, 50 Mbps and 100 Mbps which will be chosen according to the needs and facilities of the ground station. As error correction coding (ECC) scheme, a nested structure that is recommended by CCSDS is chosen which combines powerful parts of the subcodes. As the outer code, Reed Solomon with $(255,223,33)_{256}$ is used for error correction for burst errors due to multipath fading. As inner code, a convolutional code with rate $(1/2)$ is utilized, which provides correction for random errors in the channel with a moderate bandwidth expansion. Between inner and outer codes, convolutional interleaver with depth 5 is used.

1 System Design of the Transmitter

For satellite applications, it is very important to have simple and reliable systems. For this purpose, a simple heterodyne transmitter structure is chosen. In the design

H.K. Sunay

Tubitak-Uzay Technologies, METU Campus, Inonu Bulvari, 06531, Balgat, Ankara, Türkiye
e-mail: hacer.sunay@bilten.metu.edu.tr

N. İsmailoglu

Tubitak-Uzay Technologies, METU Campus, Inonu Bulvari, 06531, Balgat, Ankara, Türkiye

T. Kirılmaz

Tubitak-Uzay Technologies, METU Campus, Inonu Bulvari, 06531, Balgat, Ankara, Türkiye

C. Dudak

Tubitak-Uzay Technologies, METU Campus, Inonu Bulvari, 06531, Balgat, Ankara, Türkiye

O.A. Sen

Tubitak-Uzay Technologies, METU Campus, Inonu Bulvari, 06531, Balgat, Ankara, Türkiye

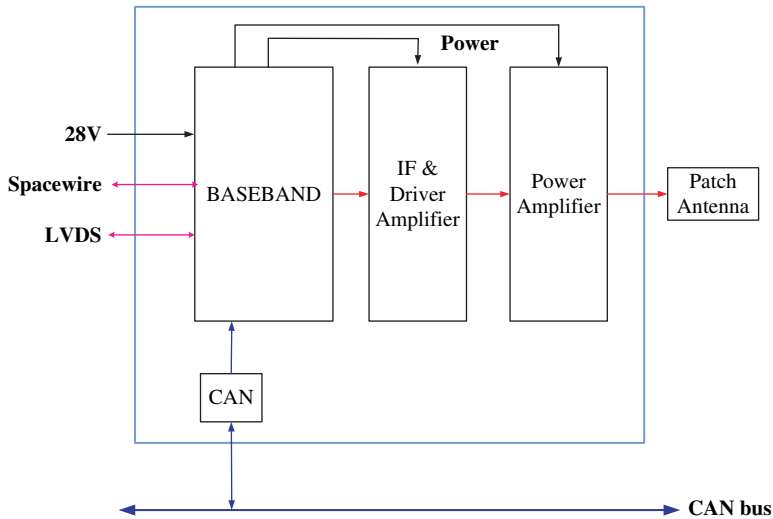


Fig. 1 Block diagram of XBAND-Tx

process, mainly commercial off the shelf components are used. Transmitter system is composed of mainly three stages: Baseband, IF Stage and RF Stage.

1.1 Baseband Stage

In the baseband stage of the transmitter (Fig. 1), the modulation scheme of the transmitter can be chosen as OQPSK or QPSK. In addition to the QPSK/OQPSK modulation scheme choice, the transmitter will have three different data rates, 50 Mbps, and 100 Mbps which will be chosen according to the needs and facilities of the ground station, i.e., for mobile ground stations, it is possible to download the signal at low data rates with a small antenna. With 100 Mbps a state of the art technology will be demonstrated and the demand for high data rates will be satisfied.

Appropriate nested-interleaving and scrambling techniques are used to minimize DC component of the signal, to improve the timing recovery at receiver; and hence effectively making the bursty channel appear like a random error channel to the decoder. As error correction coding (ECC) scheme, a nested structure is chosen which combines powerful parts of the subcodes. As the outer code, Reed Solomon with $(255,223,33)_{256}$ is used for error correction for burst errors due to multipath fading [12]. As inner code, a convolutional code with rate $(\frac{1}{2})$ is utilized, which provides correction for random errors in the channel with a moderate bandwidth expansion. Between inner and outer codes, convolutional interleaver with depth 5 is used. This concatenated encoder structure is also recommended by CCSDS [1].

Then, the output is pulse shaped by an FIR-RRC (finite impulse response root raised cosine) filter, which is implemented digitally in Xilinx Virtex-II FPGA. For

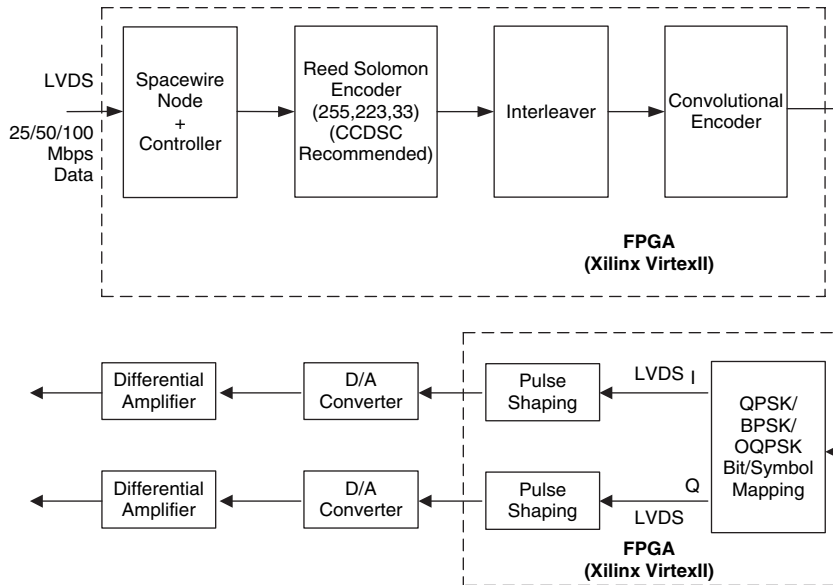


Fig. 2 The block diagram of the baseband stage

filter tap length, binary coefficient approximation simulations are realised. 4 tap per symbol and 65 tap length for RRC filter gives the best trade off number giving good BER performance, meeting certain spectral masks for space communications and boosting up communication data rate to limits in our structure. For reliability against Single Event Upset logic errors in FPGA configuration, Xilinx “Readback” Capability is used. For the necessity of reconfiguration, a CRC checksum, based upon all the configuration bits that have been read back, is generated and this CRC is compared with the expected checksum.

1.2 The IF Stage

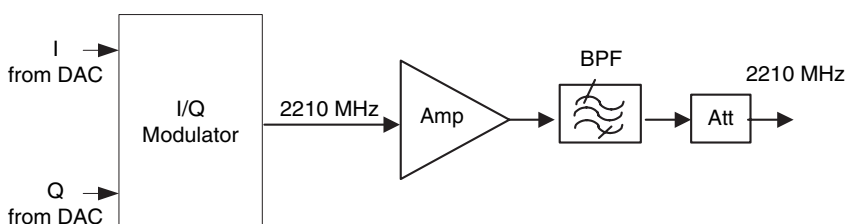


Fig. 3 Block diagram of the IF stage

The signal is direct quadrature modulated at 2210 MHz as the IF stage (Fig. 3) Then, it is filtered and amplified properly in order to obtain the required signal level.

In Fig. 4, EVM for 20 Mbps QPSK signal at 2210 MHz centre frequency is given. Additionally in Fig. 5, EVM for 20 Mbps OQPSK signal at 2210 MHz centre frequency is given.

Fig. 4 EVM for 20 Mbps QPSK signal at 2210 MHz

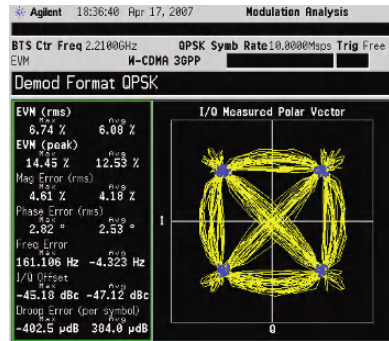
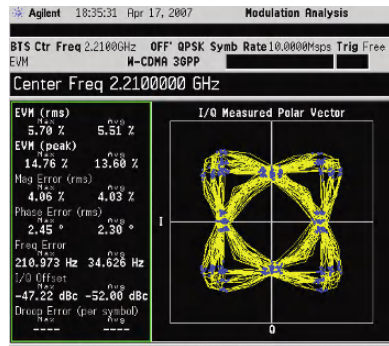


Fig. 5 EVM for 20 Mbps OQPSK signal at 2210 MHz



1.3 The RF Stage and the Power Amplifier

RF stage includes bandpass filter and three stage (including one driver stage) power amplifier that works at 8.2 GHz (Fig. 6). The analog signal at 2210 MHz is upconverted to 8.2 GHz, operating center frequency, with the help of a phase locked source oscillating at 5990 MHz. Then required attenuation and filtering operations are accomplished, taking related current, voltage and impedance matching conditions.

One of the main parts of RF stage is designed as a solid state power amplifier. It has 7 W (38.5 dBm) output power with a gain of 20.5 ± 0.6 dB in 8.17–8.265 GHz bandwidth at 8.2 GHz centre frequency and overall efficiency of 26%. The first stage of the power amplifier is realized as a Class AB amplifier with an output power of 30 dBm and an efficiency of 22%. The second stage is also realised as class

AB amplifier with 38.5 dBm output and 37% efficiency. Drain current decreases with the decrease in the input power so that efficiency degradation in the low input power is limited. This concept is very important since it increases efficiency without sacrificing linearity for the modulations with high peak to average ratio.

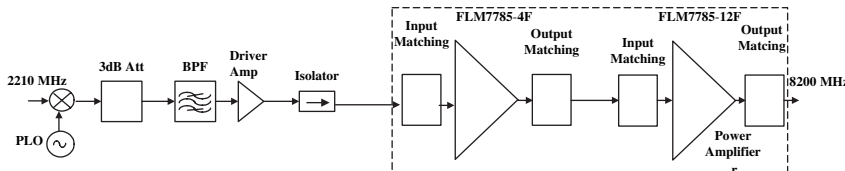
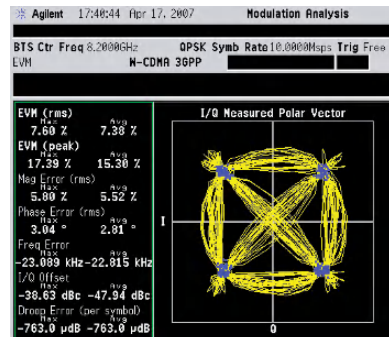


Fig. 6 Block diagram of the RF stage

Figure 7, gives EVM results of the RF stage when target power output (38.5 dBm) is reached with 20 Mbps QPSK signal. When we compare the EVM results of the IF and the RF stages' we can see that EVM results of the RF stage are slightly increased quantities. That difference arises because of nonlinearities in the line-up (mainly from that of PA stages). Nonlinearities of PA stages are different on different modulation schemes depending on CCDF of the signal (effected by both modulation and α), operating point of the PA, 1 dB compression point of PA and maximum output power of PA. For our operating point with $\alpha = 0.65$ (same as QPSK case), the EVM of OQPSK modulated 20 Mbps data rate signal is given in Fig. 8. As can be seen from these results for the conditions at 38.5 output power, EVM results of OQPSK signal is slightly better.

Fig. 7 EVM for 20 Mbps QPSK signal at 8200 MHz



Second stage of PA used in this system is characterized by power added efficiency (PAE), gain and output power curves and the results are given in Fig. 9. As can be seen from these curves, at 38.5 dBm output, power added efficiency is 38% and PA is only 0.2 dB compressed. When both two stages of PA are considered, the results are in Fig. 10.

Figure 11 Gives output of whole system when target power output (38.5 dbm) is reached with 100 Mbps QPSK signal. this spectrum also satisfies general linearity

Fig. 8 Eye Diagram of 20 Mbps OQPSK signal at 8200 MHz

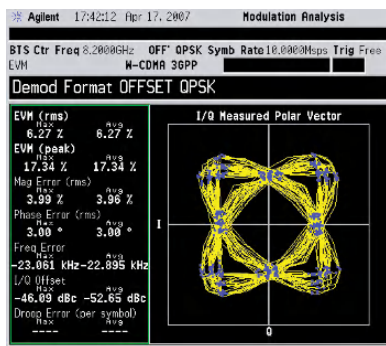


Fig. 9 Measured gain, PAE and output power vs. input power for second stage of PA

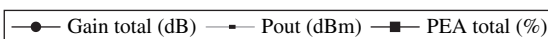
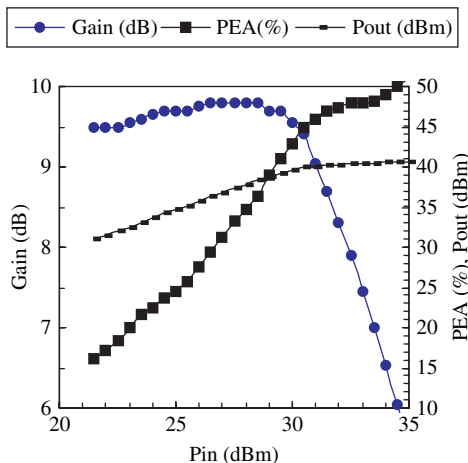
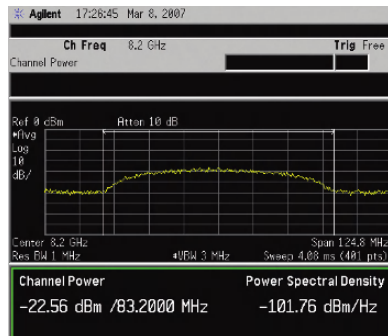


Fig. 10 Measured gain, PAE and output power vs. input power for two stage PA

requirements imposed by the recommendations of satellite communication institutions, including consultative committee for space data systems (CCSDS) [1].

Fig. 11 Power spectrum of 100 Mbps QPSK signal at 8200 MHz



2 Conclusion

In this paper, a high data rate transmitter with 38.5 dBm (7 W) output working at X-band for LEO satellite communication is given. Transmitter blocks consist of mainly commercial of the shelf components. Baseband is implemented digitally on Xilinx Virtex-II FPGA for speed-up considerations. Solid state amplifier makes the system small in volume and light.

Realization of X-band transmitter system is completed. This transmitter planned to be utilized in the LEO satellite named RASAT which will be launched at 2008 by TÜBİTAK-Space Technologies Institute. RASAT will be a Earth Observation satellite with 8 m resolution RGB camera.

References

1. Telemetry Channel Coding, CCSDS Recommendation for Space Data System Standart, Blue Book, Newport Beach, California, USA, May 1999
2. Razavi B., RF Microelectronics, New Jersey: Prentice Hall, 1998
3. Lee T.H., The design of CMOS Radio Frequency Integrated Circuits, Cambridge University Press, Cambridge, 1998
4. Proakis J., Digital Communications, McGraw-Hill, Inc., New York, 1995
5. Cripps S.C., High-Efficiency Power Amplifier Design, Lecture given in Short Course: RF ICs for wireless communication, Portland, Oregon, June, 1996
6. Cripps S.C., RF Power Amplifier for Wireless Communications, Artech House, Boston, 1999
7. Lee T.H., The Design of CMOS Radio Frequency Integrated Circuits, Cambridge University Press, Cambridge, 1998
8. Blahut R.E., Theory and Practice of Error Control Codes, Addison-Wesley Publishing Company, New York, 1983
9. Bryerton E. W., Weiss M. Popovic D., Z., "Efficiency of Chip-level Versus External Power Combining", IEEE Transactions on MTT, vol. 48, pp. 1482–1485, August 1999

10. Raab Frederick H., "Maximum Efficiency and Output of Class-F Power Amplifiers", IEEE Transactions on MTT, vol. 49, pp. 1162–1165, June 2001.
11. Hang C.Y., Deal W.R., Qian Y., "High- Efficiency Push-Pull Power Amplifier Integrated with Quasi-Yagi Antenna", IEEE Transactions on MTT, vol. 49, pp. 1155–1160, June 2001
12. Morelos-Zaragoza Robert H., The Art of Error Correcting Coding, John Wiley & Sons, 2002

Flowing Tasks: Scalable Software Dependability and Performance

Sergio Montenegro and Raffaele Vitulli

Abstract Dependability is a major challenge when designing space computing systems, both at software and hardware level. After 30 years of contentious research on how to achieve high dependability, not a single solution has been found. A huge effort has been invested to improve reliability, using reliable radiation hardened components. However, failures cannot be eliminated totally.

Nowadays, it is not imaginable the use of the same (general purpose) computer in a cube sat ($10 \times 10 \times 10 \text{ cm}^3$, 1 Kilogram) and in a mini satellite. For each satellite, a special purpose computer configuration need to be assembled, consisting of board computer, payload for cameras, star tracker, power control, reaction wheels, etc.

1 Conceptual Obstacles

From our experience we can identify at least 4 important very common conceptual obstacles when designing a fault tolerant system.

- 1) Any digital control system is a team work of software and hardware. Trying to solve any problem or challenge using only one of them means to loosing a lot of possibilities, like a team (Software-Hardware) where one player in software, but very few try to face the challenge in a team work of software and hardware.
- 2) Another wrong assumption is to think that to provide fault tolerance you just have to replicate resources. For example if you can control a water tank level opening and closing a valve, like in Fig. 1.

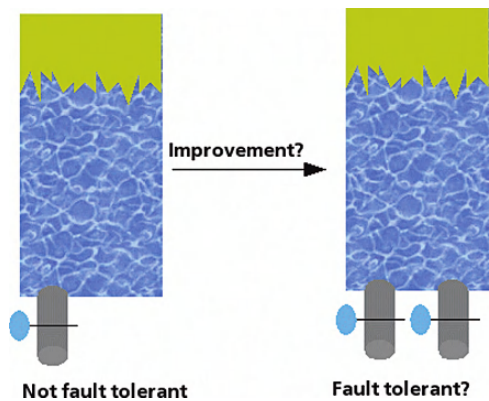
S. Montenegro

DLR, Institute of Space Systems, Am Fallturm 1, 28359 Bremen, Germany
e-mail: sergio.montenegro@dlr.de

R. Vitulli

ESA/ESTEC, Keplerlaan 1, 2201AZ Noordwijk, The Netherlands

Fig. 1 Replication alone is not fault tolerance



Then you may think: The valve can fail; let's add another valve (Fig. 1). Now one of the redundant valves fails in open position, you can not control the tank any longer. What you got is a higher possibility of failure and not more dependability. This was not right the solution!

- 3) Another wrong assumption is to think you can reach an absolute failure free system. Then an enormous effort is invested to reach what you can not reach. See Fig. 1. You can do what you want, but any system will crash some day.

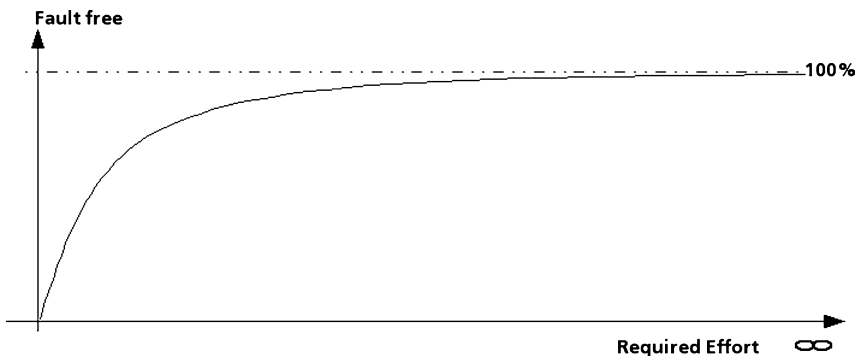


Fig. 2 Infinite effort to reach a total fault free system

- 4) Another important consideration is what to do after so many resources are permanently damaged, that no normal operation is possible any longer.

2 A Non Conventional Way to Dependability

Let's consider (in this paper) 4 (from 0 to 3) stages of fault tolerance:

- 0: No fault tolerance. One failure is enough to cause a system failure or system crash
- 1: Any single failure can collapse some critical functions, but the system remains in a safe operation. (Gracefully degradation)
- 2: Like 1, but after a short time period the system can reconfigure itself to go back to normal operation (resilience)
- 3: No single failure can disturb the normal operation of the system.

Stage 3 sounds very nice, but it requires at least a 3 fold replication of (almost) all resources, including volume, mass, power consumption, heat production, etc. For some space applications this can be a prohibitive condition. Furthermore after the first permanent failure, the system will go down to stage 2 or 1. For long operations where permanent failures are expected, stage 3 will be possible only at the beginning of the mission.

It is therefore advisable to create a resources economical system which provides stage 2 for the whole mission even after several failures. Our target is to get the highest possible dependability using very limited resources. The system has to be operable always in a safe way, but temporally loose of advanced features is allowed. Thereby it was very important not to do again the common mistakes listed in chapter 1.

2.1 Step 1: Let it Crash!

A realistic node computer operation can be represented like in Fig. 3.

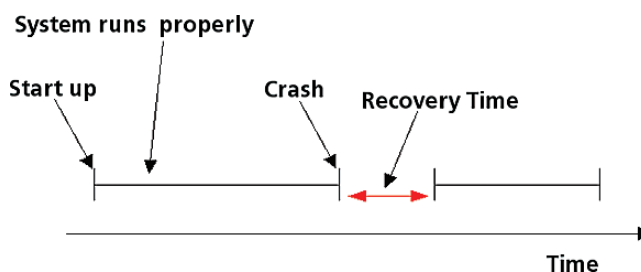


Fig. 3 realistic node computer operation

After start up a node computer will work properly for a time period (may be years) but some day it will crash and no one can impede this. Better than trying to create a (sub)system which shall never fail or where a failure is an extraordinary exception, we count with failures, they are not exceptions, but expected events which will be handles smoothly. The paradox situation is: to be safe, be ready to crash at any time.

To increase the dependability of the system we can increase the reliability of each node (eg. mean time to failure MFTF) and reducing the recovery time after crashes (increasing Availability).

Much more important than try to avoid crashes (we can not) it is to provide an ultra fast recovery. Recovery includes reboot, restore context of applications and update the context to the current situation. Having a very short recovery time, we can tolerate very easily multiple node crashes, and if we use some kind of redundancy, the probability of two redundant nodes to be down at the same time becomes lower. See Fig. 4.

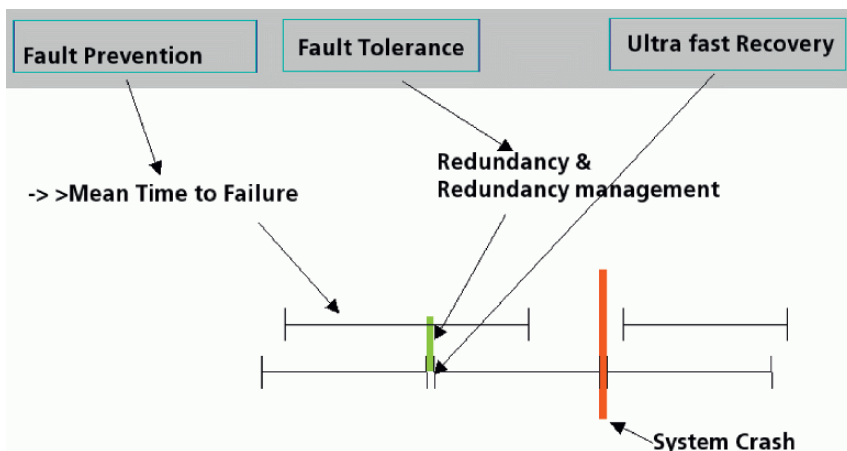


Fig. 4 Increasing dependability

Today the recovery time is very long, depending on the operating system it can range from 10 seconds to some minutes. This long period increase the probability of a total system failure if redundant nodes are down at the same time (see Fig. 4). Our target is to have a recovery time of a few milliseconds. If so, we can tolerate several crashes per second without problems.

2.2 Step 2: Do Not Paddle Only on One Side, Use Both: Software and Hardware

Better than trying to have fault tolerance in Hardware and to make it transparent to the software (e.g. Maxwell approach), we implement robustness as a harmonized team work of software and hardware. If you have a legacy or extreme complex software, which you cannot modify (or even understand) then you have to make fault tolerance transparent to the software, but doing so you lose an enormous potential from HW-SW team work: Hardware provides redundancy and software provides an intelligent redundancy management.

Using an intelligent dynamic redundancy management it is possible to adapt the redundancy degree to the current situation and mission phase. The resources usage can vary to provide high performance (no/low redundancy) or high dependability (high redundancy).

3 Our Approach/Our Solutions

Contrary to most other approaches who try to minimise the possibility of failures, this approach considers that failures will occur and tries to handle them efficiently. Dependability is implemented using smart and efficient resource and redundancy management. The novel approach is to focus on efficient software solution instead on adding more hardware.

We aim an artificial brain computing model which controls the whole spacecraft. It consists of a network of computing nodes capable of executing different tasks and autonomous task re-distribution. The brain metaphor implies capability of self organisation and adaptability. If some nodes fail, their tasks will be automatically moved to other working nodes (imitating the brain feature of healthy cells being capable of overtaking the functions of damaged or decease-affected cells). This simplifies the spacecraft/satellite construction having only one computer with autonomous configuration and continuity of service.

On the Hardware side our approach is based on a network of computing nodes (more than 3). On the software side our Approach is based on the BOSS operating system (Originally: Bird Operating System) which was designed to support dependability. Two major objectives are the ultra fast task recovery and ultra fast task migration mechanisms. An application with multiple tasks running on BOSS is distributed over a set of node computers. The communication between tasks is performed using named ports with a producer/subscriber protocol. The number of tasks, ports and the topology are transparent to the application. This allows redistribution of tasks without any programmer intervention. Consequently, any task can be replicated for redundancy purposes making the running system highly reconfigurable.

Dependably is based on a team work of software and undependable and inexpensive hardware. The designer assumption is that a node computer may crash each second. No other approach can handle such an extreme high crash ratio. This is an enormous advantage for example for satellites which operate in environments with very high radioactivity and electromagnetic noise. This approach is ready to handle crashes at any time.

4 BOSS Kernel and Middleware

The BOSS real time kernel and middleware offer an integrated framework (OO) interface. There is no need to differentiate what is a RT kernel and what is middleware functionality. Both together will be called the BOSS-framework. The BOSS

framework aims to offer the most simple and small possible interface to users tasks, which still provides all required functionality and flexibility.

The BOSS-framework includes time management, resource management and communication functionality. Without an application the framework is inactive, it just reacts to interrupts doing nothing. An application can add actions to the BOSS-framework by inheriting classes and creating active objects. These objects will be integrated automatically in the framework. In this way the framework will be extended with user functionality.

4.1 Communicating Tasks

Let's take as example a task network to control 3 arms using an environment model. The task distribution is shown in Fig. 5.

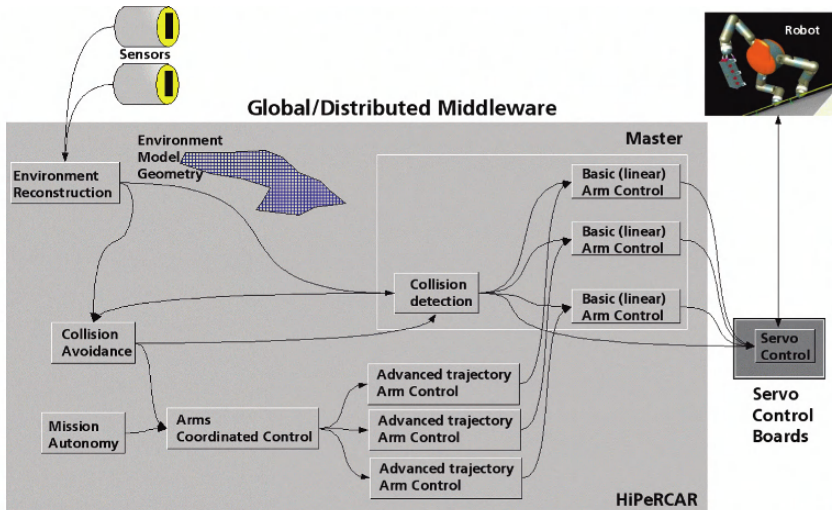


Fig. 5 Hypothetical Example of Task Distribution

For the implementation there is no difference where the tasks will be deployed. The position of tasks can even change at run time, without requiring any explicit reaction of the other involved tasks. Task communicate using the BOSS Middleware, but its only interface are messages, the rest is transparent. Tasks just define input and output messages. The rest is some one else job (Middleware and real time kernel).

4.2 Structure of the BOSS Framework

A BOSS controller is implemented as a collection of building blocks on the top of a middleware, which creates a virtual totally interconnection network for all tasks

running on it. The middleware allows every task to communicate with any other task independent of their position. It imposes no limitations to communication paths, but the application shall use/create a meaningful, reasonable and efficient inter-task communication structure.

There may be different system configurations for BOSS applications. The system supports to migrate from any of these configurations to another without having to change the application. This will be achieved by implementing a layered system.

The application tasks run on the top of a virtual global middleware which cross node boundaries and interconnect all threads/tasks in the system. They do not need to know the details of lowered layers. Applications can interact without having to know about locations and hardware architectures.

The global middleware is implemented on local middleware running on each node. This local middleware runs on the top of a real time kernel or operating system which administrates the time and local resources in the node. The real time kernel is implemented using a virtual hardware abstraction, which is implemented by the hardware dependent layer. To move from any hardware platform to another one, only this small layer has to be re-implemented.

References

1. P.A. Marra, et al. – “*HiPeRCAR: the High Performance Resilient Computer for Autonomous Robotics*” – DASIA 2006, Berlin
2. D. Jameux – “*Application of the Payload Data Processing and Storage System to MOSREM Multi-processor On-board System for Robotic Exploration Missions*”, 2003
3. Astrium/Scisys – “*UNIONICS Advanced On-Board Distributed Processing Architecture*” – Initial results from the Bench-Top Demonstrator”, 2003
4. M. Johnson, B. Green, O. Eman – EADS Astrium “*Improving the efficiency of spacecraft systems with the Unionics Advanced On-board Architecture*” – SDSS 2005
5. Guy Estaves, Alcatel Alenia Space – *Super Computers for Space Applications-* SDSS 2005, 17–20 October 2005, ESTEC, Noordwijk
6. *SpaceWire – Links, Nodes Routers and Networks*, ECSS-E-50-12A, ESA ITT AO/1-4497/NL/AG – *SpaceWire Remote Terminal Interface ASIC*, 2003

Index

A

AERL, 156–158
Albedo, 103, 159, 234, 236, 237, 245, 249, 360
ALMASat, 309–312, 314–317
Altimeter, 9, 160, 170
Antenna system, 20, 21, 73, 216
ARGO, 168, 339, 341
ARGUS, 72
ASAP, 41–43
ASIM, 27, 29
ASPIICS, 154–155
Atmosphere, 3, 4, 6, 129, 146, 156, 157, 180, 245–251, 333–338
A-Train, 6
Attitude determination, 211–219, 255–263, 310, 315, 346
Aurora imager, 187, 195
Automation, 71, 75, 379
Autonomy, 33, 37, 68, 75, 154, 267–269, 275, 321, 352

B

Basic research, 5, 335, 337
BeeSat, 255–263
Beijing, 1, 58, 60, 62, 63, 357–364
BIRD, 277–283, 358, 399
BSAR, 134

C

Calibration, 7, 102, 112, 115, 116, 150, 200, 259, 274, 317, 361
CAN bus, 50, 51, 313, 388
CASSIOPE, 169
CHAMP, 144, 148, 150, 167, 169
Chibis, 337, 339–342
CHRIS, 64–66, 67–68, 69, 80
CLARREO, 9–10
Climate, 4–6, 9, 19, 138, 156, 159, 303, 335–337

Cluster, 13–14, 22, 24, 37, 107, 134, 151, 294–296, 298, 329
Communication payload, 15, 347
Constellation(s), 57–60, 64, 80–81, 123–132, 143–145, 153, 156, 165–167, 172, 212, 245, 248, 285, 287–291, 293, 345–346, 348, 353, 359, 362, 364, 383
COSMIC, 19, 167, 169
COSMO, 134, 340, 358, 379
COSMOS launcher, 358
Cost-effective, 23, 27–31, 35–36, 38–39, 73, 78
CubeSat, 126–127, 170, 256–257, 319–321, 327

D

Darwin, 134, 268
Data analysis, 5, 39
Delfi-C3, 319–329
Demonstration, 5, 30, 38, 68, 75, 90, 94, 95, 98–99, 153–155, 167, 169–170, 172, 186, 231, 256, 267, 268, 273, 274, 290, 377, 381
Dependability, 395–401
Disaster monitoring, 31, 35, 57, 58, 61, 67, 167, 253, 313, 345, 346, 357, 359, 362
DMC, 36, 57–66, 80, 81, 154, 250, 252, 357–362
DMC+4, 58, 358
Doppler shift, 293–298
DORIS, 170
Download, 17, 18, 20, 50, 71, 175, 177, 271, 279, 285, 289, 379, 388
DSS, 267–270, 276

E

EarthCARE, 111
Earth science, 3, 5, 6, 8, 12, 365, 367–368, 374
Earth surface, 4, 312

Electro-optical, 63, 89

EMFF, 221–229

ETM, 61, 64

F

FASAT, 101–102, 109

Ferro-probe magnetometer, 337

Fluxgate magnetometer, 125, 147

Flying Laptop, 168, 175, 211–219, 231–241

Formation concept, 134

FORMOSAT, 13, 14, 19, 24, 345–349, 353, 358, 365–374

Frequency variation, 295

G

GALILEO, 160, 165, 166, 171

GENIUS, 211–214

GEO, 73, 74, 135, 159, 166, 222, 382

GEOSS, 82–83

Geostationary, 5, 58

GIPSY, 170

GMES, 64

GNSS, 33, 64, 160–161, 166, 168–172, 317

GOCE, 155, 169

GOES, 5

GOME, 245, 246, 357

GOX, 20

GPM, 5, 7, 8

GPS, 9, 20, 31, 35, 39, 124, 125, 126–129, 137, 160, 165–172, 199–207, 211–219

GRACE, 9, 10, 11, 37, 155, 169, 172, 397

Gravity, 9, 34, 124, 155, 166, 167, 191, 200, 206

Greenhouse gas, 33–337, 64

GTO, 73, 74

H

High resolution, 9, 58, 63, 65–67, 72–74, 76, 80, 90, 99, 146, 170, 304, 337, 357–364, 365, 366, 368

HPOP, 233–236

Hyperspectral, 64, 65, 73

Hyper-spectral, 89, 90, 99

I

Imaging spectrometer, 64, 65, 157, 158, 245–251

Imaging system, 61

INDEX, 36, 186, 197

Induction magnetometer, 337

INS, 199–206

InSAR, 134

INTAμSAT, 41–42, 45, 46, 53–54

Ionosphere, 19, 20, 124, 125, 146, 166, 167, 201, 336–339, 342

IRIS, 53

ISUAL, 365–366, 374

J

Jason, 1, 169, 170

JERS, 304, 393

JPEG2000, 313–314

K

Ka-band, 232, 237

Ka band, 9

KANOPUS, 62

Kolibri, 2000, 339–341

L

LAPAN-TUBSat, 301, 358

LEO, 144, 154, 161, 165–167, 170, 172, 191, 222, 294, 387, 393

LEON, 3, 345, 346, 353

LIM, 159–160

LISA, 134

M

Magnetic field, 4, 123–131, 143–150, 188, 191–193, 196, 197, 200, 234, 258, 260–261, 335

Magnetic torque, 185–186, 188–189, 191, 193, 196, 232

MAGSAT, 124, 144, 150

Mailbox Ground Station, 285, 287–292

Mapping, 9, 58, 61, 65, 66, 68, 80, 81,

101–102, 123, 124, 128, 144, 158, 159, 177, 245, 252, 303, 306, 357–359, 362–363, 389

MDVE, 232, 234–242

MEMS, 27, 29, 125

MEO, 73

Meteorology, 19

METOP, 167, 169

Microsatellite, 9, 11, 13, 19, 22–24, 43, 54, 57–58, 63–64, 80, 101, 134, 165–171, 185–186, 191, 196, 248, 277–284, 309–317, 334, 340, 341, 358, 360

Microthruster, 310

Microwave, 7, 9, 11, 18, 20, 57, 63, 73, 134, 135

MINISAT, 6, 7, 9, 42, 44, 53

MISAT, 72, 73, 319, 328–330

Modeling, 144

MODIS, 304, 305, 306

- MODTRAN, 245, 246
Modularity, 46, 50, 75
MOSAIC, 57, 58, 168, 348
MOST, 185
MTF, 90, 93–99, 360–361
MTG, 159–160
Multimission, 45
Multispectral, 58, 59, 61–65, 68, 73, 76, 80,
 157, 158, 232, 309–353, 361–363
- N**
NANOSAT, 37, 41–54, 124, 134
Natural hazard(s), 4
New technology, 30, 89, 133, 154
NigeriaSAT, 58, 61–62
NOAA, 5, 6, 9, 304, 305
- O**
OCO, 5, 6, 36
OLME, 101, 102
OMAD, 101–108
OMC, 53
OMI, 245, 247
On-board computer, 14, 15, 72, 75, 212, 232
Opto-mechanical, 89, 90
ORACUL, 337
Ørsted, 124, 126, 127, 144, 148, 150, 151
OSIRIS, 53
OSTM, 5, 6
OUBI, 101, 102
Ozone, 101–109, 245, 246, 249, 252
- P**
PAN, 53, 62, 64, 68, 90, 93, 95, 359, 363, 365,
 366
PARASOL, 36, 157
PARIS, 160–161
POES, 5
Pointing accuracy, 75, 185, 195, 197, 315
Pointing stability, 75
Polar, 5–9, 15, 64, 105, 109, 124, 125, 138,
 140, 144, 157, 169, 186, 211, 285, 287,
 289, 320, 346
POLDER, 157
PRISMA, 168, 175
PROBA, 41, 45, 52, 53, 65–66, 67–75, 94–97,
 119, 138, 153–156, 160–161, 168–169,
 175, 350, 358, 398
PROTEUS, 6
Prototype, 77–78, 82, 84, 85, 89, 90, 92, 99,
 309, 329
- Q**
QPSK, 51, 387–393
- R**
Radiance, 9, 104, 157, 247, 250, 251
RapidEye, 38, 59–62, 65, 345–350,
 352, 353
RAPIDS ground station, 380
RASAT, 393
Reaction wheel, 185–186, 233, 239, 240,
 256, 261
Reflectance, 102, 107–108, 157, 306, 361
Reflectivity, 102–103, 108
REIMEI, 185–197
Revisit time, 31, 36, 38, 81, 248, 252, 346
ROCKOT, 37
RSI, 347, 350, 352, 365, 366
RSI, 347, 350, 352, 365, 366
- S**
SABRINA, 134
SAC-C, 144, 150
SAR, 31, 64, 67, 72, 133–140, 156, 170
Satellite attitude, 20, 125, 329
S-band, 15, 18, 20, 21, 45, 50, 53, 60, 187,
 232, 310, 351, 359
SCIAMACHY, 245
SDR, 50, 293–298
Security, 61, 72, 256, 285, 301–307, 379
Sentinel, 64
SEOSAT, 53
Sich-1M, 338
Small satellite program, 42, 84, 231
SMART, 1, 175
Smart, 2, 134
SMOS, 155, 358, 379
Solar cells, 16, 27, 29, 128, 257, 310,
 319–321
Solar panel, 16, 45, 46, 52, 53, 129, 195, 212,
 237, 278–279, 283, 316, 321, 324, 325,
 328
Solar sensor, 20, 53
SOLST, 82–85
Space plasma, 337
Space program, 13–14, 22, 24–25, 41, 170,
 276, 345, 353
Space qualified, 13–24, 33, 165
Spectral bandwidth, 103
Spectral filter, 89
Spectral resolution, 89–92, 104, 157, 245–252,
 312, 336, 337
Spectrometer, 6, 64, 65, 91, 98, 101, 111, 114,
 118, 120, 157, 158, 245–251, 337, 342,
 348
SPHERES, 267–276, 337
SPOT, 61, 259, 304–305, 358, 373

Star Tracker, 52, 144, 146, 147, 149–150, 175–181, 186–188, 213, 232
Suborbital, 5, 258
Sun sensor, 17, 52, 125, 186–188, 232, 255–263, 310, 319, 320, 324, 329
Swarm, 135, 143–151, 169, 180
SWOT, 9, 11

T

TBB, 20
Technology transfer, 14, 30, 31, 81
TechSat21, 134, 135, 140
Telemetry, 15, 24, 45, 232, 240, 241, 278–283, 294, 310, 315, 320–322, 326, 328, 352
TET, 168, 169, 238
Thermal control, 46, 49, 114, 118, 119, 232, 242, 277–284, 350, 352, 359
TIP, 20, 223, 321
TIS, 90–98
TLEs, 365, 366, 374
TMA, 90, 92
TOMS, 101–108, 245, 247

TOPSAT, 57, 59, 60, 67, 70–72, 134, 358,

377–384

TUBSAT, 255, 263, 301, 358

U

UHF, 45, 50, 52, 232, 293, 294, 310, 315, 319, 320, 321

Uplink, 15, 20, 51, 310, 320, 381

V

Vibration, 48, 97, 99, 126, 168, 360

W

Water, 4, 9, 10, 62, 65, 81, 102, 157–159, 303, 306, 347, 361, 374, 395

Wavelength, 91–94, 103, 111, 117–118, 136, 139, 213, 245, 248–251, 306, 313, 361

Weather, 4, 34, 35, 65, 111, 146, 167, 335, 346

X

X-band, 49, 51, 53, 54, 60, 62, 313, 315, 317, 357, 359, 387–393

X-Sat, 168